Tampere University

HATAI JONGPRASITKUL

Tailoring the Printability of Photocrosslinkable Polypeptide and Polysaccharide-based Bioinks for Extrusion-based 3D Bioprinting

Tampere University Dissertations 878

Tampere University Dissertations 878

HATAI JONGPRASITKUL

Tailoring the Printability of Photocrosslinkable Polypeptide and Polysaccharide-based Bioinks for Extrusion-based 3D Bioprinting

ACADEMIC DISSERTATION
To be presented, with the permission of
the Faculty of Medicine and Health Technology
of Tampere University,
for public discussion in the auditorium TB109
of Tietotalo, Korkeakoulunkatu 1, Tampere,
on October 20th 2023, at 12 o'clock.

ACADEMIC DISSERTATION
Tampere University, Faculty of Medicine and Health Technology
Finland

Responsible supervisor and Custos
Professor
Minna Kellomäki
Tampere University
Finland

Supervisors
Postdoctoral Research Fellow
Vijay Singh Parihar
Tampere University
Finland

Postdoctoral Research Fellow
Sanna Turunen
Tampere University
Finland

Pre-examiners
Associate Professor
Riccardo Levato
Utrecht University
Netherlands

Assistant Professor
Gabriella Lindberg
University of Oregon
USA

Opponent
Professor
Anna Finne Wistrand
KTH Royal Institute of Technology
Sweden

The originality of this thesis has been checked using the Turnitin Originality Check service.

Cover design: Roihu Inc.

ISBN 978-952-03-3093-4 (print)
ISBN 978-952-03-3094-1 (pdf)
ISSN 2489-9860 (print)
ISSN 2490-0028 (pdf)
http://urn.fi/URN:ISBN:978-952-03-3094-1

HIILINEUTRAALI PAINOTUOTE
ClimateCalc CC-000025/FI
PunaMusta Printing

Carbon dioxide emissions from printing Tampere University dissertations have been compensated.

PunaMusta Oy – Yliopistopaino
Joensuu 2023

"You can't change the wind but you can set your sails."

– Billie Joe Armstrong, Green Day lead singer

ACKNOWLEDGEMENTS

My doctoral studies were performed during 2019-2023 in the Biomaterials and Tissue Engineering Research Group at the Faculty of Medicine and Health Technology, Tampere University, Finland.

I would like to express my deepest gratitude to my primary supervisor, Professor Minna Kellomäki, for giving me a second chance to prove myself on this subject. Even though my doctoral studies were not a smooth journey, you always have encouraged me to move forward and never give up. Prof. Minna, you are a talented supervisor, you've never tried to mold all researchers to be the same; you have special techniques to draw out the true strength of each researcher because you understand that everyone is unique in their own way. Moreover, you have assigned me to teach many graduate students during the lectures and lab demos, which has strengthened my teaching skills. Lastly, it has been 10 years since I've known you; you offered the first opportunities in research during my Master's studies. You and Teresa Rebelo Calejo were the main reasons for pursuing a doctoral degree. I would like to tell you that this little puppy you met 10 years ago has grown into a wolf.

I would like to thank all my co-authors, Vijay Singh Parihar and Sanna Turunen, for their contributions to all publications and Shambhavee Annurakshita for the first publication. Vijay and Sanna enlightened the connection between chemistry and engineering fields, and it has been very entertaining during the last five years; we've worked together. Vijay, you never lost faith in me, despite the fact that I was a beginner in chemistry six years ago, and I always remember what you told me "I will prove that you are a talented researcher; my chemistry and your engineering knowledge, you and I will rule the world together". Sometimes, our research opinions were not in the same direction, but you've never lost patience and listened to my explanation. Lastly, I would like to thank Vijay again for teaching me advanced organic chemistry, which I could use in future research. Besides, you always treat me like a friend, telling jokes and chitchatting to reduce the pressure during labwork. Sanna, you introduced me to the realm of photocrosslinking during the 2PP project. Back then, nobody in our group had sufficient knowledge of 3D bioprinting. But

you and I have explored from back to front, and we succeeded to summarize our learnings into comprehensive studies on this subject. We have explored the world of 3D bioprinting from the very beginning together. Additionally, you were the one who introduced the practical 3D bioprinter from Brinter, and we produced four publications by using that 3D bioprinter model. Also, you are a professional writer, and I have learned a lot from you. These would not have been possible without your support. I would like to thank everyone in Minna's group for being helpful during my studies, I wish I could spend more time with you guys. Special thanks to all my students since 2017: Jani Jokela, Katri Koskinen, Niina Alén, Tuulia Taipale, Liina Koivisto, Lotta Kääriäinen, Laura Lassilla, and Miika Virpinen. Not only I taught them, but I also learned from them. Every student has a different background and knowledge, hence I could not teach all of them in the same manner. I would also like to thank my first mentor, Professor Oommen Podiyan Oommen. You have taught me basic organic chemistry since 2017. I always remember the words of advice on how to become a successful doctoral researcher on a global scale, which has shaped me into who I am today. I still recall the first day we purchased the laboratory equipment and created the SM501 lab from scratch. I always enjoyed discussing science together. I would also like to thank your lab members, even though we worked together for only two years.

Special thanks to Dr Naomi Paxton for teaching me how to analyze the printability of bioinks. Without your help, my journey could not have come this far, and I hope to thank you in person if we meet at some point. I would also like to thank Professor Gordon Wallace for being a source of inspiration for conducting research in 3D bioprinting. He is my hero in this field, and I am a big fan of his work. I attended his lecture in 2014 in Tampere, which was a turning point for me, as it sparked my interest in pursuing this research direction. And I thank the pre-examiners, Prof. Riccardo Levato and Prof. Gabriella Lindberg, for my thesis improvement.

Finally, I would like to thank my family in Thailand: my mom, papa, big brother and grandma. You are always on my side, giving personal advice, financial support, motivation and inspiration; without your support, I would not have even considered studying abroad. During the journey, I have learned that "Success is not only the result, but it is about the journey you have faced along the way". Eventually, life will find a way.

Hatai Jongprasitkul

ABSTRACT

In extrusion-based bioprinting, a bioink with appropriate rheological properties is used to achieve 3D-printed constructs. A bioink is a printable hydrogel precursor that has properties similar to those of hydrogels, including biocompatibility, biofunctionality, and biodegradability. In particular, natural polymers such as polypeptides and polysaccharides are widely used and are suitable for hydrogel and bioink research. On the other hand, natural polymers without chemical modification lack the mechanical strength and stability to maintain 3D constructs. In bioink development, natural polymers are often functionalized with methacrylate anhydride to enable photopolymerization via free-radical polymerization. Photocrosslinking approachhas been the most used in bioink development due to its tunability, accessibility and cost-effectiveness. This provides the freedom to optimize the physical and chemical properties of the precursor by varying the degree of modification, polymer concentration, photoinitiator concentration and crosslinking time.

To the best of our knowledge, this is the first comprehensive study, which offered simple tools to improve printability in respect of the connection between polymer properties, chemical modifications, rheological behaviors, and 3D biofabrication. The most suitable bioink properties should harness shear-thinning, yield stress, and recovery behaviors. Although some bioinks may exhibit these properties, they are still unable to achieve the desired printing outcomes. The two-step crosslinking strategy is the main focus of this thesis, as it comprises physical crosslinking as the pre-crosslinking step and photocrosslinking as the post-crosslinking step. The initial crosslinking was employed to modulate the rheological properties of the hydrogel precursors for 3D printing. The secondary crosslinking provided stability to the 3D constructed via covalent crosslinking from photocrosslinking. A wide range of photocrosslinkable precursors were investigated and screened as biomaterial inks, including GelMA, ColMA, HAMA, AlgMA, GGMA, GelMAGA, HAGA and GGMAGA. In addition to the methacrylate group, gallic acid was used to improve the multifunctionality and flexibility such as stimuli-responsiveness and tissue adhesion. Different polymer sources and chemical functionalization require different

pre-crosslinking techniques such as temperature, ionic crosslinking ($CaCl_2$), catechol-metal complex ($FeCl_3$), pH modulation and controlled photocrosslinking (low UV intensity).

These pre-crosslinked precursor formulations were formed through different chemistries to obtain printable precursors based on physical or covalent crosslinking. The optimization of the pre-crosslinking parameters (temperature, precursor concentration and amount of pre-crosslinker agents) influenced the printability of the hydrogel precursor in extrusion-based 3D bioprinting. For photocrosslinking, the properties of printed hydrogel, including gelation kinetics, crosslinking degree, mechanical strength, average mesh size and swelling behaviors, could be modulated by the degree of methacrylation, photoinitiator, UV light intensity and exposure time. The printability of the biomaterial inks was assessed by pre-screening via visual analysis, flow behavior, and structural integrity of 3D printed constructs. Printable precursors were defined as those that could form long, smooth, and coherent fibers and stack on top of each fiber. The printable precursors exhibited non-Newtonian fluid, sufficient yield stress, and recovery behaviors to retain their shape fidelity after the force was applied. During printing, rational printing parameters are the most important factors in achieving 3D constructs, such as printing temperature, nozzle size/type, pressure, speed, curing time, and the selection of CAD models. The results showed that the use of pre-crosslinkers (GGMA-$CaCl_2$ and GelMAGA-$FeCl_3$) offered the highest printing resolution, followed by thermal crosslinking, pH modulation and controlled photocrosslinking. For 3D printed constructs, GelMA60 at 16 °C, GGMA-$CaCl_2$, GelMAGA-$FeCl_3$ and HAGA20-HAMA15 inks were successfully printed in cylinders with high structural integrity and stability in the swelling studies. In summary, a two-step crosslinking technique in the hydrogel precursor not only enhanced the printability but also significantly improved the mechanical strength and stability of the final printed structure. This doable crosslinking strategy demonstrates the potential for producing robust and durable constructs through 3D printing technology in the field of hydrogel-based scaffolds. The proposed characterization in this study could be used as the key to screen the printable precursors in bioink development in the future.

CONTENTS

ABBREVIATIONS

3D	Three-dimensional
Alg	Alginate
AlgMA	Alginate methacrylate
CA	Contact angle
CAD	Computational-aided design
CLIP	Continuous liquid interface production
CNF	Cellulose nanofibers
CNS	Central nervous system
Col	Collagen
ColMA	Collagen methacrylate
CT	Computerized tomography
dECM	Decellularized extracellular matrix
DI	Deionized
DLP	Digital light processing
DMEM	Dulbecco's Modified Eagle Medium
DMSO	Dimethyl sulfoxide
DPBS	Dulbecco's phosphate-buffered saline
ECM	Extracellular matrix
EDC	1-ethyl-3-(3-dimethylaminopropyl)-carbodiimide hydrochloride
FDA	Food and Drug Administration
FRESH	Freeform reversible embedding of suspended hydrogels
GA	Gallic acid
Gel	Gelatin
GelMA	Gelatin methacrylate
GelMAGA	Gallic acid functionalized gelatin methacrylate
GG	Gellan gum
GGMA	Gellan gum methacrylate
GGMA-GA	Gallic acid functionalized gellan gum methacrylate
HA	Hyaluronic acid

HAGA	Gallic acid functionalized hyaluronic acid
HAMA	Hyaluronic acid methacrylate
HOBt	1- hydroxybenzotriazole hydrate
I2959	Irgacure 2959
LAP	Lithium phenyl-2,4,6-trimethylbenzoylphosphinate
LVR	Linear viscoelastic region
MA	Methacrylate anhydride
MD	Modification degree
MWCO	Molecular weight cutoff
NMR	Nuclear magnetic resonance
OEGCG	Oligo-epigallocatechin gallate
PBS	Phosphate-buffered saline
PEGDA	Poly(ethylene glycol) diacrylate
PPO	Hydrophobic polypropylene oxide
Pr	Printability
RT	Room temperature
TNBS	Trinitrobenzene sulfonic acid
u.p.	Ultra-pure
UV	Ultraviolet
VA-086	2,2'-azobis[2-methyl-N-(2-hydroxyethyl)propionamide]

SYMBOLS

A	Area
C	Circularity
G'	Storage modulus
G''	Loss modulus
G^*	Complex modulus
G_e	Average value of storage modulus from LVR
K	Flow consistency index
L	Length
n	Shear-thinning index
n_e	Crosslinking density
N	Avogadro constant ($6.023 \times 1023\ mol^{-1}$)
R	Universal gas constant (8.314 J/K·mol)
T	Temperature
W_0	Initial weight
W_s	Swollen weight
γ	Shear rate
δ	Phase angle
η	Shear viscosity
η^*	Complex viscosity
μ	Micro
ξ	Mesh size
τ	Shear stress
τ_0	Yield stress
ω	Angular frequency

ORIGINAL PUBLICATIONS

The thesis is based on the following publications denoted as **Publications I–IV**. **Publications I–IV** have been published. The publications are reprinted with the kind permission of the publishers.

Original publications

Publication I Jongprasitkul, H.; Turunen, S.; Parihar, V.S.; Annurakshita, S; Kellomäki, M. Photocross-linkable Methacrylated Polypeptides and Polysaccharides for Casting, Injecting, and 3D Fabrication, *Biomacromolecules* 2021, 22(2), 481–493. DOI: https://doi.org/10.1021/acs.biomac.0c01322

Publication II Jongprasitkul, H.; Turunen, S.; Parihar, V.S.; Kellomäki, M. Two-Step Crosslinking to Enhance the Printability of Methacrylated Gellan Gum Biomaterial Ink for Extrusion-Based 3D Bioprinting. *Bioprinting* 2022, 25, No. e00185. DOI: https://doi.org/10.1016/j.bprint.2021.e00185

Publication III Jongprasitkul, H.; Turunen, S.; Parihar, V.S.; Kellomäki, M. Sequential Cross-linking of Gallic Acid-Functionalized GelMA-Based Bioinks with Enhanced Printability for Extrusion-Based 3D Bioprinting. *Biomacromolecules* 2023, 24(1), 502-514. DOI: https://doi.org/10.1021/acs.biomac.2c01418

Publication IV Jongprasitkul, H.; Parihar, V.S.; Turunen, S.; Kellomäki, M. pH-Responsive Gallol Functionalized Hyaluronic Acid-based Tissue Adhesive Hydrogels for Injecting and 3D Bioprinting. ACS Applied Materials & Interfaces 2023, 15(28), 33972-33984. DOI: https://doi.org/10.1021/acsami.3c02961

AUTHOR'S CONTRIBUTION

I. The study was designed by all authors. The author performed the experiments, which included polymer synthesis and functionalization. The author also performed material characterizations and data analysis. The author contributed to the writing of the whole manuscript. The final version of the manuscript was revised by the author.

II. The author was responsible for designing and conducting all experiments presented in this study. In addition, the author wrote the entire manuscript, including the conceptualization of the study, data analysis, and interpretation of the results. All aspects of the research process, from data collection to manuscript preparation, were performed by the author.

III. The study was designed by all authors. The author performed material synthesis, characterizations and data analysis. The author interpreted the data and contributed to the writing of the whole manuscript. The final version of the manuscript was revised by the author.

IV. The study was designed by all authors. The conceptualization of the research, analysis of data, and interpretation of results were performed by the author. Every stage of the research process, including data collection and finalization of the manuscript, was also undertaken solely by the author.

1 INTRODUCTION

3D bioprinting is an emerging technology in tissue engineering because of its suitability for the fabrication of complex 3D biological constructs[1]. The main advantage of 3D bioprinting over conventional scaffolds is to fuse cells and materials into a complex structure with micrometer resolution, which provides cell-friendly conditions and mimics the human body environment[2]. Extrusion-based bioprinting requires the use of bioinks, which are primarily composed of soft hydrogels, hydrogel precursors or water-soluble polymers[3,4].

So far, hydrogels have been popular options as bioinks in extrusion-based 3D bioprinters due to their several advantages, including biocompatibility, high hydrophilicity, cell-friendly properties that promote cell growth, mimicking ECM, and tunability of mechanical properties[5]. The hydrogels for extrusion-based bioprinting should possess biocompatible, biodegradable, present appropriate mechanical properties relevant to the tissue type, and have good printability and shear-thinning properties to facilitate the printing process[6]. The development of bioinks requires specific fluid properties such as shear viscosity, shear-thinning, layer stackability, and cell encapsulation[7]. During bioink preparation for an extrusion-based 3D bioprinter, the pre-hydrogel solution, or "precursor" is mildly crosslinked to transform into a "weak hydrogel"[8,9]. A weak hydrogel is a soft extrudable hydrogel that exhibits shear-thinning behavior (a decrease in viscosity as the shear rate increases), as this property enables printability during the printing process[10]. This weak hydrogel is considered a bioink, as it can be extruded smoothly from the nozzle, followed by regaining its initial viscosity after being deposited on the printing bed[11]. This property is called recovery behavior or thixotropy, as it provides shape fidelity and stackability after printing[12]. Depending on the polymer backbone properties and polymer functional groups, the precursor can be crosslinked via physical, chemical, enzymatic, or combined methods[13]. The printed weak hydrogel is later transformed and stabilized into a "true hydrogel" via irreversible covalent crosslinking[9]. The most popular crosslinking technique for 3D bioprinting is photocrosslinking[14].

Photocrosslinking is well known as a rapid crosslinking method, providing a precise, stable scaffold construct for 3D bioprinting applications[15]. Lately, reviews from various literature sources have concentrated on developing new formulations of bioinks for biomedical purposes. Here in this thesis, I focus on the improvement of printability and shape fidelity in the layer-by-layer process of photocrosslinkable bioinks by applying pre-crosslinking techniques, such as temperature change, ionic cross-linking, metal-ligand interaction, pH change, and controlled photocrosslinking. In addition, researchers do not often assess the printability of the newly developed bioinks because of the tedious process of rheological analysis and evaluation of the printability window. There exist only a few studies reporting an insight evaluation of methacrylated polysaccharide and polypeptide-based bioinks[8,10,16]. However, the bioink properties, such as printability and rheological behaviors, can be systematically assessed with various parameters to improve the printing performance[17]. These bioinks based on polypeptides/polysaccharides will open the possibility for reliable and scalable 3D bioprinting of tissue engineering scaffold structures.

2 REVIEW OF LITERATURE

2.1 3D bioprinting technology

2.1.1 Light-based 3D bioprinting

Light-based 3D bioprinting techniques such as stereolithography (SLA), digital light processing (DLP), volumetric bioprinting and continuous liquid interface production (CLIP) have been used to fabricate complex biological 3D scaffolds[18]. These techniques provide high tunability of optical, chemical, and mechanical properties of the scaffolds[19]. In general, light-based 3D printers can be categorized according to the light source used for the polymerization[20]. The most used approach for photopolymerization is utilizing ultraviolet (UV) light or visible light[21]. The main advantage of light-based 3D bioprinting over other manufacturing techniques, such as polymer molding is its ability to generate high-resolution 3D biofabrication from the micro (μm) to macroscale (mm)[22]. In addition, it offers patient-specific 3D scaffolds, as they can be fabricated using a computer-aided design (CAD) model from imaging data such as computed tomography (CT) and magnetic resonance imaging (MRI)[23,24]. However, photopolymerization in 3D bioprinting may cause cell damage during fabrication[25]. Recently, researchers have been trying to compromise UV light intensity and exposure time to achieve high cell survivability as well as maintain the high resolution of 3D constructs[26]. Another alternative method is to replace UV light with visible light to yield higher cell compatibility and a wider range of applications[27]. Typically, an extrusion-based 3D bioprinter integrated with a UV-curing module is used in 3D bioprinting applications[28].

2.1.2 Extrusion-based 3D bioprinting

Extrusion-based bioprinting has been widely used in tissue engineering and biofabrication due to its simplicity, tunability, and cost effectiveness[29]. These mechanisms involve the extrusion of a viscous polymer with or without cells, as they

produce a continuous filament from a nozzle controlled by pneumatic, piston-driven, or screw-driven systems[30]. The main advantage of this approach is that it can print viscous bioinks with high cell densities into 3D constructs[14]. After printing, the printed construct is crosslinked layer-by-layer either via physical or chemical crosslinking[12]. In general, extrusion-based 3D bioprinters contain temperature-controlled and UV-curing modules, which are often employed to adjust printing parameters during fabrication. Temperature control is applied to adjust the viscosity of bioink with temperature-sensitive properties[31]. UV-curing modules are attached to the robotic arm of the printer, providing the additional crosslinking method for photocrosslinkable bioinks to ensure shape fidelity and structural stability during and after printing[32]. For photocrosslinkable bioinks in extrusion-based 3D bioprinting, the photocuring process may be applied before (pre-crosslinking), after (post-crosslinking), or during (in-situ-crosslinking) extrusion, as shown in Figure 1[33]. The main disadvantages of extrusion-based 3D bioprinting are the limited resolution and printing speed due to the size of the nozzles (the smallest diameter is 100 μm)[34]. Extrusion-based 3D bioprinting requires bioinks with optimal rheological properties, crosslinking abilities, and biocompatibility. Several researchers have utilized high-concentration bioinks as the primary strategy to achieve high printability in extrusion-based methods, which can limit cell mobility within the polymer network and might lead to adverse effects on cell viability[35].

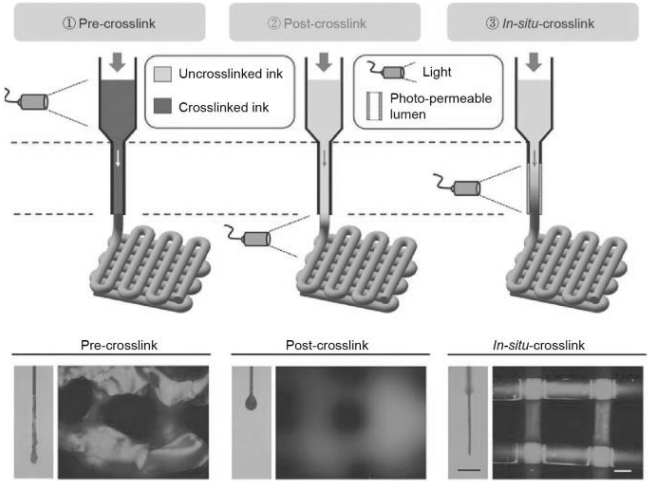

Figure 1. Schematic diagram of three crosslinking techniques for extrusion-based bioprinting: pre-crosslink, post-crosslink, and in-situ-crosslink. Reprinted with permission from ref [33]. Copyright Wiley 2017.

2.2 Precursor, bioink and biomaterial ink

Over the past decade, several researchers have focused on developing novel bioinks, but the terminology of precursor, bioink, and biomaterial ink has still remained unclear. The precursor or hydrogel precursor is a monomer/polymer solution or the initial stage of hydrogel formation before the sol-gel transition. The precursor will transform into a hydrogel in the presence of a crosslinking agent. Groll et al. have clearly defined the terms bioink and biomaterial ink (Figure 2). According to their definitions, cells are the main components of a bioink. On the other hand, polymer solutions or hydrogel precursors that contain biologically active molecules without living cells are typically referred to as biomaterial inks rather than bioinks[36]. The development of bioinks, which encapsulate the cells during the printing process, is essential for the development of functional organs or tissue structures. Recently, numerous studies have reported the modelling of human diseases and conducting drug development research with the help of 3D bioprinting, which can reduce the need for animal tests, research costs, and the duration of experiments[37]. The choice of bioink varies depending on the application (e.g., soft/hard tissue, biosensors) and the type of 3D bioprinter available (inkjet, extrusion, laser-assisted, etc.)[38]. So far, hydrogels have been used as bioink materials in the bioprinting of 3D tissue and organ constructs[39].

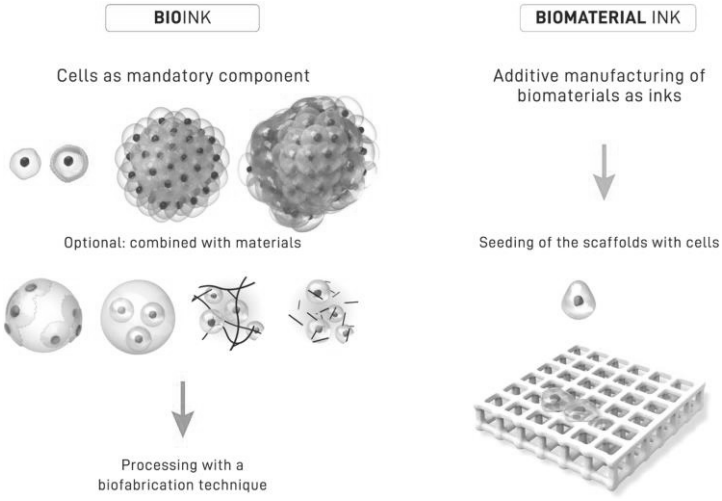

Figure 2. The difference between a bioink (left side), where the cells are the main component in the hydrogel precursor and a biomaterial ink (right side), where an individual biomaterial is printed without cells, and the cells are introduced in the ready biomaterial scaffold. Reprinted with permission from ref [36]. Copyright 2019 IOPscience.

2.2.1 Hydrogel in 3D bioprinting

Hydrogels have been the most used materials in 3D bioprinting applications because of their biocompatibility, high hydrophilicity, cell-friendly characteristics and tunability of mechanical properties[40]. Usually, the hydrogels are loaded with cells and then bioprinted into 3D constructs[39]. Hydrogels are defined as three-dimensional hydrophilic polymer networks capable of absorbing and retaining a significant amount of water or solution in their structure[41–43]. Hydrogels have unique properties because they can mimic the extracellular matrix (ECM) and are thus widely used as scaffolds for tissue engineering applications and as drug carriers in drug delivery[44]. Hydrogels can be derived from both natural and synthetic polymers. Polysaccharide- and polypeptide-derived hydrogels especially are of great interest in biomedical applications[45]. In bioprinting applications, a wide variety of polymers, including natural, synthetic, and semi-synthetic materials, have been used[46]. Various hydrogels derived from polypeptides and polysaccharides, such as gelatin (Gel), collagen (Col), alginate (Alg) and hyaluronic acid (HA), have been synthesized[47–50]. The main advantages of natural hydrogels are low cellular cytotoxicity, the presence of essential properties for cell-matrix interactions (for example, adhesion domains), biodegradability, lack of toxicity, high hydrophilicity, and the possibility to be tailored into injectable gels[51]. However, the disadvantages of natural hydrogels limit their utilization, as they have quite weak mechanical properties, and their quality is not easily controlled due to the batch-to-batch variation[52,53]. Most natural biomaterials are in the form of polypeptides and polysaccharides[54]. However, the current challenges of using polypeptides and polysaccharides include the use of hazardous solvents or reagents during hydrogel synthesis and the insufficient mechanical strength, limited ductility and recoverability attributed to most of the conventional polysaccharide gels[55]. As native polymers without any chemical modification, polypeptides and polysaccharides lack the crosslinking groups needed for hydrogel formation, limiting the range of fabrication methods or applications[56]. Chemical modification of the polymer backbone is a feasible method to improve the properties of these natural hydrogels, such as gelation time, stability, and tunability of their mechanical properties[1,57]. Modified natural polymers are also called semi-synthetic polymer. Hydrogels and bioinks share similarities in their properties and requirements for tissue engineering and biofabrication. They should mimic the mechanical and biological properties of targeted tissues. On the other hand, hydrogels in 3D bioprinting should not only maintain cell viability but also must be printable and have a fast gelation time to achieve 3D constructs[58]. As shown in

Figure 3, collagen, alginate, and gelatin are the most popular choices for bioink development.

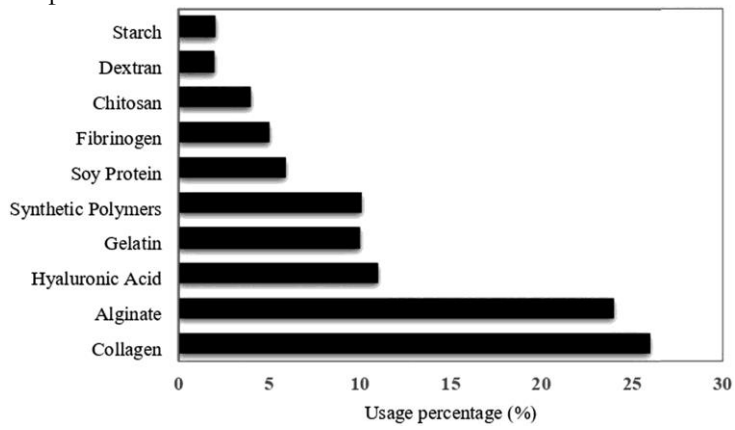

Figure 3. Most used polymers in bioprinting-related research. Reprinted with permission from ref [59]. Copyright 2019 Frontiers.

2.2.2 Polypeptide-based hydrogels

Polypeptide-based hydrogels are intrinsically biocompatible and biologically diverse and thus have been widely used and studied for several decades for various tissue engineering targets[60,61]. Polypeptides have a variety of functional groups specific to each amino acid, which provide more flexibility to modify and tune the properties of the resulting hydrogels[41]. However, polypeptide-based bioinks still have several limitations, such as poor mechanical properties, low stability, difficulties in purification and reproducible production[62]. The range of tunability of polypeptide-based bioinks is relatively narrow due to the need for a minimum protein concentration in the bioink to ensure effective gelation. Furthermore, at the higher end, the tunability is limited by the maximum solubility of the polypeptide in the aqueous solvent[63].

Gelatin has been extensively used as a main bioink in combination with other natural or synthetic bioinks due to its tunability of mechanical and biological properties[64]. Gelatin has thermosensitive properties, which means it can form into a hydrogel at low temperatures (<20 °C), but it can easily transform into a liquid when the temperature increases[65]. Due to this property, gelatin is one of the first choices for bioink development, enabling printability and stability at a controlled temperature[66]. Gelatin is able to be chemically modified because of the number of side chains (free

amine groups in the gelatin backbone) that allow for chemical crosslinking and modification[67]. Gelatin is often modified with methacrylate groups (GelMA), which have been used for a wide range of tissue engineering applications, including bone, cartilage, skin, and vascular networks[68]. Gelatin and GelMA are widely used natural bioinks because they share thermosensitive properties and the ability to change their viscosity as a function of temperature[26]. In practical approaches, a high concentration of GelMA (>5%) has been used extensively; however, this might result in lower cell viability. Janmalek et al. and Yin et al. used a low concentration (<5%) of GelMA and controlled temperature to produce stable soft 3D printed constructs. They employed a two-step thermo-/photocrosslinking strategy to improve shape fidelity while maintaining cell viability[26,69]. Due to the thermosensitive properties of GelMA, it exhibited self-healing at concentrations of 3% and 4% w/v, shear-thinning properties and faster gelation time at low temperature compared to room or physiological temperature[70]. Bartnikowsk et al. used GelMA and GGMA blends to obtain better elastic response (physical and chemical crosslinking)[71]. Moreover, Ouyang et al. utilized 5% w/v of gelatin as the main bioink to combine with low printability bioinks, such as HAMA and AlgMA, to create a complementary network, resulting in the improvement of printability and shape fidelity of 3D printed constructs[72]. Xu et al. also found that dual crosslinking with Ca^{2+} and light enabled the successful printing of low-concentration GelMA (< 1% w/v) and nanocellulose (CNFs), and this technique also provides tremendous mechanical strength up to 5 kPa[73].

Collagens are natural-derived proteins obtained from most mammals, occupying approximately 30% of the entire mammalian protein mass. Collagen facilitates cell adhesive properties, offering cell attachment and growth[74]. It is among the most popular bioinks in the market and biomedical research[75]. However, it exhibits several disadvantages, as it has low viscosity at low temperatures and forms a fibrous structure when the temperature increases or at neutral pH[65]. Several studies have also explored various approaches to enhance the printability of collagen-based bioinks by modifying them with active functional groups, controlling the gelation kinetics, and shear-thinning behavior of collagen-based bioinks[76]. For instance, Kim et al. used various concentrations of tannic acid as pre-crosslinker agents to improve the rheological properties and printability of 3D printed villi structures[77]. Despite the enhancement efforts, utilizing non-modified collagen is not recommended to be used as a standalone bioink due to its mechanical instability and slow gelation rate at physiological temperature. These factors may disrupt its ability to maintain shape

fidelity after extrusion. Collagen is often blended with other bioinks to improve its printability, shape fidelity, and biological properties. Mazzocchi et al. proposed that the combination of methacrylated collagen I and thiolated hyaluronic acid (HA) can be utilized to form a hydrogel with feasible characteristics for extrusion-based bioprinting. For example, Mörö et al. added collagen type I as a shear-thinning enhancer, and it also increased cytocompatibility[78]. A similar report found that collagen-chitosan blends showed shear-thinning behavior and did not exhibit cytotoxicity on NIH-3T3 fibroblasts. In addition, Yang et al. reported that adding collagen type I to an alginate-based bioink gained better overall mechanical strength, which helped preserve chondrocyte phenotypes and reduced unpredicted differentiation during the printing of cartilage scaffolds[79]. Collagen is often mixed with Pluronic® to provide promising results in extrusion-based 3D bioprinting[80]. Collagen type I can be modified with methacrylate groups to enable photocrosslinking due to free amines in the collagen backbone, which share similarities to gelatin[76]. This photocrosslinkable bioink was denoted as ColMA. Another study showed that ColMA and sodium alginate blends provided successful 3D bioprinting of the human cornea, and these findings might demonstrate promising results for corneal tissue engineering applications[5]. In contrast, plain collagen can be photocrosslinked without a methacrylate group. Bell et al. revealed that without even further modification, collagen type I from bovine skin could be printed into 3D microstructures via multiphoton crosslinking[81].

2.2.3 Polysaccharide-based hydrogels

Polysaccharide-based precursors, including chitosan, hyaluronic acid, and alginate, are extensively selected for hydrogel preparation. These materials offer the ability to mimic ECM and possess adjustable viscoelastic properties and excellent permeability, which can promote improved cell adhesion, spreading, and proliferation.[82,83]. They have several functional groups (hydroxyl, acetal, and amine functional groups), which can be chemically modified to improve the existing mechanical or biological properties[84,85]. Furthermore, they are easily formed into hydrogels, mixed with other polymers, or modified into photocrosslinkable precursors[86].

Alginate is the most used natural-derived polysaccharide biomaterial in various industries, including food, pharmaceutical and bioprinting, because of its biocompatibility, tunability of crosslinking techniques, affordability, and ease of

use[3,87]. Alginate is produced from marine brown algae, containing block copolymers, and the exact sequence and ratio of guluronate and mannuronate residues, depending on the source[88]. Alginate hydrogels have good mechanical properties that can mimic the ECM of tissues. Alginate bioink has the main advantage of forming hydrogels via ionic crosslinking in calcium chloride ($CaCl_2$) or calcium sulfate ($CaSO_4$) solutions due to the interaction between divalent calcium ions and negative charge of carboxylic acid groups between alginate polymer chains. This ionic interaction between alginate and divalent cations enables versatility and expands the variety of combinations of alginate-based bioinks. An alternative way to improve the printability of alginate bioink in extrusion-based 3D bioprinters is to utilize a crosslinker bath containing divalent cations. Alginate-based bioink is extruded directly into the bath, resulting in successful 3D bioprinting with high resolution; however, excessive use of high concentrations of cations may reduce cell viability because of the osmotic shock[89]. However, alginate alone has low bioactivity, which means it lacks material-cell interaction and cannot support cell proliferation. Therefore, alginate is often chemically modified or blended with other bioactive materials to overcome these drawbacks. For instance, nanocellulose has been employed with alginate to improve the ink's printability and the printed construct's mechanical strength. Müller et al. added nanocellulose to alginate sulfate to improve the bioink's rheological profile and bioactivity. In addition, Lee et al. showed that adding methacrylated dECM to an alginate-based bioink can improve bioactivity. Yang et al. also added collagen to alginate bioinks, resulting in improved mechanical strength, cell adhesion and cell proliferation in cartilage tissue engineering. Gonzalez-Fernandez et al. evaluated the various combinations of alginate-based bioinks ($CaCl_2$, $CaSO_4$, gelatin, and nanocellulose) for 3D bioprinting anatomical bone grafts[90].

Hyaluronic acid (HA) is a linear non-sulfated glycosaminoglycan found in the ECM of mammalian connective tissues, including cartilages and the central nervous system (CNS). HA contains repeating disaccharide units of D-glucuronic acid and N-acetyl-D-glucosamine moieties linked by alternating β-1,4 and β-1,3 glycosidic linkages[39]. There are three main functional groups that provide chemical activity of HA, which are a glucuronic carboxylic acid group, hydroxyl group and N-acetyl group[91]. HA is also popular among biomaterial choices in tissue engineering because it has excellent biocompatibility for cell growth and proliferation, and it can form transparent and flexible hydrogel after the HA backbone is chemically modified[92]. Additionally, HA hydrogel has a high water-retaining capacity and porosity (maintaining a hydrated

environment and easy-to-transport nutrients or waste products), resulting in an ideal choice for promoting wound healing[93]. In bioprinting, HA is often modified with methacrylate (HAMA), which can be polymerized via photocrosslinking[94]. However, Low molecular weight HA-based bioink cannot be used as an independent bioink because of its poor printability, mechanical properties, poor cell adhesion, and slow gelation time. Adding a viscosity enhancer, such as a high-molecular-weight polymer or highly printable bioink, into HA can enhance its properties. For example, Salzlechner et al. reported that high molecular weight (1 MDa) HA was added to the hydrogel to increase its viscosity and rheological properties for injecting in maxillofacial applications[95]. Several studies have blended GelMA with HA-based bioinks to improve shape fidelity and printability during printing via two-step crosslinking with temperature and photocrosslinking. The two-step crosslinking of HA and GelMA not only improved printability during printing but also provided an elastic and compact hydrogel structure. Moreover, the researchers have used HAMA and GelMA blends to gain better bioactivity of the microenvironment for the endothelial cells, as the blends facilitate the reproduction of epithelial cells, and they also support vascularization[72,96]. To improve the cell adhesion of HA, Hou et al. developed a HA hydrogel modified with laminin, in which laminin assisted cell adhesion and improved the mechanical properties as this combination demonstrated improved wound healing and mechanical properties[97].

Gellan gum is a linear, anionic polysaccharide containing a repeating pattern of one L-rhamnose, one D-glucuronic acid, and two D-glucose subunits. Gellan gum has been widely used in food industries and has been approved by the FDA as a food additive[98]. It has many advantageous properties such as biocompatibility, biodegradability, non-toxicity, and good mechanical properties with high efficiency of gelation kinetics[99]. Recently, it has been an interesting option in the field of tissue engineering and bioprinting as well and has been used in cartilage, skeletal tissue, and brain-like 3D printed scaffolds[100]. In bioprinting, gellan gum-based bioink has many advantages over other bioinks due to the low costs, simplicity, good shear-thinning behavior, and fast gelation at physiological temperature[101,102]. However, gellan gum bioink alone cannot provide sufficient printability and shape fidelity for extrusion-based 3D bioprinting[11]. In addition, the structure of the gellan gum hydrogel has intrinsic brittleness, which might limit its mechanical properties, leading to poor stability during the implantion[103]. Consequently, several researchers have developed gellan gum-based bioinks by mixing gellan gum with other components or modifying the gellan gum backbone[104]. Mouser et al. blended GG and GelMA bioinks for

cartilage bioprinting[105]. Moreover, Hu et al. reported that a gellan gum-PEGDA bioink blend creates good mechanical and rheological properties and high cell viability[100]. Moreover, Chen et al. found that the mixed combination of gellan gum, sodium alginate, and a thixotropic magnesium phosphate-based gel has been shown to increase bioactivity, as a hybrid bioink was formed with favorable characteristics, including strong gelation, mechanical stability, rheological properties, and excellent printing performance, leading to enhanced cell proliferation and increased cell survival. In the utilization of gellan gum as a solo bioink, functionalization of the GG backbone, such as GGMA or incorporation with viscosity enhancers, such as starch, have been explored to improve the processability and flexibility of applications[106–110]. For instance, GG precursor was mixed with starch and fabricated by extrusion printing[111]. Another interesting GG bioink example is the GG modification with a surfactant to improve rintability[112]. In addition, GG/PEGDA and GGMA/chitosan have exhibited double network crosslinking by combining non-covalent and covalent crosslinking, which resulted in a strong and stretchable interpenetrating polymer network structure[101,106].

2.3 Crosslinking methods for hydrogel precursors

The crosslinking mechanism of the hydrogel precursor in extrusion-based 3D bioprinting plays an essential role in achieving a high sol-gel transition degree to maintain the structural integrity of the printed construct. Optimization of crosslinking methods in pre- and post-printing steps is crucial for the bioink development process. There are two types of crosslinking between polymer chains: physical and chemical crosslinking, as shown in Figure 4. The choice of crosslinking method influences the gelation kinetics, mechanical properties and biofunctionality of the resulting hydrogels. Physical or noncovalent crosslinking in hydrogels relies on weak interaction forces, including thermal and ionic crosslinking, self-assembly and electrostatic interaction[113]. On the contrary, chemical crosslinking is based on covalent bond formation, which is more stable than the bonds formed via physical crosslinking. Among the chemical crosslinking methods in bioprinting, photopolymerization has been used in bioink development due to its unique characteristics[15,114].

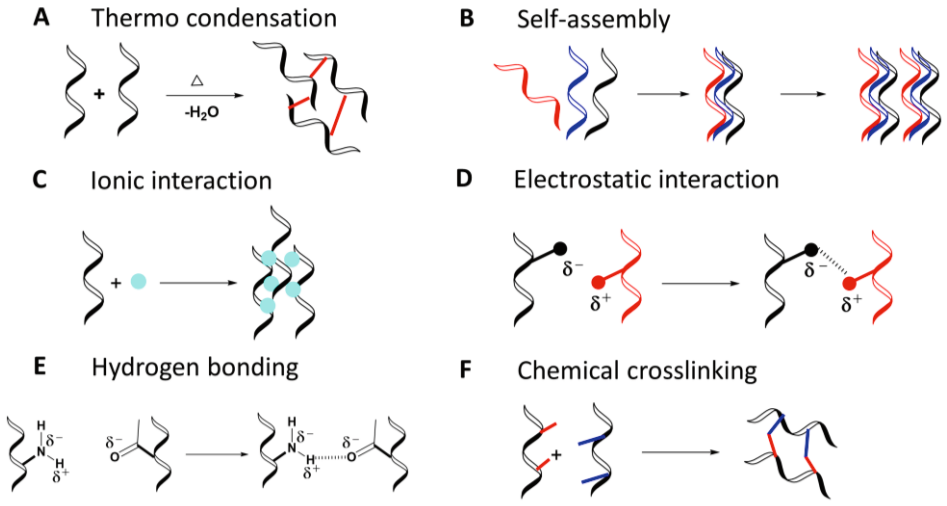

Figure 4. Different crosslinking mechanisms of hydrogels: (A) Thermal crosslinking or thermo condensation; (B) self-assembly; (C) ionic interaction; (D) electrostatic interaction; (E) hydrogen bonding; (F) chemical crosslinking.[113,115]

2.3.1 Noncovalent crosslinking

Thermal crosslinking or thermo condensation involves heating or cooling of the precursor to increase/decrease the viscosity or initiate hydrogel formation[116]. Thermal crosslinking is the simplest method for thermosensitive polymers, such as gelatin, collagen and poloxamers. The main disadvantage of this method is the long gelation time and the inability to control the degree of crosslinking[117]. Moreover, either excessive heat or cold may lead to irreversible cell damage[26]. So far, several studies have used gelatin-based bioink blends (with alginate or HA) to enhance the printability of bioinks in extrusion-based bioprinting[72]. Gelatin-based bioink undergoes a sol-gel transition from high to low temperatures, which might vary according to the functional group, degree of modification, and molecular weight of gelatin[118]. The thermal crosslinking of gelatin is highly reversible (thermally reversible properties) and can be exploited in 3D bioprinting[119]. At high temperatures, gelatin loses its triple-helix formation, behaving as a more Newtonian fluid; however, gelatin becomes more viscous and forms a gel again at a low temperature[120]. In extrusion-based 3D bioprinters, the printing machine and platform have temperature-controlled features that precisely control the temperature inside the cartridge and on

the substrate during printing. In general, GelMA bioinks have been used at high concentrations (<15% w/v) and high temperatures (< 25 °C) to increase printability[121]. However, a high polymer concentration creates a high crosslinking density, inhibiting cell growth and nutrient or waste transportation[122]. Liu et al. reported that a low concentration of GelMA (3–5% w/v) can be used in extrusion-based 3D bioprinting by cooling GelMA bioink to 4 °C for 20 mins and printing at 21 °C[70]. On the other hand, it might lead to cold injury because the cells are exposed to two different temperatures (4 and 21 °C). Zhao et al. used gelatin-alginate bioink containing cancer cells. They used low temperature during printing and subsequently crosslinked the gel with $CaCl_2$[123]. Poloxamer or P407 has been an interesting option in bioink composition due to its thermoresponsive properties. Hence, it has been used widely as a sacrificial material during printing, as it turns into an aqueous solution at low temperatures[124]. Poloxamer also undergoes sol-gel transition, but it exhibits thermal gelation from low to high temperature. On the other hand, P407 turns into a solid as the temperature rises due to hydrophobic interactions between the P407 copolymer chains[125]. At high temperatures (Figure 5), the P407 copolymer chains become aggregated into a micellar structure by dehydration of the hydrophobic polypropylene oxide (PPO) repeating units as it begins to gelate, and P407 molecules form an array of thermodynamically stable self-assembled structures[126]. Moreover, the thermal reversibility of bioink not only provides improvement of printability in 3D bioprinting but also has potential in drug release applications, making this bioink combination an attractive option for various administrations[117].

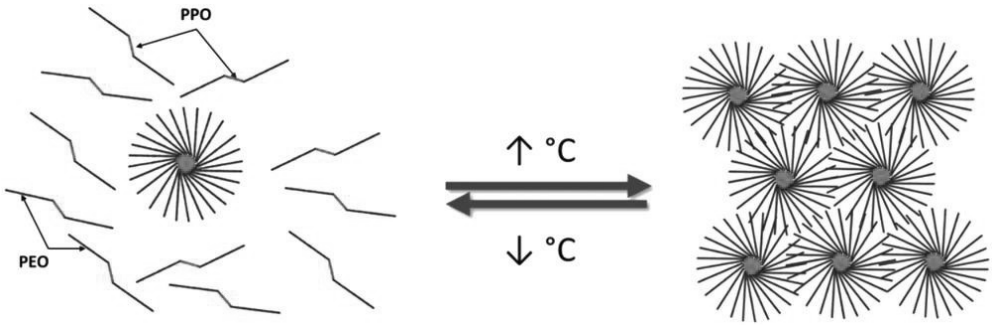

Figure 5. The schematic illustrated P407 gelation when the temperature rises. Reprinted with permission from ref [127]. Copyright 2019 Wiley.

Ionic interaction is one of key strategies for pre- and post-crosslinking of bioinks in 3D bioprinting[16]. This method utilizes the addition of multivalent cations to a

precursor to form a hydrogel. The free carboxylic groups of the polymer chain, such as alginate's linked β-d-mannuronic acid (M) and α-l-guluronic acid (G), are able to bind with multivalent cations, such as Ca^{2+} (G-G and M-G blocks), Sr^{2+} (G-G block) and Ba^{2+} (G-G and M-M blocks)[128,129]. Consequently, the polymer chain is ionically crosslinked and forms a hydrogel. This process is described as the "egg-box" model (Figure 6), in which divalent ions are entrapped within cavities formed by the cooperative coupling of contiguous G or M units[130]. However, there are several drawbacks to using ionic crosslinking, such as poor mechanical properties and stability, and ions might be accidentally released after crosslinking, which can induce an adverse effect on cells or allergic reactions after implantation[116]. The number of blocks in the polymer chain and the concentration of polymer solution determine the degree of crosslinking and the mechanical strength of the polymer[131]. Ionic crosslinking is an attractive choice in 3D bioprinting, as the bioink can be formed into a hydrogel at room and physiological temperatures and pH[132]. As mentioned earlier, polymer chains with free carboxylic groups, such as alginate, can be crosslinked with several multivalent cations, including calcium, barium, zinc, ferric, and strontium. Calcium ion has been frequently used in tissue engineering and 3D bioprinting due to the increased stability of the constructs[133]. In several studies, alginate-based polymers have been used as bioinks with ionic crosslinking, such as calcium chloride ($CaCl_2$), calcium sulphate ($CaSO_4$) and calcium carbonate ($CaCO_3$), to form more complex 3D printed constructs. Among all available crosslinkers, $CaCl_2$ is widely used in 3D bioprinting due to its high solubility in water or media and ability to form hydrogels faster than other crosslinkers[133]. However, a fast gelation time might lead to nonhomogeneous crosslinking, as gelation occurs only on the surface, leaving unreacted polymer inside the gel, resulting in poor stability after printing[134]. Therefore, several approaches have been proposed to tackle this weakness. For example, alginate bioink can be printed through direct extrusion into a calcium bath[12]. Each printed filament is immediately crosslinked in a crosslinker bath to stabilize the structure in a layer-by-layer fashion. A low concentration of $CaCl_2$ can also be used as a pre-crosslinker to modulate the viscosity of alginate-based bioinks, resulting in improved printability[10]. Besides alginate-based bioinks, other polysaccharides, such as gellan gum, can also be crosslinked by the addition of multivalent ions[107]. Similar to alginate, polymer concentrations and the type of divalent cations influence the mechanical properties of gellan gum[135]. However, gellan gum-based bioinks have not been widely explored in 3D bioprinting applications. Coutinho et al. used dual crosslinking of methacrylate gellan gum using physical (temperature and cations) and chemical crosslinking (photocrosslinking) to

improve mechanical properties without affecting biocompatibility[107]. Khademhosseini et al. also found that GGMA provided better compressive stress than pure gellan gum. Jongprasitkul et al. utilized a strategy similar to alginate-Ca^{2+}, in which $CaCl_2$ solution was used as a pre-crosslinker to increase the viscosity and printability of GGMA. After that, pre-crosslinked GGMA was then chemically crosslinked through photocrosslinking to stabilize the 3D-printed structures[11]. A high concentration of ionic crosslinkers may lead to permanent cell damage during ink preparation or after printing. Even though ionic crosslinking is safer than harsh thermal or chemical exposure, it is still not an ideal environment for cells, as it can reduce their viability. Several studies have found that excessive use of $CaCl_2$ crosslinker, for example, more than 500 mM, can harm the cells in the 3D bioprinted structures, as a high concentration of calcium damages the cell membrane leading to a disturbed state of cell electrolytes[89].

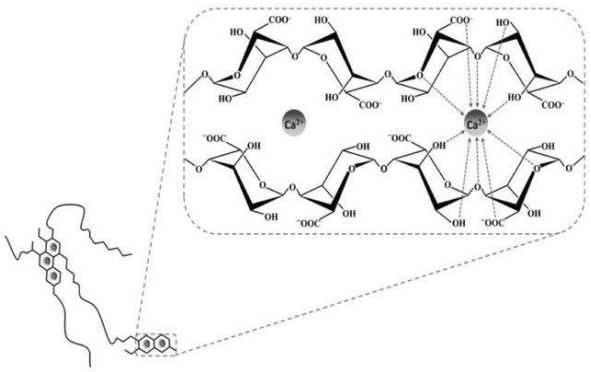

Figure 6. Egg-box model representing the interactions between alginate G-blocks and calcium ions. Reprinted with permission from ref [136]. Copyright 2019 MDPI.

In the wide selection of non-covalent crosslinking in hydrogels, hydrogen bonds have attracted interest in tissue engineering and 3D bioprinting applications. Hydrogen bonds are non-covalent interactions between the hydrogen atoms attached to electronegative atoms, such as oxygen and nitrogen, forming intermolecular bonds between the vicinity of electronegative atoms[137]. In general, hydrogen bonding is weaker than covalent or ionic interactions. Due to their reversible bonding interactions and low toxicity, hydrogen bonds have been extensively used in dynamic hydrogels with shear-thinning or self-healing properties and stimuli-responsive or smart hydrogels[13]. Various strategies have been explored to develop highly efficient hydrogen-bond crosslinking systems. Recently, phenolic moieties, including gallol or catechol groups, have been used in hydrogels. In Figure

7, Shin et al. reported hyaluronic-based hydrogel using gallol conjugation and oligo-epigallocatechin gallate (OEGCG). The main driving forces for hydrogel formation are multiple gallol-to-gallol and gallol-to-HA hydrogen bonding interactions[138]. This gallol-functionalized hydrogel was reversible and could recover from a high shear strain. In addition, this hydrogel exhibited shear-thinning properties and could be used as an injectable hydrogel[139]. For bioinks, hydrogen bonding or hydrophobic interactions are often environmentally dependent; therefore, temperature or pH changes will mainly influence the rheological behavior of the ink, such as the viscosity of precursors and the viscoelasticity of hydrogels. The gelatin-chitosan blend has been utilized for the 3D bioprinting of the skin constructs. Gelatin contains a carboxylate group that exhibits a negative charge when the pH of the medium is above 4.7. In contrast, chitosan carries positively charged ammonium ions, which can interact with the carboxylate groups of gelatins, resulting in the formation of network structure[140]. Silk-based bioinks have also been employed in 3D bioprinting and can undergo physical crosslinking through pH- or sonication-induced formation of β-sheet crystallization[141]. However, additional crosslinking is still required to improve the overall stability of the printed constructs of β-sheet mediated crosslinking and other types of non-covalent crosslinking methods[142].

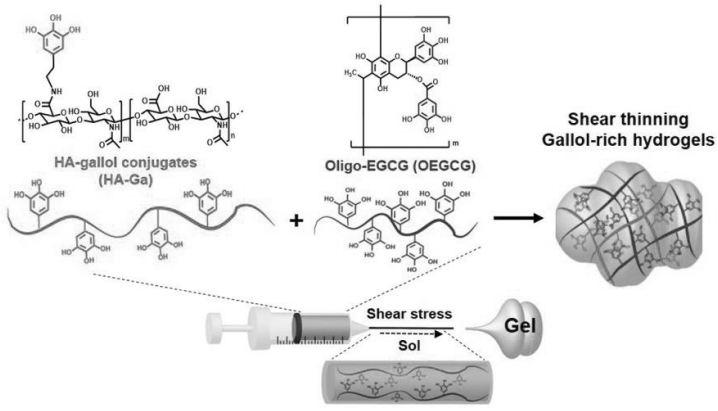

Figure 7. Schematic illustration for preparing gallol-rich, shear-thinning hydrogels of HA-Ga/OEGCG. Reprinted with permission from ref [138]. Copyright 2017 American Chemical Society.

Catechol-metal coordination bonds have offered wide versatility to dynamic polymeric networks, especially in self-healing hydrogels, as the coordination interactions between organic ligands and metallic ions generate reversible crosslinks in hydrogels[13,143]. In addition, catechol-metal coordination bonds or metal complexes have been widely used in hydrogel preparation due to the tunability of

mechanical strength. Catechol-functionalized polymers are often mixed with metal ions such as V^{3+}, Fe^{3+} and Al^{3+} to obtain self-healing hydrogels[144]. Among all combinations of catechol-metal bonds, catechol-Fe^{3+} complexes have been an interesting choice as reversible crosslinks to produce dynamic polymeric networks (Figure 8)[145]. In bioprinting, only a few reports have explored metal-ligand complexes to obtain printable hydrogels[146]. Cathechol metal ligands provide strong interactions with metal ions, which can be utilized as pre-crosslinkers for bioinks. Wodarczyk-Biegun et al. used metal ions (V^{3+}, Fe^{3+}, Al^{3+}) to crosslink with catechol-functionalized polymers. The results of the study indicated that these combinations exhibited a pH-tunable crosslinking degree, rapid formation of a network structure and self-healing properties. As a result, the extruded filaments of these ink formulations were smooth with high shape fidelity[17]. In addition, Shin et al. reported that gallol-containing compounds, such as gallic acid, have been used in injectable hydrogels through a combination of hydrogen bonding and metal coordination interactions[138]. In addition, Han et al. applied the addition of Fe^{3+} ions to catechol-modified HA, which can form a dual network via chelation, resulting in enhanced cohesiveness and shock-absorbing properties[147].

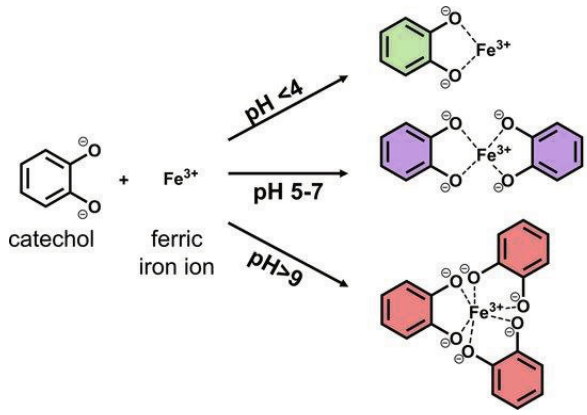

Figure 8. Coordination of ferric iron by catechol at different pH values, resulting from ligand-to-metal charge transfer. Reprinted with permission from ref [148]. Copyright 2020 Springer Nature.

2.3.2 Photocrosslinking

Bioinks with photocrosslinkable properties have gained significant attention in 3D bioprinting because light provides spatiotemporal control over the reaction behavior of the material, which can be used for controlling the accurate fabrication of 3D

structures. Furthermore, light-based crosslinking is typically very efficient and results in minimal byproducts, which in turn enables the fabrication of cell-containing constructs. The basic components in photopolymerization are polymer precursors, photoinitiators, photoreactive groups, and light energy[149]. Typically, there are two types of photocrosslinkable bioinks used in 3D bioprinting: methacrylated (free radical polymerization) and non-methacrylated groups (bio-orthogonal click reaction and redox crosslinking)[25]. The most common way to engineer photocurable bioinks is to modify them with methacryloyl groups via the esterification of methacrylic anhydride. Polymerization of methacrylate-based materials involves free radical or chain polymerization. The photocrosslinkable bioink contains a photoinitiator, which initiates photopolymerization via radical or cationic mechanisms when exposed to light and reacts with monomers or oligomers to create polymer chain reactions and growth. The photocrosslinking reaction proceeds through three stages: initiation, propagation, and termination (Figure 9)[149]. In the initiation step, free radicals are generated via homolytic cleavage of the photoinitiator. In the propagation, the rapid addition of unreacted monomers or polymers to the radical intermediate results in the formation of radical-terminated polymers. In the termination step, the chain-growth reaction on the polymer is terminated via radical coupling, chain transfer agents or disproportionation reaction.

The selected photoinitiator should efficiently generate free radicals with low toxicity, and the choice should be made according to the absorption wavelength used in the fabrication technique (one- and multi-photon polymerization)[149]. For example, Irgacure 2959, LAP, VA-086 and Eosin Y require wavelengths of 257, 375, 385, and 514 nm, respectively[150]. For bioprinting, UV or visible light-sensitive photoinitiators are frequently used. Recently, methacrylated polymers with a high degree of MA modification, such as hyaluronic acid and gelatin, have been used for light-based 3D bioprinting, such as stereolithography (SLA) and digital light processing (DLP)[151]. Previously published research by O'Connell et al. reported the fabrication of hydrogels using methacrylated polymers with a tuned molecular weight of the polymer, modification degree, polymer concentration, and even combinations with other materials to better suit the applications[1]. Figure 10 illustrates the synthesis of GelMA and the fabrication of photocrosslinked GelMA hydrogel[152]. However, the printing of photocrosslinkable bioinks with an extrusion-based 3D bioprinter still remains a challenge due to their low viscosity, poor printability, and poor printing accuracy. In this regard, direct extrusion printing is often combined with *in situ* photocrosslinking to improve printability during printing, or the bioink is exposed

to light immediately after printing (post-crosslinking). Ouyang et al. introduced *in-situ* photocrosslinking to enhance the printability of nonviscous bioinks[33]. Even though photocrosslinking with UV light (320−365 nm) has been widely used in 3D bioprinting, photocrosslinking with UV light may permanently damage cells in the printed constructs and can be harmful to users as well. In this case, visible light or blue light (<400 nm) crosslinking has been introduced as an alternative because wavelengths in the visible range are not harmful to cells. In addition, the crosslinking parameters, including light intensity, exposure time, photoinitiators and polymer concentrations, should be optimized because they may influence cellular behaviors, such as cell proliferation, cell viability and cytotoxicity[116]. The low crosslinking density of bioinks provides a more suitable environment for incorporating biomolecules due to their higher swelling ratio and larger pore size. However, bioinks with low crosslinking density suffer from poor processability, which leads to printing difficulties and ultimately results in the poor structural integrity of the final 3D printed structure[153]. Thus, printability and biological functionality must be compromised by choosing the proper printing parameters, polymer concentration, and degree of functionalization of polymers.

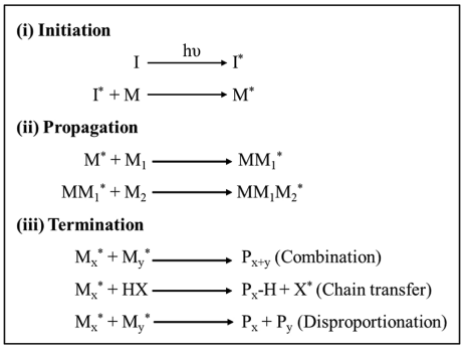

Figure 9. Mechanism of free radical polymerization (methacrylated group). Reprinted with permission from ref [149]. Copyright 2022 Elsevier.

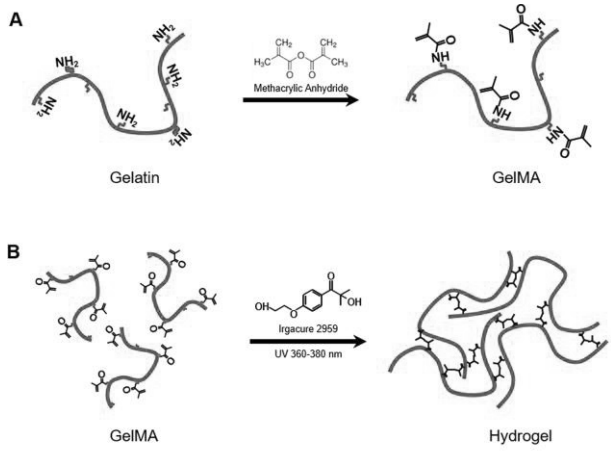

Figure 10. Fabrication of photocrosslinked GelMA hydrogel. Reprinted with permission from ref[152]. Copyright 2016 PLOS.

2.4 Modulating unprintable precursor to biomaterial ink

A bioink is a printable hydrogel precursor that contains cells. In general, the viscosity of the precursor can guarantee successful 3D printing, as the viscosity provides shape fidelity and stackability for each printed layer[154]. Low to moderate viscosity is recommended during extrusion because a high shear force disturbs the smoothness of the printed filament and may negatively impact cell viability. On the other hand, higher viscosity provides better structural stability, which is able to maintain shape fidelity longer after printing[155]. For instance, Duan et al. have shown that with a viscosity of HAMA and GelMA blends of more than 104 Pa·s, the deposition of the printed precursor was difficult, even though the shape fidelity was improved. In contrast, if the viscosity of the blend was lower than 100 Pa·s, the precursor could be extruded easily, but the printed layer failed to maintain its own weight, resulting in construction collapse in post-printing[156]. Typically, natural-derived hydrogel precursors lack processability and have inadequate viscosity and shape fidelity. Hence, proper modulations are required, such as increasing the polymer concentration, crosslinking density, and functionalization[54,157]. As a result, hydrogels gain more stiffness but become less permeable, which may limit cell migration and impair biofunctionality[122]. To achieve higher hydrogel permeability, soft hydrogels and low crosslinking densities are preferred; however, they exhibit insufficient mechanical properties to maintain the shape[158]. To solve this issue, several

researchers have introduced various strategies to create shear-thinning precursors with proper viscosity and shape fidelity during printing while maintaining high bioactivity during and after printing. So far, there are five strategies to convert unprintable precursors to printable precursors (bioinks) for extrusion-based printing, which are two-step crosslinking, blending of bioinks, *in situ* photocrosslinking, extrusion in crosslinker bath and extrusion in supporting bath (FRESH).

2.4.1 Two-step crosslinking

Two-step crosslinking refers to the combination of more than one crosslinking method to the precursor to improve its processability with extrusion-based 3D bioprinting. This approach often utilizes physical and chemical crosslinking of the precursor before and after printing or vice versa (Figure 11). The initial step is to utilize mild crosslinking agents to form reversible hydrogels, such as thermal crosslinking, ionic interactions, and hydrogen bonding, which is called pre-crosslinking [10,13,116,159–163]. The pre-crosslinked precursor with improved rheological properties is considered ink for 3D printing[10]. The second step is to stabilize the ink further after it is printed on the platform by applying irreversible covalent crosslinking. This approach offers a major advantage over other methods. In general, using a high concentration of polymer provides optimum printability, but it has an adverse effect on cell viability, proliferation, and migration. However, with this approach, low-concentration bioinks can be printed. The simplest method is to apply a lowered temperature with thermo-sensitive bioinks, such as pure gelatin, pure collagen, GelMA and ColMA, which results in higher viscosity bioinks, followed by photocrosslinking to stabilize the printed structures. This thermal crosslinking can regulate the viscosity throughout the printing process via a temperature regulator in the printer, as it provides reversible thermo-crosslinking to improve the processability of the hydrogel precursors. However, lowering the temperature of the bioink further increases its viscosity, leading to higher shear stress that may potentially cause cell injuries. Moreover, the low temperatures produced can injure the cells and cause irreversible cell damage. Cooling the GelMA surges the viscosity, which results in irregular filaments, discontinuity of extrusion or frequent clogging[26,69]. Another technique is to incorporate multivalent cations in polysaccharide-based precursors, which have free carboxylic groups in polymer chains such as alginate and gellan gum. An alginate or gellan gum-based precursor is pre-crosslinked by mixing with a low concentration of ionic crosslinker during the

ink preparation. Next, the ink is fully crosslinked after the ink is extruded on the substrate by exposure to the ions in the post-printing phase. For photocrosslinkable alginate (AlgMA) and gellan gum (GGMA), the ink is pre-crosslinked in the presence of ions, and instead of using ions to fully crosslink the ink, photocrosslinking is applied to the printed structure[2,11,164].

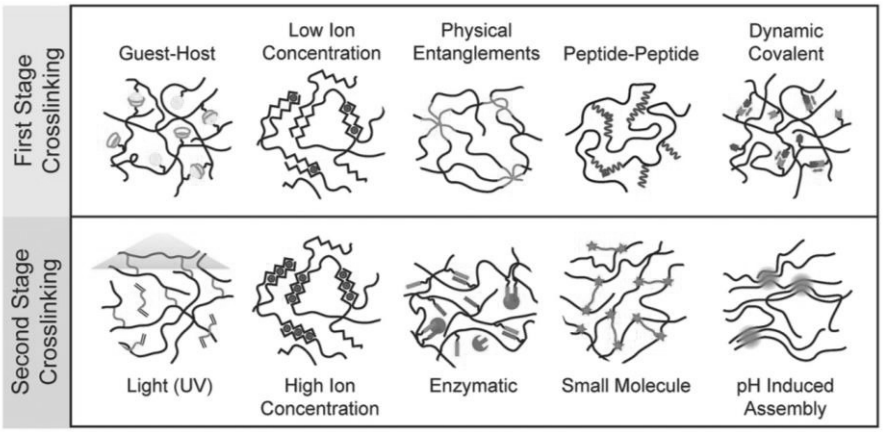

Figure 11. The selection of crosslinking methods for a two-step crosslinking strategy: (1) The precursor is mildly crosslinked to obtain the optimum rheological behavior for printing. (2) The second step is also called the curing step, as the printed construct is crosslinked more intensively to obtain greater structural integrity and with an improved mechanical property. Reprinted with permission from ref [165]. Copyright 2021 Wiley.

2.4.2 Blending of bioinks

Single component bioink has a main limitation, as it is difficult to optimize the printability to support high shape fidelity while maintaining the biological function supporting high cell viability and proliferation, resulting in a narrow biofabrication window[122,166]. The difficulty of biofabrication window adjustment can be acceptable, but it might create a compromise between printability and bioactivity for extrusion-based 3D bioprinting[58]. In this case, bioink blends or multicomponent bioinks are a combination of two or more biomaterials, which is the most used and easiest way to overcome the limitations of single-component bioinks, such as printability and biological performance. Moreover, they can provide a wider biofabrication window[58]. The bioink blend contains various polymers; each polymer has different properties, such as shear-thinning behavior and high cellular activity[155]. For example, a bioink blend is comprised of polymers A and B. The rheological properties of

polymer A can be easily adjusted during the preparation, printing or after printing, whereas polymer B, with bioactive properties, improves cell-material interactions. As a result, the printed structure of the polymer A and B blend provides better and longer-term mechanical properties and stability and biofunctionality. In addition, the functionalization of two or more polymers can create an interpenetrating network, which can significantly enhance the mechanical properties of the printed construct as well[167]. Recently, several combinations of bioink blends have been developed, which are categorized into multi-material, interpenetrating networks, nanocomposites and supramolecular bioinks (Figure 12)[52,155]. Multimaterial bioinks are composed of two or more bioinks that are covalently crosslinked with each other after printing[58]. A prominent example is GelMA and HAMA bioink blends, as GelMA improves printability via thermal gelation and HAMA enhances cell adhesion. After the GelMA component is physically crosslinked via low temperature, GelMA-HAMA bioink blends are covalently crosslinked through photocrosslinking in the final 3D printed structure[168]. Interpenetrating networks are among the most used approaches for blending bioinks. Similar to multi-material bioink, two or more bioinks are simply mixed together, but each bioink is independently crosslinked without covalently crosslinked to one another[169]. An interpenetrating network can maintain the advantages of each polymer because those two are only entangled physically without chemical interactions. An example is to use alginate-based bioink; the alginate components are crosslinked through ionic interactions, while the other parts, such as any photocrosslinkable bioinks, are chemically crosslinked through photocrosslinking[170]. The two bioink components have two independent gelation mechanisms but are combined into one final printed construct. Furthermore, multi-material and interpenetrating network bioinks can be printed using coaxial extrusion from separate printing cartridges as well[32]. The two types of bioinks can be printed simultaneously. The pre-crosslinked bioink is extruded as an outer shell to ensure shape fidelity, while the more biofunctional bioink is extruded as the core of the fiber. This process enables a simple single-step 3D bioprinting of tissue constructs with high printability and cell viability[171]. Nanocomposite bioink contains nanoparticles incorporated into the formulations, which can improve overall stiffness and biocompatibility[172]. Lastly, supramolecular bioinks are hydrogel systems based on non-covalent reversible bonds. The reversible properties of non-covalent bonding in hydrogels offer high shear-thinning and self-healing properties, which are essential for direct extrusion printing. Highly et al. developed a guest-host system by modifying HA with different groups, specifically adamantane and cyclodextrin, that improved printability with high resolution[173].

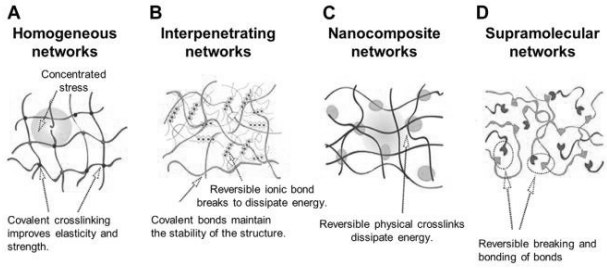

Figure 12. The illustration of four kinds of networks in bioink blends: (A) Homogeneous networks, (B) Interpenetrating networks, (C) Nanocomposite networks, and (D) Supramolecular networks. Reprinted with permission from ref [174]. Copyright 2021 Frontiers.

2.4.3 *In situ* photocrosslinking

An *in-situ* crosslinking or *in-situ* photocrosslinking is a unique bioprinting approach, which can turn non-viscous precursor into smooth, uniform extruded filament via photocrosslinking through a photopermeable capillary (Figure 13)[25]. The method has various advantages over pre- or post-photocrosslinking: viscosity modulation is not required, this method can be applied to any photocrosslinkable precursors, it does not inhibit cell viability due to the low extrusion force and low intensity of light energy, and it can be used to print more complex structure with high resolution. Moreover, *in situ* photocrosslinking allows an extrusion printing of nonviscous bioinks without adding a viscosity enhancer or post-curing step. However, the precursor must have rapid gelation kinetics to be able to form a weak gel during deposition. Ouyang et al. and Galarraga et al. introduced the concept of an *in-situ* crosslinking technique for bioprinting nonviscous bioink. They investigate various aspects of this technique, including the assessment of photorheology parameters during curing, light attenuation across the capillary, and design specifications such as capillary width and length, bioink flow rate, and light intensity[33,175].

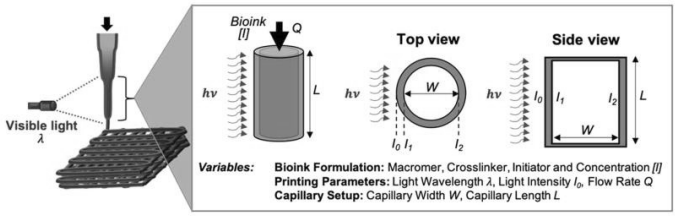

Figure 13. The schematic of *in situ* photocrosslinking for 3D bioprinting. Reprinted with permission from ref [175]. Copyright 2019 Springer Nature.

2.4.4 Extrusion in crosslinker bath

This approach involves extruding a bioink directly into a bath containing a crosslinking agent or coagulation bath such as metal ions, enabling rapid gelation, as it can support shape fidelity after printing[176]. In this printing technique (Figure 14), it is crucial to optimize the concentration of metal ions for rapid gelation of the bioinks while biocompatibility remains intact[116]. According to these studies, alginate-based bioinks have been mostly utilized in this approach, as alginate ink is extruded in a calcium chloride solution[177]. The concentration of calcium chloride bath is approximately 100 mM or less to maintain the shape fidelity and cell viability during the processing[178]. However, there are several disadvantages that might limit the use of this method[179]. For example, frequent nozzle clogging has been observed during printing due to the rapid gelation between the bioink and crosslinker. Another obvious example is the low proper adhesion between the printed layer, which might lead to instability of the printed construct and structural failure[180]. Moreover, the bioink must have rapid gelation kinetics, enabling it to form into hydrogel after being exposed to a crosslinker. Lastly, removing residual crosslinker from the complex structures can be difficult, causing a possible reduction in biocompatibility[176]. Moreover, washing the residual crosslinker might deform the printed structure[179].

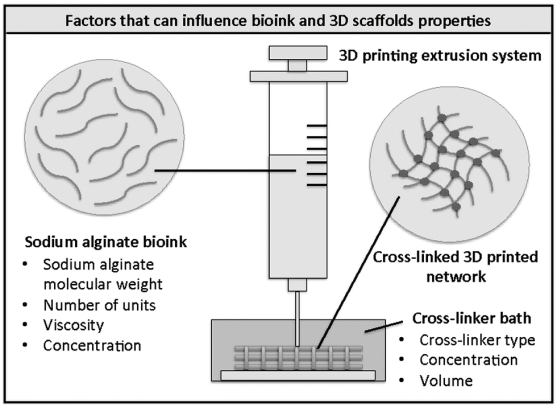

Figure 14. Schematic representation of direct extrusion 3D printing of alginate bioinks in a crosslinker bath. Reprinted with permission from ref[177]. Copyright 2020 Royal Society of Chemistry.

2.4.5 Extrusion in supporting bath

Direct printing in a supporting bath was first proposed by Hinton et al. The approach is called the freeform reversible embedding of suspended hydrogels (FRESH) method[181]. With this printing technique, low-viscosity bioinks can be printed, as the support bath assists in maintaining shape fidelity during the printing process. The support bath contains gelatin slurry, which acts as Bingham plastic (a solid at low shear stress but flows as a viscous fluid at high shear stress). This plastic-like rheological behavior provides mild resistance against the nozzle as it moves through the bath while supporting the extruded precursor in place[182]. The FRESH method supports a broad range of bioinks and cells for advanced biofabrication because it provides successful complex constructs that were previously impossible to achieve[182]. In 2019, parts of the human heart were 3D printed from collagen precursor using the FRESH method (Figure 15)[183].

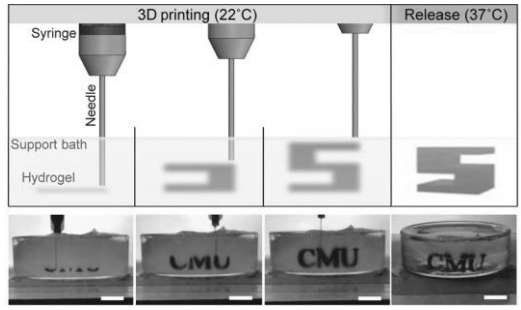

Figure 15. The FRESH printing method is performed by directly printing a liquid precursor in a supporting bath (made from gelatin microparticles). Reprinted with permission from ref [181]. Copyright 2015 Science Advances.

2.5 Biomaterial ink properties and their characterizations

2.5.1 Flow behavior of precursor

Hydrogel precursors usually exhibit Newtonian fluid behavior, as the viscosity (η) remains constant, even at a higher shear rate (γ) or shear stress (τ)[8]. In other words, the viscosity of these fluids does not change when the force is applied. This liquid-like behavior of the precursor is often found at low concentrations and low polymer molecular weight[184]. These precursors are often used in preparing bulk hydrogels

with a mold or by pipetting because, with these techniques, the viscosity does not affect the end result[54]. However, most precursors used in direct extrusion printing behave as non-Newtonian fluids, which means that the viscosity is highly affected by the shear rate and shear stress[185]. Non-Newtonian behavior is caused by the disorientation of polymer chains due to the applied external force, such as flow. This is the main property of a printable precursor, aka bioink[52]. In extrusion-based 3D bioprinting, the flow behavior of bioink greatly impacts processability. At rest, a bioink is present in a viscoelastic state, after which it undergoes a change in viscosity at a higher shear rate while being extruded through the nozzle as a fiber, and ultimately reaches a new resting state. However, using high-viscosity bioinks may lead to high shear stress during extrusion, which can kill the cells in the bioink[166]. The series of rheological characterizations of bioinks, including shear-thinning, yield stress, and thixotropy, is important to ensure the successful printing of 3D constructs (Figure 16).

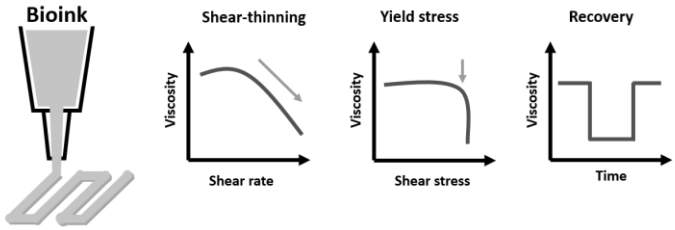

Figure 16. The series of flow behavior of bioinks: Shear-thinning, yield stress and recovery behaviors.

Shear-thinning is a time-independent non-Newtonian fluid behavior, where the external force, such as shear rate and shear stress, highly affect the viscosity[186]. This property is important for polymers used in the extrusion process, including 3D printing[185]. For a bioink in extrusion-based 3D bioprinting, shear-thinning is an important property because it provides high printability and shape fidelity for the ink while maintaining high cell viability due to the low extrusion force during the printing process[52]. Shear-thinning properties are commonly found in polymers with high concentrations and high molecular weight[187]. For instance, in polymer solutions with very high concentrations, the critical shear rate may not be apparent. The transition of decreasing viscosity as a function of shear rate may occur gradually rather than instantly. As shown in Figure 17, increasing concentration also causes a faster decrease in viscosity as the shear rate increases. The molecular weight (Mw) of the polymer, as well as Mw distribution, can also influence the shear-thinning behavior. In polymers with a broad Mw, the critical shear rate and shear-thinning behavior are also not clearly seen compared to polymers with a narrow Mw distribution[188]. A low-

viscosity bioink is often a partially crosslinked precursor, as the polymer chain of bioink is rearranged in the direction of the flow. The simple flow model to determine the shear-thinning behavior of bioink is the Power law model (Figure 18), where shear stress (τ) is related to the shear rate (γ) by the flow behavior index (n) and consistency index (K), which is the zero viscosity at the lowest shear rate (0.01 s^{-1})[189]. The Power law model, also referred to as the Ostwald de Waele relationship, is utilized to fit non-Newtonian data in the range shear rates where the Newtonian plateau is not present in this slope region[190]. In this model, if the n value is equal to 1, the ink behaves like a Newtonian fluid, whereas if the n value is lower than 1, the ink is progressively more non-Newtonian[10]. The Power law model is useful and easy to use for bioink development, in which the shear rate value can mimic the printing pressure under real printing conditions. For instance, Paxton et al. demonstrated that a shear-thinning bioink was formed into a smooth filament and was able to stack layer-by-layer into a 3D construct. Furthermore, the Power law model was applied to confirm the shear-thinning behavior of this bioink[10].

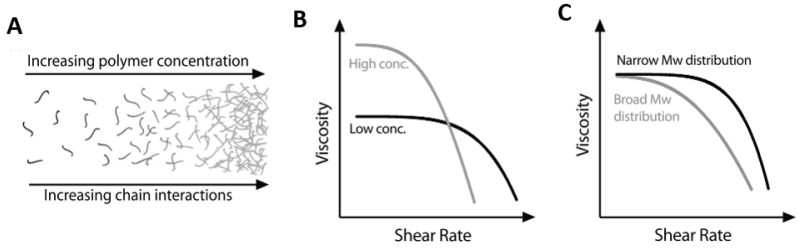

Figure 17. Effects of the polymer concentration on (A) chain interactions and (B) viscosity-shear rate curves. (C) Effect of molecular weight distribution on shear-thinning behavior. Reprinted with permission from ref [188]. Copyright 2021 AIP.

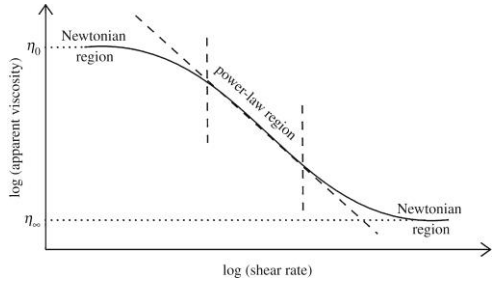

Figure 18. Qualitative representation of flow curve for shear-thinning polymer solution. Reprinted with permission from ref[189]. Copyright 2020 The Royal Society.

In general, shear-thinning bioinks also exhibit another unique behavior called yield stress, which significantly impacts the flow behavior. The yield stress is the minimum shear stress required to initiate the flow. The shear-thinning bioink behaves like a solid at rest; if shear stress is applied and reaches the yield stress point, the viscosity of the bioink starts to decrease, assuming good printability[10]. The ink exhibiting yield stress will remain solid-like and maintain the shape after extrusion due to the resistance of deformation[191]. The benefit of the material with a yield stress is shown in Figure 19, in which a precursor solution without yield stress cannot hold its shape after placement, compared to a hydrogel precursor solution with a yield stress[8]. In bioprinting, the ink can protect the cells from high shear force during extrusion by exhibiting plug flow in the center of the flow profile; thus, shearing is confined to a narrow region along the walls[192]. However, high yield stress can cause difficulty in handling and a high printing pressure is required to extrude the ink from the nozzle, which can damage the cells[193]. Malda et al. reported that the yield stress could be beneficial for a bioink, as it could stabilize the 3D structure and prevent sedimentation of the cells. In addition, Malda et al. discussed the relevance of high viscosity and yield stress in injecting and printing and concluded that the yield stress had more impact on processability, as it could prevent deformation, while high viscosity only delays the deformation of the bioink[122]. Townsend et al. reported that yield stress values above 100 Pa are recommended for 3D bioprinting to achieve a high print fidelity[8]. Although bioinks with less than 100 Pa could be printable, the 100 Pa is the setpoint to support layer stacking. Another flow model for printability evaluation is the Herschel–Bulkley model. It is often used to determine the yield stress values. The Herschel–Bulkley model is similar to the Power Law model with an additional term (τ_0) for the yield stress[8]. The Herschel–Bulkley model was first introduced by Winslow Herschel and Ronald Bulkley in 1926 and provided a simple and general model to explain the behavior of a non-Newtonian fluid. It can also predict the behavior of non-Newtonian fluids exhibiting shear-thinning and yield stress[8,10].

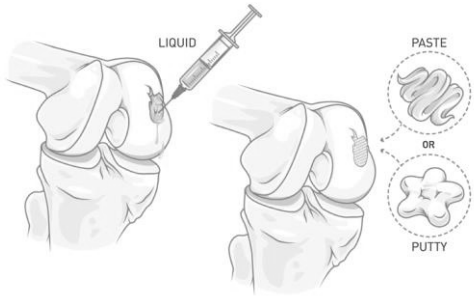

Figure 19. Illustration of the importance of materials with a yield stress, as it allows the placement of the material on the defect site. (Left) Precursor materials without yield stress lack shape fidelity, compared to (Right) precursor materials exhibiting desirable paste and putty behavior. Reprinted with permission from ref [8]. Copyright 2019 Elsevier.

Shear-thinning behavior and yield stress are essential to ensure printability and shape fidelity in extrusion-based 3D bioprinting. However, the bioink's ability to return to its original viscosity after extrusion is also vital in achieving high-resolution bioprinting[13]. Thixotropy or recovery behavior is a time-dependent shear-thinning behavior, which causes the ink to exhibit low viscosity during printing and recover its original viscosity after printing[194]. The recovery time after extrusion through the nozzle must be fast to ensure good shape fidelity. A material with a slow recovery rate may encounter difficulties during the placement, as the material would not adequately retain its position within the defect site. In terms of injectable hydrogels, a short recovery time after injection is necessary for gel manipulation or shaping. Townsend et al. reported that the viscosity should recover more than 85% of the original viscosity within a few seconds after extrusion[8]. In a study by Abouzeid et al., the initial and final viscosities of various nanocellulose-alginate blends were measured after the shear rate of 1000 s^{-1} for 100 s was applied, and the results demonstrated that the best shape fidelity was in the blends that also had the highest viscosity recovery percent[195]. Paxton et al. mitigated a slow bioink recovery using chemical crosslinking agents to crosslink the printed construct between layers[10]. Although a bioink exhibits a short recovery time, it must also have the ability to resist external force, such as the weight of the stacked layers, which might lead to structural deformation and poor shape fidelity[8].

2.5.2 Viscoelastic properties of hydrogel

Hydrogels are viscoelastic, which means that they exhibit both viscous and elastic behaviors. The storage modulus (G') represents the stored energy within a material when subjected to a force, indicating its elastic behavior. On the other hand, the loss modulus (G") measures the energy dissipated by the material when a force is applied, reflecting its viscous behavior. The loss tangent, denoted as tan δ, is the ratio of the loss modulus (G") to the storage modulus (G') and provides insights into the balance between these two behaviors in the material.[196]. The tan δ value represents the relationship between the viscous and elastic behaviors of the material. When the tan δ value is lower than 1, the material behaves more elastic, when the tan delta value is more than 1, the material behaves more viscous. The tan δ value is often used to observe the point of sol-gel transition or gelation kinetics of the hydrogel and the point at which the hydrogel starts to deform under shear force. Typically, these values are determined within the linear viscoelastic region (LVR) via an amplitude sweep in oscillatory measurements, in which the frequency is constant and the strain is increased[13,196]. In bioprinting, the concentration and functionalization degree of the bioink influence the rheological parameters of the printed hydrogel structure, including shape fidelity, structural integrity, stability, viscoelasticity, and gelation kinetics[117,122].

Several studies have explained the relationship between viscoelasticity and structural integrity. Diamantides et al. conducted a study by comparing the rheological properties to the shape fidelity of their collagen-based bioinks, including G' pre-and post-photocrosslinking, crosslinking rate, and exposure time. They found that within the range of testing conditions, the G' value was the best indication of structural integrity[197]. In addition, O'Connell et al. measured G' and gelation time by varying the UV intensities and polymer concentrations to estimate the crosslinking rate of GelMA[1,198]. Gao et al. showed a direct relationship between tan δ and the structural integrity of printed structures by comparing the height of a 5-layer tubular structure printed from different ink formulations (gelatin-alginate)[16].

3 AIMS

The overall aim of my thesis is to develop photocrosslinkable hydrogel precursors with excellent shear-thinning profiles by utilizing various noncovalent chemical interactions for pre-crosslinking. The hypothesis is that each pre-crosslinking technique will improve the printability of natural polymer-based biomaterial inks for extrusion-based 3D bioprinting. The investigated pre-crosslinking techniques comprise thermal crosslinking, ionic interactions, metal coordination and hydrogen bonding. The post-crosslinking with UV light will provide the final shape fidelity and stability to the printed structure. I also hypothesize that the interpenetrating network (IPN) in hydrogels via a dual-crosslinking approach (noncovalent and covalent crosslinking) will significantly enhance the viscoelasticity, structural integrity and stability of 3D printed constructs. The steps for biomaterial ink printability assessment are addressed in this thesis through an evaluation process illustrated in Figure 20. In addition, the study also compares the mechanical properties of hydrogels formed via a single crosslinking mechanism and dual crosslinking.

In order to accomplish the overall goal, the following steps are defined as follows:

1. The photocrosslinkable precursors: GelMA, ColMA, HAMA, AlgMA, and GGMA are synthesized through methacrylation chemistry (**Publications I–IV**). The grafting of gallic acid on GelMA and HA (**Publications III & IV**) is achieved to enhance the tunability of GelMAGA and HAGA precursors.

2. The precursor formulations are optimized by tuning the polymer concentration and degree of functionalization. The optimized precursors are later pre-crosslinked by using various noncovalent chemistry interactions, including thermal crosslinking (**Publication I**), ionic interactions (**Publication II**), metal coordination (**Publication III**), and hydrogen bonding (**Publication IV**) to turn unprintable precursors into biomaterial inks.

3. A method for screening the precursor printability is developed in this thesis. The precursors are pre-screened to obtain the best biomaterial ink candidates through stepwise characterizations: fiber formation, stackability and rheological profiles (**Publications I–IV**). The series of rheological characterizations for precursors are based on flow behavior determination: viscosity, shear-thinning, yield stress and recovery behavior. The photocrosslinking parameters, including UV light intensity and exposure time (**Publication I**), are optimized to ensure the structural integrity of the hydrogel constructs.

4. The printing parameters are optimized to achieve the 3D printed constructs. The study focuses on the quantitative measurement of the printability of biomaterial inks from the printed grid structures (**Publications II–IV**).

5. The physical attributes of dual-crosslinked hydrogel constructs are characterized: viscoelastic properties, structural integrity and swelling behavior (**Publications II–IV**).

4 MATERIALS AND METHODS

4.1 Materials

Hyaluronic acid (100 kDa in molecular weight) was purchased from Lifecore Biomedical, USA. Bovine dermal collagen type I solution (PureCol, 3.0 mg/mL in 0.01 M HCl) was purchased from Advanced BioMatrix, USA. Sodium alginate, gelatin type A (300 bloom strength, porcine skin), low acyl gellan gum (Gelzan), methacrylic anhydride, gallic acid (3,4,5-trihydroxybenzoic acid), 1-ethyl-3- (3-dimethylaminopropyl)-carbodiimide hydrochloride (EDC), 1- hydroxybenzotriazole hydrate (HOBt), calcium chloride ($CaCl_2$), iron(III) chloride ($FeCl_3$) and cell culture media (Dulbecco's Modified Eagle's medium, DMEM), trinitrobenzene sulfonic acid (TNBS), deuterium oxide (D_2O) and 2-hydroxy-4'-(2- hydroxyethoxy)-2-methylpropiophenone (Irgacure 2959) were purchased from Merck KGaA, Darmstadt, Germany. Dialysis membranes with a molecular weight cutoff (MWCO) of 3.5 and 14 kDa were purchased from Spectra/Por, Repligen Corp., USA. DI water (deionized water, Miele Aqua Purificator G 7795, Siemens) and u.p. water (ultra-pure, Sartorius Arium Mini, 0.055 μS/cm) were used in the synthesis and dialysis. Dulbecco's phosphate-buffered saline (DPBS) was prepared in the laboratory. All solvents were of analytical quality. Nivea Crème (Beiersdorf Global AG, Germany) was used as a control printing material.

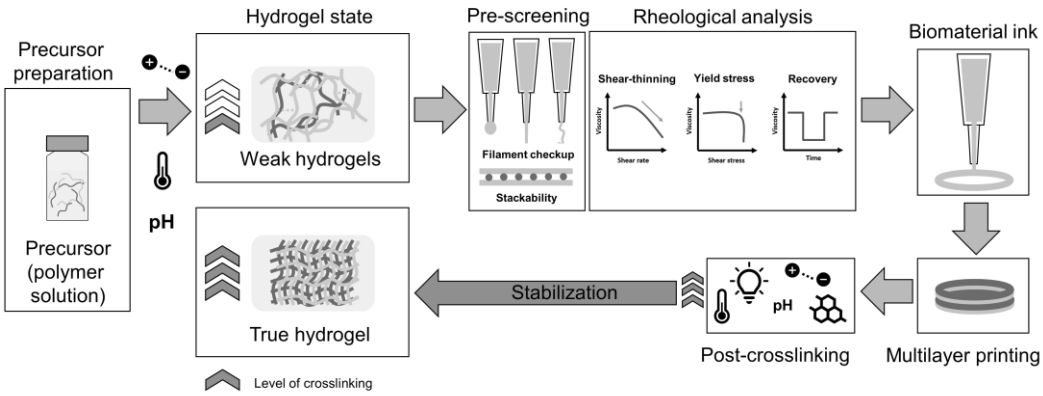

Figure 20. The flow chart demonstrates the process of biomaterial ink evaluation through the definitions of precursor, weak hydrogel, true hydrogel, and biomaterial ink. (precursor → weak hydrogel → biomaterial ink → true hydrogel). Precursor = polymer solution or pre-hydrogel solution without crosslinking. Weak hydrogel = weakly crosslinked hydrogel (extrudable). Biomaterial ink = printable precursor (weak hydrogel) or precursor candidate for 3D bioprinting that has been screened for printability through stepwise evaluation steps: precursor preparation, pre-crosslinking, pre-screening for printability (filament formation and stackability), rheological analysis (degree of shear-thinning, yield stress and recovery behavior), 3D printing (multilayer printing) and post-crosslinking (stabilization). True hydrogel = crosslinked hydrogels with mechanically stable to maintain the structural integrity after printing

4.2 Synthesis of precursors

4.2.1 Methacrylation of precursors

HA, Alg and GG were functionalized with methacrylate anhydride through hydroxyl groups to obtain HAMA, AlgMA and GGMA, respectively (Figure 21 & 22, Table 1). The detailed descriptions are shown in **Publications I, II & IV**. The methacrylic anhydride was added dropwise into the system in an amount corresponding to the desired modification for each material. Afterwards, the reaction mixture was dialyzed with a 3.5 kDa molecular-weight-cutoff (MWCO) membrane against deionized water for 72 h (2 × 2 L, 12 h) at RT. Thereafter, the solution was lyophilized to obtain a white and fluffy final product. The degree of methacrylation was quantified using ^{1}H-NMR.

The gelatin and collagen were modified through a methacryloyl reaction involving free amine and hydroxyl groups (Figure 21, Table 1). The detailed descriptions are shown in **Publications I & III**. The methacrylic anhydride was added dropwise into the system in an amount corresponding to the desired modification for each material. After that, the reaction mixture was dialyzed with a 14 kDa MWCO membrane against deionized water for 72 h (2 × 2 L, 12 h) at 37 °C. Thereafter, the solution was lyophilized, and the GelMA and ColMA product was obtained. The degree of modification of gelatin and collagen after methacrylation was determined using TNBS assay.

4.2.2 Gallic acid-functionalized precursors

GelMA was grafted with gallic acid (GA) using a previously reported method (**Publication III**) (Figure 23, Table 1). The synthesis of methacryloyl gelatin-GA involved a carbodiimide coupling reaction using EDC. The excess GA and EDC were removed through dialysis using a 3.5 kDa MWCO in 1 M NaCl solution at pH 5.3, carried out at 4 °C for 3 d. This was followed by dialysis against deionized water for 24 h. The resulting solution was then freeze-dried. The degree of GA functionalization was characterized using UV spectra.

HA and GGMA were functionalized with gallic acid hydrazide via EDC coupling reaction (HAGA and GGMAGA). The details of synthesis (HAGA and GA hydrazide) and characterizations are shown in **Publication IV**. For the 10% and 20% GA modification, EDC was added, corresponding to the desired degree of modification. The reaction mixture was then dialyzed against a dilute HCl solution (pH = 3.5) containing 100 mM sodium chloride (NaCl) (6 × 2 L, 48 h) and subsequently dialyzed against deionized water (4 × 2 L, 24 h). The resulting solution was freeze-dried to obtain a white solid fluffy material. The conjugation of gallic acid and the degree of gallic acid modification in hyaluronic acid was confirmed by the presence of characteristic aromatic peaks at 6.98 and 6.93 ppm in the ^{1}H nuclear magnetic resonance (NMR) spectrum.

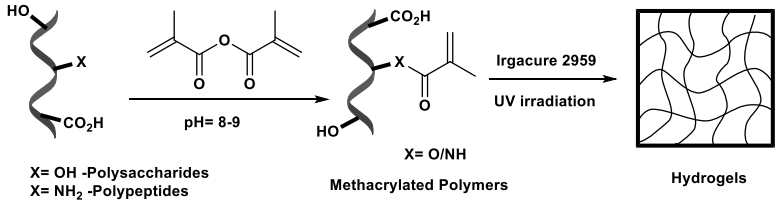

Figure 21. Methacrylation of polysaccharides/polypeptides and formation of photocrosslinked hydrogels.

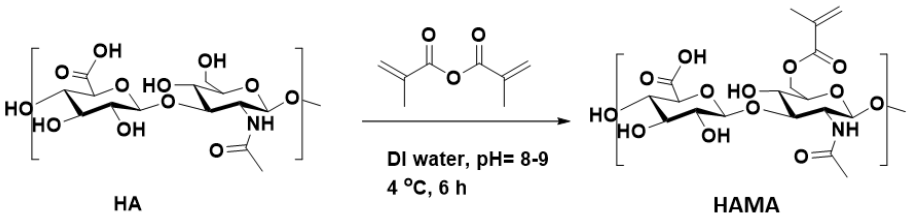

Figure 22. Synthesis of hyaluronic acid methacrylate (HAMA).

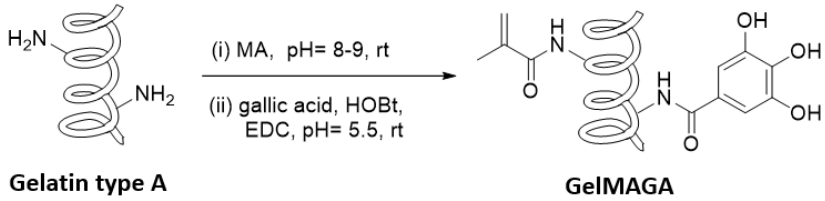

Figure 23. The synthesis of GelMAGA biomaterial inks.

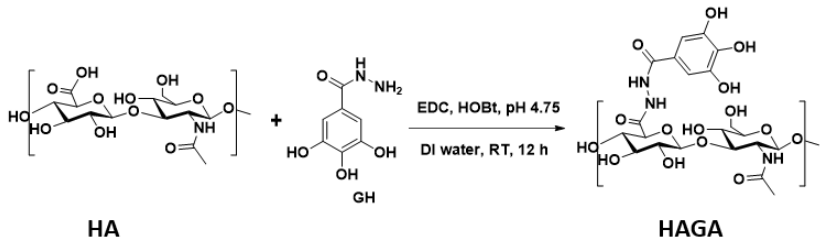

Figure 24. Synthesis of gallic acid conjugated hyaluronic acid (HAGA).

Table 1. The percentage of methacrylate anhydride (MA%) and gallic acid (GA%) functionalization is indicated by the number in the name. Polymer concentration is expressed in weight by volume (%).

Precursor code	Polymer	MA [%]	GA [%]	Polymer concentration [%w/v]	#
HAMA15	Hyaluronic acid	15	0	5	**IV**
HAMA30	Hyaluronic acid	30	0	5	**I**
HAMA60	Hyaluronic acid	60	0	5	**I**
HAGA10	Hyaluronic acid	0	10	5	**IV**
HAGA20	Hyaluronic acid	0	20	5	**IV**
AlgMA30	Alginate	30	0	5	**I**
AlgMA60	Alginate	60	0	5	**I**
1% GGMA15	Gellan gum	15	0	1	**II**
2% GGMA15	Gellan gum	15	0	2	**II**
3% GGMA15	Gellan gum	15	0	3	**II**
GGMA15GA	Gellan gum	15	15	2	**-**
GelMA30	Gelatin	30	0	5	**I**
GelMA60	Gelatin	60	0	5	**I, III**
GelMA30GA	Gelatin	30	15	5	**III**
GelMA60GA	Gelatin	60	15	5	**III**
ColMA30	Collagen	30	0	5	**I**
ColMA60	Collagen	60	0	5	**I**

4.2.3 Characterization of functionalized precursors

For HAMA, HAGA, AlgMA, GGMA and GGMA-GA, The NMR spectra were recorded using a Varian Mercury 300 MHz spectrometer. The sample concentrations were prepared at 0.8% w/v, using D_2O as a solvent. For GelMA, GelMAGA and ColMA, the modification degree was characterized by TNBS assay. Spectrophotometric analysis was recorded using UV spectroscopy (UV-3600 Plus, Shimadzu Corp., Japan) at a wavelength of 350–500 nm. The modification degree was calculated by estimating the number of free amines before and after methacrylation. The number of free amine groups in gelatin and collagen was determined by using a calibration curve of the glycine standard.

4.3 Pre-processing

4.3.1 Preparation of precursors

All precursors used in the study are listed in Table 1. The precursors HAMA30, HAMA60, AlgMA30, AlgMA60, GelMA30, GelMA60, ColMA30 and ColMA60 for **Publication I** were prepared at a concentration of 5% w/v in DPBS at 37 °C. The pH of the precursors was adjusted to 7.5 to gain proper viscosity.
In **Publication II**, GGMA with different concentrations (1, 2 and 3% w/v) was investigated at RT. The pH of the precursors was adjusted to 7.5 to gain proper viscosity, and they were dissolved at 37 °C.
For **Publication III**, GelMA30GA and GelMA60GA precursors were prepared at a concentration of 5% w/v in DPBS at 37 °C. The pH of precursors was adjusted to 7.5 to gain proper viscosity.
For **Publication IV**, the precursor formulations were prepared at 37 °C by mixing HAMA (5% w/v) and HAGA (5% w/v) in a ratio of 1:1 and the pH was adjusted into the range of basic, neutral and acidic.
GGMA and GGMA-GA were prepared at a concentration of 3% w/v at 37 °C. The pH of precursors was adjusted to 7.5 to gain proper viscosity.
In all **Publications I–IV**, the photoinitiator, Irgacure 2959, was used at the same concentration (0.5% w/v) in all precursor formulations.

4.3.2 Gelation time of photocrosslinkable precursors

The gelation kinetics of the precursors was measured via a rotational rheometer (Discovery HR-2, TA Instruments Inc., USA) at RT as a function of time (for 500 s, the UV lamp was activated at 100 s) while strain and frequency were kept constant at 1% and 1 Hz, respectively. UV lamp (BlueWave 50 UV curing spot lamp, DYMAX Corp., USA) was used for photorheology.

4.3.3 Pre-crosslinking approaches (precursors to biomaterial inks)

In **Publication I**, the temperature of GelMA30 and GelMA60 precursors was lowered to 16 °C to observe the change in viscosity (Table 2). The viscosity of the precursors was observed as a function of the temperature (4–37 °C).

In **Publication II**, GGMA precursors with different formulations were prepared by incorporating different concentrations of $CaCl_2$ (0, 22.5, 45, and 90 mM) for ionic pre-crosslinking (as shown in Table 2). The pH of all GGMA precursors was adjusted to 7.5 to achieve the desired viscosity. The tested formulations included $GGMA_{\_4°C}$ (GGMA at 4 °C), $GGMA_{\_22.5mM}$ (GGMA with 22.5 mM $CaCl_2$), $GGMA_{\_45mM}$ (GGMA with 45 mM $CaCl_2$), and $GGMA_{\_90mM}$ (GGMA with 90 mM $CaCl_2$).

In **Publication III** (Table 2), the precursor formulations were investigated: GelMA, GelMAGA, and GelMAGA with a pre-crosslinker ($FeCl_3$). Gelatin methacryloyl with 30% and 60% degree modifications were denoted as GelMA30 and GelMA60, respectively. GelMA30 and GelMA60 functionalized with gallic acid, were referred to as GelMA30GA and GelMA60GA. Additionally, GelMA30GA and GelMA60GA with $FeCl_3$ were named GelMA30GA-xFe and GelMA60GA-xFe, where "x" represented the concentration of $FeCl_3$ (2.5 corresponding to 15 mM and 5 corresponding to 30 mM).

In **Publication IV**, the pH of all HAMA-HAGA precursor formulations was slowly adjusted using NaOH (0.5 M) and varied into acidic (pH = 4, 5), neutral (pH = 7), and basic (pH = 8, 9) pH values (Table 2).

The GGMA and GGMA-GA precursors (Table 2) were pre-crosslinked with UV light at an intensity of 10 mW/cm^2 for 30 s at 37 °C, and then the precursor was loaded into the cartridge. The pH of the precursors was set at 7.5 to gain the proper viscosity.

Table 2. Biomaterial ink compositions with different pre-crosslinkers, including temperature, $CaCl_2$, $FeCl_3$, pH level and UV light. The ink code denotes the polymer type, concentration, percentage of functionalization, and pre-crosslinking. The bold font indicated the pre-crosslinker condition.

Ink code	Temp. [°C]	$CaCl_2$ [mM]	$FeCl_3$ [mM]	pH level	UV light [mW/cm^2]
1% GGMA15	**4**	0	0	Neutral	0
2% GGMA15	**4**	0	0	Neutral	0
3% GGMA15	**4**	0	0	Neutral	0
1% GGMA15-22.5mM	RT	**22.5**	0	Neutral	0
2% GGMA15-45mM	RT	**45**	0	Neutral	0
3% GGMA15-90mM	RT	**90**	0	Neutral	0
GGMA15GA	RT	0	0	Neutral	**10**
HAGA10-HAMA15	RT	0	0	Acidic	0
HAGA10-HAMA15	RT	0	0	Neutral	0
HAGA10-HAMA15	RT	0	0	**Basic**	0
HAGA20-HAMA15	RT	0	0	Acidic	0
HAGA20-HAMA15	RT	0	0	Neutral	0
HAGA20-HAMA15	RT	0	0	**Basic**	0
GelMA30	RT	0	0	Neutral	0
GelMA60	RT	0	0	Neutral	0
GelMA60*	**16**	0	0	Neutral	0
GelMA30GA	RT	0	0	Neutral	0
GelMA60GA	RT	0	0	Neutral	0
GelMA30GA-2.5Fe	RT/37 °C	0	**15**	Neutral	0
GelMA30GA-5Fe	RT/37 °C	0	**30**	Neutral	0
GelMA60GA-2.5Fe	RT/37 °C	0	**15**	Neutral	0
GelMA60GA-5Fe	RT/37 °C	0	**30**	Neutral	0
ColMA30	RT	0	0	Neutral	0
ColMA60	RT	0	0	Neutral	0

4.4 Pre-evaluation of printability

In this study, the precursor is defined as a hydrogel solution pre-screened for its injectability and printability.

4.4.1 Filament classification

A series of pre-screening and filament classification tests were performed in **Publications I–IV**. The pre-crosslinked precursor was transferred into a 1 mL syringe capped with a printing nozzle. 250 μm of steel nozzles (Optimum General-

Purpose Stainless-Steel Tips) were used in **Publication I**. UV-shielded tapered nozzles (200 μm, SmoothFlow™) were used in **Publications I & II**. Steel nozzles (410 μm) were used in **Publication IV**. All nozzles were purchased from Nordson EFD, USA. To maintain a consistent temperature, the syringe was positioned vertically and secured with a clamp. This setup prevented temperature fluctuations during the experiment. The precursor material was then manually extruded by applying pressure to the syringe plunger. The filament quality was classified based on the ability of the precursor to form a smooth filament after being extruded from the nozzle. The filament formation of the precursors was observed using a contact angle camera (Theta Lite, CMOS 1/2" USB 3.0 digital camera with fixed zoom, a resolution of 1280 × 1024 pixels, Biolin Scientific, Sweden), and a video was recorded. The filament was deposited as a grid structure on the glass surface to investigate its layer-stacking performance. The precursor compositions were selected for 3D printing based on filament characteristics (undergelated, smooth and overgelated filaments). As shown in Figure 25, the undergelated filament, forming a droplet, indicates an unprintable precursor, whereas a smooth filament indicates a printable precursor and has a high potential as a biomaterial ink candidate. The overgelated filament exhibited ununiformed and irregular filament, which is not recommended for 3D printing.

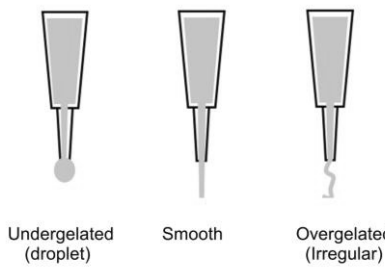

Figure 25. The illustration of three filament conditions observed during the pre-screening test for 3D bioprinting. The droplet filament indicates that the extruded filament is too liquid. The smooth filament indicated that the extruded filament exhibits smooth and uniform filament. The irregular filament indicates overgelation condition of the extruded filament, exhibiting ununiformed and fractured filament after being extruded from the nozzle.

4.4.2 Flow behavior

The flow behavior of the precursors in **Publications I–IV** was measured on a rotational rheometer in parallel plate geometry (12 mm plate, 2.5 mm gap size). For the temperature-dependent behavior of the precursors in **Publications I & II**, the measurement was conducted in flow mode (temperature sweep, 4–37 °C) with a constant shear rate (0.01 s^{-1}). The results were plotted as viscosity as a function of the temperature graph.

In the flow mode, viscosity, yield stress, shear-thinning, and recovery behavior were evaluated. The determination of yield stress involved analyzing the shear rate-shear stress curve, from which the yield point was identified as the intersection point on the Y-axis when the shear rate was nearly zero. This specific point indicated the onset of material flow. Shear-thinning behavior was examined by varying the shear rate from 0.01 to 800 s^{-1}. Recovery behavior measurements were performed to evaluate the material's ability to recover, involving the application of a low shear rate of 0.01 s^{-1} for 200 s, followed by a high shear rate of 500 s^{-1} for 100 s, and finally, a low shear rate of 0.01 s^{-1} for 200 s.

Power law regression analysis was employed to confirm the shear-thinning properties of the materials. This analysis involved fitting a Power law equation to the linear region of the viscosity-shear rate plots (Figure 18), calculated using Equation 1.

$$\eta = K\gamma^{n-1}, \quad (1)$$

The flow behavior index, denoted as "n", is a parameter that characterizes the shear-thinning ability of a material. A value of n equal to 1 indicates Newtonian behavior, where the viscosity remains constant regardless of the shear rate. If the value of n is greater than 0.6, the material exhibits weak shear-thinning behavior. On the other hand, if the value of n is less than or equal to 0.2, the material possesses strong shear-thinning properties, which are highly desirable for excellent printability.

In **Publication IV**, the viscosity of the highly pre-crosslinked precursors was obtained from the Cox-Merz rule (Equation 2), transformed from the oscillatory measurement (frequency sweep, 0.1–500 rad/s, constant strain 1%).

$$|\eta^*(\omega, rad/s)| = |\eta\,(\gamma, s^{-1})|_{,(\gamma)=(\omega)}\,, \quad (2)$$

The Cox-Merz Rule explains the relationship between the shear viscosity (η) and complex viscosity (η^*) from oscillatory measurement, describing the correspondence between the shear viscosity, η, against shear rate, γ, and the complex viscosity (η^*) from the oscillatory measurement of frequency sweep (angular frequency, ω). The yield stress values were obtained from the yield stress-shear rate plot, where the shear stress starts to deviate from the origin (Y-axis) and exhibits an increase. The calculation of yield stress was based on the Herschel-Bulkley model, which is a rheological model specifically employed to describe non-Newtonian fluids. By fitting the data to this model, the yield stress value is quantified, providing insight into the resistance of the material to flow and its ability to maintain its structural integrity. (Equation 3).

$$\tau = \tau_0 + K\gamma^n, \quad (3)$$

where τ represents the shear stress measured on the inks, and τ_0 refers to the yield stress. The yield point indicates the point at which the ink starts to flow under the applied shear stress. It represents the minimum stress required to initiate flow in the precursor.

The gelation or crosslinking time was determined using an *in situ* polymerization method. This involved employing a rotational rheometer and an external UV lamp emitting light at a wavelength of 365 nm and UV intensity of 25 mW/cm^2. The gelation/crosslinking process was monitored in real-time using the rheometer, allowing the measurement of the time for the ink to undergo polymerization and form a true hydrogel.

4.5 Processing (3D printing)

The term "biomaterial ink" or ink was used for the screened precursor(s)/or precursor formulation(s) that exhibited high shear-thinning behavior and were assumed to be printable with an extrusion-based 3D bioprinter (BRINTER® ONE 3D bioprinter, Brinter Ltd., Finland). CAD models were drawn with AutoDesk Fusion 360 software.

4.5.1 Printability window

After the ideal printable biomaterial ink composition and printing settings were determined, the evaluation of structural integrity was conducted. The shape and stackability of the printed filament were key parameters. These parameters ensure the success of the printing process and contribute to achieving a high printing resolution. The overall quality and reliability of the printed structures can be assessed by evaluating the shape and stackability of the printed filament. Pre-screened biomaterial ink formulations were loaded into a 10 mL cartridge and transferred to an incubator (37 °C) for 30 min to remove any air bubbles. Next, the cartridge (Optimum® syringe barrels, Nordson EFD, USA) was installed into a 3D bioprinting platform by capping it with a printing nozzle (200 μm for **Publications II–III** and 410 μm for **Publication IV**). The printing was conducted using a pneumatically operated Pneuma Tool print head. To determine the printability window, lines were printed at various pressures and printing speeds. The printability window was achieved by printing lines with different pressures and printing speeds. For example, in **Publication IV**, the extrusion pressure ranged between 2000–3000 mbar, and the printing speed was set to 4, 6 or 8 mm/s. The filament widths were recorded and analyzed using image processing software (Fiji-ImageJ) to obtain accurate measurements. The printability of the filaments was assessed by comparing their widths to the size of the nozzle. To achieve an optimal 3D construct, the lag time for pre-flow and post-flow was calculated to determine the appropriate delays before and after the ink deposition. The flow behavior of the inks exhibited a noticeable delay following the application of pressure and during the transition between printing layers. This delay resulted in the deformation and collapse of the structure after fiber deposition in subsequent layers.

4.5.2 Pr value

Biomaterial inks exhibiting optimal rheological characteristics, such as shear-thinning and recovery behavior, result in the formation of cohesive filaments that can be stacked without merging. Despite sufficient printability results being achieved in both rheological and quantitative printability assessments, certain precursor candidates cannot deliver a successful 3D-printed construct. A quantitative approach was utilized to assess the shape of the printed pores, employing Equation 4 for this analysis.

$$Pr = \frac{\pi}{4} \cdot \frac{1}{C} = \frac{L^2}{16A}, \quad (4)$$

The circularity of the enclosed pore (C) is calculated based on the perimeter (L) and pore area (A) using Equation 4. The printability (Pr) of the biomaterial inks is determined by examining the geometry of the pores within a grid structure. A Pr value of 1 signifies a perfectly square shape. A Computer-Aided Design (CAD) model of the square grids measuring 20 × 20 × 0.4 mm^3 was created using Autodesk Fusion 360 software. This model served as the established standard for the evaluation process. The optimized conditioned inks demonstrate the capability to generate smooth and uniform filaments of consistent width, effectively stacking to form a cohesive 3D structure. This ultimately results in the creation of square pores within the fabricated construct, achieving a Pr value of 1, signifying a perfect square shape (Figure 26). On the other hand, inadequately conditioned inks manifest as either having a liquid-like appearance or producing filaments with irregular shapes. This leads to Pr values that are lower than 1 or higher than 1, signifying deviations from the desired perfect square shape. Excessive pre-crosslinking leads to a higher Pr value. A lower Pr value serves as a clear indicator of insufficient pre-crosslinking. To ascertain the Pr value for each ink across different printing parameter combinations, optical images of the printed constructs were meticulously analyzed using ImageJ software. This analysis involved measuring the circularity of the pores (n=5).

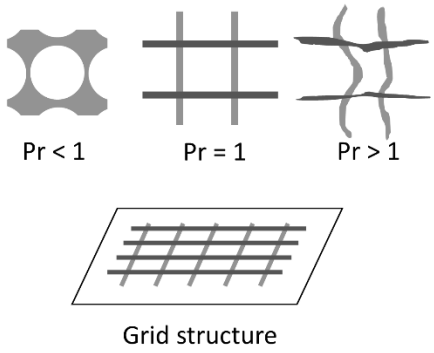

Figure 26. Pore geometry evaluation and calculation of the printability (Pr) value. The ideal outcome is characterized by Pr = 1, signifying perfectly square-shaped pores.

4.6 Post-processing

4.6.1 Accuracy and structural integrity

The structural integrity was then evaluated after achieving the best printable biomaterial ink formulation and optimal printing parameters. Nivea Creme (**Publication I**) and Poloxamer (**Publication III**) were chosen as control printing materials because they offer the highest geometric accuracy, which exhibits minimal deviation in comparison to the original CAD model. The ink was printed into cylinders with varying heights (1, 2.5 and 5 mm), while the outer diameters of 10 mm were kept constant. The curing process of each structure was performed in a layer-by-layer fashion using a built-in UV/Vis LED module in the bioprinter. The curing was carried out at a wavelength of 365 nm with an intensity of 25 mW/cm^2 for 10 seconds for each layer. The post-curing step was conducted for 60 seconds after the printing process. An overview of the printing process is illustrated in Figure 27. The dimensions of the cylinders, including the wall height, outer diameter, and inner diameter, were compared to those of the printed control structure to assess the printing accuracy. The deviation or accuracy of the printed cylinders was determined by comparing these measurements. The wall height was measured from the side view, while the outer and inner diameters were measured from a top view. The structural integrity of each 3D printed structure was assessed by determining the ratio between the dimensions of the biomaterial ink cylinders and the control structure. A value of 1 indicated a perfect structure, values less than 1 indicated smaller dimensions than the control, and values more than 1 indicated larger dimensions than the control.

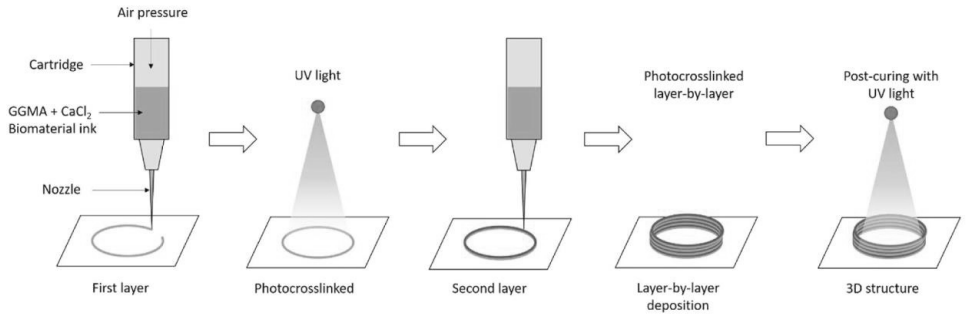

Figure 27. An example of the process flow of extrusion-based 3D bioprinting.

4.6.2 Viscoelastic properties

To assess the viscoelastic properties of the biomaterial inks, oscillatory measurements were performed within the linear viscoelastic region (LVR). An amplitude sweep was conducted, ranging from 0.1% to 100% strain, while maintaining a constant frequency of 1 Hz. In addition, a frequency sweep was performed, varying a frequency range of 0.1 Hz to 100 Hz, with a constant strain of 1%. The biomaterial inks were cast into molds with dimensions of 2.5 mm height and a diameter of 12 mm. Subsequently, the samples were exposed to 365 nm UV light at an intensity of 25 mW/cm^2 for 120 s. During the measurements, each sample was positioned between the 12 mm geometry and the platform, with a gap size of 2.5 mm. The storage modulus (G') and loss modulus (G") were calculated from the slopes obtained during the measurements. The ratio of G" to G', known as tan δ, was then determined to evaluate the viscoelastic properties and plotted as a tan δ-strain curve.

For microstructural analysis, the average mesh size (ξ) and crosslinking density of the hydrogels were determined based on the results obtained from the oscillatory measurements. Specifically, the storage moduli (G') of the hydrogels, which were obtained using the optimal ink formulation, were used. The calculation of the average mesh size (ξ) was performed at a UV exposure time of 120 s, and Equation 5 was used to estimate the average mesh size at different exposure times.

$$(\xi) = \left(\frac{G'N}{RT}\right)^{-1/3}, (5)$$

where G' is the storage modulus of the hydrogel, N is the Avogadro constant (6.023 × 10^{23} mol^{-1}), R is the molar gas constant (8.314 JK^{-1}mol^{-1}), and T is the temperature (298 K).

The hydrogels' crosslinking density (n_e, mol/m^3) was determined by calculating the storage modulus obtained from the linear region of the frequency sweep test curve. The data yields the total count of elastically active junction points within the network per unit volume, as described by Equation 6.

$$n_e = \frac{G_e}{RT}, (6)$$

where G_e is the average value of the storage modulus from the linear region of the oscillatory frequency sweep measurements.

4.6.3 Swelling behavior

The selected biomaterial ink was utilized to 3D print grid structures with dimensions of 10 × 10 × 5 mm^3 and cylindrical shapes. Subsequently, an additional photocrosslinking technique was employed on the printed structures to enhance their stability during incubation. The swelling ratio was calculated as W_s /W_0, where W_s is the equilibrium weight of swollen hydrogels, and W_0 is the weight of hydrogels at a zero time point.

In **Publication II**, cylinders with a height of 1 mm were 3D printed using GGMA ink. For each condition, 2% $GGMA_{\_90mM}$ was used. The printed samples were cured layer-by-layer using 365 nm UV light at an intensity of 25 mW/cm^2. The exposure time for each layer was 10 s, followed by a 60-second post-curing step. The initial weight of the hydrogels at zero time points was recorded as W0. Subsequently, the hydrogels were immersed in either DI water or DMEM until equilibrium was reached, and their weights were measured as W_s. The swelling ratio was calculated at various time points (1, 2, 3, 4, 5, 24, 36, and 48 h) using W_s/W_0.

In **Publication III**, the printed structures were submerged in DPBS solution containing 0.05% w/v of Irgacure 2959. They were then exposed to UV light at an intensity of 10 mW/cm^2 for 5 min. After post-stabilization, the printed samples were transferred to a solution (DI water, DPBS, or DMEM). The hydrogels were maintained at 37 ± 0.5 °C in a shaking incubator at 90 rpm for various times (0, 1, 2, 3, 5, 7 and 15 d). At zero time point, the samples were characterized by a weight denoted as W_0. At each subsequent time point, the samples were extracted from the solution, and any residual solution on the surface was eliminated to acquire the weight labeled asW_s.

In **Publication IV**, the stability of hydrogels under different pH conditions was examined, and all hydrogel samples with and without post-crosslinking were immersed in PBS solution at different pH values (5, 7.5 and 9). The procedure employed was derived from **Publication III**.

5 RESULTS

5.1 Modification of polypeptide and polysaccharide-based precursors

5.1.1 Methacrylation of HA, Alg, GG, Gel and Col

In **Publications I & II & IV**, the degree of modification in HAMA was calculated as the ratio of the N-acetyl peak of hyaluronic acid and olefinic protons from the methacrylate groups (reference peak at 1.9–2.1 and defined MA peak at 5.7–6.2). The degree of methacrylation in AlgMA was calculated using the area under the peak for the anomeric protons in the guluronic unit (reference peak at 4.6–5.2 and defined MA peak at 5.3–6.5). The degree of methacrylation of GGMA was determined by comparing the integrated peaks of specific protons and rhamnose ring. The peak was selected from the methyl group on the rhamnose ring of gellan gum (reference peak at 1.2−1.3 and defined MA peak at 1.90 and 5.7−6.2). In **Publications I & III**, the UV-vis spectra (TNBS assay) showed the absorption peaks of free amine groups in gelatin and collagen at 350–500 nm absorption range. The degree of modification (methacryloyl) of GelMA and ColMA was quantified based on the measurement of free amine and hydroxyl groups in modified gelatin with respect to unmodified gelatin (same as collagen). Table 3 provides an overview of the different precursors with a defined degree of functionalization and the reference peak of each precursor.

5.1.2 Gallic functionalization of GelMA and HA

In **Publication III**, gallic acid modification in GelMA was calculated based on the measurements of free amines in modified gelatin with respect to unmodified gelatin. In **Publication IV**, the spectra of HAGA showed the presence of distinctive peaks of aromatic protons of GA. In addition, the GA conjugation was further confirmed by checking the precursor's color change at the basic conditions (~pH 8). The conjugation of gallic acid and the degree of gallic acid modification in hyaluronic acid

was confirmed by the presence of characteristic aromatic peaks at 6.9−7 ppm in the ^{1}H nuclear magnetic resonance (NMR) spectrum (Table3).

Table 3. Percentage modification of MA and GA in polysaccharide (^{1}H-NMR) and polypeptide (UV-vis)-based precursors

Method	Precursor code	MA [%]	GA [%]	Ref. peak [ppm]	MA peak [ppm]	GA peak [ppm]	Free NH_2 [%]
^{1}H-NMR	HAMA15	17±2	0	1.9−2.1	5.7−6.2	-	-
	HAMA30	32±5	0	1.9−2.1	5.7−6.2	-	-
	HAMA60	59±3	0	1.9−2.1	5.7−6.2	-	-
	HAGA10	0	10±3	1.9−2.1	-	6.9-7	-
	HAGA20	0	20±2	1.9−2.1	-	6.9-7	-
	AlgMA30	35±8	0	4.6−5.2	5.3−6.5	-	-
	AlgMA60	61±6	0	4.6−5.2	5.3−6.5	-	-
	GGMA15	15±1	0	1.2−1.3	1.90, 5.7−6.2	-	-
UV-vis	GelMA30	31±5	0	-	-	-	69±5
	GelMA60	64±5	0	-	-	-	36±5
	GelMA30GA	32±4	16±1	-	-	-	53±4
	GelMA60GA	66±7	15±1	-	-	-	19±7
	ColMA30	37±3	0	-	-	-	63±3
	ColMA60	62±8	0	-	-	-	38±8

5.2 Pre-evaluation of printability

5.2.1 Filament classification and pre-crosslinking approaches

In **Publications I–IV**, pre-evaluation of printability was performed using visual analysis to screen the filament formation and layer stacking capability of precursors under the influence of different pre-crosslinking approaches: temperature (**Publication I**), $CaCl_2$ (**Publication II**), $FeCl_3$ (**Publication III**), pH modulation (**Publication IV**) and controlled photocrosslinking.

In **Publication I** (Figure 28), the GelMA60 precursor was highly affected by the low temperature (16 °C) as it was able to form a coherent filament and maintain its shape. In addition, ColMA60 formed a coherent filament at RT with a relatively low applied pressure. It showed good layer-stacking ability without merging. However, the other precursors (GelMA30, ColMA30, HAMA30, HAMA60, AlgMA30 and AlgMA60) did not form coherent filaments and did not retain their shape, even at a low

temperature. Moreover, the filament formation ability of GelMA60 precursors were tested at concentrations of 5 and 10% w/v (Figure 29). The results showed that GelMA60 with the higher concentration formed better filaments than the lower concentrations. The produced filaments of 10% GelMA60 were longer and retained their shape better than those of 5% GelMA60 at 16 °C. The filament produced by Nivea crème was used as a control.

In **Publication II** (Figure 30), a low temperature was also applied to observe the viscosity change; GGMA at 4 °C became more viscous, but it was unable to maintain its shape after extruding from a nozzle. As a result, $CaCl_2$ was chosen as a pre-crosslinker for the GGMA precursor to get coherent and extrudable filaments. The concentrations of GGMA (1, 2 and 3% w/v) and $CaCl_2$ (22.5, 45 and 90 mM) were varied to obtain a set of formulations for rheology testing and 3D printing. Tested concentrations were 1% $GGMA_{\_45mM}$, 1% $GGMA_{\_90mM}$, 2% $GGMA_{\_45mM}$, 2% $GGMA_{\_90mM}$, 3% $GGMA_{\_45mM}$ and 3% $GGMA_{\_90mM}$. Nivea crème was used as a control to compare the filament quality.

In **Publication III**, as also shown in **Publication I**, 5% w/v of GelMA at RT and 37 °C did not produce smooth and coherent fibers. To obtain high printability and stability at RT and 37 °C, the pre-crosslinker $FeCl_3$ was applied to GelMAGA using two different concentrations (0.25 and 0.5 %w/v), as shown in Figure 31. The GA functionalization and addition of $FeCl_3$ to GelMA30 (GelMA30GA-2.5Fe) and GelMA60 (GelMA60-2.5GA) hindered the formation of coherent filaments during extrusion at room temperature (RT), resulting in discontinuous fibers. However, GelMA30GA-5Fe was able to produce coherent filaments of approximately 5 cm in length at both RT and 37 °C. On the other hand, GelMA60-5Fe exhibited heterogeneous filaments consisting of a mixture of overgelated filaments and droplets. In addition, the concentration of Fe^{3+} was tuned to 1% w/v in both GelMA30GA and GelMA60GA, but the inks became hydrogels in the cartridge, which clogged the nozzle.

In **Publication IV**, the HAGA-HAMA precursor at pH 3–5 exhibited droplet-like filaments, whereas filaments produced at pH 7.5 were smooth and coherent (Figure 32). A further extent of the pH towards basic conditions (pH <8) required higher pressure to extrude the filament out of the nozzle due to overgelation and caused frequent nozzle clogging.

GGMA and GGMA-GA precursors were able to produce long continuous filaments, but all filaments were irregular in shape, as shown in Figure 33.

	MA			
	30%		60%	
	RT	16 °C	RT	16 °C
HA	droplet	droplet	droplet	droplet
Alg	droplet	droplet	droplet	droplet
Gel	droplet	droplet	droplet	smooth
Col	droplet	droplet	smooth	smooth

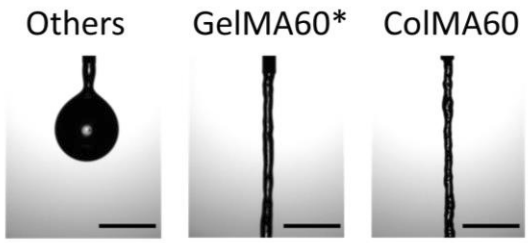

Figure 28. Filament formation of the precursors: GelMA60* (GelMA60 at 16 °C), ColMA60 at RT, Others at RT (GelMA60, GelMA30, ColMA30, AlgMA30, AlgMA60, HAMA30, and HAMA60), Scale bar = 1 mm. (**Publication I**)

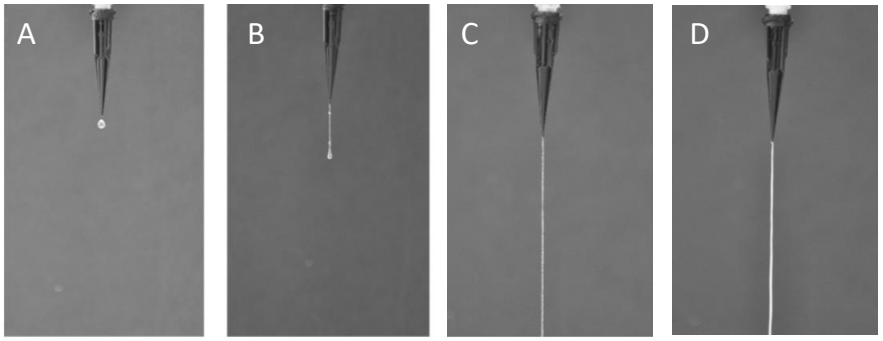

Figure 29. Filament formation test: (A) 5% w/v GelMA60 at RT, (B) 5% w/v GelMA60 at 16 °C, (C) 10% w/v GelMA60 at RT, and (D) Nivea crème as a control at RT. (200 µm nozzle size)

GGMA (%w/v)	$CaCl_2$ (mM)			
	0	22.5	45	90
1	droplet	droplet	viscous	smooth
2	viscous	droplet	smooth	smooth
3	viscous	droplet	smooth	irregular

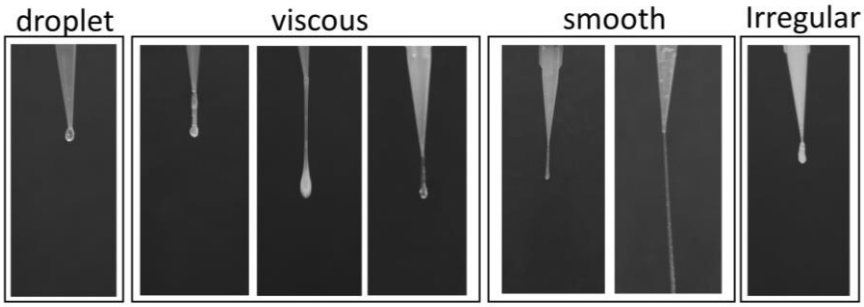

Figure 30. Filament formation quality testing in various materials, GGMA at 4 °C and various concentrations of GGMA with $CaCl_2$. (200 µm nozzle size) (**Publication II**)

	$FeCl_3$ (mM)		
	0	15	30
GelMA30GA	droplet	droplet	smooth
GelMA60GA	droplet	droplet	irregular

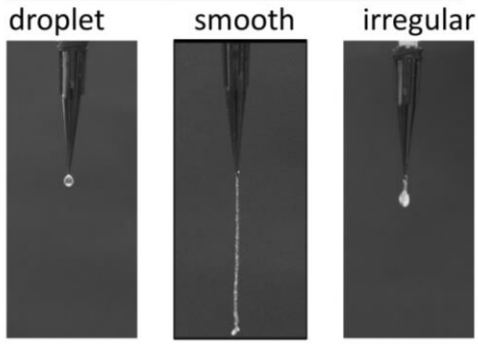

Figure 31. Filament formation quality testing of GelMA30GA with $FeCl_3$, GelMA60GA with $FeCl_3$ and other formulations without $FeCl_3$. (200 µm nozzle size) (**Publication III**)

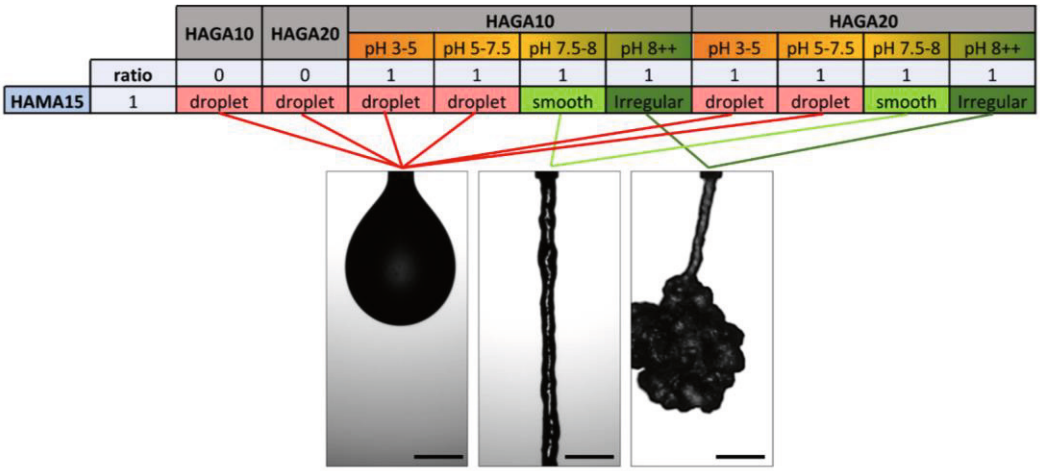

Figure 32. Filament quality of plain HAMA15, HAGA10-HAMA15 and HAGA20-HAMA15 at pH 3–5, 7.5–8 and > 8 (410 µm nozzle size), 1 mm scale bar. (**Publication IV**)

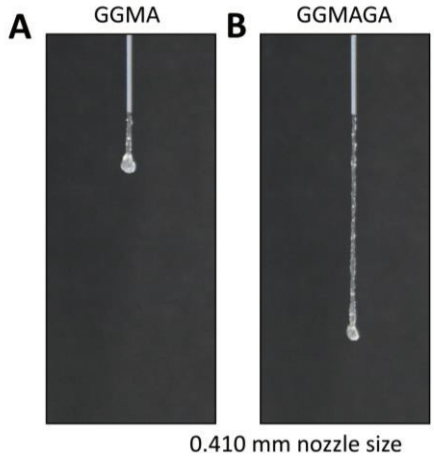

Figure 33. Filament quality of GGMA (A) and GGMAGA (B) after pre-crosslinked with UV light. 410 µm nozzle size, steel type was used.

5.2.2 Flow behavior

The flow behavior of the precursors was measured to deepen the study of precursor properties in terms of printability. The measurements were performed using a rheological test in flow mode. Rheological testing was conducted using the same measurement methods in all publications (**I–IV**). The flow measurements were divided into shear-thinning, yield stress, and recovery behavior. The Power law model fit was applied in all publications (**I–V**) to predict shear-thinning behavior from shear-thinning coefficients (*K* and *n* values). The linear region was chosen from the middle of the slope, and the power trendline was fitted to obtain all shear-thinning coefficients. All viscosity values, calculated shear-thinning coefficients and recovery are listed in Table 4.

Figure 34 (**Publication I)** illustrates the relationship between viscosity and modification degree of the precursors at different shear rates. GelMA exhibited temperature-dependent behavior, resulting in the formation of coherent filaments at 16 °C. Most of the precursors (AlgMA30, AlgMA60, and HAMA30) displayed Newtonian fluid behavior, where viscosity remained constant with increasing shear rate. Power law analysis confirmed that the 30% modification degree precursors had high shear-thinning coefficients (*n*) close to 1. AlgMA60 and HAMA60 also showed shear-thinning behavior with n coefficients ranging between 0.7 and 0.9. Shear-thinning precursors such as ColMA60, GelMA30, GelMA60, and GelMA60 at 16 °C exhibited low n values close to 0.1. The details of the calculation can be found in Equation 1 of **Publication I**.

In **Publication II**, the temperature-dependent viscosity of the 3% GGMA precursor was evaluated, and it showed shear-thinning behavior with decreasing viscosity as a function of the increasing shear rate (n = 0.29). However, filament formation showed contradictory results, as the filament of 3% GGMA was formed in a short period after extrusion from the nozzle. 1 and 2% GGMA at 4 °C exhibited Newtonian fluid behavior (Figures 36A and B). Applying ionic pre-crosslinking ($CaCl_2$) in GGMA significantly improved shear-thinning behavior, as presented in Figure 37. The concentrations of $CaCl_2$ (22.5 and 45 mM) were insufficient to provide shear-thinning behavior in GGMA, resulting in many variations in the viscosity curves. Most of the 2 and 3% GGMA with 45 or 90 mM $CaCl_2$ increased the viscosity, leading to the enhancement of shear-thinning properties. The GGMA formulations were arranged according to *n* values (from the lowest): 2%

$GGMA_{\_90mM}$, 1% $GGMA_{\_90mM}$, 3% $GGMA_{\_90mM}$, 3% $GGMA_{\_45mM}$, 3% $GGMA_{\_22.5mM}$, 2% $GGMA_{\_45mM}$ and 2% $GGMA_{\_22.5mM}$. The details of the calculation can be found in Equation 1 of **Publication II**.
In **Publication III**, the temperature dependence of the viscosity of GelMA and GelMAGA was measured in terms of viscosity as a function of temperature (Figure 38). GelMAGA with a pre-crosslinker ($FeCl_3$) was able to maintain viscosity levels, which steadily decreased after 30 °C. All pre-crosslinked GelMAGA had shear-thinning behavior, as confirmed by $n < 1$ (Figure 39). However, GelMAGA without an additional pre-crosslinker showed poorer viscosity and shear-thinning coefficients than pure GelMA. In Table 4, the shear-thinning coefficients of the pre-crosslinked GelMAGA are arranged from best to poor: GelMA30GA-5Fe, GelMA60GA-5Fe, GelMA60GA-2.5Fe and GelMA30GA-2.5Fe. The details of the calculation can be found in Equation 1 of **Publication III**.

In **Publication IV** (Figure 40), all HAGA-HAMA formulations at low pH (3-5) were liquid (Newtonian fluid), as confirmed by the shear-thinning coefficients of $n > 0.9$. The viscosity of the precursors increased with increasing pH, and they became true hydrogels after reaching a pH of 8. In detail, the viscosity curve of HAGA10-HAMA15 at pH 7.5–8 showed a plateau region at a low shear rate, but the viscosity steadily decreased at 10 s^{-1}. HAGA20-HAMA15 at 5–7.5 pH also started behaving as a weak non-Newtonian fluid when the shear rate reached 10 s^{-1}. On the other hand, HAGA20-HAMA15 at pH 8 showed an improvement in the shear-thinning behavior at a shear rate above 1 s^{-1}, giving $n < 0.2$. The details of the calculation can be found in Supporting information of **Publication IV**.

GGMA and GGMAGA pre-crosslinked with UV light were high shear-thinning, as presented in Figure 41, which was confirmed by shear-thinning coefficients from the Power law fit ($n=0.35$ and 0.19, respectively).

In all publications (**I–IV**), the Herschel−Bulkley model was used to determine the yield stress from the shear stress-shear rate and viscosity-shear stress plots. In **Publication I**, the viscosity curve was plotted as a function of increasing shear stress. Figure 35 shows that both GelMA60 at 16 °C and ColMA60 clearly exhibited yield stress, after which the precursor began to flow easily under a certain level of shear stress. On the other hand, the other precursors showed flatlines in viscosity, even at high levels of shear stress. In **Publication II**, all pre-crosslinked GGMA precursors with $CaCl_2$ exhibited yield stress from the first point of the shear rate (Figure 37).

The pre-crosslinked GGMA, denoted as 1-3% GGMA_22.5mM, had low yield points and did not exhibit yield stress. Highly shear-thinning pre-crosslinked GGMA showed clear yield points after increasing the shear rate. In **Publication III**, the $FeCl_3$ pre-crosslinker improved the clarity of the yield point in all GelMAGA precursors and the shear-thinning coefficients of the precursors were confirmed via this model (Figure 39). In **Publication IV**, HAGA10-HAMA15 and HAGA20-HAMA15 at pH 8 showed obvious yield points (Figure 40), but they did not have high yield stress, implying that high printing pressure is not required to extrude the material.

Recovery testing was performed to estimate the thixotropic behavior of the precursors and biomaterial inks after extrusion from a needle or a printing nozzle (**Publications II–IV**). In **Publication II**, the viscosity measurements could not be performed on 1% $GGMA_{\_22.5mM}$ and 1% $GGMA_{\_45mM}$ due to their low viscosity, which caused the inks to dislocate from the geometry at high centrifugal force. In addition, 3% $GGMA_{\_90mM}$ exhibited overgelation, resulting in the ink being shattered and slipping out during the measurement. The GGMA formulations that exhibited proper recovery behavior were: 1% $GGMA_{\_90mM}$, 2% $GGMA_{\_22.5mM}$, 2% $GGMA_{\_45mM}$, 2% $GGMA_{\_90mM}$, 3% $GGMA_{\_22.5mM}$, and 3% $GGMA_{\_45mM}$. However, 2% $GGMA_{\_22.5mM}$, 2% $GGMA_{\_45mM}$, 3% $GGMA_{\_22.5mM}$, and 3% $GGMA_{\_45mM}$ required a longer recovery time (100 s for 2% GGMA) to regain their initial viscosity, indicating slower recovery compared to other formulations. In **Publication III**, GelMA30GA-5Fe and GelMA60GA-5Fe exhibited rapid recovery of their viscosities, reaching approximately 70% recovery after the high shear rate was removed. On the other hand, the inks containing 0.25% w/v $FeCl_3$ were unable to recover their viscosity and permanently lost their characteristic properties. In **Publication IV**, HAGA20-HAMA15 at pH 8 rapidly recovered back to its original viscosity (~80%) after removing the high shear rate. In contrast, at pH 9, HAGA10-HAMA15 and HAGA20-HAMA15 lost half of their viscosity after removing the shear rate.

Table 4. Overview of properties of the biomaterial inks in the studies: flow behavior (shear-thinning, yield stress and recovery) and pre-crosslinking.

Ink code	Pre-crosslinking	Viscosity [Pa·s]	n	K	τ_0 [Pa]	Recovery [%]
HAMA30	-	0.302	0.95	0.08	0	0
HAMA60	-	2.66	0.77	0.58	0	0
AlgMA30	-	0.62	0.93	0.15	0	0
AlgMA60	-	1.83	0.86	0.95	0	0
1% GGMA15	Low temp.	0.65	0.92	0.07	0	0
2% GGMA15	Low temp.	23.4	0.78	3.88	0	0
3% GGMA15	Low temp.	286	0.29	146	0.05	0
1% GGMA15-22.5mM	$CaCl_2$	1.94	-	-	0.01	0
1% GGMA15-45mM	$CaCl_2$	8.56	-	-	0.12	0
1% GGMA15-90mM	$CaCl_2$	3872	0.16	61.6	17	~87
2% GGMA15-22.5mM	$CaCl_2$	52.2	0.55	21	0.46	~56
2% GGMA15-45mM	$CaCl_2$	596	0.35	33.2	3.64	~57
2% GGMA15-90mM	$CaCl_2$	8042	0.10	115.8	48	~96
3% GGMA15-22.5mM	$CaCl_2$	86.8	0.34	40.6	0.78	~53
3% GGMA15-45mM	$CaCl_2$	1121	0.26	77.4	13.4	~58
3% GGMA15-45mM	$CaCl_2$	3375	0.22	83.3	26.3	~51
GGMA15GA	UV light	1297	0.28	24.8	117.7	~54
HAGA10-HAMA15	Basic pH	13.43	0.21	265	215	~72
HAGA20-HAMA15	Basic pH	125.42	0.27	96.2	209	~81
GelMA30	-	1.22	0.82	0.01	0.04	0
GelMA60	-	4.62	0.41	0.01	0.07	0
GelMA60*	Low temp.	915	0.11	14.3	79.4	~95
GelMA30GA	-	4.62	0.28	0.43	0.08	0
GelMA60GA	-	0.05	0.92	0.01	0.02	0
GelMA30GA-2.5Fe	$FeCl_3$	76	0.42	0.8	0.74	0
GelMA30GA-5Fe	$FeCl_3$	7940	0.03	276	83	~73
GelMA60GA-2.5Fe	$FeCl_3$	4.16	0.26	0.16	0.04	0
GelMA60GA-5Fe	$FeCl_3$	6371	0.23	21	21	~72
ColMA30	-	0.941	0.78	0.14	0	0
ColMA60	-	208	0.14	0.39	126	~86

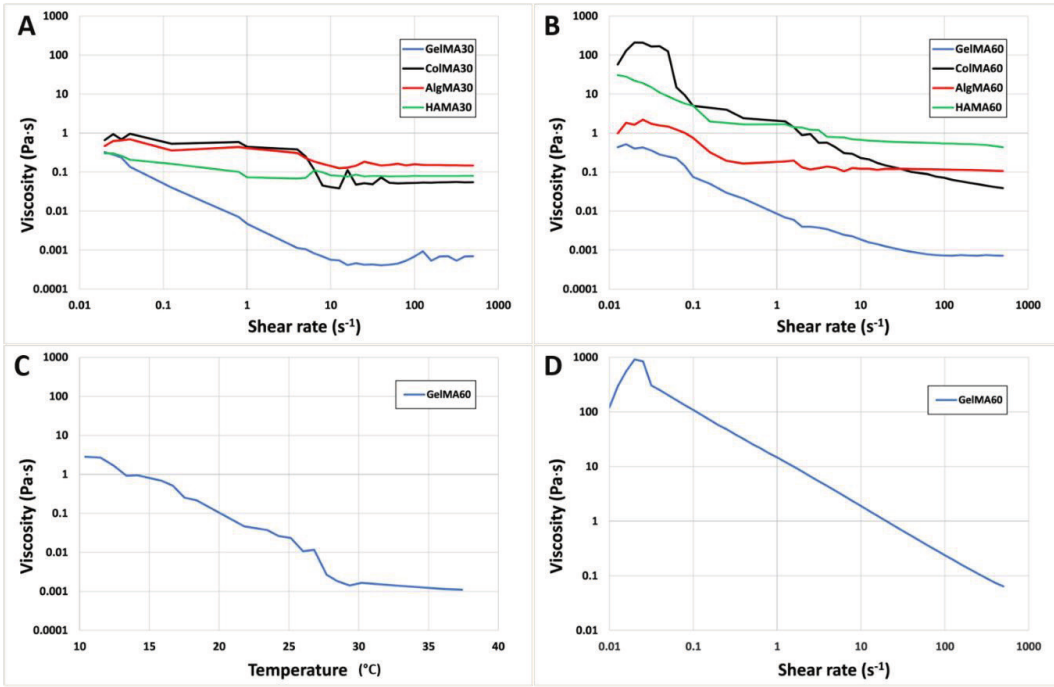

Figure 34. The viscosity-shear rate plots of the hydrogel precursors with varying %MD: (A) with a 30% modification degree, (B) with a 60% modification degree. Additionally, the figure displays the viscosity-temperature relationship (C) of GelMA60 at a constant shear rate of 0.1 s^{-1} and a concentration of 5% w/v. Finally, the figure showcases the viscosity-shear rate profile (D) of GelMA60 at 16 °C, demonstrating its shear-thinning behavior.

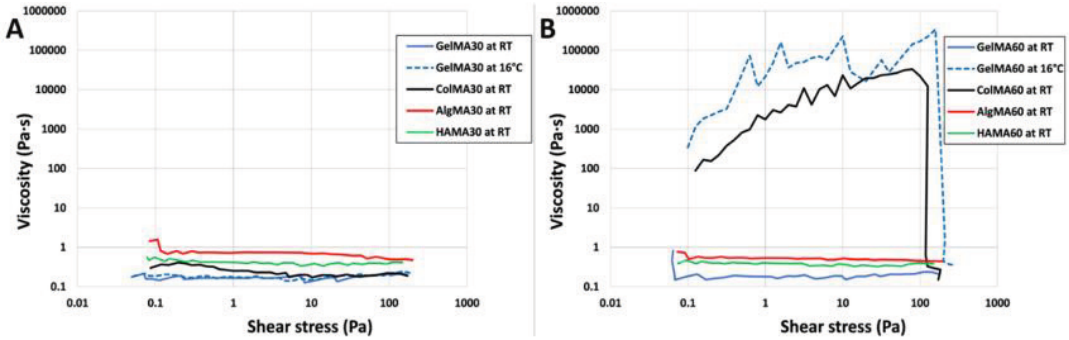

Figure 35. Yield stress measurement data for all precursors at RT and for GelMA30 and GelMA60 also at 16 °C. Figures (A) and (B) represent precursors with a 30% modification degree (MD) and precursors with a 60% MD, respectively.

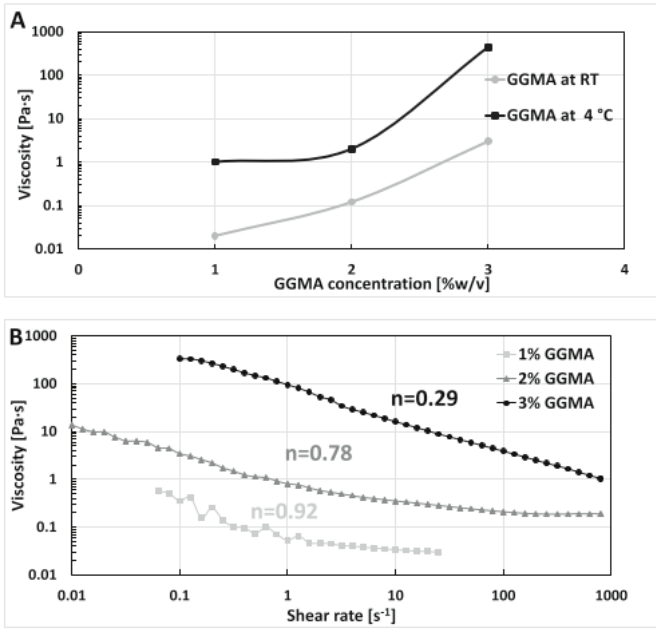

Figure 36. The viscosity measurements provide insights into the temperature sensitivity of GGMA hydrogels. (A) The effect of temperature on GGMA at RT and 4 °C for various concentrations (1, 2 and 3%), (B) Shear-thinning properties of 1, 2 and 3% GGMA concentrations. The viscosity decreases with increasing shear rate, indicating the weak shear-thinning behavior of GGMA hydrogels at 4 °C.

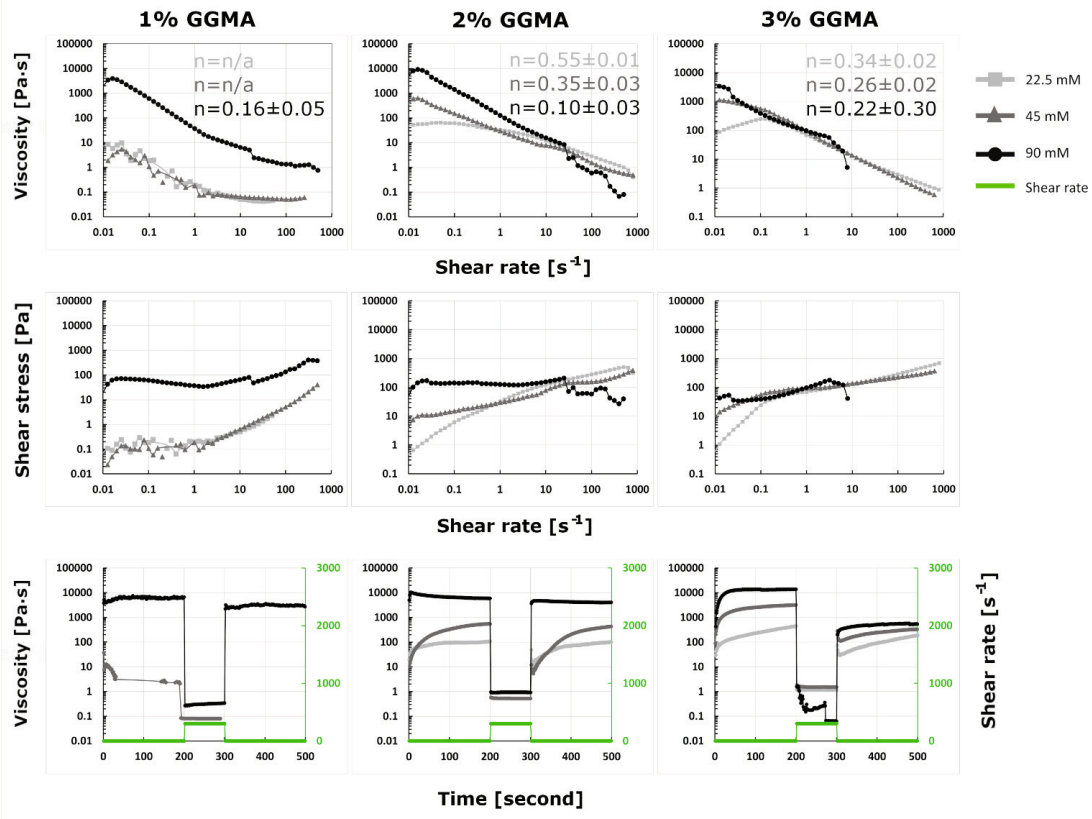

Figure 37. Rheological properties: shear-thinning, yield stress and recovery for various GGMA and $CaCl_2$ concentrations at RT. The plot includes the shear-thinning behavior, yield stress, and recovery of the hydrogels, providing insights into their flow characteristics and mechanical properties.

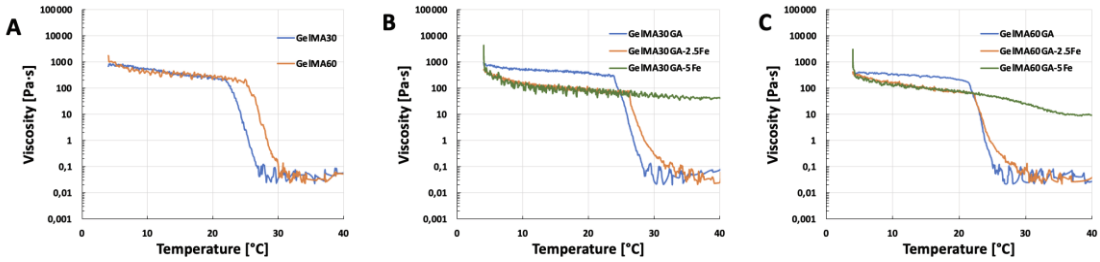

Figure 38. Rheological measurement of viscosity as a function of temperature. All samples were measured over the temperature range from 4°C to 40°C. (A) GelMA with 30% and 60% degrees of methacrylation, (B) GelMA30GA group with/without Fe^{3+}, (C) GelMA60GA group with/without Fe^{3+}. The plots provide insights into the thermostability and rheological behavior of the different hydrogel formulations.

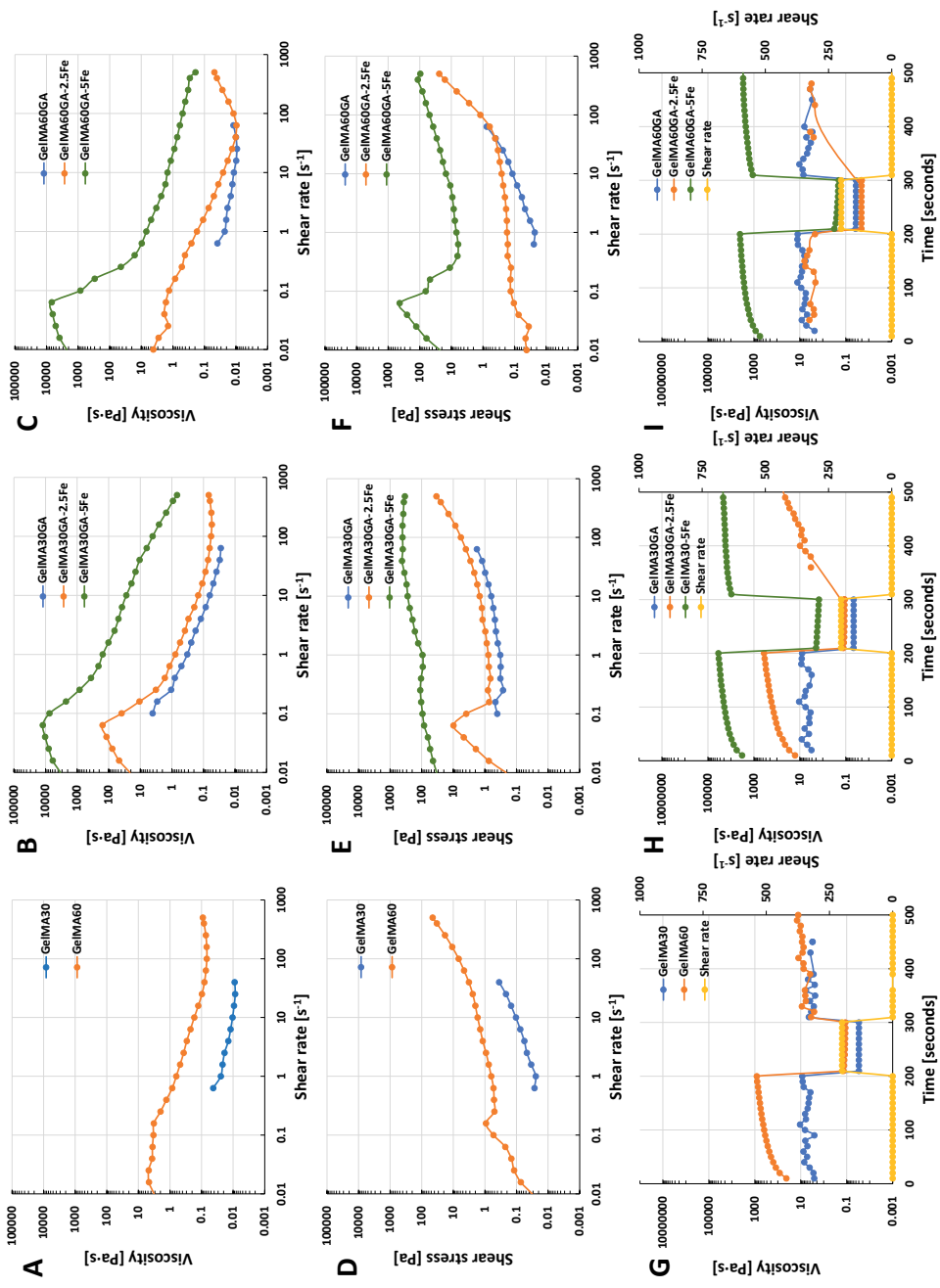

Figure 39. The plots illustrate insights into the flow properties, including shear-thinning, yield stress, and recovery behavior of the different GelMAGA formulations at RT. Rheological measurements in flow mode: shear-thinning (A-C), yield stress (D-F) and recovery behavior (G-I) at RT. (A, D, G) pure GelMA30 and GelMA60, (B, E, H) GelMA30GA group with/without Fe^{3+}, (C, F, I) GelMA60GA group with/without Fe^{3+}.

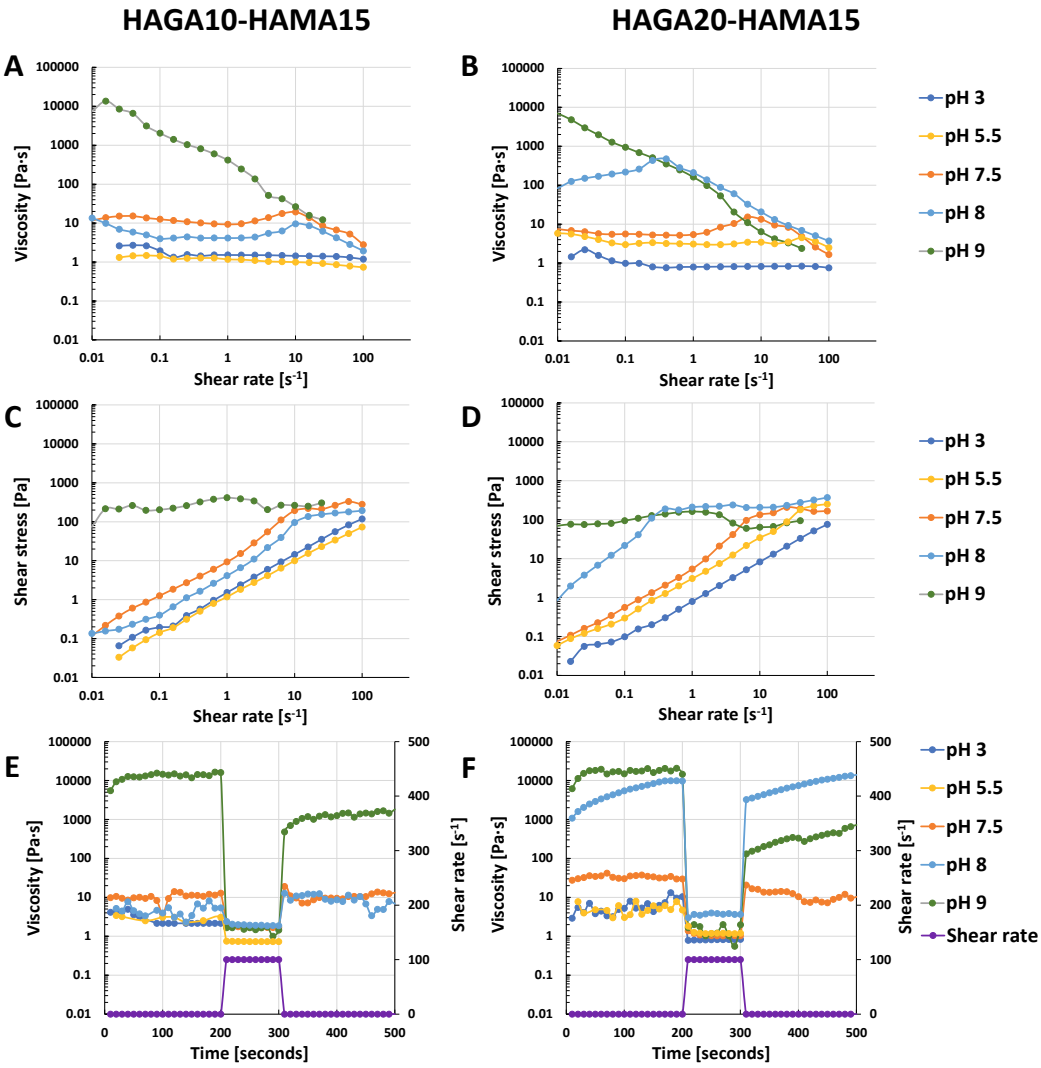

Figure 40. Rheological measurements of precursor mixtures of HAGA10-HAMA15 and HAGA20-HAMA15 at different pH (3, 5.5, 7.5, 8 and 9): shear-thinning (A, B), yield stress (C, D) and recovery behavior (E, F) at 37 °C.

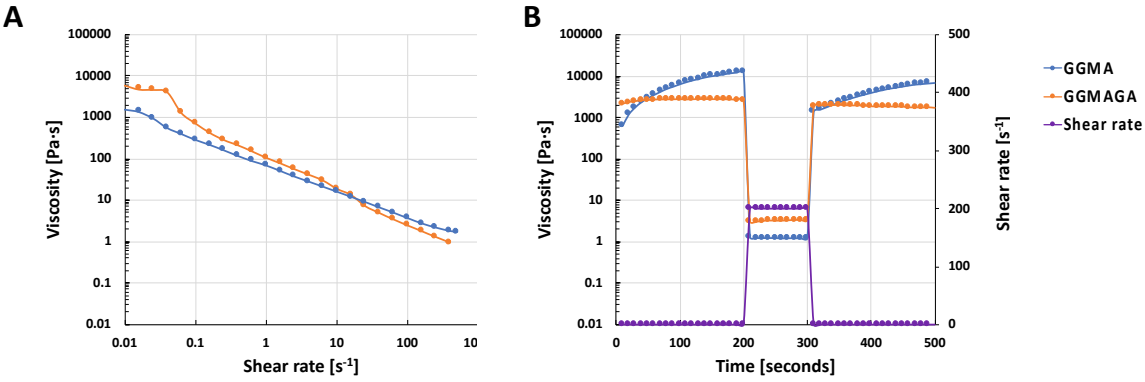

Figure 41. The shear-thinning properties and recovery behavior of GGMA and GGMAGA hydrogels after undergoing pre-crosslinking with UV light. Rheological measurements of GGMA and GGMAGA after being pre-crosslinked with UV light: (A) shear-thinning and (B) recovery behavior.

5.2.3 Gelation kinetics

In **Publication I**, the gelation kinetics of GelMA30, GelMA60, ColMA30, ColMA60, AlgMA30, AlgMA60, HAMA30 and HAMA60 precursors were analyzed based on the storage moduli of the resulting hydrogels under different UV crosslinking conditions: UV light intensity and exposure time. Figure 56 illustrates that increasing the UV intensity, exposure time, or %MD resulted in G' and a more rigid structure in all hydrogels. The results also demonstrated that both G' and G" increased with longer exposure times and higher UV intensities. A higher MD indicated a greater degree of cross-linking, which in turn led to stiffer hydrogels. To be more precise, in the hydrogels with 30% and 60% MD, higher UV intensities facilitated faster polymerization processes. In the unpublished data (Figure 45), the photoinitiator selection (LAP or Irgacure2959) highly influenced the gelation kinetics of GelMA60 precursors, as LAP provided faster gelation time and higher final storage moduli, compared to Irgacure2959.

In **Publication II**, Figure 42 demonstrates the gelation kinetics of GGMA at different concentrations (1%, 2%, and 3%) upon exposure to UV light. The results indicate that all GGMA concentrations exhibited rapid gelation and crosslinking in less than 10 seconds, reaching a maximum crosslinking state within 60 seconds. While the concentration of GGMA had a significant impact on the final storage modulus, the gelation time did not show significant differences among the different polymer concentrations.

In **Publication III,** In Figure 43, the *in situ* photorheology results show the gelation time of various ink formulations, as indicated by the storage modulus over time. All ink formulations exhibited an initial increase in storage modulus upon UV light exposure. Within 60 seconds, the ink formulations reached their maximum cross-linking degree, indicating the completion of gelation. The gelation time and storage modulus of GA-functionalized GelMA showed no significant differences compared to pure GelMA. However, the addition of $FeCl_3$ in GelMAGA resulted in a slower gelation process, as the storage modulus took more than 60 s to reach a plateau. These findings suggest that the incorporation of $FeCl_3$ in GelMAGA may potentially reduce the gelation time compared to other formulations.

In **Publication IV**, the *in situ* photorheology (Figure 44) shows the gelation time of all precursor formulations (HAGA10-HAMA15 and HAGA20-HAMA15) at different pH after being exposed to UV light (storage modulus as a function of time). At basic pH, the initial storage moduli of HAGA-HAMA reached the maximum value, resulting in no difference in storage moduli after photocrosslinking. On the other hand, the precursors at acidic pH responded to the UV light actively, but they were not able to reach the same level of final storage moduli as the precursors at neutral or basic pH.

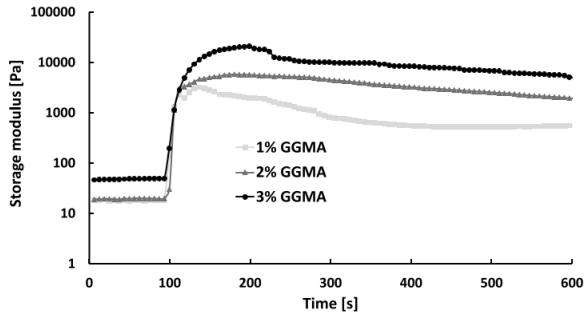

Figure 42. *In situ* photorheology of 1%, 2% and 3% GGMA at RT. The figure showcases the real-time monitoring of the rheological behavior of GGMA hydrogels during UV light exposure.

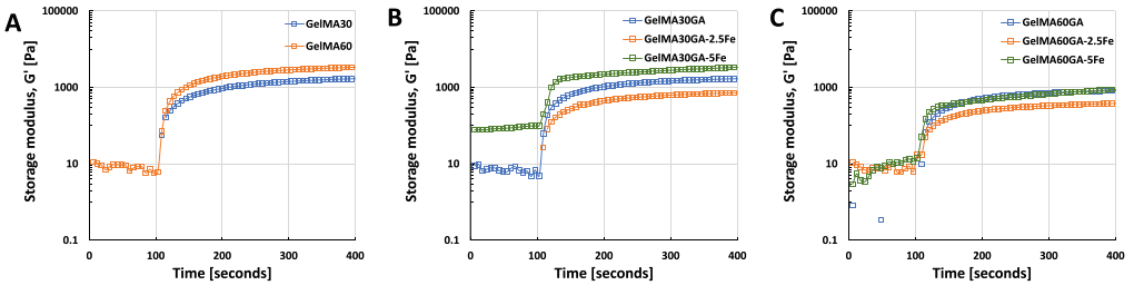

Figure 43. *In situ* photo-polymerization test to observe the gelation time of each ink formulation (time sweep of oscillatory measurement, 25 mW/cm^2 for 300 s, at RT). (A) Pure GelMA30 and GelMA60, (B) GelMA30GA group with/without Fe^{3+}, and (C) GelMA60GA group with/without Fe^{3+}.

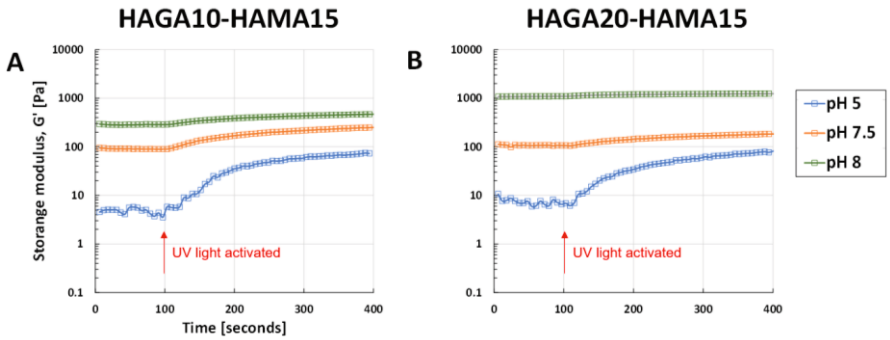

Figure 44. Gelation time of (A) HAGA10-HAMA15 and (B) HAGA20-HAMA15 precursors after photocrosslinking.

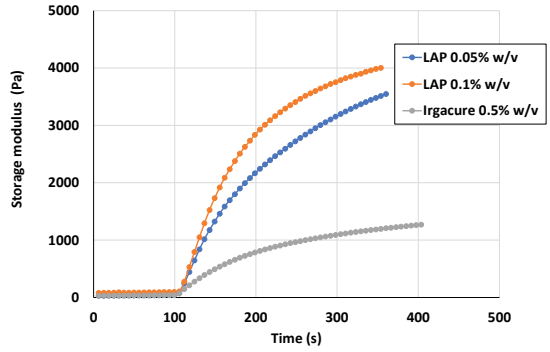

Figure 45. The comparison of gelation kinetics of GelMA60 in the presence of different photoinitiators: 0.05 % LAP, 0.1% LAP and 0.5% Irgacure2959. The experiment was performed at RT.

5.3 Processing (3D printing)

In all publications (**I–IV**), screened precursor formulations with high shear-thinning properties are defined as biomaterial inks and were prepared for 3D printing test (**Publications II–IV**). The printability assessment quantitatively evaluates printability (Pr value), printing accuracy and structural integrity.

5.3.1 Pr value

The Pr values were calculated from the average squareness of the pores (pore geometry) in the printed grid structure for each biomaterial ink formulation. The highly printable ink has a Pr value between 0.9-1.1.

In **Publication II,** 1,2 and 3% w/v of GGMA with $CaCl_2$ concentrations of 0, 22.5, 45 and 90 mM were printed into the grids. Figure 46 showcases the ability of the inks to form coherent filaments and their successful application in printing grid structures. It was obvious that GGMA inks without a pre-crosslinker were unprintable (too liquid) when deposited on the substrate. The Pr value of 1-3% $GGMA_{\_22.5mM}$ could not be measured because of the undergelation of the ink. The Pr values were improved as the concentrations of GGMA and $CaCl_2$ increased, as presented in Figure 47. 1% $GGMA_{\_90mM}$ and 2% $GGMA_{\_45mM}$ inks were printable, but they were insufficient to maintain the structures intact (Pr values = 0.78 ± 0.4 and 0.82 ± 0.04). However, 3% $GGMA_{\_90mM}$ appeared as an overgelated ink because of the excessive ionic crosslinking. High pressure was required for extrusion and to form a tough hydrogel inside the nozzle, resulting in the fluctuating size of printed fibers and irregularly shaped pores (Pr = 1.1 ± 0.3). The Pr values of 2% $GGMA_{\_90mM}$ and 3% $GGMA_{\_45mM}$ were in a proper region, being 0.97 and 1.1, respectively. However, 2 % $GGMA_{\_90mM}$ produced smooth and coherent grid structures, compared to the irregular grids of 3% $GGMA_{\_45mM}$.

In **Publication III**, Figure 48 illustrates the printing process of the pre-selected precursors, namely GelMA30GA-5Fe and GelMA60GA-5Fe, which were used to create grid structures at RT. Additionally, GelMA30GA-5Fe was printed at a temperature of 37 °C. The grid structures were printed into 2 and 6 layers, respectively. The microscopic images also showed the intersection between the two filaments to observe the stackability. GelMA30GA-5Fe produced smooth and

coherent 2-layered grid structures at RT and 37 °C. However, the grid started to collapse and merge when the 6-layered structure was printed at 37 °C. The Figure 49 indicates that the average Pr values for GelMA30GA-5Fe, GelMA30GA-5Fe at 37 °C, and GelMA60GA-5Fe were quite similar (Pr ≈ 1.1). These structures exhibited irregular shapes and were positioned in the overgelation region on the graph. However, the standard deviation values increased as the degree of methacrylation increased, as evidenced by the filament formation data and the printing results.

In **Publication IV**, the printability assessment (Figure 50) was performed in the same way as in the previous publications, but the pore size of the printed structures was fabricated into two sizes (adjusted from the filling in the CAD model). The Pr values of HAGA20-HAMA15 were between 0.9-1. In Figure 51, the Pr values of GGMA and GGMAGA were 0.85 and 1.1. In Figure 52, the microscopic images present the comparison between different pre-crosslinking approaches: temperature, pre-crosslinkers and photocrosslinking. Pre-crosslinked precursors with pre-crosslinkers exhibited homogeneous fibers, resulting in perfect grid structures, whereas the thermal gelation was unable to provide coherent and smooth fibers due to the temperature gradient after extrusion. On the other hand, pre-crosslinking with UV was the worst approach, observed by the poor printing resolution.

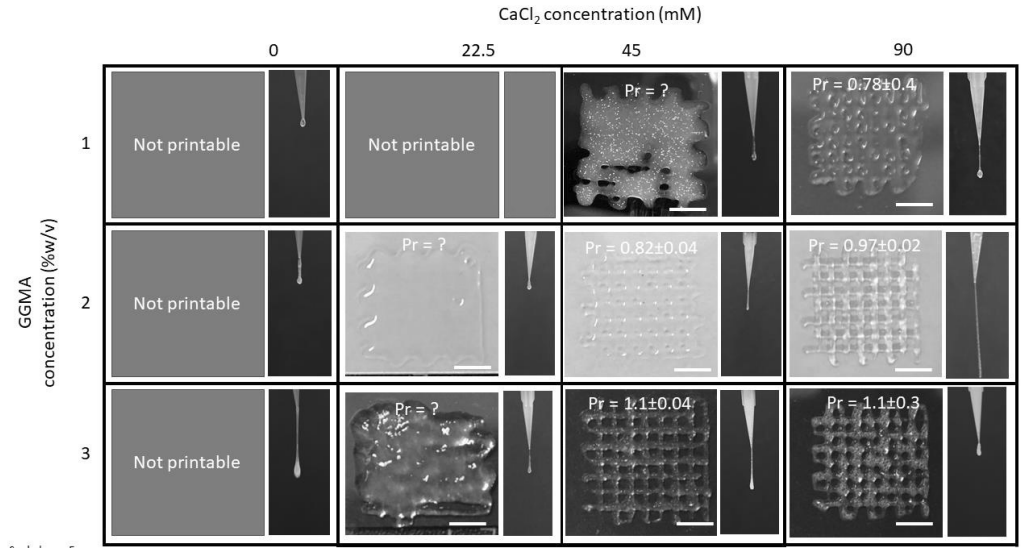

Figure 46. The results of filament formation results and printed grid structures of GGMA/$CaCl_2$ inks were evaluated in terms of printability. The scale bar is 5 mm.

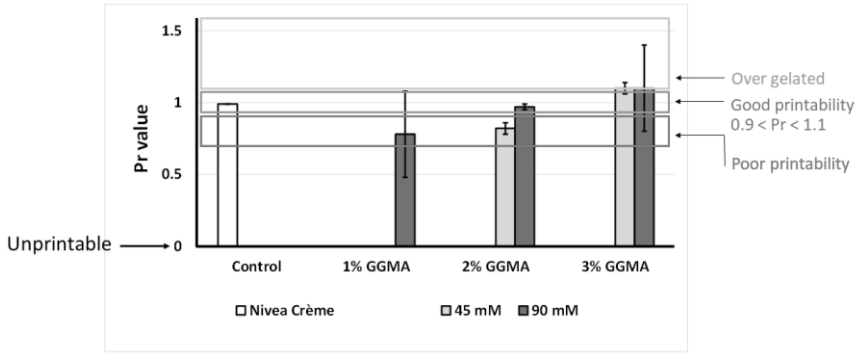

Figure 47. The calculated Pr values for Nivea Creme (control) and various GGMA formulations with different amounts of $CaCl_2$ pre-crosslinking.

Ink composition	Fiber formation	Grids (2 layers)	Grids (6 layers)	Intersection
GelMA30GA-5Fe (RT)				
GelMA30GA-5Fe (37 °C)				
GelMA60GA-5Fe (RT)				
Others (RT)				

Figure 48. Pre-screening of biomaterial inks: fiber formation, two-layered and six-layered printed grids and close-ups of filament intersections. Scale bar = 10 mm (white), 1 mm (black).

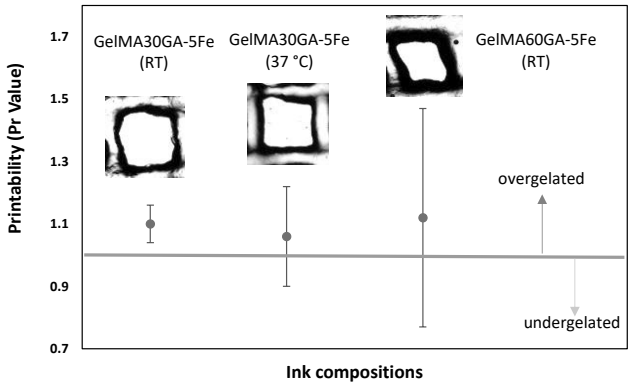

Figure 49. Calculated Pr values for the determination of the actual printability of GelMA30GA-5Fe at RT, GelMA30GA-5Fe at 37 °C and GelMA60GA-5Fe at RT. The green line indicates the perfect printability value of 1. The Pr values are represented as the mean ± standard deviation (n=20).

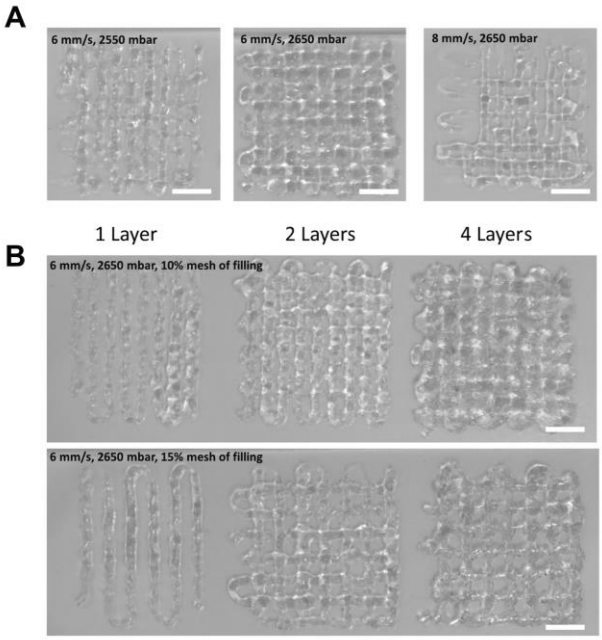

Figure 50. Printability of biomaterial inks (HAGA20-HAMA15 at pH 7.5–8, 37 °C) and 3D printing for Pr value calculation. (A) The images of 2 layers printed grid structures varying the printing speed and printing pressure to optimize the printing resolution. (B) The images of 1, 2 and 4 layers using the screened printed parameters, but the filling of the grids are 10 and 15%. The scale bar is 5mm.

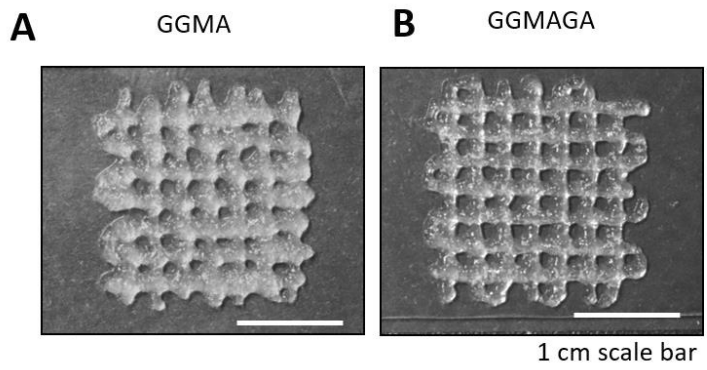

Figure 51. The printed grid structures of GGMA (A) and GGMAGA (B) precursors pre-crosslinked with UV light.

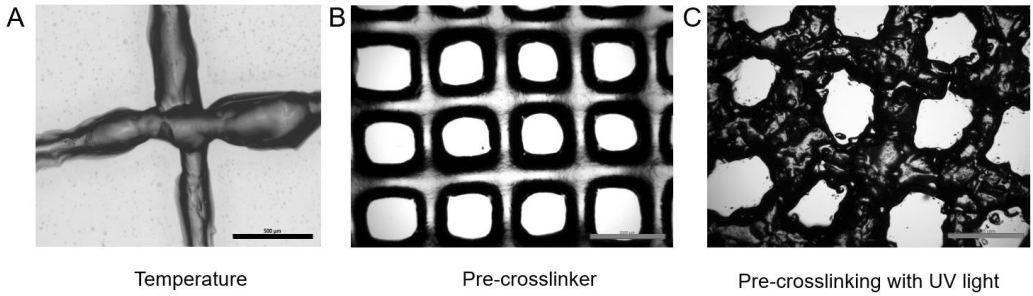

Figure 52. Illustration of the comparison of three crosslinking techniques: (A) low temperature (500 µm scale bar), (B) pre-crosslinker (2000 µm scale bar) and (C) pre-crosslinking with UV light (2000 µm scale bar).

5.3.2 Printability window

Ideally, the proper printing parameters provide stability and shape fidelity for the printed structure, which allows the 3D stacking of filaments in a layer-by-layer fashion. In **Publications I–IV**, the printing pressures were obtained from the automatic dispenser during the filament formation tests. The tested printing speeds were 6, 8 and 10 mm/s. The relationship between the printing pressure and speed was formulated into a printability window (Figure 53). In all ink formulations, low printing speed (4 mm/s) fed excessive inks on the printing bed, resulting in over-deposited and irregular filaments. However, when the inks started to extrude at a particular pressure, they could not adhere to the substrate and formed discontinuous

filaments. The optimal printing speed in all the materials was 8 mm/s, which resulted in continuous thin filaments without breaking. The blank sections displayed where the printing pressure and speed were unmatched, which would lead to unfeasible filament shapes (discontinuous shapes or dots). The green sections show the perfect combination of printing parameters, which leads to smooth filament shapes. The sections displayed in blue and dark blue show that the printing pressure was exceeded, leading to the over-deposition of filaments on the substrate. In **Publication IV**, the printed filaments were assessed using different nozzle sizes due to the high viscosity of the ink, as the ink could not pass through the small nozzle orifices (200 and 250 μm).

Nivea crème — 200 μm nozzle

speed	10				
	8				
	6				X
pressure		1500	2000	2500	3000

Poloxamer — 200 μm nozzle

speed	10				X
	8				X
	6			X	X
pressure		900	1000	1100	1200

GelMA60 at 16 °C — 200 μm nozzle

speed	10				
	8				
	6		X	X	X
pressure		400	600	800	1000

GGMA-$CaCl_2$ — 200 μm nozzle

speed	10				
	8				
	6				X
pressure		400	600	800	1000

GelMA30GA-$FeCl_3$ — 200 μm nozzle

speed	10				
	8				
	6			X	X
pressure		1200	1300	1400	1500

HAGA20-HAMA15 — 410 μm nozzle

speed	8				
	6				X
	4	X	X	X	X
pressure		2450	2550	2650	2750

Figure 53. Printability window of all precursor formulations and controls in **Publications I–IV**, Nivea Creme, 40% Poloxamer, 5% GelMA60 at 16 °C, GGMA-$CaCl_2$, GelMA30GA-$FeCl_3$ and HAGA20-HAMA15. The optimal printing parameters (green) were a compromise between printing pressure and speed. Light blue indicates the irregular filament, and dark blue (x) indicates the over-deposition of the material on the substrate.

5.4 Post-processing

5.4.1 Accuracy and structural integrity

CAD models of cylinders (height of 1, 2.5 and 5 mm) were chosen for post-printing characterizations and used in **Publications II & III**. The dimensions of printed

structures in **Publication II** (Figure 54, Table 5), **III** (Figure 55), **IV** (Figure 56) and Figure 57 showed the same pattern, but they were larger than the CAD models, especially the wall thickness. In detail, the filament sizes produced from both Nivea crème and Poloxamer were close to the nozzle orifice (Figure 54 and Figure 55). However, the filament width of the pre-crosslinked inks in **Publications II, III & IV** swelled after being extruded from the nozzle, resulting in larger printed structures. The structural integrity was confirmed by calculating the ratio between the printed constructed of the developed inks and the control ink, and they were able to maintain good shape fidelity and enabled the printing of multilayered 3D constructs.

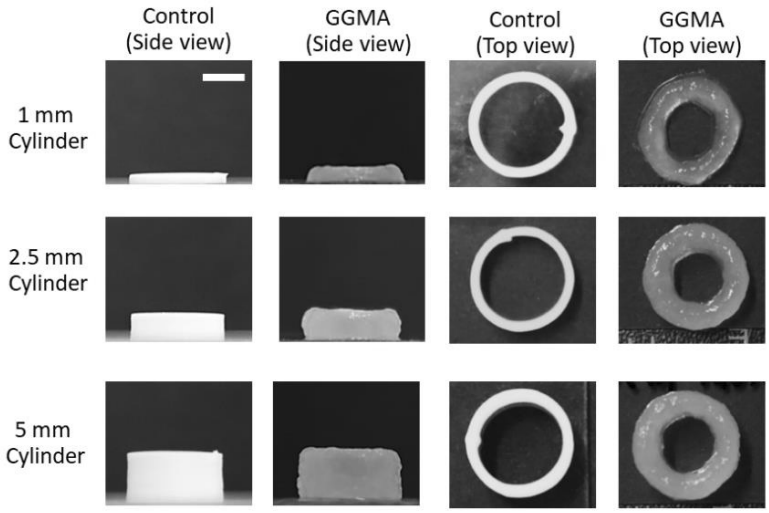

Figure 54. Side-views and top-views of printed cylinders for the evaluation of printing accuracy and structural integrity, The scale bar = 5 mm.

Table 5. The dimensions of the printed cylinders, including the percentage error, compared to the control cylinder and structural integrity ratio.

1 mm cylinder [6 layers]	Control dimensions [mm]	GGMA dimensions [mm]	Error [%]	Structural integrity ratio
Height	1.3±0.1	1.7±0.2	30.7±5.1	1.31±0.05
Outer diameter	11.0±0.2	11.2±0.2	1.8±0.2	1.02±0.01
Inner diameter	8.80±0.2	6.5±0.3	26.2±2.7	0.73±0.04
Wall thickness	1.2±0.1	3.0±0.1	150.7±10.8	2.50±1.30

2.5 mm cylinder [16 layers]	Control dimensions [mm]	GGMA dimensions [mm]	Error [%]	Structural integrity ratio
Height	3.2±0.1	3.7±0.3	15.6±3.7	1.15±0.06
Outer diameter	11.0±0.1	11.7±0.2	6.3±1.5	1.06±0.01
Inner diameter	8.8±0.2	6.2±0.1	28.5±2.8	0.70±0.04
Wall thickness	1.2±0.2	3.1±0.1	158.7±12.5	2.58±0.28

5 mm cylinder [33 layers]	Control dimensions [mm]	GGMA dimensions [mm]	Error [%]	Structural integrity ratio
Height	5.8±0.1	7.2±0.2	24.21±1.2	1.24±0.02
Outer diameter	11.2±0.2	11.2±0.1	10.7±5.8	1.04±0.02
Inner diameter	8.4±0.2	5.6±0.2	33.3±5.3	0.66±0.01
Wall thickness	1.4±0.2	3.2±0.1	128.5±7.2	2.28±0.22

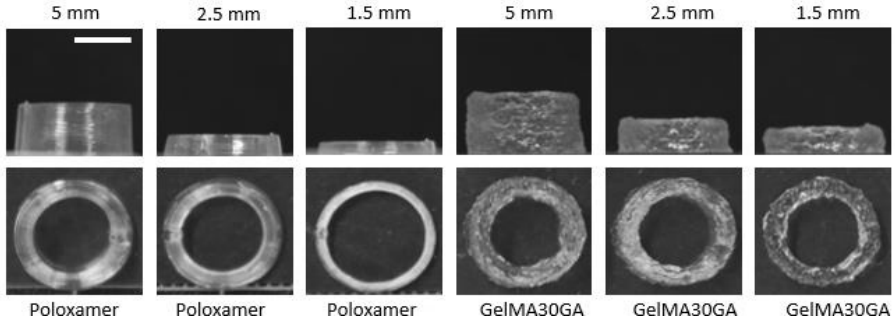

Figure 55. The 3D printed structures of GelMA30GA-5Fe ink and control material (Poloxamer).Top and side views of printed structures with 1.5, 2.5- and 5-mm wall height (Theoretical heights from CAD models). The scale bar = 5 mm (white).

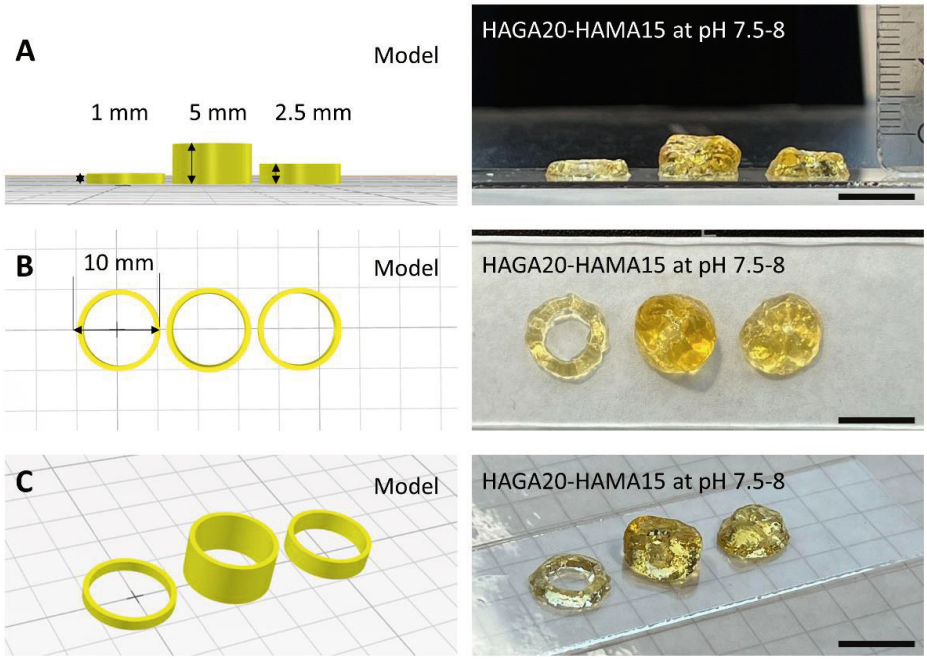

Figure 56. The images of 3D printed cylinders (HAGA20-HAMA15 at pH 7.5–8), varying the height: 1, 2.5 and 5 mm, compared to the CAD model. (A) Side view, (B) top view, and (C) isometric view. Scale bar = 10 mm.

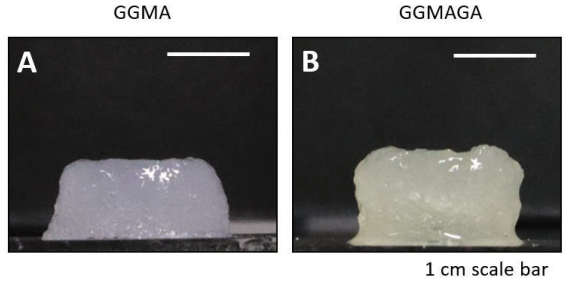

Figure 57. The printed structures of (A) GGMA and (B) GGMAGA using the pre-crosslinking with UV light.

5.4.2 Viscoelastic properties

The viscoelastic properties of the hydrogels were determined using small amplitude oscillatory shear (SAOS) tests. The rheological tests included amplitude, frequency sweep and stress relaxation. The obtained parameters were storage (G'), loss modulus (G"), tan δ, average mesh size (ξ) and crosslinking density (n_e), as shown in Table 6. The amplitude and frequency sweeps were performed in **Publications I–IV**. The parameters: G', G", tan δ and n_e of different precursors with and without pre-crosslinking are presented in Table 6. For all hydrogels, the G' was higher than G" (the elastic modulus is higher than the viscous modulus), as confirmed by the tan δ value being lower than 1. The results also showed that pre-crosslinking and % MD of methacrylate significantly increased the G' and tan δ values were lower than 0.1, compared to the hydrogel without pre-crosslinking.

In detail, in **Publication I**, the G' and G" measurement plots of different %MD, UV intensity and curing time from the LVR strain are presented in Figure 58. The results showed that the G' of hydrogels increased when the UV curing dosage (intensity and exposure time) and %MD increased. Moreover, high MD and UV curing corresponded to a higher degree of crosslinking and a smaller average mesh size, which led to stiffer hydrogels. The contact angle measurements also confirmed that the denser hydrogel network led to more hydrophobic hydrogel samples. In **Publication II**, the results show the corresponding effect of the $CaCl_2$ pre-crosslinker and UV curing time on the viscoelasticity, mesh size and crosslinking density of GGMA hydrogels (Table 6). In **Publication III** (Figure 59), GelMA30 and GelMA60 were used as controls to assess the effects of gallic acid functionalization and a pre-crosslinker. Gallic acid functionalized GelMA30 significantly increased G', but no significant increase of G' was observed in GelMA60. On the other hand, GelMA30GA and GelMA60GA yielded higher G' values when the $FeCl_3$ was added. Moreover, hydrogel samples increased the elasticity when gallic acid was grafted to the GelMA backbone and the elasticity showed further improvement when $FeCL_3$ was added to GelMAGA hydrogels, as observed in Figure 59B. The GelMAGA hydrogels exhibited higher cross-linking density, resulting in stiffer hydrogels and smaller average mesh sizes. Among all ink formulations, GelMAGA with $FeCl_3$ had a significantly smaller average mesh size due to higher values of G' and crosslinking densities. As shown in Figures 59C, D and E, the rapid transition between elastic and viscous states between low and high strain indicates the strain recovery behavior of the hydrogels during the cyclic test.

The HAGA-HAMA hydrogels showed high recoverability of the polymeric networks (especially HAGA20-HAMA15), suggesting the dynamic nature of the complementary network between gallol moieties and photocrosslinking. On the other hand, HAMA15 groups lost their initial properties after the first high strain. In **Publication IV** (Figure 60), HAGA-HAMA was shown to have the ability to transform into a true hydrogel at high pH. As a result, the viscoelasticity of hydrogels with and without photocrosslinking was evaluated to compare the influence of gallic acid functionalization, %MD of gallic acid and photocrosslinking. The results showed that HAGA-HAMA with photocrosslinking yielded a slightly higher G' than HAGA-HAMA without photocrosslinking. There were no significant differences in viscoelastic properties between the two groups. On the other hand, the HAGA-HAMA blend had an improved stress relaxation compared to pure HAMA, as shown in Figure 62. Figure 61 shows that GA grafted to the GGMA backbone gained higher storage moduli than plain GGMA. In contrast, GGMAGA traded the mechanical strength with viscoelastic properties, observed in the reduction in the storage modulus as the frequency increased. GGMA remained more stable, and the storage modulus dominated the loss modulus.

Table 6. Overview of all precursor formulations: pre-crosslinking conditions and rheological properties of resulting hydrogels.

Precursors	Pre-crosslinking	G' [Pa]	G" [Pa]	tan δ	ξ [nm]	n_e	#
GelMA30	-	478±32	9±5	0.01	20.5±0.1	0.19	**I**
GelMA60	-	594±56	45±4	0.07	19.0±0.1	0.24	**I**
GelMA30	Temperature	1022±40	16±5	0.01	16.0±0.2	0.41	**I**
GelMA60	Temperature	1100±40	62±6	0.05	15.5±0.2	0.44	**I**
ColMA30	-	1655±38	78±85	0.04	13.5±0.1	0.66	**I**
ColMA60	-	1800±60	38±2	0.02	13.2±0.1	0.71	**I**
HAMA30	-	2420±250	840±45	0.34	12.0±0.4	0.98	**I**
HAMA60	-	3650±150	150±5	0.04	10.4±0.1	1.47	**I**
AlgMA30		2200±85	360±8	0.16	12.3±0.2	0.88	**I**
AlgMA60		3700±850	2020±250	0.54	10.3±0.6	1.50	**I**
2% GGMA	-	2450±56	79±13	0.03	12.0±0.3	0.97	**II**
2% GGMA	90 mM of $CaCl_2$	3375±61	46±21	0.01	10.6±0.2	1.47	**II**
GelMA30GA	-	1631±14	39±5	0.02	13.6±0.2	0.65	**III**
GelMA60GA	-	662±63	94±11	0.14	18.8±0.5	0.26	**III**
GelMA30GA-5Fe	30 mM of $FeCl_3$	4454±224	135±14	0.03	9.7±0.7	1.79	**III**
GelMA60GA-5Fe	30 mM of $FeCl_3$	2166±346	116±4	0.05	12.3±0.8	0.87	**III**
HAGA10 HAMA15	Basic pH	594±2	58±3	0.09	19.0±0.1	0.24	**IV**
HAGA20 HAMA15	Basic pH	1000±66	57±6	0.05	16.0±0.5	0.40	**IV**
2%GGMA	Photocrosslinking	1118±37	101±2	0.09	15.4±0.1	0.45	**-**
2%GGMAGA	Photocrosslinking	1752±14	63±1	0.03	13.3±0.2	0.70	**-**

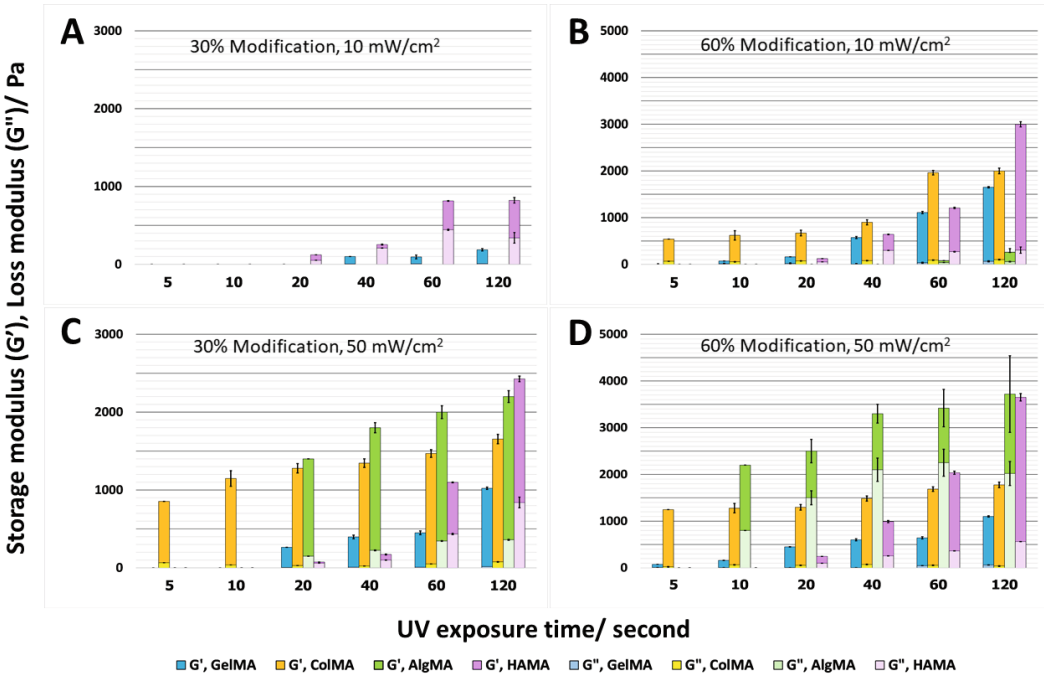

Figure 58. The storage (G') and loss moduli (G'') of the crosslinked hydrogels with different modification degrees (30% and 60%) crosslinked with low/high UV intensity and varying exposure time. (A) Hydrogels with 30% modification degree, and (B) 60% modification degree at 10 mW/cm^2 UV intensity for 5–120 s. (C) 30% modification degree, and (D) 60% modification degree at 50 mW/cm2 UV intensity for 5–120 s.

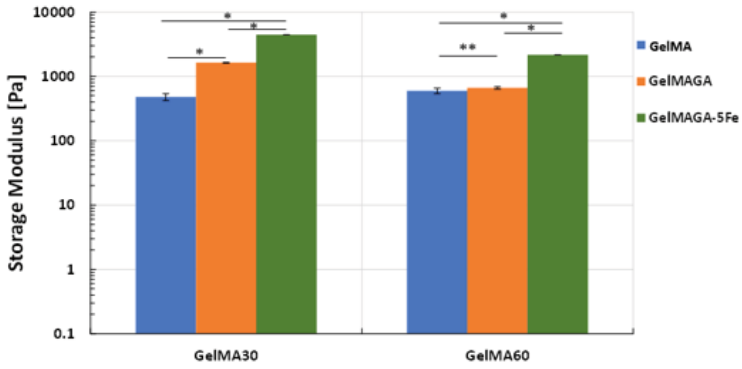

Figure 59. Oscillatory measurements of all hydrogel samples: GelMA30, GelMA60, GelMA30GA, GelMA60GA, GelMA30GA-5Fe and GelMA60GA-5Fe, measured via amplitude sweeps at RT. The error bars indicate the standard deviation of storage modulus for each ink, presented as Mean ±SD (n=10, *p < 0.05, **insignificant).

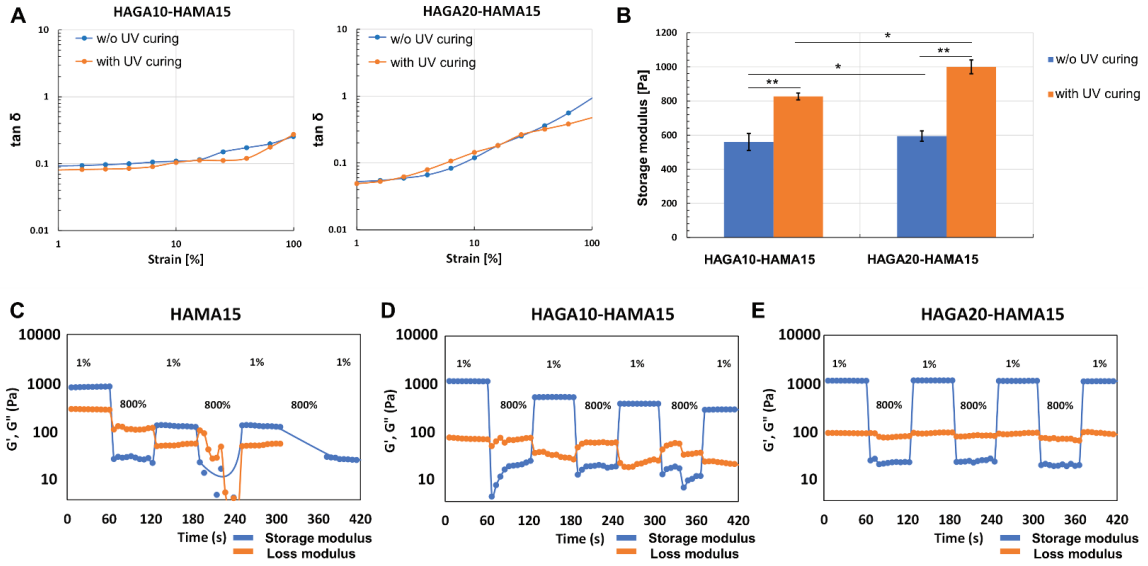

Figure 60. Oscillatory measurements of all hydrogel samples were tested using frequency and amplitude sweeps. (A) tan δ value, calculated from the ratio between G' and G" from the amplitude sweep to observe the viscoelasticity of hydrogels (with and without UV). (B) Storage moduli of hydrogels (with and without UV) obtained from the linear region of amplitude and frequency curves. The error bars indicate the standard deviation of storage modulus for each ink, presented as mean ±SD (n = 10, *p < 0.05, **insignificant). (C, D, E) The comparison of strain recovery behavior of hydrogels with the complementary network (HAGA10-HAMA15 and HAGA20-HAMA15) and without the complementary network (HAMA15). The strain recovery behavior was measured through seven cycles of strain (1% strain → 800% strain → 1% strain).

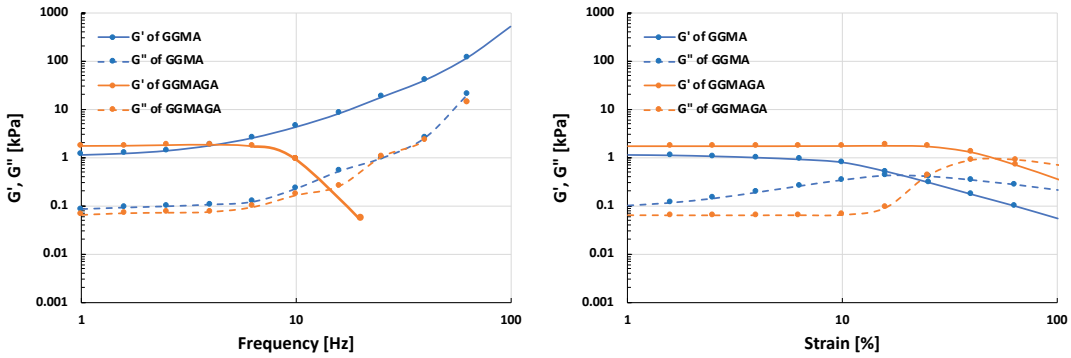

Figure 61. The oscillatory measurement of GGMA and GGMAGA was performed by frequency and amplitude sweep (n = 3).

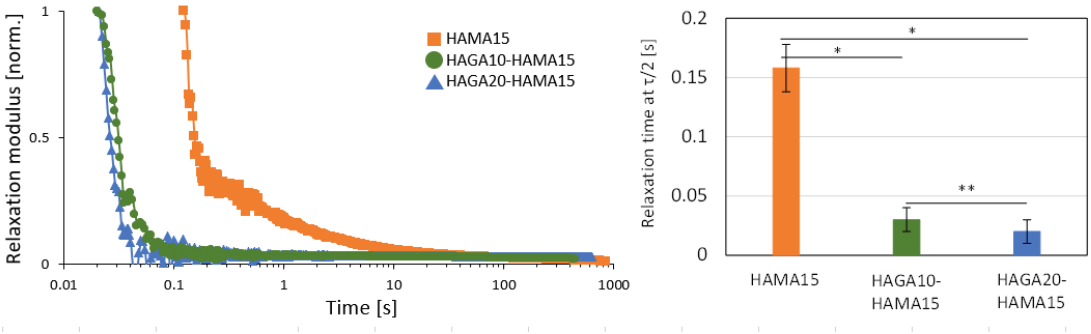

Figure 62. Stress relaxation tests on HAGA-HAMA and HAMA hydrogels. The hydrogel samples were tested with 5% strain, which was then held at a constant rate for 1000 seconds. The error bars indicate the standard deviation of storage modulus for each ink, presented as mean ±SD (n = 10, *p < 0.05, **insignificant).

5.4.3 Swelling behavior

The swelling kinetics of all hydrogel samples in this study were determined from the swelling ratio as a function of time. The swelling tests were performed in deionized water, cell culture media (**Publications II & III**) and DPBS (**Publication III**). The pH of DPBS in **Publication IV** was adjusted into 5, 7 and 8. The swelling ratios of the hydrogel samples are shown in Figures 63-66. The unpublished results show the swelling kinetics of GelMA60, which was used as a control. GelMA60 hydrogels in DI water, DPBS and DMEM swelled slightly on the first day, leading quickly to the dissolution of the structures after 24 h, however, the data is not included in any Figure. In **Publication II**, the results showed that hydrogels (2% GGMA-90mM) in deionized water significantly swelled in the first three days and became stable until the end of the observation period, as shown in Figure 63. In contrast, 2% GGMA-90mM started to shrink in DMEM because of the presence of divalent ions. When compared to other hydrogels (GelMA30GA, HAGA-HAMA and plain GGMA) in DMEM, 2%GGMA-90mM shrank the most because of the carboxylic group in the gellan gum backbone and $CaCl_2$ residual. Similar behavior was observed in DPBS. In **Publication III** (Figure 64), GelMA30GA hydrogels in DI water swelled the most, whereas the hydrogels in DPBS shrank rapidly on the first day. In contrast, the GelMAGA hydrogels were stable in DMEM. In **Publication IV**, Figure 65 shows that all HAGA-HAMA swelled rapidly after the first time point and stabilized after 2-3 days of observation. On the other hand, all HAGA-HAMA hydrogels

revealed a huge difference when submerged at acidic pH, as the swelling ratio was higher than those at neutral and basic pH. Moreover, the HAGA10-HAMA15 groups showed a greater swelling ratio than the HAGA20-HAMA15 (4 and 2, respectively). In GGMA-GA hydrogels (Figure 66), the swelling tests showed that in the cell culture medium, GGMA-GA started to shrink rapidly on the first day, whereas GGMA hydrogels remained stable. Both the GGMA and GGMA-GA hydrogels shrank slightly and became stable until the end of the observation period, but the hydrogels containing GA shrank somewhat more.

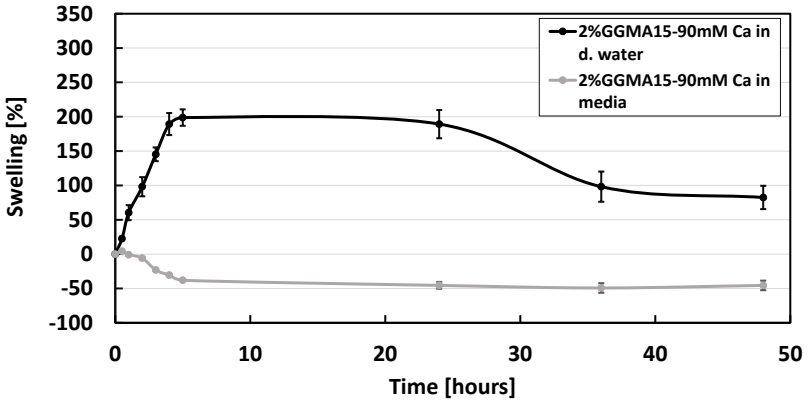

Figure 63. Swelling behavior of the printed GGMA structures. The samples were immersed in two different media: DI water and DMEM.

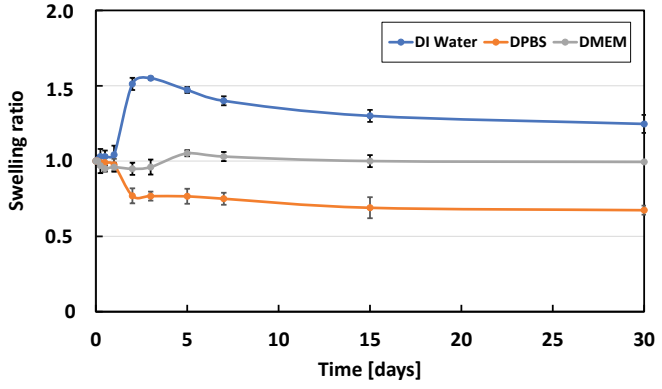

Figure 64. Stability test of 3D printed GelMA30GA-5Fe structures in DI water, DPBS and DMEM for 30 days. The mean (n = 3) and standard deviation are shown.

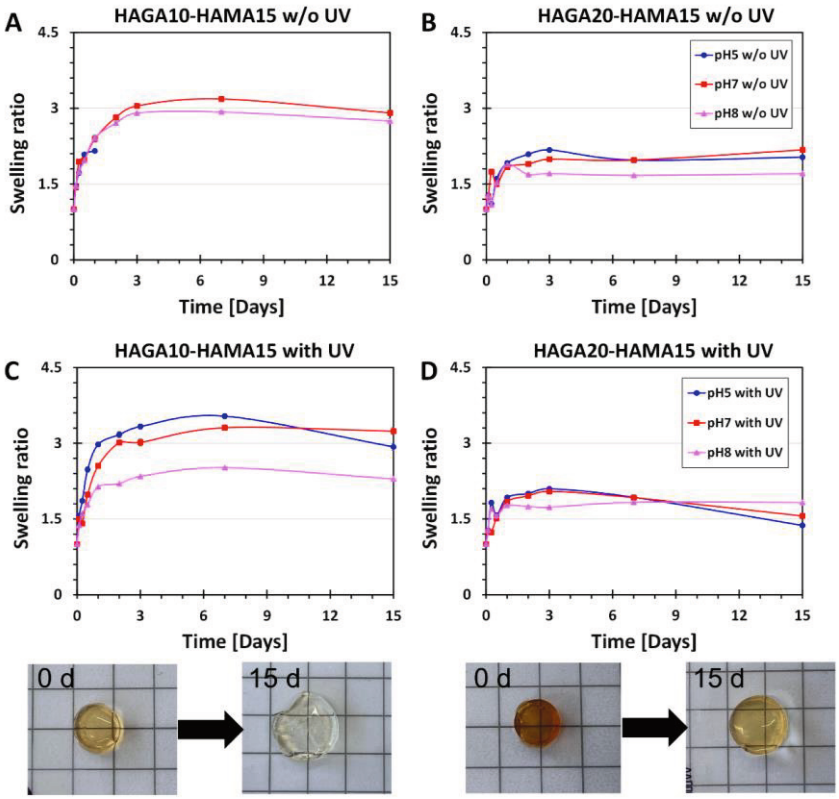

Figure 65. The time-dependent swelling behavior of HAGA10-HAMA15 and HAGA20-HAMA gels as a response to different pH (5–8). The swelling ratio of hydrogels (A) HAGA10-HAMA15 and (B) HAGA20-HAMA15. The hydrogels before and after swelling are shown here as examples, 1 cm^2 grid scale. The mean (n = 3) and standard deviation are shown.

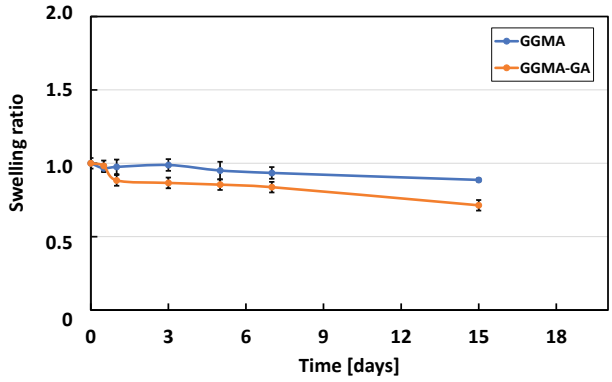

Figure 66. Swelling behavior of the printed GGMA and GGMA-GA structures. The samples were immersed in DMEM. The mean (n = 3) and standard deviation are shown.

6 DISCUSSION

6.1 Precursor functionalization and hydrogel properties

Photocrosslinkability offers flexibility to the hydrogels, enabling them to be processed into various shapes or forms, such as thin films and 3D structures, which provides advantages over other crosslinking methods[164,200]. The selection of natural precursors, such as polypeptides and polysaccharides in bioprinting technology, varies in properties depending on the polymer backbone, crosslinking kinetics, cellular cytotoxicity, and printability. Precursors may be modified depending on the properties of the polymers and target applications. Precursors for injecting and direct extrusion printing usually share similar requirements, such as polymer concentration, degree of modification, and crosslinking types[8]. In **Publications I–IV**, photocrosslinkable natural precursors were achieved by the methacrylation of polypeptides and polysaccharides and crosslinked in the presence of a photoinitiator. The degree of methacrylation in polypeptides and polysaccharides was adjusted by modulating the nucleophilicity of hydroxy groups in polysaccharides and amine groups in polypeptides at a basic pH. This modulation facilitated the rapid nucleophilic attack of the hydroxy/amine groups onto the anhydride linkage. The reaction between the carboxylic group of methacrylic anhydride in GelMA primarily interacts with the primary amine of gelatin (methacrylamide), but hydroxyl groups are also involved in this substitution reaction (methacrylate)[32]. The tunability of the precursors enabled us to control the properties of the materials, which is crucial for various hydrogel-based applications[54]. The precursor concentrations were held at 5% w/v; however, GGMA has low solubility at 5% w/v, which resulted in lower concentrations (2–3% w/v). It has also been reported that low precursor concentrations are more suitable for biomaterial ink preparation because they can maintain high cell stability and viability[201,202]. However, low-concentration precursors lose their processability during extrusion, which will be discussed below. The modification degree for polysaccharide and polypeptide-based polymer have been determined using different methods: ^{1}H-NMR for polysaccharide and UV-vis for polypeptide because UV-vis spectroscopy revealed a more distinctive peak for free primary amines in pure polypeptides. Moreover, the viscoelasticity parameters

of hydrogels, such as the storage modulus, reflect the structural properties of hydrogels, including crosslinking density and mesh size. These properties directly influence the structural integrity and swelling behaviors of final hydrogel constructs. The calculation of crosslinking density and mesh size from rheology allows us to briefly investigate the network structure of hydrogels[153]. It is important to note that these calculations only provide the theoretical values of the structure.

In **Publication I**, the concentration of hydrogels was fixed at 5% w/v. It is important to note that the viscosity of the precursors and the rigidity of the resulting hydrogels were influenced by the varying molecular weight ranges of the initial biopolymers (300 bloom strength in gelatin, 100 kDa in hyaluronan). Environmental factors such as temperature played a role in these variations[1]. As a result, the crosslinking density and the average mesh size of the hydrogels were also influenced by these factors[153]. To tailor the end products, such as scaffolds, according to the specific needs of cells or tissues, two different degrees of methacrylation (30% and 60%) were used to achieve hydrogels with variable crosslinking densities and stiffness properties[203]. In addition, the exposure time and UV intensity could be adjusted to match the mechanical stiffness of the specific cell type (native tissue varying from neural tissue to liver tissue)[203]. The degree of methacrylation can also be adjusted to modulate the hydrogel properties, such as gelation time and mechanical strength[204]. For instance, in **Publication I**, the gelation kinetics of the precursors were adjusted by varying the degree of methacrylation, UV intensity and exposure time. In addition to the main study, the use of different types of photoinitiators also influenced the gelation time of hydrogel. For example, GelMA60 in the presence of LAP resulted in faster gelation time and higher storage modulus, compared to Irgacure 2959 at the same concentration because LAP can be activated in visible light and broader wavelength due to its higher molar extinction coefficient at 365 nm (218 M^{-1} cm^{-1})[56]. The *in situ* photorheology results showed that the storage moduli of the hydrogels increased with time and reached a plateau after 60 s of UV exposure, indicating that the precursors were fully crosslinked, as explained in the literature[1]. In **Publication II**, the final storage modulus of GGMA was highly dependent on the precursor concentration, but the gelation time did not differ significantly among the various tested polymer concentrations. In 3D bioprinting, the gelation kinetics of the precursors are crucial because the precursor must be crosslinked immediately after deposition on the substrate. Therefore, in these studies, the UV exposure times for layer-by-layer curing during printing and post-curing phase were determined based on the conditions of the *in situ* photorheology.

To be more specific, a UV intensity of 25 mW/cm^2 was applied for 10 s for each layer during printing and 60 s for the post-curing process. These UV dosages were chosen to ensure sufficient crosslinking and achieve the desired structural integrity for the printed constructs.

In Publication III, by adding GA to the GelMA hydrogel backbone, mechanical properties and tissue adhesion improved. This enhancement is attributed to the covalent bonds formed between the catechol group in GA and the amine group in GelMA. In the preparation of GelMAGA, GelMA was synthesized with two degrees of methacrylation (30 and 60%), followed by the grafting of 10% gallic acid onto the backbone of GelMA. The methacrylation was achieved by nucleophilic reaction of residual amine on gelatin molecules and methacrylic anhydride, whereas the gallic conjugation was achieved by EDC-mediated amide coupling reaction. As a confirmation of the successful conjugation of gallic acid, GelMAGA solution turned brown at a basic pH. Several studies have highlighted that increasing the modification degree of gelatin leads to reduced physical interactions among polymer chains. This effect results in lower viscosities of the precursors and lower temperatures for the sol-gel transition, as reported in multiple studies[161]. The difference in the results of GelMA60 between Publication I and III could be from batch-to-batch variations in the gelatin source. According to the results, GelMA60GA precursor displayed less thermostability compared to GelMA30GA. Similarly, the higher modification degree of GelMA led to the lower formation of the triple helix structure because of reduced ionic and dipole-dipole interactions between gelatin molecules. As a result, the physical network of the hydrogel becomes looser, leading to decreased thermostability[161].

In **Publication IV**, pH-responsive hyaluronic acid-based (HA) precursors were synthesized and grafted with GA moiety. GGMA backbone was also functionalized with GA. The degrees of GA functionalization were ~10 and 20% with respect to the disaccharide repeat units. In HA and GG, GA was conjugated to polysaccharides via carbohydrazide linkages utilizing the carboxylic group on the polymer backbone and hydrazide group from amine-functionalized GA using carbodiimide coupling chemistry. The carboxylate residues of GA were modified to a hydrazide derivative as they are known to undergo proficient EDC coupling at acidic pH (4.7–4.8). The successful conjugation of GA was confirmed as the solution turned light brown at basic pH (~8), indicating that GA functionalization was successful in grafting to the HA backbone, as also demonstrated in **Publication III**. The GA modification

degree was confirmed by H-NMR. The HAGA-HAMA hydrogels in **Publication IV** demonstrated improved viscoelastic behavior compared to plain HAMA hydrogels. The dual crosslinking of gallol-mediated network and covalent bonds from photocrosslinking created a complementary network in the HAGA-HAMA hydrogels. An increase in the storage modulus and elasticity was observed, indicating a more stable matrix formation. This complementary network in HAGA-HAMA hydrogels displayed more stress relaxation than HAMA alone. In order to evaluate the effectiveness of complementary networks in HAGA-HAMA hydrogels, a series of rheological recovery tests were performed on G' and G" with seven cycles of low and high strain. It was found that HAMA hydrogels lost their initial G' value after the first cycle because they were formed via a single network, resulting in a brittle hydrogel structure. According to the results, the G' of the HAGA10-HAMA15 and HAGA20-HAMA15 hydrogels under high dynamic strain decreased due to the deformation of the hydrogel network. After the low strain, they quickly returned to the original G' value as the hydrogel construct recovered, especially in hydrogels with higher GA modification. The strain recovery of hydrogels may increase due to the addition of secondary crosslinking, such as interpenetrating and complementary networks. In addition to the other features, GA-functionalized hydrogels in **Publications III–IV** demonstrated tissue adhesion.

6.2 From precursor to biomaterial ink

A biomaterial ink is a printable hydrogel precursor. The wide range of precursors and their functionalization in the performed studies allow flexibility in choosing a proper precursor for each fabrication method: casting, injecting, or extrusion-based 3D bioprinting. It is important to note that not all single biomaterial ink is suitable for all bioprinting methods. Each bioprinting technique requires bioinks/biomaterial inks with specific rheological and mechanical properties to ensure highest quality of printing outcomes. It has been reported that temperature[26], ionic[16], and metal chelation crosslinking[17] result in the formation of noncovalent hydrogels. For instance, Ouyang et al. and Yin et al. employed the two-step crosslinking approach by utilizing low temperature as a primary crosslinking to maintain shape fidelity of gelatin-based bioink, followed by photocrosslinking as a secondary crosslinking[26, 72]. Another example is the blend of alginate with photocrosslinkable bioinks, such as GelMA. In this blend, the ionic crosslinking of alginate serves as the primary mechanism, while the photocrosslinking of GelMA acts as the secondary crosslinking[170]. Based on this understanding, I utilized these crosslinking techniques

as a pre-crosslinking method to enhance printability. The photocrosslinking in the post-printing stage was then employed to produce self-supporting hydrogels. Hence, I developed a two-step crosslinking strategy inspired by noncovalent interactions and covalent crosslinking to enhance the printability of biomaterial ink. In this thesis, I focus on extrusion-based methods, which requires shear-thinning properties of biomaterial inks. All plain precursors in the studies (**Publications I–IV**) exhibited relatively low viscosity, limiting the processability, as they can be fabricated in 3D hydrogels only by casting into a mold. For biomaterial ink, precursors with sufficient viscosity, yield stress, shear-thinning and recovery behavior can be achieved using pre-crosslinking methods. These properties are required for extrusion-based 3D bioprinting. However, some precursors possess inherent shear-thinning properties; for example, ColMA60 in **Publication I** has the optimum properties to be printed into 3D constructs without any pre-crosslinkers. Another notable example is using a high concentration of GelMA (<10% w/v), which has good shear-thinning properties, resulting in successful 3D constructs. On the other hand, high concentrations of the precursor may increase the difficulty in processing, and it also affects cell viability when mixing the cells in it. In addition, blending biomaterial inks with other polymers or peptides to enhance their processability have been used widely. However, multi-component inks could draw more complexity between research and commercialization[117]. The physical blending of two different molecular weight polymers may create an immiscible mixture as blending requires compatibility of polymer properties[16].

In this thesis, two-step crosslinking methods were introduced to widen the processing window in 3D bioprinting, as they offer higher tunability, printability, shape fidelity and mechanical properties. In general, noncovalent interaction have been used for injectable hydrogels due to their reversibility, which was considered as a primary crosslinking in this study. The long-term stability of the printed constructs was ensured by photocrosslinking to form dual-crosslinking (noncovalent, followed by covalent). The comprehensive set of different pre-crosslinking methods used in the two-step crosslinking approach was created to match the intrinsic properties of the precursor. Each pre-crosslinking method can be used specifically for each type of precursor. For example, thermal crosslinking was used in thermosensitive precursors, ionic crosslinking in alginate or gellan gum based-precursors, the metal ion in catechol-functionalized precursor, pH modulation in precursors containing phenolic moieties and controlled photocrosslinking in photocrosslinkable precursors. Two-step crosslinking in the studies enhanced the processability of low-

concentration precursors. In the initial step, the precursor is mildly crosslinked via physical crosslinking, which is reversible. The pre-crosslinked precursor demonstrates a weak and extrudable hydrogel, making it suitable for direct extrusion printing. After that, the weak hydrogel is covalently crosslinked into a true hydrogel via photocrosslinking.

In **Publication I** (temperature), The study highlighted importance of utilizing lower temperatures to enhance the printability of both GelMA30 and GelMA60 by comparing the shear-thinning coefficients between the two groups (RT and low temperature). GelMA60 at 16 °C exhibited shear-thinning and was able to maintain high viscosity during the printing process. Moreover, GelMA60 is cost-friendly, which would be beneficial for biomaterial ink preparation in high-volume 3D bioprinting. According to the results, GelMA30 and GelMA60 did not exhibit a significant difference in their sol state at room temperature (RT). GelMA precursors at low temperature were able to maintain shape fidelity during printing, followed by photocrosslinking after printing. The shear-thinning of GelMA at low temperature could be influenced by the intermolecular of GelMA when the energy of the physical bond is similar in magnitude to the thermal energy. When the shear rate reaches the critical point, GelMA coils have the ability to disorientate and align themselves in the direction of the flow, which can cause shear-thinning behavior[69]. A similar phenomenon is observed in collagen-based hydrogels, where lower temperatures can also limit the nucleation of new fibers, resulting in the thickening and elongation of existing collagen fibers, and the formation of heterogeneous networks[76]. Similar studies have used a different combination of gelatin-based bioinks such as GelMA-HAMA, alginate-gelatin, alginate-gelatin-hydroxyapatite, and GelMA-alginate blends[170,205,206]. However, the low temperature can be difficult to control throughout the printing process, as the temperatures in the cartridge, nozzle and printing bed are not equal[26,69]. Moreover, the printer also generates heat in the printing environment, which might lead to droplet formation and structural collapse during printing. According to the microscope images in the results part, the printed filament at low temperature resulted in heterogeneous structures, which could compromise the printing resolution. From a biofunctionality perspective, prolonged exposure to low temperatures can also damage the cells due to cold injury[160].

In **Publication II** ($CaCl_2$), the printability of the GGMA precursor was tuned by varying the concentration of polymer and $CaCl_2$. This pre-crosslinking technique using $CaCl_2$ is a well-known and widely used approach for improving the printability

of alginate and nanocellulose precursors, but it has not been previously used for GGMA precursors[2,89,90,134,162–164]. Gellan gum-based precursor exhibits thermo- and ionotropic gelation, in which the viscosity of gellan gum increases when the temperature decreases because it can self-orientate from a random coil state into a double helix structure, which can be further improved in the presence of cations[99,106]. These unique properties exhibit behavior similar to that of the combination of gelatin and alginate-based hydrogels, making them potential candidates for bioink development. Several studies have reported that the mixture of gellan gum and divalent ions has been used to increase the elastic modulus of the resulting bulk hydrogels[102,107,108]. A limitation of gellan gum lies within its advantages, which is the temperature-dependent and ionic crosslinking, leading to fluctuating mechanical properties when the environment changes[108]. However, the combination between ionic and photocrosslinking has not been widely used in bioprinting. Incorporating calcium ions into the GGMA precursor turns the liquid precursor into a shear-thinning precursor, even at low GGMA concentrations, enabling them to maintain the 3D shape before photocrosslinking. Although the technique is simple and easy to access, the inappropriate concentrations of GGMA and $CaCl_2$, either too low or too high, can affect the fiber quality during printing because GGMA precursor can form into a true hydrogel at a high $CaCl_2$ concentration[135].

In **Publication III** ($FeCl_3$), the shear-thinning behavior and thermostability of GelMA were enhanced by pre-crosslinking with $FeCl_3$ via catechol−Fe^{3+} chelation, allowing lower polymer concentrations to be printable at RT or physiological temperature (37 °C). Adding a proper amount of Fe^{3+} to GelMAGA precursor can enhance its viscosity and yield a weak hydrogel by providing primary crosslinking of the precursor. After printing each layer, the ink was stabilized by secondary crosslinking using UV light. This two-step crosslinking approach significantly improved the printability of low-concentration GelMA-based biomaterial inks (5% w/v) due to noncovalent interactions of catechol−Fe^{3+} chelation[207]. The formation of a loose hydrogel network is a result of the coordination bonding between trivalent ferric ions and the hydroxyl groups of GA. This phenomenon significantly enhances the viscosity of the inks[17,138]. Moreover, the $FeCl_3$ pre-crosslinked GelMAGA was not affected by the temperature transition from low to high due to the primary crosslinking with Fe^{3+}. The same rule is applied when the pre-crosslinking agents are involved in the pre-processing step; the precursor can turn into a true hydrogel if the concentration of the pre-crosslinker is too high.

In **Publication IV** (pH modulation), the precursor blend (HAGA-HAMA) exhibited pH-responsive properties necessary to improve both printability and injectability. Furthermore, blending enhanced the viscoelastic behavior of printed hydrogels after photocrosslinking. The shear-thinning precursors prepared by gallol-containing polymers utilized direct gallol-to-gallol covalent linkages at a basic condition (pH 8). The benefits of using pH-responsive precursors in the clinics are that the precursors can be bioprinted at neural-basic pH (7.3–9.8) on damaged skin[208] and be triggered to degrade at low pH (4–6) on healthy skin[209]. In bioprinted wound dressing applications, the pH-responsive non-Newtonian precursors enable the *in situ* bioprinting of the precursor in the wound, allowing shape-specific fitting and stability of the printed construct[8]. In addition, among all reversible bonds of hydrogels, this pH-responsive behavior offers wide flexibility in terms of bonding strength and dynamics by varying the pH of the precursor, as it provides pH-tunable crosslinking degree, fast network formation, and self-healing behavior[138,210]. However, too high basic pH can result in a rapid sol-gel transition, ultimately forming the precursor into a true hydrogel that is not extrudable.

The controlled photocrosslinking was applied to GGMA-GA to ensure the improvement of processability. Pre-crosslinking with UV light (UV intensity of 10 mW cm^{-2} for 30 s) caused high and inconsistent extrusion forces during printing, which resulted in irregular and heterogeneous printed structures[33]. In contrast, the precursors formed using pre-crosslinking agents were printed with consistent filaments. However, some parameters need further exploration to improve the resolution of 3D-printed structures. For example, a higher gallic acid conjugation could provide better self-healing properties to hydrogels, leading to a smooth and regular filament after extrusion[138,210]. It is important to note that the flow behavior of these precursors, including viscosity values and shear-thinning coefficients, varied across **Publication I-IV**. This due to the properties of modified-natural polymer, in which the natural polymers are derived from biological sources (production and extraction process), leading to a broad molecular weight distribution. In addition, modified natural polymers possess innate functional groups distributed randomly along their chains, unlike synthetic polymers[52]. These functional groups can participate in hydrogen bonding, ionic interactions, and other secondary interactions, which influence the efficiency of crosslinking and, consequently, their rheological properties. The degree of MA (methacrylated in polysaccharides and methacryloyl in polypeptides) modification in precursors can vary due to batch-to-batch inconsistencies during the functionalization[53]. The chemical modification for natural

polymers is influenced by various factors including reaction time, and environmental conditions. Even slight changes in these parameters can lead to variations in the degree of modification.

6.3 Printability of biomaterial ink

Several researchers have investigated the critical parameters to determine a precursor "printable" and various quantitative methods to evaluate the true printability of a precursor. In my thesis, the assessment of true printability was conducted in a step-by-step process, including pre-screening via visual analysis (fiber formation and stackability), flow behavior (rheology), a score of printability value (Pr), and quantification of the structural integrity of 3D printed construct.

The first step to assess the printability of a precursor is to pre-screen the fiber formation and stackability after extruding from a nozzle. An extruded precursor with high printability should produce smooth fibers that can hold their own weight in the air and stack layer-by-layer to form a 3D structure. Generally, the precursors require sufficient viscosity to exhibit these behaviors. The droplet-smooth filament transitions have been achieved by raising precursor concentration, crosslinking agent concentration, and thermal gelation. This transition indicates a dominant factor influencing the precursor behavior. The precursor exhibiting droplets is dominated by surface tension and water molecule interactions, while filament formation is associated with the formation of the polymer network as precursor concentration and gelation increase. A droplet formation of a precursor, after being extruded from a nozzle, generally has poor printability. However, smooth filament formation cannot guarantee good printability. Therefore, filament quality checkup is used as a pre-screening tool to quickly screen biomaterial ink candidates. Thermal crosslinking was utilized in **Publications I & II** to increase the viscosity of thermo-responsive precursors. During the pre-screening test, the GelMA60 precursor formed a droplet at RT, but it was able to produce a smooth fiber after cooling to 16 °C. On the other hand, GGMA, at low temperature was able to produce a smooth fiber and stack only a short period of time before deforming. The viscosity of GGMA increased after exposure to low temperature, but it was not able to hold its shape. The explanation for this result could be the rapid change in temperature of GGMA precursor during and after printing, as the printed filament suffered from

the significant temperature difference between the nozzle and external environment (4 °C to RT).

As mentioned in the literature review, high precursor viscosity does not guarantee the shear-thinning ability or high shape fidelity after printing. The printable precursor must possess sufficient yield stress, which contributes to its extrudability and retention after printing. A precursor with yield stress will demonstrate better shape fidelity after deposition on the printing bed compared to those without yield stress. A precursor with proper yield stress value forms good fibers and stacks into 3D structures without collapse, as it can flow consistently from the nozzle and retain its shape after deposition. In addition, the recovery behavior or thixotropy is the precursor's ability to return to the original properties after extrusion. Therefore, the values of shear-thinning coefficients and yield stress were used to explain printability in extrusion-based 3D bioprinting. Choosing the correct method to evaluate the deeper relationship between printability and rheological properties is also important. Mathematical models such as Power Law and Herschel-Bulkley models are used to determine printability from shear-thinning coefficients. For example, in **Publication II**, GGMA precursor was pre-crosslinked with $CaCl_2$, resulting in improved shape fidelity, as it was able to form a smooth fiber after being extruded from a nozzle. According to the rheological data, the viscosity of GGMA changed as a function of the $CaCl_2$ concentration and obtained yield stress. In **Publication III**, a catechol metal complex was introduced into GelMA-based precursors, and $FeCl_3$ was used as a pre-crosslinker to improve the precursor's printability and stability at physiological temperature. According to **Publication I**, low-concentration GelMA is highly dependent on temperature change, which may cause a narrow fabrication window during printing. In **Publications II & III**, pre-crosslinked precursors shared the similarity that they all possess yield stress, which was confirmed by the Herschel−Bulkley model. In addition, the Power Law model confirmed shear-thinning performance in these precursors, giving n values < 0.3. The recovery test results also showed that a higher pre-crosslinker amount in precursors improved recovery behavior in all precursor concentrations. This improvement can be attributed to the reversible interaction of ionic crosslinking (**Publication II**) and GA-Fe^{3+} ions (**Publication III**). However, it is important to note that the tuning of the pre-crosslinker concentration needs to be meticulous, as an incorrect pre-crosslinker amount can lead to poor printability, such as liquid-like or over-viscous ink. In **Publication II**, a low concentration of $CaCl_2$ in GGMA generated low ionic strength in the hydrogel network, resulting in weak extrudable hydrogels.

Publications III & IV demonstrated that the catechol and gallol moieties acted similarly and could be used as pre-crosslinkers to form dynamic physical networks. In **Publication III**, the results were interpreted that the favorable shear-thinning and recovery behavior of the inks was due to the multiple long-range ionic interactions caused by quadruple hydrogen bonds between Fe^{3+} and the phenolic groups. In **Publication IV**, the formation of shear-thinning precursors was based on weak phenolic interactions between HA and GA, primarily through hydrogen bonding. The HAGA component acted as a pre-crosslinker, activated by the pH change. This precursor's printability depended on the modification of GA and the concentration of HAGA in the blends. However, this blend was observed to undergo a fast reversible sol-gel transition at basic pH, resulting in the formation of a soft hydrogel. Flow behavior measurement was not possible to obtain the rheological data because the blend slipped from the parallel plate at high-velocity centrifugal movement during the measurement. Therefore, the Cox-Mertz rule was applied to convert the frequency sweep via oscillatory measurement to a viscosity-shear rate plot, followed by Power law analysis to obtain shear-thinning coefficients, giving n values < 0.2.

Based on the prescreening and rheological measurements, the precursor that meets the printability requirements is then chosen to be printed into a grid structure to determine the printability score (Pr). The score is obtained by calculating the average pore geometry inside the grid structures. Nivea crème and poloxamer were used as controls for evaluation because the extruded fibers were highly consistent and maintained their shape fidelity without merging/breaking during printing, giving Pr values close to 1. In **Publication II**, it was clear that plain high-viscosity precursors that exhibited poor shape fidelity according to pre-screening results could not be printed into grid structures, even if the temperature was adjusted to 4 °C. In **Publications II & III**, the pre-crosslinkers improved the printability of the precursor when either the concentration precursor or pre-crosslinker was increased. In **Publication IV**, the printable precursor exhibited more viscoelastic behavior (i.e. a hydrogel-like precursor). As a result, the precursor was difficult to extrude from a small-sized nozzle. However, the pore filling of a grid CAD model needed to be adjusted because the precursors exhibited die swelling after extrusion, resulting in each filament in the grid structure being wider than the nozzle size. For the printed precursors with low Pr values (below 0.8), the pores within the grid structures were observed to be fused together, leading to an assessment of poor printability. On the other hand, in the case of printed precursors with high Pr values (above 1.1), the

square shape of the pores deviated from the CAD model, also leading to an assignment of poor printability.

The precursor with the best Pr value was selected as a "biomaterial ink" for printing into a 3D printed construct. The structural integrity of 3D printed constructs was evaluated from the best ink formulations. Nivea crème and poloxamer were also used as controls for the 3D printed constructs because the deviation from the CAD model was not noticeable, and they can represent a perfect example of material behavior during the printing process. The structural analysis of printed 3D structures and comparison to control samples followed the methodology described by Paxton et al. and Gao et al. According to the structural integrity analysis, the structures of GGMA inks (**Publication II**) exhibited higher errors compared to the control structures. It was assumed that the reason was the low rheological recovery degree of GGMA, which was only 70–90%, and the structural integrity ratio exceeding 1.0. The deposited fibers on the glass substrate exhibited swelling and increased dimensions in each printed layer. The wall thickness showed the highest error, and the deviation accumulated with the number of printed layers. For GelMAGA inks in **Publication III**, the measured diameters of the printed cylinders matched relatively well with the control group. However, the wall heights were larger, indicating the die swelling of the extruded filament. The inaccuracy of the 3D printed constructs was also supported by the characterization of the filament shape displaying die swelling of GelMA30GA-5Fe (RT). A comparison of the top and side views of the cylinders clearly indicates that GelMA30GA-5Fe managed to maintain satisfactory structural integrity and was successful in multilayered printing. However, in **Publication IV**, only four-layer high 3D-printed constructs were achieved as they started to deform on the fifth layer, indicating poor structural integrity. According to the literature review, the storage modulus and tan delta of hydrogels can also predict the structural integrity of the printed construct. The printed hydrogel structures that possess a high storage modulus and a tan delta value of less than 1 can sustain their own weight after multiple layers of printing, assuming high structural integrity. These results proved that the crosslinking density and mesh size of hydrogels were not only factors to determine the swelling behaviors or diffusion properties. In **Publications II & III**, the printed constructs in the presence of pre-crosslinkers provided high storage modulus with small tan delta values, as they exhibited uniform and multi-layer printing without collapse. The storage moduli of GGMA inks (**Publication II**) increased because the GGMA was influenced by the presence of Ca^{2+} ions. The hydrogel network was formed via both physical and

chemical crosslinking. In the swelling study, the stiff GGMA hydrogel printed constructs demonstrated high crosslinking density and small average mesh size due to high storage moduli, which minimized the hydrogel deformation and swelling. The stability of GGMA hydrogels was further enhanced due to divalent ions in the cell culture medium, which can slow down the degradation of printed hydrogel constructs[211]. In the case of GelMAGA-Fe (**Publication III**), the storage moduli were significantly higher than plain GelMA. The addition of GA and Fe^{3+} improved the elasticity of the resulting GelMA hydrogels because of the double network formed between GA and Fe^{3+}. Photocrosslinking and catechol–Fe^{3+} chelation provided more interconnectivity and integrity than a single GelMA network, resulting in a more stable network compared to a single photocrosslinking approach. Crosslinking density and average mesh size affect the swelling kinetics of a hydrogel, as the higher crosslinking density results in additional network formation. As expected in the swelling test, GelMAGA-Fe swelled less than 10%, and the printed structure was able to maintain its architecture until the end of the observation period. The GelMAGA-Fe printed construct displayed high structural integrity because of high crosslinking density and small average mesh size. The higher crosslinking density resulted from dual network formation via metal-ligand complex and photocrosslinking. However, in **Publication IV**, the hydrogel swelling kinetics changed as a function of pH. The HAGA20-HAMA15 hydrogels demonstrated a slower swelling rate than the HAGA10-HAMA15 hydrogels, especially after day 1. The complementary network reduced the average mesh size, limiting the hydrogel swelling and reducing water uptake into the hydrogels. The higher crosslinking density results in additional network formation; as a result, the network structure of hydrogel is formed, which reduces water absorption.

6.4 Printing parameters: Printability window

The quality of the bioink for extrusion-based 3D bioprinters is strongly influenced by various parameters during the preparation or pre-processing phase, such as temperature, polymer concentration, and crosslinking time. From the rheological perspective of the precursor, a printable precursor with ideal properties for direct extrusion printing should have the following characteristics: (1) a weak extrudable hydrogel stage (pre-crosslinked precursor) before printing with shear-thinning, yield stress and recovery behavior, (2) fast sol-gel transition after printing to maintain shape fidelity and structural integrity, (3) low die swelling of the filament after being

extruded from the nozzle to yield the highest possible resolution for complex printed structures. In practice, a combination of these parameters can be achieved during the pre-processing phase; however, the precursor may behave differently during the processing because of the mismatch of the printing parameters, such as printing temperature, pressure, speed, nozzle size/type and more. It is worth to mention that the printability window discussed in this thesis is based on the 3D bioprinter from Brinter. Although different brands might employ the same method, values for temperature, printing speed, and pressure might vary.

The temperature adjustment in the cartridge and printing bed affects the quality of the printed filaments, particularly in thermosensitive biomaterial inks. As highlighted in the literature review section, physical crosslinking based on hydrogen bonding or hydrophobic interactions is affected by the change in temperature. The studies (**Publications I–III**) showed that the printability of thermoresponsive precursors relied on the temperature. Therefore, it is necessary to modulate the temperature in the cartridge to compensate for the rise in temperature in the nozzle. For example, GelMA at a concentration of 5% w/v demonstrated the best printability at 16-18 °C. Thus, the temperature in the cartridge needs to be cooled lower in order to achieve the optimal temperature during printing[26,31,69].

For photocrosslinkable precursors, the precursor might be accidentally cured during the printing process due to premature exposure to the light in the environment or UV-integrated module, which can result in frequent nozzle clogging or irregular filaments. However, this issue can be solved by using UV-shielded nozzles and cartridges. In addition, previous studies have shown that UV light may have limited penetration through larger 3D structures. However, photocrosslinking in a layer-by-layer manner during printing can increase the homogeneity of the printed structures. Furthermore, during printing, it is important to minimize the curing time to prevent overcuring of the printed layer, which can cause a reduction in adhesion between layers due to the photo-oxidation on the hydrogel's surface[212]. UV radiation can cause photo-oxidation, which breaks down the polymer bonds on the surface of the hydrogel[213]. If the molecular bonds on the surface are degraded, it is assumed that the surface adhesion of another layer of cured filament would be interfered. As a result, overcured filaments may become less flexible, more hydrophobic and more brittle, leading to structural collapse. For example, **Publication I** showed that the high percentage of methacrylation and high UV intensity led to a higher crosslinking density in the hydrogel network, resulting in more hydrophobic hydrogels. It is

assumed that high hydrophobicity may also disrupt the surface adhesion during printing. In addition, the concentration of the photoinitiator (Irgacure2959) in the study was fixed at 0.5% w/v, providing the absorption peak in the range of 280–365 nm (UV-A and UV-B). Irgacure2959 is water-soluble and non-cytotoxic, however, it is not an ideal choice for future bioprinting because it is insufficient when using the UV-A spectrum or visible light for photocrosslinking[214,215]. LAP is well-known as an alternative photoinitiator that has higher water solubility than Irgacure2959 and can be activated under visible light[216]. Figure 44 shows the direct comparison of Irgacure 2959 and LAP as photoinitiators. The gelation time and final storage moduli of GelMA were 10x higher with LAP compared to Irgacure2959 using 365 nm UV light at similar concentrations and exposure times. GelMA60 containing 0.05% and 0.1% LAP exposed to 365 nm UV light reached the same final storage modulus. The combination of using a lower concentration of LAP and visible light activation provides better properties than Irgacure2959. This assumes that it offers lower cytotoxicity to the cells, as the UV-B light may produce a greater genotoxic effect[217]. However, the cells were not included in the precursor mixtures in these studies, instead, they were planted in the printed structures after fabrication. In addition, Irgacure2959 provides more flexibility in choosing the microfabrication method utilizing laser-assisted 3D printers such as SLA and multiphoton polymerization, as they utilize UV-B wavelength[218,219].

Apart from the precursor properties and pre-crosslinking methods, the printability of the precursor during processing is also highly affected by the printing parameters, including nozzle type/size, layer height, printing speed and pressure. Moreover, the selection of the CAD model, such as line width, line height, solid 3D shape, and the height of the model, can affect the quality of the printing outcome. Several printability assessments from printing parameters have been performed by visual inspection and user judgement, involving a photograph from a camera or microscope, followed by image analysis with software such as ImageJ. The initial screening is to determine the relationship between the line width and printing pressure. In practice, the printing pressure, speed, nozzle size, and pre- or post-flow settings can control line width and height. The line width increases when the printing pressure rises, and the printing speed is slow. The optimal relationship between these parameters will provide a smooth line width with the same diameter as the nozzle without breaking. However, some materials may behave differently, which depends on the rheological and material properties. For example, pre-crosslinked precursor conventionally exhibits die swelling after being extruded from the nozzle. This

phenomenon will influence the line width in the first layer, which ultimately creates more errors in the final printed construct. Several researchers have reported the methodologies to address the issues. For instance, if the height of the final printed construct is more than the original CAD model, the number of printed layers can be reduced to match the desired height, resulting in better printing accuracy. Another example is when the printed filaments overlap during printing, which occurs especially in wood piles or grid structures. The filaments merge together when the gap between the two filaments is too short. For example, if the pores in the original design are too small, filaments will merge, and the pores will disappear. A similar study has been reported by Ribeiro et al., in which a filament fusion test demonstrated how the distances between filaments affect the fusion between filaments[166]. Moreover, the hydrogel bioinks are generally non-Newtonian fluids; hence, they have a response lag when starting, stopping, or changing the direction of the printing[220]. This lag may cause a collapse during printing. The time delay of the extruded materials during printing can be adjusted to match the material deposition and the moving direction of the print head.

7 CONCLUSION

My thesis provides insightful studies into synthesizing photocrosslinkable precursors, pre-screening the printability, a two-step crosslinking approach, and post-processing characterizations of dual-crosslinked 3D printed hydrogels. The basic understanding of material properties, chemistry, gelation kinetics and mechanical properties is crucial for developing or improving biomaterial inks for direct extrusion 3D bioprinting. In photocrosslinkable biomaterial ink, the selection of an appropriate type of polymer, polymer concentration, functionalization, photoinitiators, light intensity and exposure time are the fundamental factors to achieve a 3D printed construct. However, most plain hydrogel precursors are unsuitable for 3D bioprinting because they lack proper rheological properties, including shear-thinning, yield stress and recovery behavior. The studies (**Publications I–IV**) emphasized the importance of a two-step crosslinking strategy to improve the printability of hydrogel precursors with various noncovalent chemical interactions, including thermal crosslinking, ionic interactions, metal coordination, and hydrogen bonding. This customization enhanced the overall printability of photocrosslinkable biomaterial inks, facilitating the successful fabrication of complex 3D structures. In summary, the study highlighted the importance of tailoring a suitable noncovalent crosslinking method for specific polymer types and functional groups to improve the printability of biomaterial ink formulations. This knowledge will guide the development of functional tissue constructs and biomedical applications. The following conclusions were organized based on the results of **Publications I–IV**.

The synthesis of photocrosslinkable precursors and their formulations for extrusion-based 3D bioprinting (**Publications I–IV**)

- Polypeptides and polysaccharides were successfully functionalized through methacrylation chemistry with varying degrees of modification.
- GA-functionalized GelMA and HA-based biomaterial inks were synthesized via EDC coupling reaction with specific GA concentrations.

The pre-screening of printability of plain GelMA, ColMA, HAGA, AlgMA, and GGMA (**Publications I & II**).

- The concentration and degree of modification influenced the processability, viscosity, shear-thinning behavior, and fiber-forming capability of the precursors.
- The pre-screening tests, such as fiber-forming ability assessment, predicted the flow behavior of precursors, including shear-thinning, yield stress and recovery behaviors.
- Precursors with low viscosity, low yield stress, and poor shear-thinning properties are not recommended for injecting and 3D bioprinting.

Two-step crosslinking approach of precursors for extrusion-based 3D bioprinting (**Publications II–IV**)

- A two-step crosslinking technique involving pre-crosslinkers and photocrosslinking for GelMA, GGMA, GelMAGA, and HAGA-HAMA biomaterial inks was implemented.
- The optimal concentration of pre-crosslinkers transformed liquid precursors into weak, printable hydrogels that exhibited smooth and coherent fiber extrusion.
- Due to ionic interactions, the rheological profiles of GGMA with $CaCl_2$ were significantly improved compared to plain GGMA.
- Due to metal coordination bonding, the rheological profiles and thermostability of GelMAGA precursors with Fe^{3+} were improved compared to plain GelMA.
- Blending HAGA (hydrogen bonding) with other nonviscous precursors enhanced processability and reduced costs.

Post-processing characterizations of dual-crosslinked 3D printed hydrogels (**Publications I–IV**)

- Methacrylation degree and UV crosslinking conditions influenced precursor properties and resulting hydrogel stiffness and hydrophobicity.
- 3D printed structures demonstrated high shape fidelity, structural integrity, and enhanced mechanical stability.
- Dual-crosslinked hydrogels achieved through ionic interactions, catechol-Fe^{3+} chelation, and hydrogen bonding showed improved viscoelasticity and stability.

- Catechol-based adhesive precursor exhibited intrinsic adhesive properties, enhancing scaffold integration and stability.
- The swelling properties of printed GGMA and GelMAGA-Fe structures confirmed their mechanical stability in aqueous media. HAGA-HAMA hydrogels exhibited controlled swelling properties depending on the pH conditions.

REFERENCES

(1) O'Connell, C. D.; Zhang, B.; Onofrillo, C.; Duchi, S.; Blanchard, R.; Quigley, A.; Bourke, J.; Gambhir, S.; Kapsa, R.; Di Bella, C.; Choong, P.; Wallace, G. G. Tailoring the Mechanical Properties of Gelatin Methacryloyl Hydrogels through Manipulation of the Photocrosslinking Conditions. *Soft Matter* **2018**, *14* (11), 2142–2151. https://doi.org/10.1039/c7sm02187a.

(2) Mishbak, H. H.; Cooper, G.; Bartolo, P. J. Development and Characterization of a Photocurable Alginate Bioink for Three-Dimensional Bioprinting. *Int J Bioprint* **2019**, *5* (2), 12–26. https://doi.org/10.18063/IJB.V5I2.189.

(3) Ozbolat, I. T.; Hospodiuk, M. Current Advances and Future Perspectives in Extrusion-Based Bioprinting. *Biomaterials* **2016**, *76*, 321–343. https://doi.org/10.1016/j.biomaterials.2015.10.076.

(4) Amr, M.; Counts, M.; Kernan, J.; Mallah, A.; Mendenhall, J.; Wie, B. van; Abu-lail, N.; Gozen, B. A. Bioprinting 3D Printed, Mechanically Tunable, Composite Sodium Alginate, Gelatin and Gum Arabic (SA-GEL-GA) Scaffolds. *Bioprinting* **2021**, *22* (December 2020), e00133. https://doi.org/10.1016/j.bprint.2021.e00133.

(5) Isaacson, A.; Swioklo, S.; Connon, C. J. 3D Bioprinting of a Corneal Stroma Equivalent. *Exp Eye Res* **2018**, *173* (May), 188–193. https://doi.org/10.1016/j.exer.2018.05.010.

(6) Li, H.; Liu, S.; Li, L. Rheological Study on 3D Printability of Alginate Hydrogel and Effect of Graphene Oxide. *Int J Bioprint* **2016**, *2* (2), 54–66. https://doi.org/10.18063/IJB.2016.02.007.

(7) Bertassoni, L. E.; Cecconi, M.; Manoharan, V.; Nikkhah, M.; Hjortnaes, J.; Cristino, A. L.; Barabaschi, G.; Demarchi, D.; Dokmeci, M. R.; Yang, Y.; Khademhosseini, A. Hydrogel Bioprinted Microchannel Networks for Vascularization of Tissue Engineering Constructs. *Lab Chip* **2014**, *14* (13), 2202–2211. https://doi.org/10.1039/c4lc00030g.

(8) Townsend, J. M.; Beck, E. C.; Gehrke, S. H.; Berkland, C. J.; Detamore, M. S. Flow Behavior Prior to Crosslinking: The Need for Precursor Rheology for Placement of Hydrogels in Medical Applications and for 3D Bioprinting. *Prog Polym Sci* **2019**, *91*, 126–140. https://doi.org/10.1016/j.progpolymsci.2019.01.003.

(9) Morris, E. R.; Nishinari, K.; Rinaudo, M. Gelation of Gellan - A Review. *Food Hydrocoll* **2012**, *28* (2), 373–411. https://doi.org/10.1016/j.foodhyd.2012.01.004.

(10) Paxton, N.; Smolan, W.; Böck, T.; Melchels, F.; Groll, J.; Jungst, T. Proposal to Assess Printability of Bioinks for Extrusion-Based Bioprinting and Evaluation of Rheological Properties Governing Bioprintability. *Biofabrication* **2017**, *9* (4), 44107. https://doi.org/10.1088/1758-5090/aa8dd8.

(11) Jongprasitkul, H.; Turunen, S.; Parihar, V. S.; Kellomäki, M. Two-Step Crosslinking to Enhance the Printability of Methacrylated Gellan Gum Biomaterial Ink for Extrusion-Based 3D Bioprinting. *Bioprinting* **2022**, *25* (November 2021), e00185. https://doi.org/10.1016/j.bprint.2021.e00185.

(12) Schwab, A.; Levato, R.; D'Este, M.; Piluso, S.; Eglin, D.; Malda, J. Printability and Shape Fidelity of Bioinks in 3D Bioprinting. *Chem Rev* **2020**, *120* (19), 11028–11055. https://doi.org/10.1021/acs.chemrev.0c00084.

(13) Lee, S. C.; Gillispie, G.; Prim, P.; Lee, S. J. Physical and Chemical Factors Influencing the Printability of Hydrogel-Based Extrusion Bioinks. *Chem Rev* **2020**, *120* (19), 10834–10886. https://doi.org/10.1021/acs.chemrev.0c00015.

(14) Pereira, R. F.; Bartolo, P. J. 3D Bioprinting of Photocrosslinkable Hydrogel Constructs. *J Appl Polym Sci* **2015**, *132* (48). https://doi.org/10.1002/app.42889.

(15) Choi, G.; Cha, H. J. Recent Advances in the Development of Nature-Derived Photocrosslinkable Biomaterials for 3D Printing in Tissue Engineering. *Biomaterials Research*. BioMed Central Ltd. November 19, **2019**. https://doi.org/10.1186/s40824-019-0168-8.

(16) Gao, T.; Gillispie, G. J.; Copus, J. S.; PR, A. K.; Seol, Y.-J.; Atala, A.; Yoo, J. J.; Lee, S. J. Optimization of Gelatin Alginate Composite Bioink Printability Using Rheological Parameters: A Systematic Approach. *Biofabrication* **2018**, *10* (3), 34106. https://doi.org/10.1088/1758-5090/aacdc7.

(17) Włodarczyk-Biegun, M. K.; Paez, J. I.; Villiou, M.; Feng, J.; Del Campo, A. Printability Study of Metal Ion Crosslinked PEG-Catechol Based Inks. *Biofabrication* **2020**, *12* (3), 035009. https://doi.org/10.1088/1758-5090/ab673a.

(18) Bagheri, A.; Jin, J. Photopolymerization in 3D Printing. *ACS Appl Polym Mater* **2019**, *1* (4), 593–611. https://doi.org/10.1021/acsapm.8b00165.

(19) Layani, M.; Wang, X.; Magdassi, S. Novel Materials for 3D Printing by Photopolymerization. *Advanced Materials*. Wiley-VCH Verlag October 11, 2018. https://doi.org/10.1002/adma.201706344.

(20) Zheng, Z.; Eglin, D.; Alini, M.; Richards, G. R.; Qin, L.; Lai, Y. Visible Light-Induced 3D Bioprinting Technologies and Corresponding Bioink Materials for Tissue Engineering: A Review. *Engineering* **2021**, *7* (7), 966–978. https://doi.org/10.1016/j.eng.2020.05.021.

(21) Khoshakhlagh, P.; Bowser, D. A.; Brown, J. Q.; Moore, M. J. Comparison of Visible and UVA Phototoxicity in Neural Culture Systems Micropatterned with Digital Projection Photolithography. *J Biomed Mater Res A* **2019**, *107* (1), 134–144. https://doi.org/10.1002/jbm.a.36540.

(22) Galarraga, J. H.; Dhand, A. P.; Enzmann, B. P.; Burdick, J. A. Synthesis, Characterization, and Digital Light Processing of a Hydrolytically Degradable Hyaluronic Acid Hydrogel. *Biomacromolecules* **2023**, *24* (1), 413–425. https://doi.org/10.1021/acs.biomac.2c01218.

(23) Haleem, A.; Javaid, M. Role of CT and MRI in the Design and Development of Orthopaedic Model Using Additive Manufacturing. *J Clin Orthop Trauma* **2018**, *9* (3), 213–217. https://doi.org/10.1016/j.jcot.2018.07.002.

(24) Cengiz, I. F.; Pitikakis, M.; Cesario, L.; Parascandolo, P.; Vosilla, L.; Viano, G.; Oliveira, J. M.; Reis, R. L. Building the Basis for Patient-Specific Meniscal Scaffolds: From Human Knee MRI to Fabrication of 3D Printed Scaffolds. *Bioprinting* **2016**, *1–2*, 1–10. https://doi.org/10.1016/j.bprint.2016.05.001.

(25) Lim, K. S.; Galarraga, J. H.; Cui, X.; Lindberg, G. C. J.; Burdick, J. A.; Woodfield, T. B. F. Fundamentals and Applications of Photo-Cross-Linking in Bioprinting. *Chem Rev* **2020**, *120* (19), 10662–10694. https://doi.org/10.1021/acs.chemrev.9b00812.

(26) Yin, J.; Yan, M.; Wang, Y.; Fu, J.; Suo, H. 3D Bioprinting of Low-Concentration Cell-Laden Gelatin Methacrylate (GelMA) Bioinks with a Two-Step Cross-Linking Strategy. *ACS Appl Mater Interfaces* **2018**, *10* (8), 6849–6857. https://doi.org/10.1021/acsami.7b16059.

(27) Petta, D.; Armiento, A. R.; Grijpma, D.; Alini, M.; Eglin, D.; D'Este, M. 3D Bioprinting of a Hyaluronan Bioink through Enzymatic-and Visible Light-Crosslinking. *Biofabrication* **2018**, *10* (4). https://doi.org/10.1088/1758-5090/aadf58.

(28) Groll, J.; Boland, T.; Blunk, T.; Burdick, J. A.; Cho, D. W.; Dalton, P. D.; Derby, B.; Forgacs, G.; Li, Q.; Mironov, V. A.; Moroni, L.; Nakamura, M.; Shu, W.; Takeuchi, S.; Vozzi, G.; Woodfield, T. B. F.; Xu, T.; Yoo, J. J.; Malda, J. Biofabrication: Reappraising the Definition of an Evolving Field. *Biofabrication*. Institute of Physics Publishing January 8, **2016**. https://doi.org/10.1088/1758-5090/8/1/013001.

(29) Valmikinathan, C. M.; Mukhatyar, V. J.; Jain, A.; Karumbaiah, L.; Dasari, M.; Bellamkonda, R. v. Photocrosslinkable Chitosan Based Hydrogels for Neural Tissue Engineering. *Soft Matter* **2012**, *8* (6), 1964–1976. https://doi.org/10.1039/c1sm06629c.

(30) Jakab, K.; Norotte, C.; Damon, B.; Marga, F.; Neagu, A.; Besch-Williford, C. L.; Kachurin, A.; Church, K. H.; Park, H.; Mironov, V.; Markwald, R.; Vunjak-Novakovic, G.; Forgacs, G. Tissue Engineering by Self-Assembly of Cells Printed into Topologically Defined Structures. *Tissue Eng Part A* **2008**, *14* (3), 413–421. https://doi.org/10.1089/tea.2007.0173.

(31) Wüst, S.; Godla, M. E.; Müller, R.; Hofmann, S. Tunable Hydrogel Composite with Two-Step Processing in Combination with Innovative Hardware Upgrade for Cell-Based Three-Dimensional Bioprinting. *Acta Biomater* **2014**, *10* (2), 630–640. https://doi.org/10.1016/j.actbio.2013.10.016.

(32) Liu, W.; Zhong, Z.; Hu, N.; Zhou, Y.; Maggio, L.; Miri, A. K.; Fragasso, A.; Jin, X.; Khademhosseini, A.; Zhang, Y. S. Coaxial Extrusion Bioprinting of 3D Microfibrous Constructs with Cell-Favorable Gelatin Methacryloyl Microenvironments. *Biofabrication* **2018**, *10* (2). https://doi.org/10.1088/1758-5090/aa9d44.

(33) Ouyang, L.; Highley, C. B.; Sun, W.; Burdick, J. A. A Generalizable Strategy for the 3D Bioprinting of Hydrogels from Nonviscous Photo-Crosslinkable Inks. *Advanced Materials* **2017**, *29* (8), 1604983. https://doi.org/10.1002/adma.201604983.

(34) Miri, A. K.; Mirzaee, I.; Hassan, S.; Mesbah Oskui, S.; Nieto, D.; Khademhosseini, A.; Zhang, Y. S. Effective Bioprinting Resolution in Tissue Model Fabrication. *Lab Chip* **2019**, *19* (11), 2019–2037. https://doi.org/10.1039/c8lc01037d.

(35) Zhuang, P.; Ng, W. L.; An, J.; Chua, C. K.; Tan, L. P. Layer-by-Layer Ultraviolet Assisted Extrusion-Based (UAE) Bioprinting of Hydrogel Constructs with High Aspect Ratio for Soft Tissue Engineering Applications. *PLoS One* **2019**, *14* (6), 1–21. https://doi.org/10.1371/journal.pone.0216776.

(36) Groll, J.; Burdick, J. A.; Cho, D. W.; Derby, B.; Gelinsky, M.; Heilshorn, S. C.; Jüngst, T.; Malda, J.; Mironov, V. A.; Nakayama, K.; Ovsianikov, A.; Sun, W.; Takeuchi, S.; Yoo, J. J.; Woodfield, T. B. F. A Definition of Bioinks and Their Distinction from Biomaterial Inks. *Biofabrication* **2019**, *11* (1), 013001. https://doi.org/10.1088/1758-5090/aaec52.

(37) Yi, H. G.; Kim, H.; Kwon, J.; Choi, Y. J.; Jang, J.; Cho, D. W. Application of 3D Bioprinting in the Prevention and the Therapy for Human Diseases. *Signal Transduction and Targeted Therapy*. Springer Nature December 1, **2021**. https://doi.org/10.1038/s41392-021-00566-8.

(38) Maiz-Fernández, S.; Pérez-álvarez, L.; Silván, U.; Vilas-Vilela, J. L.; Lanceros-Méndez, S. PH-Induced 3D Printable Chitosan Hydrogels for Soft Actuation. *Polymers (Basel)* **2022**, *14* (3), 650. https://doi.org/10.3390/polym14030650.

(39) Hospodiuk, M.; Dey, M.; Sosnoski, D.; Ozbolat, I. T. The Bioink: A Comprehensive Review on Bioprintable Materials. *Biotechnology Advances*. Elsevier Inc. March 1, **2017**, pp 217–239. https://doi.org/10.1016/j.biotechadv.2016.12.006.

(40) Mancha Sánchez, E.; Gómez-Blanco, J. C.; López Nieto, E.; Casado, J. G.; Macías-García, A.; Díaz Díez, M. A.; Carrasco-Amador, J. P.; Torrejón Martín, D.; Sánchez-Margallo, F. M.; Pagador, J. B. Hydrogels for Bioprinting: A Systematic Review of Hydrogels Synthesis, Bioprinting Parameters, and Bioprinted Structures Behavior. *Front Bioeng Biotechnol* **2020**, *8* (August). https://doi.org/10.3389/fbioe.2020.00776.

(41) Darge, H. F.; Andrgie, A. T.; Tsai, H. C.; Lai, J. Y. Polysaccharide and Polypeptide Based Injectable Thermo-Sensitive Hydrogels for Local Biomedical Applications. *Int J Biol Macromol* **2019**, *133*, 545–563. https://doi.org/10.1016/j.ijbiomac.2019.04.131.

(42) Akhtar, M. F.; Hanif, M.; Ranjha, N. M. Methods of Synthesis of Hydrogels … A Review. *Saudi Pharmaceutical Journal* **2016**, *24* (5), 554–559. https://doi.org/https://doi.org/10.1016/j.jsps.2015.03.022.

(43) Ahmed, E. M. Hydrogel: Preparation, Characterization, and Applications: A Review. *J Adv Res* **2015**, *6* (2), 105–121. https://doi.org/https://doi.org/10.1016/j.jare.2013.07.006.

(44) Saravanan, S.; Vimalraj, S.; Thanikaivelan, P.; Banudevi, S.; Manivasagam, G. A Review on Injectable Chitosan/Beta Glycerophosphate Hydrogels for Bone Tissue Regeneration. *Int J Biol Macromol* **2019**, *121*, 38–54. https://doi.org/https://doi.org/10.1016/j.ijbiomac.2018.10.014.

(45) Mathew, A. P.; Uthaman, S.; Cho, K. H.; Cho, C. S.; Park, I. K. Injectable Hydrogels for Delivering Biotherapeutic Molecules. *Int J Biol Macromol* **2018**, *110*, 17–29. https://doi.org/10.1016/j.ijbiomac.2017.11.113.

(46) Shams, E.; Barzad, M. S.; Mohamadnia, S.; Tavakoli, O.; Mehrdadfar, A. A Review on Alginate-Based Bioinks, Combination with Other Natural Biomaterials and Characteristics. *J Biomater Appl* **2022**, *37* (2), 355–372. https://doi.org/10.1177/08853282210856907

(47) Möller, L.; Krause, A.; Dahlmann, J.; Gruh, I.; Kirschning, A.; Dräger, G. Preparation and Evaluation of Hydrogel-Composites from Methacrylated Hyaluronic Acid, Alginate, and Gelatin for Tissue Engineering. *International Journal of Artificial Organs* **2011**, *34* (2), 93–102. https://doi.org/10.5301/IJAO.2011.6397.

(48) Kwiecień, I.; Kwiecień, M. Application of Polysaccharide-Based Hydrogels as Probiotic Delivery Systems. *Gels* **2018**, *4* (2), 47. https://doi.org/10.3390/gels4020047.

(49) Black, K. A.; Lin, B. F.; Wonder, E. A.; Desai, S. S.; Chung, E. J.; Ulery, B. D.; Katari, R. S.; Tirrell, M. v. Biocompatibility and Characterization of a Peptide Amphiphile Hydrogel for Applications in Peripheral Nerve Regeneration. *Tissue Eng Part A* **2015**, *21* (7–8), 1333–1342. https://doi.org/10.1089/ten.tea.2014.0297.

(50) Du, X.; Zhou, J.; Shi, J.; Xu, B. Supramolecular Hydrogelators and Hydrogels: From Soft Matter to Molecular Biomaterials. *Chem Rev* **2015**, *115* (24), 13165–13307. https://doi.org/10.1021/acs.chemrev.5b00299.

(51) Catoira, M. C.; Fusaro, L.; di Francesco, D.; Ramella, M.; Boccafoschi, F. Overview of Natural Hydrogels for Regenerative Medicine Applications. *J Mater Sci Mater Med* **2019**, *30* (10), 115. https://doi.org/10.1007/s10856-019-6318-7.

(52) Chimene, D.; Kaunas, R.; Gaharwar, A. K. Hydrogel Bioink Reinforcement for Additive Manufacturing: A Focused Review of Emerging Strategies. *Advanced Materials* **2020**, *32* (1), 1–22. https://doi.org/10.1002/adma.201902026.

(53) Annabi, N.; Tamayol, A.; Uquillas, J. A.; Akbari, M.; Bertassoni, L. E.; Cha, C.; Camci-Unal, G.; Dokmeci, M. R.; Peppas, N. A.; Khademhosseini, A. 25th

Anniversary Article: Rational Design and Applications of Hydrogels in Regenerative Medicine. *Advanced Materials* **2014**, *26* (1), 85–124. https://doi.org/10.1002/adma.201303233.

(54) Jongprasitkul, H.; Turunen, S.; Parihar, V. S.; Annurakshita, S.; Kellomaki, M. Photocross-Linkable Methacrylated Polypeptides and Polysaccharides for Casting, Injecting, and 3D Fabrication. *Biomacromolecules* **2021**, *22* (2), 481–493. https://doi.org/10.1021/acs.biomac.0c01322.

(55) Zhu, T.; Mao, J.; Cheng, Y.; Liu, H.; Lv, L.; Ge, M.; Li, S.; Huang, J.; Chen, Z.; Li, H.; Yang, L.; Lai, Y. Recent Progress of Polysaccharide-Based Hydrogel Interfaces for Wound Healing and Tissue Engineering. *Adv Mater Interfaces* **2019**, *6* (17), 1–22. https://doi.org/10.1002/admi.201900761.

(56) Pahoff, S.; Meinert, C.; Bas, O.; Nguyen, L.; Klein, T. J.; Hutmacher, D. W. Effect of Gelatin Source and Photoinitiator Type on Chondrocyte Redifferentiation in Gelatin Methacryloyl-Based Tissue-Engineered Cartilage Constructs. *J Mater Chem B* **2019**, *7* (10), 1761–1772. https://doi.org/10.1039/c8tb02607f.

(57) Duchi, S.; Onofrillo, C.; O'Connell, C. D.; Blanchard, R.; Augustine, C.; Quigley, A. F.; Kapsa, R. M. I.; Pivonka, P.; Wallace, G.; di Bella, C.; Choong, P. F. M. Handheld Co-Axial Bioprinting: Application to in Situ Surgical Cartilage Repair. *Sci Rep* **2017**, *7* (1), 1–12. https://doi.org/10.1038/s41598-017-05699-x.

(58) Cui, X.; Li, J.; Hartanto, Y.; Durham, M.; Tang, J.; Zhang, H.; Hooper, G.; Lim, K.; Woodfield, T. Advances in Extrusion 3D Bioprinting: A Focus on Multicomponent Hydrogel-Based Bioinks. *Advanced Healthcare Materials*. Wiley-VCH Verlag August 1, **2020**. https://doi.org/10.1002/adhm.201901648.

(59) Montero, F. E.; Rezende, R. A.; da Silva, J. V. L.; Sabino, M. A. Development of a Smart Bioink for Bioprinting Applications. *Front Mech Eng* **2019**, *5*, 56. https://doi.org/10.3389/fmech.2019.00056

(60) Nichol, J. W.; Koshy, S. T.; Bae, H.; Hwang, C. M.; Yamanlar, S.; Khademhosseini, A. Cell-Laden Microengineered Gelatin Methacrylate Hydrogels. *Biomaterials* **2010**, *31* (21), 5536–5544. https://doi.org/https://doi.org/10.1016/j.biomaterials.2010.03.064.

(61) Koivisto, J. T.; Gering, C.; Karvinen, J.; Maria Cherian, R.; Belay, B.; Hyttinen, J.; Aalto-Setälä, K.; Kellomäki, M.; Parraga, J. Mechanically Biomimetic Gelatin-Gellan Gum Hydrogels for 3D Culture of Beating Human Cardiomyocytes. *ACS Appl Mater Interfaces* **2019**, *11* (23), 20589–20602. https://doi.org/10.1021/acsami.8b22343.

(62) Ravichandran, R.; Islam, M. M.; Alarcon, E. I.; Samanta, A.; Wang, S.; Lundström, P.; Hilborn, J.; Griffith, M.; Phopase, J. Functionalised Type-I Collagen as a Hydrogel Building Block for Bio-Orthogonal Tissue Engineering Applications. *J Mater Chem B* **2015**, *4* (2), 318–326. https://doi.org/10.1039/c5tb02035b.

(63) Khoury, L. R.; Popa, I. Chemical Unfolding of Protein Domains Induces Shape Change in Programmed Protein Hydrogels. *Nat Commun* **2019**, *10* (1), 1–9. https://doi.org/10.1038/s41467-019-13312-0.

(64) Kim, D.; Kim, M.; Lee, J.; Jang, J. Review on Multicomponent Hydrogel Bioinks Based on Natural Biomaterials for Bioprinting 3D Liver Tissues. *Frontiers in Bioengineering and Biotechnology*. Frontiers Media S.A. February 14, **2022**. https://doi.org/10.3389/fbioe.2022.764682.

(65) Benwood, C.; Chrenek, J.; Kirsch, R. L.; Masri, N. Z.; Richards, H.; Teetzen, K.; Willerth, S. M. Natural Biomaterials and Their Use as Bioinks for Printing Tissues. *Bioengineering*. MDPI AG February 1, **2021**, 1–19. https://doi.org/10.3390/bioengineering8020027.

(66) Wang, X.; Ao, Q.; Tian, X.; Fan, J.; Tong, H.; Hou, W.; Bai, S. Gelatin-Based Hydrogels for Organ 3D Bioprinting. *Polymers (Basel)* **2017**, *9* (9). https://doi.org/10.3390/polym9090401.

(67) van den Bulcke, A. I.; Bogdanov, B.; de Rooze, N.; Schacht, E. H.; Cornelissen, M.; Berghmans, H. Structural and Rheological Properties of Methacrylamide Modified Gelatin Hydrogels. *Biomacromolecules* **2000**, *1* (1), 31–38. https://doi.org/10.1021/bm990017d.

(68) Sun, M.; Sun, X.; Wang, Z.; Guo, S.; Yu, G.; Yang, H. Synthesis and Properties of Gelatin Methacryloyl (GelMA) Hydrogels and Their Recent Applications in Load-Bearing Tissue. *Polymers (Basel)* **2018**, *10* (11). https://doi.org/10.3390/POLYM10111290.

(69) Janmaleki, M.; Liu, J.; Kamkar, M.; Azarmanesh, M.; Sundararaj, U.; Nezhad, A. S. Role of Temperature on Bio-Printability of Gelatin Methacryloyl Bioink in Two-Step Cross-Linking Strategy for Tissue Engineering Applications. *Biomedical Materials (Bristol)* **2021**, *16* (1), 015021. https://doi.org/10.1088/1748-605X/abbcc9.

(70) Liu, W.; Heinrich, M. A.; Zhou, Y.; Akpek, A.; Hu, N.; Liu, X.; Guan, X.; Zhong, Z.; Jin, X.; Khademhosseini, A.; Zhang, Y. S. Extrusion Bioprinting of Shear-Thinning Gelatin Methacryloyl Bioinks. *Adv Healthc Mater* **2017**, *6* (12). https://doi.org/10.1002/adhm.201601451.

(71) Bartnikowski, M.; Bartnikowski, N. J.; Woodruff, M. A.; Schrobback, K.; Klein, T. J. Protective Effects of Reactive Functional Groups on Chondrocytes in Photocrosslinkable Hydrogel Systems. *Acta Biomater* **2015**, *27*, 66–76. https://doi.org/10.1016/j.actbio.2015.08.038.

(72) Ouyang, L.; Armstrong, J. P. K.; Lin, Y.; Wojciechowski, J. P.; Lee-Reeves, C.; Hachim, D.; Zhou, K.; Burdick, J. A.; Stevens, M. M. Expanding and Optimizing 3D Bioprinting Capabilities Using Complementary Network Bioinks. *Sci Adv* **2020**, *6* (38), 1–14. https://doi.org/10.1126/sciadv.abc5529.

(73) Xu, W.; Molino, B. Z.; Cheng, F.; Molino, P. J.; Yue, Z.; Su, D.; Wang, X.; Willför, S.; Xu, C.; Wallace, G. G. On Low-Concentration Inks Formulated by Nanocellulose Assisted with Gelatin Methacrylate (GelMA) for 3D Printing

toward Wound Healing Application. *ACS Appl Mater Interfaces* **2019**, *11* (9), 8838–8848. https://doi.org/10.1021/acsami.8b21268.

(74) Ferreira, P.; J. Coelho, J. F.; F., J.; H., M. Photocrosslinkable Polymers for Biomedical Applications. *Biomedical Engineering - Frontiers and Challenges* **2011**. https://doi.org/10.5772/18752.

(75) Mazzocchi, A.; Devarasetty, M.; Huntwork, R.; Soker, S.; Skardal, A. Optimization of Collagen Type I-Hyaluronan Hybrid Bioink for 3D Bioprinted Liver Microenvironments. *Biofabrication* **2018**, *11* (1), 15003. https://doi.org/10.1088/1758-5090/aae543.

(76) Stepanovska, J.; Supova, M.; Hanzalek, K.; Broz, A.; Matejka, R. Collagen Bioinks for Bioprinting: A Systematic Review of Hydrogel Properties, Bioprinting Parameters, Protocols, and Bioprinted Structure Characteristics. *Biomedicines* **2021**, *9* (9). https://doi.org/10.3390/biomedicines9091137.

(77) Kim, W.; Kim, G. Intestinal Villi Model with Blood Capillaries Fabricated Using Collagen-Based Bioink and Dual-Cell-Printing Process. *ACS Appl Mater Interfaces* **2018**, *10* (48), 41185–41196. https://doi.org/10.1021/acsami.8b17410.

(78) Mörö, A.; Samanta, S.; Honkamäki, L.; Rangasami, V. K.; Puistola, P.; Kauppila, M.; Narkilahti, S.; Miettinen, S.; Oommen, O.; Skottman, H. Hyaluronic Acid Based next Generation Bioink for 3D Bioprinting of Human Stem Cell Derived Corneal Stromal Model with Innervation. *Biofabrication* **2023**, *15* (1). https://doi.org/10.1088/1758-5090/acab34.

(79) Yang, X.; Lu, Z.; Wu, H.; Li, W.; Zheng, L.; Zhao, J. Collagen-Alginate as Bioink for Three-Dimensional (3D) Cell Printing Based Cartilage Tissue Engineering. *Materials Science and Engineering C* **2018**, *83*, 195–201. https://doi.org/10.1016/j.msec.2017.09.002.

(80) Homenick, C. M.; de Silveira, G.; Sheardown, H.; Adronov, A. Pluronics as Crosslinking Agents for Collagen: Novel Amphiphilic Hydrogels. *Polym Int* **2011**, *60* (3), 458–465. https://doi.org/10.1002/pi.2969.

(81) Bell, A.; Kofron, M.; Nistor, V. Multiphoton Crosslinking for Biocompatible 3D Printing of Type I Collagen. *Biofabrication* **2015**, *7* (3), 35007. https://doi.org/10.1088/1758-5090/7/3/035007.

(82) Shelke, N. B.; James, R.; Laurencin, C. T.; Kumbar, S. G. Polysaccharide Biomaterials for Drug Delivery and Regenerative Engineering. *Polym Adv Technol* **2014**, *25* (5), 448–460. https://doi.org/10.1002/pat.3266.

(83) Raemdonck, K.; Martens, T. F.; Braeckmans, K.; Demeester, J.; de Smedt, S. C. Polysaccharide-Based Nucleic Acid Nanoformulations. *Adv Drug Deliv Rev* **2013**, *65* (9), 1123–1147. https://doi.org/https://doi.org/10.1016/j.addr.2013.05.002.

(84) Xiao, R.; Grinstaff, M. W. Chemical Synthesis of Polysaccharides and Polysaccharide Mimetics. *Prog Polym Sci* **2017**, *74*, 78–116. https://doi.org/https://doi.org/10.1016/j.progpolymsci.2017.07.009.

(85) Singh, B.; Bala, R. Polysaccharide Based Hydrogels as Controlled Drug Delivery System for GIT Cancer. *Int J Biol Macromol* **2014**, *65*, 524–533. https://doi.org/https://doi.org/10.1016/j.ijbiomac.2014.02.004.

(86) Pereira, R. F.; Bártolo, P. J. 3D Photo-Fabrication for Tissue Engineering and Drug Delivery. *Engineering* **2015**, *1* (1), 090–112. https://doi.org/10.15302/J-ENG-2015015.

(87) Hay, I. D.; Rehman, Z. U.; Moradali, M. F.; Wang, Y.; Rehm, B. H. A. Microbial Alginate Production, Modification and Its Applications. *Microbial Biotechnology*. November **2013**, 637–650. https://doi.org/10.1111/1751-7915.12076.

(88) Jungst, T.; Smolan, W.; Schacht, K.; Scheibel, T.; Groll, J. Strategies and Molecular Design Criteria for 3D Printable Hydrogels. *Chemical Reviews*. American Chemical Society February 10, **2016**, 1496–1539. https://doi.org/10.1021/acs.chemrev.5b00303.

(89) Cao, N.; Chen, X. B.; Schreyer, D. J. Influence of Calcium Ions on Cell Survival and Proliferation in the Context of an Alginate Hydrogel. *ISRN Chemical Engineering* **2012**, 516461. https://doi.org/10.5402/2012/516461.

(90) Gonzalez-Fernandez, T.; Tenorio, A. J.; Campbell, K. T.; Silva, E. A.; Leach, J. K. Alginate-Based Bioinks for 3D Bioprinting and Fabrication of Anatomically Accurate Bone Grafts. *Tissue Eng Part A* **2021**, *00* (00), 1–14. https://doi.org/10.1089/ten.tea.2020.0305.

(91) Luo, Y.; Kirker, K. R.; Prestwich, G. D. *Cross-Linked Hyaluronic Acid Hydrogel Films: New Biomaterials for Drug Delivery*; **2000**; Vol. 69. www.elsevier.com/locate/jconrel.

(92) Burdick, J. A.; Prestwich, G. D. Hyaluronic Acid Hydrogels for Biomedical Applications. *Advanced Materials* **2011**, *23* (12). https://doi.org/10.1002/adma.201003963.

(93) Collins, M. N.; Birkinshaw, C. Hyaluronic Acid Based Scaffolds for Tissue Engineering—A Review. *Carbohydr Polym* **2013**, *92* (2), 1262–1279. https://doi.org/10.1016/J.CARBPOL.2012.10.028.

(94) El-Husseiny, H. M.; Mady, E. A.; Hamabe, L.; Abugomaa, A.; Shimada, K.; Yoshida, T.; Tanaka, T.; Yokoi, A.; Elbadawy, M.; Tanaka, R. Smart/Stimuli-Responsive Hydrogels: Cutting-Edge Platforms for Tissue Engineering and Other Biomedical Applications. *Mater Today Bio* **2022**, *13* (December 2021), 100186. https://doi.org/10.1016/j.mtbio.2021.100186.

(95) Salzlechner, C.; Haghighi, T.; Huebscher, I.; Walther, A. R.; Schell, S.; Gardner, A.; Undt, G.; da Silva, R. M. P.; Dreiss, C. A.; Fan, K.; Gentleman, E. Adhesive Hydrogels for Maxillofacial Tissue Regeneration Using Minimally Invasive Procedures. *Adv Healthc Mater* **2020**, *9* (4), 1901134. https://doi.org/10.1002/adhm.201901134.

(96) Ouyang, L.; Yao, R.; Zhao, Y.; Sun, W. Effect of Bioink Properties on Printability and Cell Viability for 3D Bioplotting of Embryonic Stem Cells.

Biofabrication **2016**, *8* (3), 1–12. https://doi.org/10.1088/1758-5090/8/3/035020.

(97) Hou, S.; Xu, Q.; Tian, W.; Cui, F.; Cai, Q.; Ma, J.; Lee, I. S. The Repair of Brain Lesion by Implantation of Hyaluronic Acid Hydrogels Modified with Laminin. *J Neurosci Methods* **2005**, *148* (1), 60–70. https://doi.org/10.1016/J.JNEUMETH.2005.04.016.

(98) Zia, K. M.; Tabasum, S.; Khan, M. F.; Akram, N.; Akhter, N.; Noreen, A.; Zuber, M. Recent Trends on Gellan Gum Blends with Natural and Synthetic Polymers: A Review. *International Journal of Biological Macromolecules*. Elsevier B.V. April 1, **2018**, 1068–1087. https://doi.org/10.1016/j.ijbiomac.2017.11.099.

(99) Wu, D.; Yu, Y.; Tan, J.; Huang, L.; Luo, B.; Lu, L.; Zhou, C. 3D Bioprinting of Gellan Gum and Poly (Ethylene Glycol) Diacrylate Based Hydrogels to Produce Human-Scale Constructs with High-Fidelity. *Mater Des* **2018**, *160*, 486–495. https://doi.org/10.1016/j.matdes.2018.09.040.

(100) Hu, D.; Wu, D.; Huang, L.; Jiao, Y.; Li, L.; Lu, L.; Zhou, C. 3D Bioprinting of Cell-Laden Scaffolds for Intervertebral Disc Regeneration. *Mater Lett* **2018**, *223*, 219–222. https://doi.org/10.1016/j.matlet.2018.03.204.

(101) Robinson, T. M.; Talebian, S.; Foroughi, J.; Yue, Z.; Fay, C. D.; Wallace, G. G. Fabrication of Aligned Biomimetic Gellan Gum-Chitosan Microstructures through 3D Printed Microfluidic Channels and Multiple in Situ Cross-Linking Mechanisms. *ACS Biomater Sci Eng* **2020**, *6* (6), 3638–3648. https://doi.org/10.1021/acsbiomaterials.0c00260.

(102) Ferris, C. J.; Gilmore, K. J.; Wallace, G. G.; Panhuis, M. In Het. Modified Gellan Gum Hydrogels for Tissue Engineering Applications. *Soft Matter* **2013**, *9* (14), 3705–3711. https://doi.org/10.1039/c3sm27389j.

(103) Wang, F.; Wen, Y.; Bai, T. The Composite Hydrogels of Polyvinyl Alcohol–Gellan Gum-Ca2 + with Improved Network Structure and Mechanical Property. *Materials Science and Engineering C* **2016**, *69*, 268–275. https://doi.org/10.1016/j.msec.2016.06.084.

(104) Pacelli, S.; Paolicelli, P.; Dreesen, I.; Kobayashi, S.; Vitalone, A.; Casadei, M. A. Injectable and Photocross-Linkable Gels Based on Gellan Gum Methacrylate: A New Tool for Biomedical Application. *Int J Biol Macromol* **2015**, *72*, 1335–1342. https://doi.org/10.1016/j.ijbiomac.2014.10.046.

(105) Mouser, V. H. M.; Melchels, F. P. W.; Visser, J.; Dhert, W. J. A. Yield Stress Determines Bioprintability of Hydrogels Based on Gelatin-Methacryloyl and Gellan Gum for Cartilage Bioprinting. *Biofabrication* **2016**, *8* (3), 1–24. https://doi.org/10.1088/1758-5090/8/3/035003.

(106) Wu, D.; Yu, Y.; Tan, J.; Huang, L.; Luo, B.; Lu, L.; Zhou, C. 3D Bioprinting of Gellan Gum and Poly (Ethylene Glycol) Diacrylate Based Hydrogels to Produce Human-Scale Constructs with High-Fidelity. *Mater Des* **2018**, *160*, 486–495. https://doi.org/10.1016/j.matdes.2018.09.040.

(107) Coutinho, D. F.; Sant, S. v.; Shin, H.; Oliveira, J. T.; Gomes, M. E.; Neves, N. M.; Khademhosseini, A.; Reis, R. L. Modified Gellan Gum Hydrogels with Tunable Physical and Mechanical Properties. *Biomaterials* **2010**, *31* (29), 7494–7502. https://doi.org/10.1016/j.biomaterials.2010.06.035.

(108) Xu, Z.; Li, Z.; Jiang, S.; Bratlie, K. M. Chemically Modified Gellan Gum Hydrogels with Tunable Properties for Use as Tissue Engineering Scaffolds. *ACS Omega* **2018**, *3* (6), 6998–7007. https://doi.org/10.1021/acsomega.8b00683.

(109) Silva-Correia, J.; Zavan, B.; Vindigni, V.; Silva, T. H.; Oliveira, J. M.; Abatangelo, G.; Reis, R. L. Biocompatibility Evaluation of Ionic- and Photo-Crosslinked Methacrylated Gellan Gum Hydrogels: In Vitro and in Vivo Study. *Adv Healthc Mater* **2013**, *2* (4), 568–575. https://doi.org/10.1002/adhm.201200256.

(110) Ferris, C. J.; Gilmore, K. J.; Wallace, G. G.; Panhuis, M. In Het. Modified Gellan Gum Hydrogels for Tissue Engineering Applications. *Soft Matter* **2013**, *9* (14), 3705–3711. https://doi.org/10.1039/C3SM27389J.

(111) Silva, N. A.; Salgado, A. J.; Sousa, R. A.; Oliveira, J. T.; Pedro, A. J.; Leite-Almeida, H.; Cerqueira, R.; Almeida, A.; Mastronardi, F.; Mano, J. F.; Neves, N. M.; Sousa, N.; Reis, R. L. Development and Characterization of a Novel Hybrid Tissue Engineering-Based Scaffold for Spinal Cord Injury Repair. *Tissue Eng Part A* **2010**, *16* (1), 45–54. https://doi.org/10.1089/ten.tea.2008.0559

(112) Ferris, C. J.; Gilmore, K. J.; Beirne, S.; McCallum, D.; Wallace, G. G.; In Het Panhuis, M. Bio-Ink for on-Demand Printing of Living Cells. *Biomater Sci* **2013**, *1* (2), 224–230. https://doi.org/10.1039/C2BM00114D

(113) Gomez-Florit, M.; Pardo, A.; Domingues, R. M. A.; Graça, A. L.; Babo, P. S.; Reis, R. L.; Gomes, M. E. Natural-Based Hydrogels for Tissue Engineering Applications. *Molecules*. MDPI December 1, **2020**. https://doi.org/10.3390/molecules25245858.

(114) Seo, J. W.; Kim, G. M.; Choi, Y.; Cha, J. M.; Bae, H. Improving Printability of Digital-Light-Processing 3D Bioprinting via Photoabsorber Pigment Adjustment. *Int J Mol Sci* **2022**, *23* (10). https://doi.org/10.3390/ijms23105428.

(115) Zhang, Y. S.; Khademhosseini, A. Advances in Engineering Hydrogels. *Science (1979)* **2017**, *356* (6337). https://doi.org/10.1126/science.aaf3627.

(116) GhavamiNejad, A.; Ashammakhi, N.; Wu, X. Y.; Khademhosseini, A. Crosslinking Strategies for 3D Bioprinting of Polymeric Hydrogels. *Small* **2020**, *16* (35), 2002931. https://doi.org/10.1002/smll.202002931.

(117) Jongprasitkul, H.; Turunen, S.; Parihar, V. S.; Kellomäki, M. Sequential Cross-Linking of Gallic Acid-Functionalized GelMA-Based Bioinks with Enhanced Printability for Extrusion-Based 3D Bioprinting. *Biomacromolecules* **2023**, *24* (1), 502–514. https://doi.org/10.1021/acs.biomac.2c01418.

(118) Zheng, J.; Zhu, M.; Ferracci, G.; Cho, N. J.; Lee, B. H. Hydrolytic Stability of Methacrylamide and Methacrylate in Gelatin Methacryloyl and Decoupling of

Gelatin Methacrylamide from Gelatin Methacryloyl through Hydrolysis. *Macromol Chem Phys* **2018**, *219* (18). https://doi.org/10.1002/macp.201800266.

(119) Ashammakhi, N.; Ahadian, S.; Xu, C.; Montazerian, H.; Ko, H.; Nasiri, R.; Barros, N.; Khademhosseini, A. Bioinks and Bioprinting Technologies to Make Heterogeneous and Biomimetic Tissue Constructs. *Materials Today Bio*. Elsevier B.V. January 1, **2019**. https://doi.org/10.1016/j.mtbio.2019.100008.

(120) Zhou, M.; Lee, B. H.; Tan, Y. J.; Tan, L. P. Microbial Transglutaminase Induced Controlled Crosslinking of Gelatin Methacryloyl to Tailor Rheological Properties for 3D Printing. *Biofabrication* **2019**, *11* (2). https://doi.org/10.1088/1758-5090/ab063f.

(121) Billiet, T.; Gevaert, E.; de Schryver, T.; Cornelissen, M.; Dubruel, P. The 3D Printing of Gelatin Methacrylamide Cell-Laden Tissue-Engineered Constructs with High Cell Viability. *Biomaterials* **2014**, *35* (1), 49–62. https://doi.org/10.1016/j.biomaterials.2013.09.078.

(122) Malda, J.; Visser, J.; Melchels, F. P.; Jüngst, T.; Hennink, W. E.; Dhert, W. J. A.; Groll, J.; Hutmacher, D. W. 25th Anniversary Article: Engineering Hydrogels for Biofabrication. *Advanced Materials* **2013**, *25* (36), 5011–5028. https://doi.org/10.1002/adma.201302042.

(123) Zhao, Y.; Li, Y.; Mao, S.; Sun, W.; Yao, R. The Influence of Printing Parameters on Cell Survival Rate and Printability in Microextrusion-Based 3D Cell Printing Technology. *Biofabrication* **2015**, *7* (4). https://doi.org/10.1088/1758-5090/7/4/045002.

(124) Rohani Rad, E.; Vahabi, H.; Formela, K.; Saeb, M. R.; Thomas, S. Injectable Poloxamer/Graphene Oxide Hydrogels with Well-Controlled Mechanical and Rheological Properties. *Polym Adv Technol* **2019**, *30* (9), 2250–2260. https://doi.org/10.1002/pat.4654.

(125) Dumortier, G.; Grossiord, J. L.; Agnely, F.; Chaumeil, J. C. A Review of Poloxamer 407 Pharmaceutical and Pharmacological Characteristics. *Pharmaceutical Research*. Springer Science and Business Media Deutschland GmbH **2006**, 2709–2728. https://doi.org/10.1007/s11095-006-9104-4.

(126) Kamlungmak, S.; Dechraksa, J.; Padmavathi, A. R.; Sawatdee, S.; Tinpun, K.; Nakpheng, T.; Srichana, T. Lamellar Phase Behavior and Molecular Interaction of a Thermoresponsive Poloxamer and Crosslinked Poly (Vinyl Alcohol) Hydrogel. *Mater Today Commun* **2019**, *20*. https://doi.org/10.1016/j.mtcomm.2019.100542.

(127) Abou-Shamat, M. A.; Calvo-Castro, J.; Stair, J. L.; Cook, M. T.; Abou-Shamat, M. A.; Calvo-Castro, J.; Stair, J. L.; Cook, M. T. Modifying the Properties of Thermogelling Poloxamer 407 Solutions through Covalent Modification and the Use of Polymer Additives. *Macromol Chem Phys* **2019**, *220* (16), 1900173. https://doi.org/10.1002/MACP.201900173.

(128) de Vos, P.; Lazarjani, H. A.; Poncelet, D.; Faas, M. M. Polymers in Cell Encapsulation from an Enveloped Cell Perspective. *Advanced Drug Delivery*

Reviews. Elsevier April 10, **2014**, 15–34. https://doi.org/10.1016/j.addr.2013.11.005.

(129) Kim, D.; Kim, M.; Lee, J.; Jang, J. Review on Multicomponent Hydrogel Bioinks Based on Natural Biomaterials for Bioprinting 3D Liver Tissues. *Frontiers in Bioengineering and Biotechnology*. Frontiers Media S.A. February 14, **2022**. https://doi.org/10.3389/fbioe.2022.764682.

(130) Lee, H. R.; Jung, S. M.; Yoon, S.; Yoon, W. H.; Park, T. H.; Kim, S.; Shin, H. W.; Hwang, D. S.; Jung, S. Immobilization of Planktonic Algal Spores by Inkjet Printing. *Sci Rep* **2019**, *9* (1). https://doi.org/10.1038/s41598-019-48776-z.

(131) Paredes Juárez, G. A.; Spasojevic, M.; Faas, M. M.; de Vos, P. Immunological and Technical Considerations in Application of Alginate-Based Microencapsulation Systems. *Frontiers in Bioengineering and Biotechnology*. Frontiers Media S.A. **2014**. https://doi.org/10.3389/fbioe.2014.00026.

(132) Giuseppe, M. di; Law, N.; Webb, B.; A. Macrae, R.; Liew, L. J.; Sercombe, T. B.; Dilley, R. J.; Doyle, B. J. Mechanical Behaviour of Alginate-Gelatin Hydrogels for 3D Bioprinting. *J Mech Behav Biomed Mater* **2018**, *79* (September 2017), 150–157. https://doi.org/10.1016/j.jmbbm.2017.12.018.

(133) Demirtaş, T. T.; Irmak, G.; Gümüşderelioğlu, M. A Bioprintable Form of Chitosan Hydrogel for Bone Tissue Engineering. *Biofabrication* **2017**, *9* (3). https://doi.org/10.1088/1758-5090/aa7b1d.

(134) Hazur, J.; Detsch, R.; Karakaya, E.; Kaschta, J.; Teßmar, J.; Schneidereit, D.; Friedrich, O.; Schubert, D. W.; Boccaccini, A. R. Improving Alginate Printability for Biofabrication: Establishment of a Universal and Homogeneous Pre-Crosslinking Technique. *Biofabrication* **2020**, *12* (4), 045004. https://doi.org/10.1088/1758-5090/ab98e5.

(135) Muthukumar, T.; Song, J. E.; Khang, G. Biological Role of Gellan Gum in Improving Scaffold Drug Delivery, Cell Adhesion Properties for Tissue Engineering Applications. *Molecules* **2019**, *24* (24). https://doi.org/10.3390/molecules24244514.

(136) Martau, G. A.; Mihai, M.; Vodnar, D. C. The Use of Chitosan, Alginate, and Pectin in the Biomedical and Food Sector—Biocompatibility, Bioadhesiveness, and Biodegradability. *Polymers 2019, Vol. 11, Page 1837* **2019**, *11* (11), 1837. https://doi.org/10.3390/POLYM11111837.

(137) Vatankhah-Varnoosfaderani, M.; GhavamiNejad, A.; Hashmi, S.; Stadler, F. J. Hydrogen Bonding in Aprotic Solvents, a New Strategy for Gelation of Bioinspired Catecholic Copolymers with N-Isopropylamide. *Macromol Rapid Commun* **2015**, *36* (5), 447–452. https://doi.org/10.1002/MARC.201400501.

(138) Shin, M.; Lee, H. Gallol-Rich Hyaluronic Acid Hydrogels: Shear-Thinning, Protein Accumulation against Concentration Gradients, and Degradation-Resistant Properties. *Chemistry of Materials* **2017**, *29* (19), 8211–8220. https://doi.org/10.1021/acs.chemmater.7b02267.

(139) Samanta, S.; Rangasami, V. K.; Sarlus, H.; Samal, J. R. K.; Evans, A. D.; Parihar, V. S.; Varghese, O. P.; Harris, R. A.; Oommen, O. P. Interpenetrating Gallol Functionalized Tissue Adhesive Hyaluronic Acid Hydrogel Polarizes Macrophages to an Immunosuppressive Phenotype. *Acta Biomater* **2022**, *142* (1), 36–48. https://doi.org/10.1016/j.actbio.2022.01.048.

(140) Ng, W. L.; Ayi, T. C.; Liu, Y.-C.; Sing, S. L.; Yeong, W. Y.; Tan, B.-H. Fabrication and Characterization of 3D Bioprinted Triple-Layered Human Alveolar Lung Models. *Int J Bioprint* **2021**, *7* (2). https://doi.org/10.18063/IJB.V7I2.332.

(141) Li, Q.; Xu, S.; Feng, Q.; Dai, Q.; Yao, L.; Zhang, Y.; Gao, H.; Dong, H.; Chen, D.; Cao, X. 3D Printed Silk-Gelatin Hydrogel Scaffold with Different Porous Structure and Cell Seeding Strategy for Cartilage Regeneration. *Bioact Mater* **2021**, *6* (10), 3396–3410. https://doi.org/10.1016/j.bioactmat.2021.03.013.

(142) Huang, S.; Lin, P.; Yao, S.; Wu, M.; Zhu, Z.; Wang, L.; Wang, H. High-Performance Para-Aramid Paper Strengthened by Ultrafine Fiber Pulp of Polyphenylene Sulfide. *Compos Sci Technol* **2021**, *216*, 109073. https://doi.org/https://doi.org/10.1016/j.compscitech.2021.109073.

(143) Wang, W.; Xu, Y.; Li, A.; Li, T.; Liu, M.; Von Klitzing, R.; Ober, C. K.; Kayitmazer, A. B.; Li, L.; Guo, X. Zinc Induced Polyelectrolyte Coacervate Bioadhesive and Its Transition to a Self-Healing Hydrogel. *RSC Adv* **2015**, *5* (82), 66871–66878. https://doi.org/10.1039/c5ra11915d.

(144) Krogsgaard, M.; Andersen, A.; Birkedal, H. Gels and Threads: Mussel-Inspired One-Pot Route to Advanced Responsive Materials. *Chemical Communications* **2014**, *50* (87), 13278–13281. https://doi.org/10.1039/c4cc05293e.

(145) Zheng, S. Y.; Ding, H.; Qian, J.; Yin, J.; Wu, Z. L.; Song, Y.; Zheng, Q. Metal-Coordination Complexes Mediated Physical Hydrogels with High Toughness, Stick-Slip Tearing Behavior, and Good Processability. *Macromolecules* **2016**, *49* (24), 9637–9646. https://doi.org/10.1021/acs.macromol.6b02150.

(146) Shi, L.; Carstensen, H.; Hölzl, K.; Lunzer, M.; Li, H.; Hilborn, J.; Ovsianikov, A.; Ossipov, D. A. Dynamic Coordination Chemistry Enables Free Directional Printing of Biopolymer Hydrogel. *Chemistry of Materials* **2017**, *29* (14), 5816–5823. https://doi.org/10.1021/acs.chemmater.7b00128.

(147) Lee, J.; Chang, K.; Kim, S.; Gite, V.; Chung, H.; Sohn, D. Phase Controllable Hyaluronic Acid Hydrogel with Iron(III) Ion-Catechol Induced Dual Cross-Linking by Utilizing the Gap of Gelation Kinetics. *Macromolecules* **2016**, *49* (19), 7450–7459. https://doi.org/10.1021/acs.macromol.6b01198.

(148) Bijlsma, J.; de Bruijn, W. J. C.; Hageman, J. A.; Goos, P.; Velikov, K. P.; Vincken, J. P. Revealing the Main Factors and Two-Way Interactions Contributing to Food Discolouration Caused by Iron-Catechol Complexation. *Sci Rep* **2020**, *10* (1). https://doi.org/10.1038/s41598-020-65171-1.

(149) Zennifer, A.; Manivannan, S.; Sethuraman, S.; Kumbar, S. G.; Sundaramurthi, D. 3D Bioprinting and Photocrosslinking: Emerging Strategies & Future

Perspectives. *Materials Science and Engineering C*. Elsevier Ltd 2021. https://doi.org/10.1016/j.msec.2021.112576.

(150) Wang, Z.; Kumar, H.; Tian, Z.; Jin, X.; Holzman, J. F.; Menard, F.; Kim, K. Visible Light Photoinitiation of Cell-Adhesive Gelatin Methacryloyl Hydrogels for Stereolithography 3D Bioprinting. *ACS Appl Mater Interfaces* **2018**, *10* (32), 26859–26869. https://doi.org/10.1021/acsami.8b06607.

(151) Asvany, O.; Yamada, K. M. T.; Brünken, S.; Potapov, A.; Schlemmer, S. Experimental Ground-State Combination Differences of CH5+. *Science (1979)* **2015**, *347* (6228), 1346–1348. https://doi.org/10.1126/science.aaa3304.

(152) Yoon, H. J.; Shin, S. R.; Cha, J. M.; Lee, S. H.; Kim, J. H.; Do, J. T.; Song, H.; Bae, H. Cold Water Fish Gelatin Methacryloyl Hydrogel for Tissue Engineering Application. *PLoS One* **2016**, *11* (10), e0163902. https://doi.org/10.1371/JOURNAL.PONE.0163902.

(153) Karvinen, J.; Ihalainen, T. O.; Calejo, M. T.; Jönkkäri, I.; Kellomäki, M. Characterization of the Microstructure of Hydrazone Crosslinked Polysaccharide-Based Hydrogels through Rheological and Diffusion Studies. *Materials Science and Engineering C* **2019**, *94* (January 2019), 1056–1066. https://doi.org/10.1016/j.msec.2018.10.048.

(154) Billiet, T.; Vandenhaute, M.; Schelfhout, J.; Van Vlierberghe, S.; Dubruel, P. A Review of Trends and Limitations in Hydrogel-Rapid Prototyping for Tissue Engineering. *Biomaterials*. September **2012**, 6020–6041. https://doi.org/10.1016/j.biomaterials.2012.04.050.

(155) Chimene, D.; Lennox, K. K.; Kaunas, R. R.; Gaharwar, A. K. Advanced Bioinks for 3D Printing: A Materials Science Perspective. *Annals of Biomedical Engineering*. Springer New York LLC June 1, **2016**, 2090–2102. https://doi.org/10.1007/s10439-016-1638-y.

(156) Duan, B.; Kapetanovic, E.; Hockaday, L. A.; Butcher, J. T. Three-Dimensional Printed Trileaflet Valve Conduits Using Biological Hydrogels and Human Valve Interstitial Cells. *Acta Biomater* **2014**, *10* (5), 1836–1846. https://doi.org/10.1016/j.actbio.2013.12.005.

(157) Kyle, S.; Jessop, Z. M.; Al-Sabah, A.; Whitaker, I. S. 'Printability" of Candidate Biomaterials for Extrusion Based 3D Printing: State-of-the-Art.' *Advanced Healthcare Materials*. Wiley-VCH Verlag August 23, **2017**. https://doi.org/10.1002/adhm.201700264.

(158) Deforest, C. A.; Anseth, K. S. Advances in Bioactive Hydrogels to Probe and Direct Cell Fate. *Annual Review of Chemical and Biomolecular Engineering*. **2012**, 421–444. https://doi.org/10.1146/annurev-chembioeng-062011-080945.

(159) Bartnikowski, M.; Wellard, R. M.; Woodruff, M.; Klein, T. Tailoring Hydrogel Viscoelasticity with Physical and Chemical Crosslinking. *Polymers (Basel)* **2015**, *7* (12), 2650–2669. https://doi.org/10.3390/polym7121539.

(160) Gu, Y.; Zhang, L.; Du, X.; Fan, Z.; Wang, L.; Sun, W.; Cheng, Y.; Zhu, Y.; Chen, C. Reversible Physical Crosslinking Strategy with Optimal Temperature

for 3D Bioprinting of Human Chondrocyte-Laden Gelatin Methacryloyl Bioink. *J Biomater Appl* **2018**, *33* (5), 609–618. https://doi.org/10.1177/0885328218805864.

(161) Rebers, L.; Granse, T.; Tovar, G. E. M.; Southan, A.; Borchers, K. Physical Interactions Strengthen Chemical Gelatin Methacryloyl Gels. *Gels* **2019**, *5* (1), 4. https://doi.org/10.3390/gels5010004.

(162) Wang, M. D.; Zhai, P.; Schreyer, D. J.; Zheng, R. S.; Sun, X. D.; Cui, F. Z.; Chen, X. B. Novel Crosslinked Alginate/Hyaluronic Acid Hydrogels for Nerve Tissue Engineering. *Front Mater Sci* **2013**, *7* (3), 269–284. https://doi.org/10.1007/s11706-013-0211-y.

(163) Gao, Y.; Jin, X. Dual Crosslinked Methacrylated Alginate Hydrogel Micron Fibers and Tissue Constructs for Cell Biology. *Mar Drugs* **2019**, *17* (10). https://doi.org/10.3390/md17100557.

(164) Araiza-Verduzco, F.; Rodríguez-Velázquez, E.; Cruz, H.; Rivero, I. A.; Acosta-Martínez, D. R.; Pina-Luis, G.; Alatorre-Meda, M. Photocrosslinked Alginate-Methacrylate Hydrogels with Modulable Mechanical Properties: Effect of the Molecular Conformation and Electron Density of the Methacrylate Reactive Group. *Materials* **2020**, *13* (3), 534. https://doi.org/10.3390/ma13030534.

(165) Hull, S. M.; Brunel, L. G.; Heilshorn, S. C.; Hull, S. M.; Brunel, L. G.; Heilshorn, S. C. 3D Bioprinting of Cell-Laden Hydrogels for Improved Biological Functionality. *Advanced Materials* **2022**, *34* (2), 2103691. https://doi.org/10.1002/ADMA.202103691.

(166) Ribeiro, A.; Blokzijl, M. M.; Levato, R.; Visser, C. W.; Castilho, M.; Hennink, W. E.; Vermonden, T.; Malda, J. Assessing Bioink Shape Fidelity to Aid Material Development in 3D Bioprinting. *Biofabrication* **2018**, *10* (1), 014102. https://doi.org/10.1088/1758-5090/aa90e2.

(167) Park, Y. D.; Tirelli, N.; Hubbell, J. A. Photopolymerized Hyaluronic Acid-Based Hydrogels and Interpenetrating Networks. *Biomaterials* **2003**, *24* (6), 893–900. https://doi.org/10.1016/S0142-9612(02)00420-9.

(168) Wang, M.; Li, W.; Hao, J.; Gonzales, A.; Zhao, Z.; Flores, R. S.; Kuang, X.; Mu, X.; Ching, T.; Tang, G.; Luo, Z.; Garciamendez-Mijares, C. E.; Sahoo, J. K.; Wells, M. F.; Niu, G.; Agrawal, P.; Quiñones-Hinojosa, A.; Eggan, K.; Zhang, Y. S. Molecularly Cleavable Bioinks Facilitate High-Performance Digital Light Processing-Based Bioprinting of Functional Volumetric Soft Tissues. *Nat Commun* **2022**, *13* (1). https://doi.org/10.1038/s41467-022-31002-2.

(169) Hong, S.; Sycks, D.; Chan, H. F.; Lin, S.; Lopez, G. P.; Guilak, F.; Leong, K. W.; Zhao, X. 3D Printing of Highly Stretchable and Tough Hydrogels into Complex, Cellularized Structures. *Advanced Materials* **2015**, *27* (27), 4035–4040. https://doi.org/10.1002/adma.201501099.

(170) Aldana, A. A.; Valente, F.; Dilley, R.; Doyle, B. Development of 3D Bioprinted GelMA-Alginate Hydrogels with Tunable Mechanical Properties. *Bioprinting*

2021, *21* (September 2020), e00105. https://doi.org/10.1016/j.bprint.2020.e00105.

(171) Shyam Mohan, T.; Datta, P.; Nesaei, S.; Ozbolat, V.; Ozbolat, I. T. 3D Coaxial Bioprinting: Process Mechanisms, Bioinks and Applications. *Progress in Biomedical Engineering* **2022**, *4* (2), 022003. https://doi.org/10.1088/2516-1091/AC631C.

(172) Jaiswal, M. K.; Xavier, J. R.; Carrow, J. K.; Desai, P.; Alge, D.; Gaharwar, A. K. Mechanically Stiff Nanocomposite Hydrogels at Ultralow Nanoparticle Content. *ACS Nano* **2016**, *10* (1), 246–256. https://doi.org/10.1021/acsnano.5b03918.

(173) Highley, C. B.; Rodell, C. B.; Burdick, J. A. Direct 3D Printing of Shear-Thinning Hydrogels into Self-Healing Hydrogels. *Advanced Materials* **2015**, *27* (34), 5075–5079. https://doi.org/10.1002/adma.201501234.

(174) Li, N.; Guo, R.; Zhang, Z. J. Bioink Formulations for Bone Tissue Regeneration. *Front Bioeng Biotechnol* **2021**, *9*, 44. https://doi.org/10.3389/FBIOE.2021.630488.

(175) Galarraga, J. H.; Kwon, M. Y.; Burdick, J. A. 3D Bioprinting via an in Situ Crosslinking Technique towards Engineering Cartilage Tissue. *Sci Rep* **2019**, *9* (1). https://doi.org/10.1038/s41598-019-56117-3.

(176) Costantini, M.; Colosi, C.; Święszkowski, W.; Barbetta, A. Co-Axial Wet-Spinning in 3D Bioprinting: State of the Art and Future Perspective of Microfluidic Integration. *Biofabrication* **2019**, *11* (1). https://doi.org/10.1088/1758-5090/aae605.

(177) Piras, C. C.; Smith, D. K. Multicomponent Polysaccharide Alginate-Based Bioinks. *Journal of Materials Chemistry B*. Royal Society of Chemistry September 28, **2020**, 8171–8188. https://doi.org/10.1039/d0tb01005g.

(178) Gao, G.; Lee, J. H.; Jang, J.; Lee, D. H.; Kong, J. S.; Kim, B. S.; Choi, Y. J.; Jang, W. B.; Hong, Y. J.; Kwon, S. M.; Cho, D. W. Tissue Engineered Bio-Blood-Vessels Constructed Using a Tissue-Specific Bioink and 3D Coaxial Cell Printing Technique: A Novel Therapy for Ischemic Disease. *Adv Funct Mater* **2017**, *27* (33). https://doi.org/10.1002/adfm.201700798.

(179) Davoodi, E.; Sarikhani, E.; Montazerian, H.; Ahadian, S.; Costantini, M.; Swieszkowski, W.; Willerth, S. M.; Walus, K.; Mofidfar, M.; Toyserkani, E.; Khademhosseini, A.; Ashammakhi, N. Extrusion and Microfluidic-Based Bioprinting to Fabricate Biomimetic Tissues and Organs. *Advanced Materials Technologies*. Wiley-Blackwell August 1, **2020**. https://doi.org/10.1002/admt.201901044.

(180) Ashammakhi, N.; Hasan, A.; Kaarela, O.; Byambaa, B.; Sheikhi, A.; Gaharwar, A. K.; Khademhosseini, A. Advancing Frontiers in Bone Bioprinting. *Advanced Healthcare Materials*. Wiley-VCH Verlag April 11, **2019**. https://doi.org/10.1002/adhm.201801048.

(181) Hinton, T. J.; Jallerat, Q.; Palchesko, R. N.; Park, J. H.; Grodzicki, M. S.; Shue, H. J.; Ramadan, M. H.; Hudson, A. R.; Feinberg, A. W. Three-Dimensional Printing of Complex Biological Structures by Freeform Reversible Embedding of Suspended Hydrogels. *Sci Adv* **2015**, *1* (9). https://doi.org/10.1126/sciadv.1500758.

(182) Allencherry, J.; Pradeep, N.; Shrivastava, R.; Joy, L.; Imbriacco, F.; Özel, T. Investigation of Hydrogel and Gelatin Bath Formulations for Extrusion-Based 3D Bioprinting Using Deep Learning. In *Procedia CIRP*; Elsevier B.V., **2022**; Vol. 110, 362–367. https://doi.org/10.1016/j.procir.2022.06.064.

(183) Lee, A.; Hudson, A. R.; Shiwarski, D. J.; Tashman, J. W.; Hinton, T. J.; Yerneni, S.; Bliley, J. M.; Campbell, P. G.; Feinberg, A. W. 3D Bioprinting of Collagen to Rebuild Components of the Human Heart. *Biomedicine (Taipei)* **2019**, No. 365, 482–487. 10.1126/science.aav9051

(184) Kosik-Kozioł, A.; Costantini, M.; Mróz, A.; Idaszek, J.; Heljak, M.; Jaroszewicz, J.; Kijeńska, E.; Szöke, K.; Frerker, N.; Barbetta, A.; Brinchmann, J. E.; Święszkowski, W. 3D Bioprinted Hydrogel Model Incorporating β -Tricalcium Phosphate for Calcified Cartilage Tissue Engineering. *Biofabrication* **2019**, *11* (3), 035016. https://doi.org/10.1088/1758-5090/ab15cb.

(185) Melchels, F. P. W.; Dhert, W. J. A.; Hutmacher, D. W.; Malda, J. Development and Characterisation of a New Bioink for Additive Tissue Manufacturing. *J Mater Chem B* **2014**, *2* (16), 2282–2289. https://doi.org/10.1039/c3tb21280g.

(186) Malekpour, A.; Chen, X. Printability and Cell Viability in Extrusion-Based Bioprinting from Experimental, Computational, and Machine Learning Views. *Journal of Functional Biomaterials*. MDPI June 1, **2022**. https://doi.org/10.3390/jfb13020040.

(187) Mezger, T. G. *European Coatings Tech Files The Rheology Handbook: 3 Rd Revised Edition*; 2011.

(188) Cooke, M. E.; Rosenzweig, D. H. The Rheology of Direct and Suspended Extrusion Bioprinting. *APL Bioeng* **2021**, *5* (1), 011502. https://doi.org/10.1063/5.0031475.

(189) Ionescu, C. M.; Birs, I. R.; Copot, D.; Muresan, C. I.; Caponetto, R. Mathematical Modelling with Experimental Validation of Viscoelastic Properties in Non-Newtonian Fluids. *Philosophical Transactions of the Royal Society A* **2020**, *378* (2172). https://doi.org/10.1098/RSTA.2019.0284.

(190) Kasehagen, L. J.; Macosko, C. W. Nonlinear Shear and Extensional Rheology of Long-Chain Randomly Branched Polybutadiene. *J Rheol (N Y N Y)* **1998**, *42* (6), 1303. https://doi.org/10.1122/1.550892.

(191) Sathaye, S.; Mbi, A.; Sonmez, C.; Chen, Y.; Blair, D. L.; Schneider, J. P.; Pochan, D. J. Rheology of Peptide- and Protein-Based Physical Hydrogels: Are Everyday Measurements Just Scratching the Surface? *Wiley Interdiscip Rev Nanomed Nanobiotechnol* **2015**, *7* (1), 34–68. https://doi.org/10.1002/wnan.1299.

(192) Chimene, D.; Peak, C. W.; Gentry, J. L.; Carrow, J. K.; Cross, L. M.; Mondragon, E.; Cardoso, G. B.; Kaunas, R.; Gaharwar, A. K. Nanoengineered Ionic-Covalent Entanglement (NICE) Bioinks for 3D Bioprinting. *ACS Appl Mater Interfaces* **2018**, *10* (12), 9957–9968. https://doi.org/10.1021/acsami.7b19808.

(193) Fischer, L.; Nosratlo, M.; Hast, K.; Karakaya, E.; Ströhlein, N.; Esser, T. U.; Gerum, R.; Richter, S.; Engel, F.; Detsch, R.; Fabry, B.; Thievessen, I. Calcium Supplementation of Bioinks Reduces Shear Stress-Induced Cell Damage during Bioprinting. *Biofabrication* **2022**, *14* (4). https://doi.org/10.1088/1758-5090/ac84af.

(194) Barbucci, R.; Leone, G.; Lamponi, S. Thixotrophy Property of Hydrogels to Evaluate the Cell Growing on the inside of the Material Bulk (Amber Effect). *J Biomed Mater Res B Appl Biomater* **2006**, *76* (1), 33–40. https://doi.org/10.1002/jbm.b.30390.

(195) Abouzeid, R. E.; Khiari, R.; Beneventi, D.; Dufresne, A. Biomimetic Mineralization of Three-Dimensional Printed Alginate/TEMPO-Oxidized Cellulose Nanofibril Scaffolds for Bone Tissue Engineering. *Biomacromolecules* **2018**, *19* (11), 4442–4452. h https://doi.org/10.1021/acs.biomac.8b01325

(196) Oyen, M. L. Mechanical Characterisation of Hydrogel Materials. *International Materials Reviews*. Maney Publishing **2014**, 44–59. https://doi.org/10.1179/1743280413Y.0000000022.

(197) Diamantides, N.; Wang, L.; Pruiksma, T.; Siemiatkoski, J.; Dugopolski, C.; Shortkroff, S.; Kennedy, S.; Bonassar, L. J. Correlating Rheological Properties and Printability of Collagen Bioinks: The Effects of Riboflavin Photocrosslinking and PH. *Biofabrication* **2017**, *9* (3), 034102. https://doi.org/10.1088/1758-5090/aa780f.

(198) O'Connell, C. D.; Di Bella, C.; Thompson, F.; Augustine, C.; Beirne, S.; Cornock, R.; Richards, C. J.; Chung, J.; Gambhir, S.; Yue, Z.; Bourke, J.; Zhang, B.; Taylor, A.; Quigley, A.; Kapsa, R.; Choong, P.; Wallace, G. G. Development of the Biopen: A Handheld Device for Surgical Printing of Adipose Stem Cells at a Chondral Wound Site. *Biofabrication* **2016**, *8* (1), 0. https://doi.org/10.1088/1758-5090/8/1/015019.

(199) Kirchmajer, D. M.; Steinhoff, B.; Warren, H.; Clark, R.; In Het Panhuis, M. Enhanced Gelation Properties of Purified Gellan Gum. *Carbohydr Res* **2014**, *388* (1), 125–129. https://doi.org/10.1016/j.carres.2014.02.018.

(200) Smeds, K. A.; Grinstaff, M. W. Photocrosslinkable Polysaccharides for in Situ Hydrogel Formation. *J Biomed Mater Res* **2001**, *54* (1), 115–121. https://doi.org/10.1002/1097-4636(200101)54:1<115::AID-JBM14>3.0.CO;2-Q.

(201) Colosi, C.; Shin, S. R.; Manoharan, V.; Massa, S.; Costantini, M.; Barbetta, A.; Dokmeci, R.; Dentini, M.; Khademhosseini, A. Microfluidic Bioprinting of Heterogeneous 3D Tissue Constructs Using Low-Viscosity Bioink. *Advanced Materials* **2016**, *28* (4), 677–684. https://doi.org/10.1002/ADMA.201503310.

(202) Chung, J. H. Y.; Naficy, S.; Yue, Z.; Kapsa, R.; Quigley, A.; Moulton, S. E.; Wallace, G. G. Bio-Ink Properties and Printability for Extrusion Printing Living Cells. *Biomater Sci* **2013**, *1* (7), 763–773. https://doi.org/10.1039/C3BM00012E.

(203) Pepelanova, I.; Kruppa, K.; Scheper, T.; Lavrentieva, A. Gelatin-Methacryloyl (GelMA) Hydrogels with Defined Degree of Functionalization as a Versatile Toolkit for 3D Cell Culture and Extrusion Bioprinting. *Bioengineering* **2018**, *5* (3), 55. https://doi.org/10.3390/bioengineering5030055.

(204) Nguyen, K. T.; West, J. L. Photopolymerizable Hydrogels for Tissue Engineering Applications. *Biomaterials* **2002**, *23* (22), 4307–4314. https://doi.org/10.1016/S0142-9612(02)00175-8.

(205) Fan, Y.; Yue, Z.; Lucarelli, E.; Wallace, G. G. Hybrid Printing Using Cellulose Nanocrystals Reinforced GelMA/HAMA Hydrogels for Improved Structural Integration. *Adv Healthc Mater* **2020**, *9* (24). https://doi.org/10.1002/adhm.202001410.

(206) Koti, P.; Muselimyan, N.; Mirdamadi, E.; Asfour, H.; Sarvazyan, N. A. Use of GelMA for 3D Printing of Cardiac Myocytes and Fibroblasts. *J 3D Print Med* **2019**, *3* (1), 11–22. https://doi.org/10.2217/3dp-2018-0017.

(207) Fazary, A. E.; Taha, M.; Ju, Y. H. Iron Complexation Studies of Gallic Acid. *J Chem Eng Data* **2009**, *54* (1), 35–42. https://doi.org/10.1021/je800441u.

(208) Haidari, H.; Kopecki, Z.; Sutton, A. T.; Garg, S.; Cowin, A. J.; Vasilev, K. Ph-Responsive "Smart" Hydrogel for Controlled Delivery of Silver Nanoparticles to Infected Wounds. *Antibiotics* **2021**, *10* (1), 1–15. https://doi.org/10.3390/antibiotics10010049.

(209) Jiang, H.; Ochoa, M.; Waimin, J. F.; Rahimi, R.; Ziaie, B. A PH-Regulated Drug Delivery Dermal Patch for Targeting Infected Regions in Chronic Wounds. *Lab Chip* **2019**, *19* (13), 2265–2274. https://doi.org/10.1039/c9lc00206e.

(210) Kimura, S.; Haraya, N.; Komiyama, T.; Yokoya, M.; Yamanaka, M. Formation of PH-Responsive Supramolecular Hydrogels in Basic Buffers: Self-Assembly of Amphiphilic Tris-Urea. *Chem Pharm Bull (Tokyo)* **2021**, *69* (11), 1131–1135. https://doi.org/10.1248/cpb.c21-00539.

(211) Chen, Y.; Xiong, X.; Liu, X.; Cui, R.; Wang, C.; Zhao, G.; Zhi, W.; Lu, M.; Duan, K.; Weng, J.; Qu, S.; Ge, J. 3D Bioprinting of Shear-Thinning Hybrid Bioinks with Excellent Bioactivity Derived from Gellan/Alginate and Thixotropic Magnesium Phosphate-Based Gels. *J Mater Chem B* **2020**, *8* (25), 5500–5514. https://doi.org/10.1039/D0TB00060D.

(212) Grigoryan, B.; Miller, J. S. 3D Printing and Patterning Vasculature in Engineered Tissues. *3D Bioprinting and Nanotechnology in Tissue Engineering and Regenerative Medicine* **2015**, 171–189. https://doi.org/10.1016/B978-0-12-800547-7.00008-4.

(213) El-Hiti, G. A.; Ahmed, D. S.; Yousif, E.; Al-Khazrajy, O. S. A.; Abdallh, M.; Alanazi, S. A. Modifications of Polymers through the Addition of Ultraviolet

Absorbers to Reduce the Aging Effect of Accelerated and Natural Irradiation. *Polymers (Basel)* **2022**, *14* (1). https://doi.org/10.3390/POLYM14010020.

(214) Williams, C. G.; Malik, A. N.; Kim, T. K.; Manson, P. N.; Elisseeff, J. H. Variable Cytocompatibility of Six Cell Lines with Photoinitiators Used for Polymerizing Hydrogels and Cell Encapsulation. *Biomaterials* **2005**, *26* (11), 1211–1218. https://doi.org/10.1016/j.biomaterials.2004.04.024.

(215) Nguyen, A. K.; Goering, P. L.; Reipa, V.; Narayan, R. J. Toxicity and Photosensitizing Assessment of Gelatin Methacryloyl-Based Hydrogels Photoinitiated with Lithium Phenyl-2,4,6-Trimethylbenzoylphosphinate in Human Primary Renal Proximal Tubule Epithelial Cells. *Biointerphases* **2019**, *14* (2), 021007. https://doi.org/10.1116/1.5095886.

(216) Fairbanks, B. D.; Schwartz, M. P.; Bowman, C. N.; Anseth, K. S. Photoinitiated Polymerization of PEG-Diacrylate with Lithium Phenyl-2,4,6-Trimethylbenzoylphosphinate: Polymerization Rate and Cytocompatibility. *Biomaterials* **2009**, *30* (35), 6702–6707. https://doi.org/10.1016/j.biomaterials.2009.08.055.

(217) Ikehata, H.; Higashi, S.; Nakamura, S.; Daigaku, Y.; Furusawa, Y.; Kamei, Y.; Watanabe, M.; Yamamoto, K.; Hieda, K.; Munakata, N.; Ono, T. Action Spectrum Analysis of UVR Genotoxicity for Skin: The Border Wavelengths between UVA and UVB Can Bring Serious Mutation Loads to Skin. *Journal of Investigative Dermatology* **2013**, *133* (7), 1850–1856. https://doi.org/10.1038/jid.2012.504.

(218) Turunen, S.; Käpylä, E.; Lähteenmäki, M.; Ylä-Outinen, L.; Narkilahti, S.; Kellomäki, M. Direct Laser Writing of Microstructures for the Growth Guidance of Human Pluripotent Stem Cell Derived Neuronal Cells. *Opt Lasers Eng* **2014**, *55*, 197–204. https://doi.org/10.1016/j.optlaseng.2013.11.003.

(219) Elkhoury, K.; Zuazola, J.; Vijayavenkataraman, S. Bioprinting the Future Using Light: A Review on Photocrosslinking Reactions, Photoreactive Groups, and Photoinitiators. *SLAS Technol* **2023**. https://doi.org/10.1016/j.slast.2023.02.003.

(220) O'Connell, Cathal; Junxiang, Ren; Leon, Pope; Yifan, Li; Anushree, Mohandas; Romane, Blanchard; Serena, Duchi; Carmine, O. 3DBioprinting: Principles and Protocols. In *Method in Molecular Biology*; Crook, J. M., Ed.; Humana, New York, NY, **2020**; 111–131. https://doi.org/https://doi.org/10.1007/978-1-0716-0520-2_7.

PUBLICATIONS

Publication I Jongprasitkul, H.; Turunen, S.; Parihar, V.S.; Annurakshita, S; Kellomäki, M. Photocross-linkable Methacrylated Polypeptides and Polysaccharides for Casting, Injecting, and 3D Fabrication, *Biomacromolecules* 2021, 22(2), 481–493. DOI: https://doi.org/10.1021/acs.biomac.0c01322

Publication II Jongprasitkul, H.; Turunen, S.; Parihar, V.S.; Kellomäki, M. Two-Step Crosslinking to Enhance the Printability of Methacrylated Gellan Gum Biomaterial Ink for Extrusion-Based 3D Bioprinting. *Bioprinting* 2022, 25, No. e00185. DOI: https://doi.org/10.1016/j.bprint.2021.e00185

Publication III Jongprasitkul, H.; Turunen, S.; Parihar, V.S.; Kellomäki, M. Sequential Cross-linking of Gallic Acid-Functionalized GelMA-Based Bioinks with Enhanced Printability for Extrusion-Based 3D Bioprinting. *Biomacromolecules* 2023, 24(1), 502-514. DOI: https://doi.org/10.1021/acs.biomac.2c01418

Publication IV Jongprasitkul, H.; Parihar, V.S.; Turunen, S.; Kellomäki, M. pH-Responsive Gallol Functionalized Hyaluronic Acid-based Tissue Adhesive Hydrogels for Injecting and 3D Bioprinting. ACS Applied Materials & Interfaces 2023, 15(28), 33972-33984. DOI: https://doi.org/10.1021/acsami.3c02961

PUBLICATION I

Photocross-linkable Methacrylated Polypeptides and Polysaccharides for Casting, Injecting, and 3D Fabrication

Jongprasitkul, H.; Turunen, S.; Parihar, V.S.; Annurakshita, S; Kellomäki, M.

Biomacromolecules 2021, 22(2), 481–493
https://doi.org/10.1021/acs.biomac.0c01322

BioMACROMOLECULES

pubs.acs.org/Biomac Article

Photocross-linkable Methacrylated Polypeptides and Polysaccharides for Casting, Injecting, and 3D Fabrication

Hatai Jongprasitkul, Sanna Turunen, Vijay Singh Parihar,* Shambhavee Annurakshita, and Minna Kellomäki*

Cite This: https://dx.doi.org/10.1021/acs.biomac.0c01322 Read Online

ACCESS | Metrics & More | Article Recommendations | Supporting Information

ABSTRACT: For modern tissue engineering, we need not only develop new hydrogels but also suitable processing methods for them. Polypeptides and polysaccharides are potential candidates because they can be methacrylated, processed before photocross-linking, and yielded into hydrogels with given shape and form. In this study, we successfully methacrylated collagen, gelatin, hyaluronan, and alginate to 30 and 60% degree of modification. We studied methacrylated compositions (i.e., precursors) to investigate their processability. The precursors of collagen and gelatin with 60% methacrylation exhibited suitable yield stress, shear-thinning properties, and fiber-forming capability for injecting and 3D bioprinting. On the contrary, the 30% methacrylated precursors had properties suitable for casting purposes. Our study also showed that the mechanical properties of hydrogels corresponded to the used photocross-linking conditions and the degree of modification. These results underline the importance of tunability of the precursors and resulting hydrogels according to the specific fabrication method and tissue engineering application.

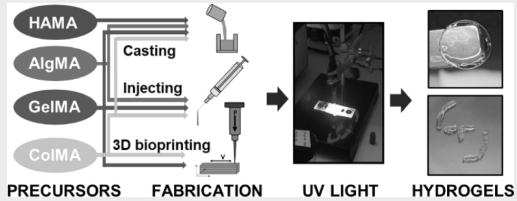

■ INTRODUCTION

Photocross-linkable hydrogels have attracted growing interest in tissue engineering because light provides spatiotemporal control over the reaction behavior of the material.[1] Hence, photocross-linking can be used to control the accurate fabrication of 3D structures.[2] Furthermore, the chemistry of photocross-linking can be controlled accurately and the cross-linking results in minimal byproducts, both of which enable safe fabrication of cell-containing constructs.[3] Photocross-linking can be used as a part of various fabrication methods—casting, injecting, and 3D bioprinting—to produce hydrogel scaffolds for tissue engineering.[4,5] All these fabrication methods have their unique prerequisites concerning the properties of the precursors (polymers with a functional group capable of being cross-linked with the energy of light), such as viscosity, shear response, yield stress, shape fidelity before cross-linking, or gelation time.[6,7]

The most common way to engineer polymers photocross-linkable is the introduction of methacryloyl groups via esterification with methacrylic anhydride.[8,9] These methacrylated precursors can then be efficiently cross-linked via free-radical chain polymerization because of the rapid nature of the reaction. Overall, the free-radical chain polymerization offers a practical way to tune the structure and cross-linking density of the formed networks via varying the photoinitiator (PI) concentration, reactive group concentration, or light intensity.[10,11]

Hydrogels can be derived both from natural and synthetic polymers and especially, polypeptide- and polysaccharide-derived hydrogels are of great interest for biomedical applications.[12] In fact, a variety of hydrogels derived from polypeptides, polysaccharides, and glycosaminoglycans, including gelatin, collagen, alginate, and hyaluronic acid, have been fabricated into scaffolds.[13−18] These polymers are widely used for hydrogel preparation because they can easily mimic extracellular matrix and have tunable viscoelasticity and high permeability, which can enhance cell adhesion, spreading, and proliferation.[19,20] The current challenges of using polypeptide−polysaccharide-based hydrogels in 2D or 3D constructs include poor mechanical properties, low stability, batch-to-batch variations of raw material, and difficulty to purify to be used with cells or clinically.[21,22] However, polypeptides and polysaccharides have a variety of functional groups, which give flexibility to the modifications and tune the mechanical and biological properties of precursors and resulting hydrogels.[23]

So far, there exist only a few studies reporting a comparison of methacrylated polypeptide and polysaccharide-based hydrogels in terms of the pre- and post-photocross-linking

Received: September 10, 2020
Revised: December 4, 2020

https://dx.doi.org/10.1021/acs.biomac.0c01322
Biomacromolecules XXXX, XXX, XXX−XXX

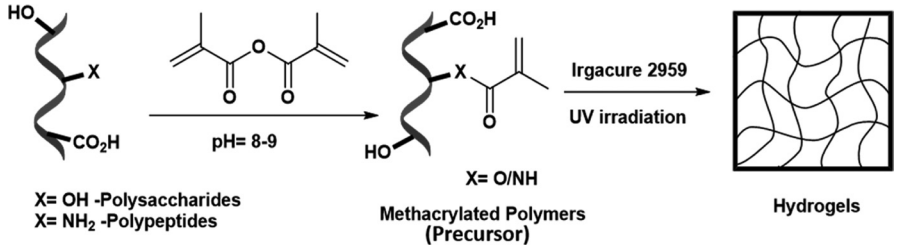

Figure 1. Methacrylation of polypeptides and polysaccharides (precursors) and formation of photocross-linked hydrogels.

conditions, such as modification degree of the precursor polymer, UV intensity and exposure time, gelation time, and mechanical properties of the resulting hydrogel.[24−27] There is a clear need for a comprehensive study that provides enough data to formulate guiding principles for the end users to select feasible materials to be used with specific cells and for different processing methods, and we wanted to meet these demands. We anticipated that the polymer type (source) and methacrylation degree (MD) of precursors would influence their properties such as viscosity, yield stress, shear-thinning behavior, and injectability/printability. We also expected that the polymer type together with the photocross-linking conditions (UV intensity and exposure time) would affect the properties of the photocross-linked hydrogel (stiffness and hydrophilicity).

To our knowledge, for the first time, two methacrylated polypeptides (collagen and gelatin) and two polysaccharides (alginate and hyaluronic acid) have been compared to this extent. We synthesized the precursors with two different MDs and characterized them thoroughly. The hydrogels were formed from the precursors by photocross-linking using various UV exposure conditions and evaluated for their viscoelastic properties. The results are reflected to meet the requirements of different fabrication methods, namely, 2D or 3D casting, injecting, or 3D bioprinting.

■ MATERIALS AND METHODS

Material Synthesis. Precursors with low (∼30%) and high (∼60%) MD were synthesized by tuning the specific ratio of methacrylic anhydride with respect to the precursor volume. In our study, we chose two polypeptides and two polysaccharides to be functionalized and studied for their properties. For modified polypeptide representatives, we synthesized gelatin methacrylate (GelMA) and collagen methacrylate (ColMA), and for modified polysaccharides, hyaluronan methacrylate (HAMA) and alginate methacrylate (AlgMA) (Figure 1).

Methacrylated polypeptides (GelMA and ColMA) with 30 and 60% MD were prepared. The different modification degrees were achieved by tuning the ratio of methacrylic anhydride in the reaction, as follows. For GelMA, 1 g of Gelatin Type A (porcine skin, 300 bloom strength, Merck KGaA, Darmstadt, Germany) was dissolved in 10 mL of deionized water at 40−50 °C and vigorously stirred until it became homogeneous. The pH was adjusted to 8 by adding a few drops of 1 M NaOH. Next, methacrylic anhydride (Merck KGaA) was added into the system dropwise, providing the amount equal to the defined modification in each material. The solution was stirred for 1 h at 40−50 °C while maintaining the pH 8. After that, the reaction mixture was diluted to 60 mL and dialyzed with a 3.5 kDa molecular weight-cutoff (MWCO) membrane (Spectra/Por, Repligen Corp., USA) against deionized water for 72 h (2 × 2 L, 12 h) at 40 °C. Thereafter, the solution was lyophilized, and 1 g of the product was obtained. For ColMA, collagen type I with 30 and 60% MD was prepared via the technique reported elsewhere in order to achieve a high degree of modification.[23] The different modification degrees were adjusted by tuning the ratio of methacrylic anhydride in the reaction, as described before. Bovine dermal collagen type I solution (PureCol, Advanced BioMatrix, USA, 3.0 mg/mL in 0.01 M HCl) was slowly adjusted to pH 7−8 at 4 °C to prevent precipitation. Next, methacrylic anhydride was added into the system dropwise, providing the equivalent amount reported for the defined modification in each material.[23] The reaction mixture was stirred and was adjusted to pH 8 by carefully adding 10 M NaOH at 4 °C for 7 h. Next, the reaction mixture was stirred overnight at room temperature (RT, 21 °C) and transferred into a dialysis bag with a 3.5 kDa MWCO membrane and dialyzed against deionized water for 72 h (2 × 2 L, 12 h). Thereafter, the solution was lyophilized, and 300 mg of the product was obtained.

Methacrylated polysaccharides (HAMA and AlgMA) with 30 and 60% MD were prepared by adjusting the ratio of methacrylic anhydride in the reaction, as described above. For HAMA, 400 mg of sodium hyaluronate (100 kDa in molecular weight, Lifecore Biomedical, USA) was dissolved in 60 mL of deionized water and vigorously stirred until it became homogeneous. The pH was adjusted to 8 by adding a few drops of 1 M NaOH. Next, methacrylic anhydride was added into the system dropwise, providing the amount equal to the defined modification in each material. The reaction was carried out for 7 h at 4 °C while maintaining pH 8. After that, the reaction mixture was diluted to 60 mL to quench the reaction and dialyzed with a 3.5 kDa MWCO membrane against deionized water for 72 h (2 × 2 L, 12 h) at RT. Thereafter, the solution was lyophilized, and 390 mg of the product was obtained. For AlgMA, 400 mg of sodium alginate (Merck KGaA) was dissolved in 60 mL of deionized water and vigorously stirred until it became homogeneous. The pH was adjusted to 8 by adding a few drops of 1 M NaOH. Next, methacrylic anhydride was added into the system dropwise, providing the equivalent amount for the defined modification in each material. The reaction mixture was stirred at 4 °C for 1 h and then continued at RT for 7 h while maintaining pH 8. After that, the reaction mixture was diluted to 60 mL and dialyzed with a 3.5 kDa MWCO membrane against deionized water for 72 h (2 × 2 L, 12 h) at RT. Thereafter, the solution was lyophilized, and 395 mg of the product was obtained.

Quantification of the Modification Degree. For GelMA and ColMA, the MD was determined by trinitrobenzene sulfonic acid (TNBS) assay using UV spectroscopy (UV-3600 Plus, Shimadzu Corp., Japan) at a wavelength 350−500 nm, as described in the literature.[24] The MD was calculated using an estimation of free amines before and after the methacrylate conjugation. The percentage decrease of amine groups after substitution matched the percentage of methacrylate conjugation. For HAMA and AlgMA, the MD in polysaccharides was quantified by ^{1}H NMR. The NMR spectra were recorded using Varian Mercury 300 MHz spectrometer [deuterium oxide (D_2O) as a solvent]. The sample concentrations were around 0.8% weight/volume (w/v). The measurement was performed at RT.

Spin-Coating Experiment of Precursors. The precursors with a concentration of 5 w/v % in deionized water were spin-coated on borosilicate coverslips with 1000 rpm for HAMA and GelMA, 2000 rpm for AlgMA and ColMA, using an acceleration of 500 m/s^2 for 40 s. The thickness of the films was measured with a profilometer (Dektak 150, Veeco Instruments Inc., USA).

https://dx.doi.org/10.1021/acs.biomac.0c01322
Biomacromolecules XXXX, XXX, XXX−XXX

Preparation of Photocross-linkable Precursors. Methacrylated precursor solutions were prepared at a concentration of 5 w/v % in deionized water. The solutions were stirred and incubated at 37 °C until they were completely dissolved. The PI, 2-hydroxy-4′-(2-hydroxyethoxy)-2-methylpropiophenone (Irgacure 2959, Merck KGaA) was added in all of the polymer solutions at a concentration of 0.5% w/v. The pH was adjusted to 7 in order to maintain proper viscosity and dissolution. Later, when precursor is referred, it is a solution prepared in this manner having PI added.

Prescreening of the Filament Formation of Precursors. All precursors were transferred into a 1 mL syringe capped with a needle having an inner diameter of 250 μm (Optimum General Purpose Stainless Steel Tips, Nordson EFD, USA). The syringe was installed in a vertical position and fixed with a clamp to prevent the variation of temperature. The solution was injected by manually pressing the plunger. The filament formation of the precursor was observed with a contact angle (CA) camera, and a video was recorded. The fiber was drawn as a grid structure on the glass surface to investigate layer stacking performance.

Rheological Characterization of Precursors. To determine the yield stress values of the precursors, steady-state stress sweep measurements were performed with a rotational rheometer (Discovery HR-2, TA Instruments Inc., USA) in a parallel plate geometry (diameter of 12 mm) at RT. The shear stress was varied from 0.1 to 1000 Pa for all precursors (the shear rate was kept constant at 0.01 s^{-1}). The yield point was determined by determining the intersection point between the linear region and viscosity-drop region from the viscosity−shear stress plot. This yield point indicates the flow initiation of the precursor at the level of the applied shear stress.

To determine the shear-thinning properties of the precursors, rotational shear−viscosity measurements were performed in a flow mode with the shear rate varying from 0.01 to 1000 s^{-1} with a gap size of 0.2 mm at RT. To characterize the effect of temperature on the viscosity of GelMA, the temperature was varied from +10 to +37 °C with a constant shear rate (0.1 s^{-1}) at the rate of 2 °C/min. The precursor volume was 250 μL to fit the diameter of the geometry.

Power Law Model for Shear-Thinning Behavior of Precursors. The Power law regression eq 1 was applied to the data to predict the shear-thinning properties of the precursors from the linear region of the viscosity−shear rate plot.[25]

$$\mu = K\dot{\gamma}^{n-1} \tag{1}$$

where μ is the viscosity, γ is the shear rate, K is the flow consistency index, and n is the flow behavior index. The consistency index K is related to the initial viscosity of the precursor, and thus, lower values indicate higher extrudability. The flow index n relates to the shear-thinning abilities of the precursor with $n = 1$ indicating Newtonian behavior, $n = 0.6$ indicating weakly shear-thinning material, and $n \leq 0.2$ meaning high shear-thinning properties and therefore good extrudability.[25]

Photocross-linking of Hydrogels. The precursors (250 μL) were pipetted into a cut 4 mL syringe used as a mold to prepare hydrogels (2.5 mm in height and 12 mm in diameter). Photocross-linking was performed by irradiating the solution at varying distances corresponding to the defined UV intensities at a wavelength of 300−450 nm (Figure 1) (BlueWave 50 UV curing spot lamp, DYMAX Corp., USA). The used intensity values were 10 mW/cm^2 (low) and 50 mW/cm^2 (high), and six different exposure times were used (5, 10, 20, 40, 60, and 120 s). All photocross-linked hydrogels were stored in the refrigerator at 4 °C overnight. On the following day, the samples were characterized by rheological measurements.

Rheological Characterization of Photocross-linked Hydrogels. To characterize the transition of the precursors into hydrogels, rheological measurements were performed on a rotational rheometer (Discovery HR-2, TA Instruments Inc., USA) in a parallel plate geometry (diameter of 12 mm) at RT. To investigate viscoelasticity of hydrogels (with varying UV exposure time and intensity), samples were gently transferred into the rheometer. The plate−plate geometry was adjusted to a measuring distance of 2.5 mm to fit the height of hydrogels. The frequency sweep was carried out to measure the viscoelasticity of the hydrogel within a frequency range of 0.1−100 Hz. The storage and loss moduli (G', G'') correlating to the elastic and viscous nature of the hydrogels were measured and plotted into a graph, which was later processed using Excel.

Cross-linking Density of Photocross-linked Hydrogels. Cross-linking density was estimated by determining the difference between G' and G'' at 120 s exposure time.[2] To be more precise, the average mesh size (ξ) calculation[24] was applied to determine the cross-linking density of resulting hydrogels at 120 s UV exposure time, using eq 2

$$(\xi) = \left(\frac{G'N}{RT}\right)^{-1/3} \tag{2}$$

where G' is the storage modulus of the hydrogels, N is the Avogadro constant (6.023 × 10^{23} mol^{-1}), R is the molar gas constant (8.314 J K^{-1} mol^{-1}), and T is the temperature (298 K).

Water CA Measurements of Photocross-linked Hydrogels. Water CA values of the photocross-linked hydrogels were measured with the Attension Theta Lite optical tensiometer (Biolin Scientific Holding AB, Sweden) using a sessile drop method. The thin films were prepared as follows: the precursor solution was pipetted in a mold (height of 1 mm and diameter of 10 mm) and photocross-linked using UV light at 50 mW/cm^2 for 120 s. Next, the mold was removed; the hydrogel was placed on a glass coverslip and put on the stage. A droplet of deionized water (5 μL) was slowly applied on the hydrogel surface and simultaneously recorded using a video recorder for 15 s after the contact. CA values (left and right) were automatically calculated with the equipment software (OneAttension v2.1).

■ RESULTS

Characterization of the Synthesized Materials. The synthesis of HAMA and AlgMA relied on the reaction of methacrylic anhydrides at pH 7−8 at low temperature. According to the results, the MD in hyaluronic acid was ∼30 and ∼60% (with +3−5% variations from batch to batch) with respect to the disaccharide units of hyaluronic acid as estimated by the NMR spectroscopy (^{1}H NMR, 300 MHz). The degree of modification was estimated by calculating the ratio of the *N*-acetyl peak of hyaluronic acid at 2.01 ppm and the olefinic protons from the methacrylate groups at 5.74 and 6.18 ppm (Figures S1 and S2 in Supporting Information).

The MD in alginate were ∼30 and ∼60% (+3−5% variations from batch to batch), which was quantified by ^{1}H NMR spectroscopy (Figures S3 and S4 in Supporting Information). The MD was calculated as per the reported procedure[26] by using the area under the peak for anomeric protons in the guluronic unit (4.6−5.2 ppm) and the two vinyl protons in the methacrylate group (5.3−6.5 ppm).

According to the UV absorption spectra, it was evident that collagen and gelatin were functionalized with the methacrylate groups, and the MD was determined by the TNBS assay. The MD of collagen (ColMA) and gelatin (GelMA) were calculated as ∼30 and ∼60% with +3−5% variations. The details can be found in Figures S5 and S6 in Supporting Information.

Spin-Coating Experiment of Precursors. All precursors were spin-coatable to a thickness range varying from 300 to 1400 nm measured with a profilometer. The thicknesses were as follows: HAMA30: 580 nm, HAMA60: 910 nm, AlgMA30: 676 nm, AlgMA60: 1360 nm, GelMA30: 281 nm, GelMA60: 420 nm, ColMA30: 531 nm, and ColMA60: 917 nm.

Initial Injectability Screening by Manual Dispensing of the Precursors. Preliminary testing was performed to screen the fiber formation capability of the precursors and the

https://dx.doi.org/10.1021/acs.biomac.0c01322
Biomacromolecules XXXX, XXX, XXX−XXX

ability for the fibers to stack layer-by-layer to form 3D constructs essential for extrusion-based 3D bioprinting. The MD had a considerable effect on the injectability and on the ability of the material to form a fiber. As shown in Figure 2, precursors with 30% MD and some of the 60% MD did not form coherent fiber (GelMA30, ColMA30, AlgMA30, AlgMA60, HAMA30, and HAMA60) and did not retain their shape.

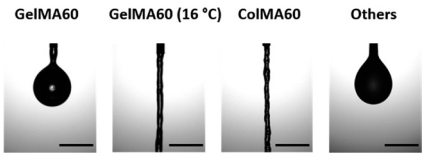

Figure 2. Fiber formation of the precursors: GelMA60 and GelMA60 at 16 °C, ColMA60 and others (GelMA30, ColMA30, AlgMA30, AlgMA60, HAMA30, and HAMA60), scale bar = 1 mm.

When injected, GelMA60 at 16 °C formed a coherent fiber, although at RT, only droplets or partial fiber formation was seen. However, the fibers maintained their shape only for a short period of time after layer deposition on a substrate at RT. Utilization of a cooling platform (4−5 °C) helped to retain the structure for longer time. Also, ColMA60 at RT formed a coherent fiber with relatively low applied pressure. It showed a good layer stacking ability without the layers merging (Figure S7 in Supporting Information). The quality of the injected fibers has been summarized in Table 1. The "printable" precursors are shown with bolded text, while the unbolded text is used for "unprintable" precursors. These preliminary screening results are compared to the rheological profiles in the next section in order to confirm the relationship between the Power law model and manual injection.

Table 1. Fiber Formation Quality Testing in Various Precursors with 30 and 60% MD[a]

	fiber formation screening	
precursors	30% of modification degree	60% of modification degree
HAMA	droplet (RT)	partial fiber (RT)
AlgMA	droplet (RT)	viscous droplet (RT)
GelMA	droplet (RT)	droplet (RT)
	droplet (16 °C)	**fiber (16 °C)**
ColMA	droplet (RT)	**coherent fiber (RT)**

[a]Bolded text refers to printable and the unbolded text to unprintable precursors.

Yield Stress Measurement (Flowability) of Precursors. In order to suggest suitable fabrication methods for each precursor, the yield stress values were evaluated. Figure 3 shows the plots of viscosity as a function of shear stress. Both GelMA60 at 16 °C and ColMA60 clearly showed a yield point, after which the precursor started to flow easily under a certain level of shear stress. The viscosity of all 30% MD precursors in Figure 3A and GelMA60 at RT and AlgMA60 and HAMA60 in Figure 3B did not change as a function of shear stress (shown as flat line), meaning they did not exhibit yield stress.

Shear-Thinning Properties of Precursors. To assess the reliability of manual dispensing method and predict the shear-thinning properties of the precursors, rheological evaluation and Power law model fit were performed. The shear-thinning profile of each precursor was obtained from the rheological measurements. The relationship between the viscosity and the modification degree in the precursors under increasing shear rate was investigated, as shown in Figure 4. For GelMA, an additional temperature−viscosity measurement was performed because of its temperature-dependent behavior, which yielded into a coherent fiber formation at low temperature. Most of the precursors exhibited weak shear-thinning behavior. AlgMA30, AlgMA60, and HAMA30 were plotted as plateaus because the viscosity did not change as a function of an increasing shear rate; instead, they exhibited Newtonian fluid behavior, as shown in Figure 4A,B. This behavior relates to the observations reported in Table 1, where these precursors were categorized as "unprintable". The MD played an essential role in the viscosity and shear-thinning profiles. As shown in Figure 4C, the viscosity of GelMA60 slowly decreased as a function of increasing temperature. Hence, GelMA60 was also examined for its shear-thinning properties at low temperature (16 °C), as shown in Figure 4D.

To confirm the shear-thinning behavior of the precursors, the Power law model was applied to the data by plotting the viscosity−shear rate on a logarithmic scale. The linear region was chosen from the middle of the slope, and the Power trend line was fitted to obtain K and n values reported in Table 3. In Table 3, n values less than 0.2 are bolded and represent

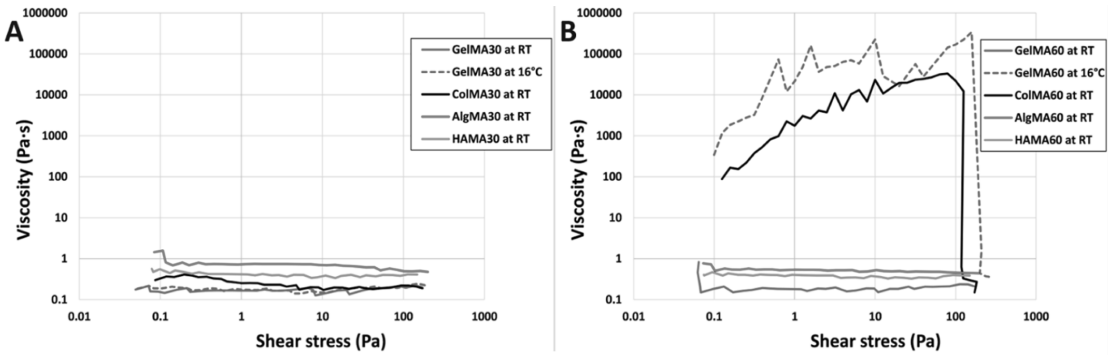

Figure 3. Yield stress measurement data for all precursors at RT and for GelMA30 and GelMA60 also at 16 °C. (A) Precursors with 30% MD, (B) precursors with 60% MD.

https://dx.doi.org/10.1021/acs.biomac.0c01322
Biomacromolecules XXXX, XXX, XXX−XXX

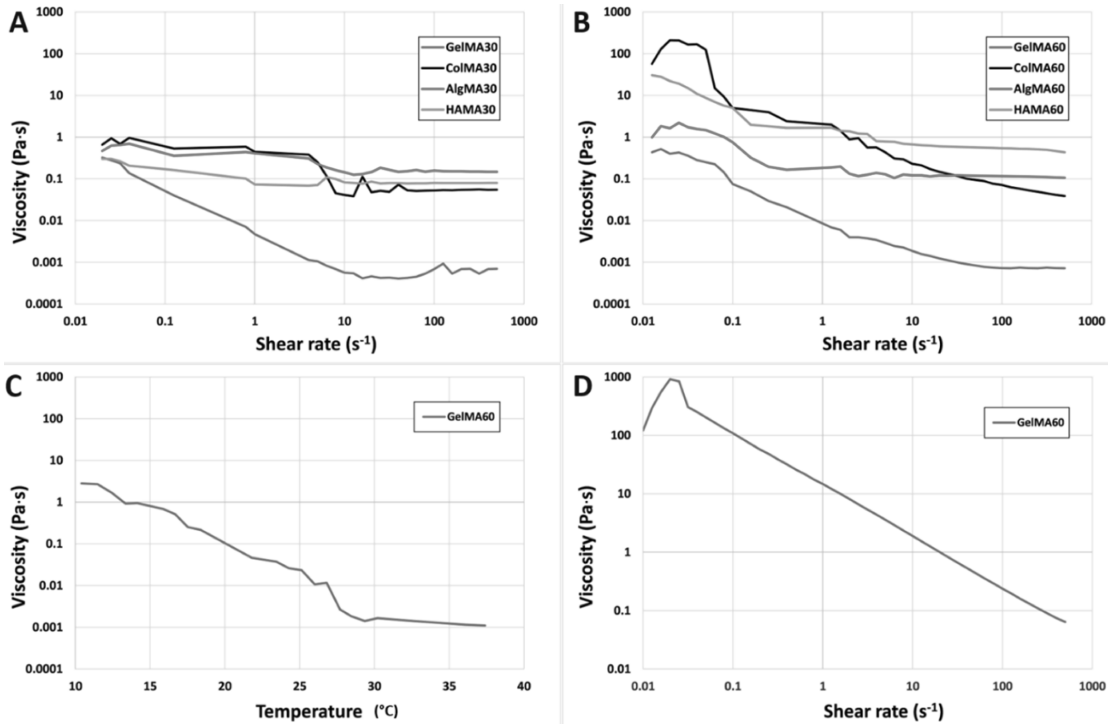

Figure 4. Viscosity−shear rate plots of the precursors: (A) with 30% MD, (B) with the 60% MD. (C) Viscosity−temperature plot of GelMA60 at 0.1 s^{-1} constant shear rate. (D) Viscosity as a function of shear rate for GelMA60 at 16 °C showing shear-thinning behavior.

Table 2. Yield Stress Values of the Investigated Precursors[a]

precursors	yield stress (Pa)
GelMA30	N/A
GelMA30 (16 °C)	N/A
GelMA60	N/A
GelMA60 (16 °C)	79.4
ColMA30	N/A
ColMA60	126
HAMA30	N/A
HAMA60	N/A
AlgMA30	N/A
AlgMA60	N/A

[a]N/A in yield stress means the precursor started flowing already at the beginning of the measurement (at a shear stress of 0.01 Pa), and thus, yield stress could not be measured.

Table 3. Values of Shear-Thinning Coefficients for Precursors with 30 and 60% MD[a]

precursors	*K*	*n*
HAMA30	0.0817	0.954
HAMA60	0.583	0.773
AlgMA30	0.152	0.937
AlgMA60	0.952	0.858
GelMA30	**0.00504**	**0.162**
GelMA60	**0.0164**	**0.141**
GelMA60 (16 °C)	**14.3**	**0.119**
ColMA30	0.138	0.787
ColMA60	**0.394**	**0.145**

[a]Precursors with values in **bold** are labeled as "printable" and have $n <$ 0.2 according to the Power law model. *K* and *n* values are given with three significant numbers.

precursors described as printable. According to the calculations, it was obvious that most of the 30% MD precursors had high *n* coefficients, that is, close to 1. On the other hand, the *n* coefficients of AlgMA60 and HAMA60 were also between 0.7 and 0.9. Shear-thinning precursors (bold text) ColMA60, GelMA30, GelMA60, and GelMA60 at 16 °C all have *n* values close to 0.1.

Viscoelasticity of Photocross-linked Hydrogels. The underlying factors affecting the mechanical properties of the resulting hydrogels are the starting strength of polymers, such as molecular weight, or bloom strength in gelatin and the concentration of hydrogels. In our research, we focused on studying the effect of MD (30% or 60%), UV intensity (10 and 50 mW/cm^2) and exposure time (5, 10, 20, 40, 60, and 120 s) on the mechanical properties of the resulting hydrogels.

According to the rheological results (Figure 5), the increase in the UV intensity, exposure time, or MD led to higher storage modulus (G') and more rigid structure in all hydrogels. The rheological measurement of hydrogels showed increase in storage G' and loss G'' moduli with increasing curing time and UV intensity. The higher MD corresponded to the higher degree of cross-linking, which led to stiffer hydrogels. In 30 and 60% MD hydrogels, the higher UV intensity resulted in faster polymerization. In addition, the average mesh size ξ values

https://dx.doi.org/10.1021/acs.biomac.0c01322
Biomacromolecules XXXX, XXX, XXX−XXX

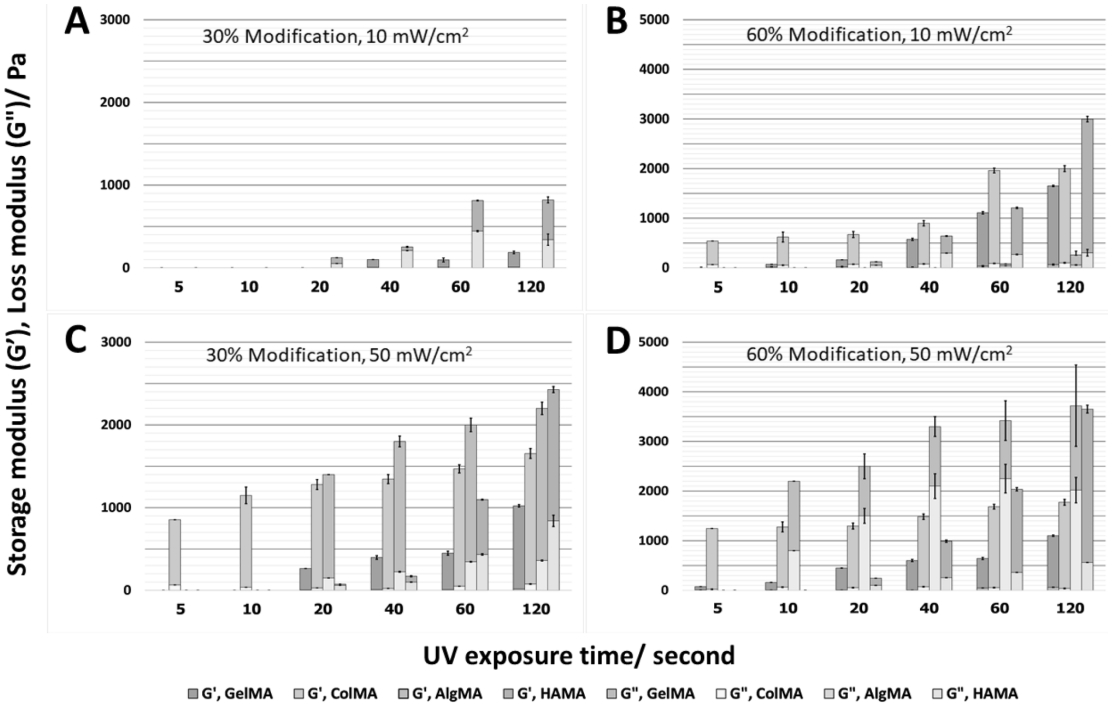

Figure 5. Storage (G') and loss moduli (G'') of the cross-linked hydrogels with different MD (30 and 60%) cross-linked with low/high UV intensity and varying exposure time. (A) Hydrogels with 30% MD and (B) 60% MD at 10 mW/cm^2 UV intensity for 5−120 s. (C) 30% MD and (D) 60% MD at 50 mW/cm^2 UV intensity for 5−120 s.

(reflecting the cross-linking density of hydrogels) are given in Table 4. Hydrogels with high MD (60%) and cross-linked with high UV intensity (50 mW/cm^2) had smaller mesh size than hydrogels with lower MD (30%) and cross-linked with low UV intensity (10 mW/cm^2). In the polypeptides (GelMA and ColMA), the MD and concentrations were equal, but ColMA tended to polymerize faster than GelMA (5 s vs 40 s), as shown in Figure 5B,D, yielding into stiffer hydrogels (Table 4).

Hydrophilicity of Photocross-linked Hydrogels. The wettability of the photocross-linked hydrogels was investigated by measuring the water CAs (Figure 6). The CA measurements determine the attraction between the water molecules and the polymer surface. The results showed that the more substantial cross-linking degree (higher MD) provided denser hydrogel network, and less water was observed on the hydrogel surface. It resulted in hydrophobic behavior in most hydrogels. On the other hand, the stiffer structure did not always give high CA values as observed in ColMA60. It showed a significant decrease of CA value compared to the ColMA30 because of the excessive water on the surface of the hydrogels (CA values of ColMA30 and ColMA60 were 105−110 and 74−78°, respectively).

■ DISCUSSION

The versatility of hydrogels has allowed them to be used in various biomedical engineering applications, such as tissue engineering scaffolds and drug delivery devices.[27] Photocross-linkable hydrogels can be achieved by methacrylation of polypeptides and polysaccharides and cross-linking them in the presence of PI. The extent of methacrylation can be adjusted to improve the hydrogel properties, such as gelation time and mechanical strength.[28] Moreover, photocross-linkability makes the hydrogels more flexible to process into different shapes or forms, such as thin films and 3D structures, which gives advantages over other cross-linking methods.[26,29] Each fabrication method has its unique pros and cons and requires different characteristics from the precursors, making the assessment critical.

In many applications, for example, in biosensing and cell culture, hydrogels are usually engineered into (2D) thin films.[30] 2D films can only swell in the direction vertical to the substrate.[31] However, swelling-induced mechanical instability and surface treatment are needed to improve cell attachment.[32,33] Spin coating has been widely used for microfabrication applications, as it can create thin films with thicknesses below 10 nm.[34,35] Spin coating is a procedure used to apply uniform thin films to flat substrates.[36] The resulting film thickness depends on the concentration of the solution, viscosity, drying rate, percent of solid material, surface tension, and the parameters chosen for the spin process such as final rotational speed, acceleration, and fume exhaust.[36,37]

3D casting of hydrogels is a fundamental approach to create 3D cell cultures in hydrogels. It can also be used for prescreening the gelation time and mechanical strength of the hydrogels.[38] Hydrogels are created by casting the precursor in a mold and then cured with UV light. High-viscosity precursors have to be centrifuged to make them homogeneous and fit to the bottom of a mold.[39]

https://dx.doi.org/10.1021/acs.biomac.0c01322
Biomacromolecules XXXX, XXX, XXX−XXX

Table 4. Overview of Properties of the Photocross-linkable Materials in Our Study: Properties and Cross-linking Conditions of the Precursors and Properties of the Resulting Hydrogels[a]

			feature value														
											storage/loss moduli after 120 s of UV crosslinking (Pa)						
					shear-thinning coefficients				UV crosslinking time (s)		10 mW/cm^2		50 mW/cm^2		average mesh size, ξ (nm)		
biopolymer	costs	handling difficulty	viscosity (Pa·s)	yield stress (Pa)	K	n	fiber formation	layer stacking	10 mW/cm^2	50 mW/cm^2	G'	G''	G'	G''	10 mW/cm^2	50 mW/cm^2	CA (deg)
GelMA30	€	++	0.001 (RT) [liquid-sticky]	0	0.005	0.162	droplet (RT)	no	20−40	10−20	190 ± 40	9 ± 5	1022 ± 40	16 ± 5	28.0 ± 1.8	16.0 ± 0.2	22 ± 1.0
GelMA60	€	++	0.515 (RT) [liquid-sticky]	n/a (RT)	0.016	0.141	droplet (RT)	no (RT)	5−10	1−5	1700 ± 45	65 ± 4	1100 ± 40	62 ± 6	13.5 ± 1.2	15.5 ± 0.2	83 ± 3.9
			915 (16 °C) [viscous]	79.4 (16 °C)			fiber (16 °C)	yes (16 °C)									
ColMA30	€€€	++	0.941 (RT) [viscous]	0	0.138	0.600	droplet (RT)	no		1−5			1655 ± 38	76 ± 85		13.5 ± 0.1	110 ± 0.3
ColMA60	€€€	++	208 (RT) [viscous]	126	0.394	0.145	fiber (RT)	yes (RT)	1−5	1−5	2000 ± 50	100 ± 12	1800 ± 60	38 ± 2	12.7 ± 0.1	13.2 ± 0.1	78 ± 1.0
HAMA30	€€	+	0.302 (RT) [liquid]	0	0.081	0.954	droplet (RT)	no	10−20	10−20	820 ± 100	340 ± 45	2420 ± 250	840 ± 45	17.2 ± 1.4	12.0 ± 0.4	35 ± 1.2
HAMA60	€€	+	2.66 (RT) [liquid]	0	0.583	0.773	droplet (RT)	no	10−20	10−20	3000 ± 200	300 ± 50	3650 ± 150	150 ± 5	11.1 ± 0.2	10.4 ± 0.1	58 ± 0.9
AlgMA30	€	+++	0.627 (RT) [liquid-sticky]	0	0.152	0.937	droplet (RT)	no		10−20			2200 ± 85	360 ± 8		12.3 ± 0.2	12 ± 0.5
AlgMA60	€	+++	1.83 (RT) [viscous-sticky]	0	0.952	0.858	droplet (RT)	no	40−60	5−10	260 ± 90	60 ± 15	3700 ± 850	2020 ± 250	25.0 ± 2.0	10.3 ± 0.6	46 ± 2.8
			precursor properties						cross-linking parameters				hydrogel properties				

[a]Costs are defined using a scale from the budget (€) to expensive (€€€). Handling difficulty is defined with a range from easy (+) to difficult (+++).

https://dx.doi.org/10.1021/acs.biomac.0c01322
Biomacromolecules XXXX, XXX, XXX−XXX

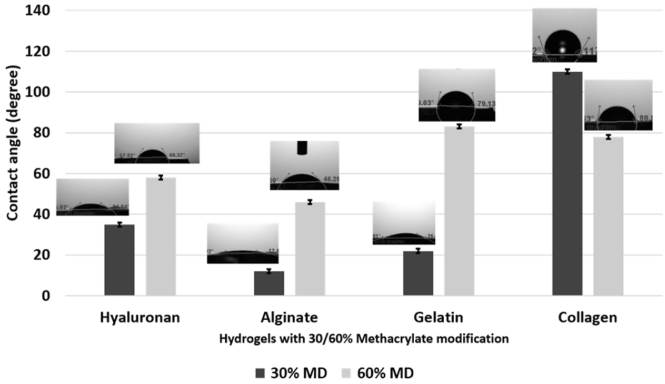

Figure 6. CA measurements of the photocross-linked polypeptide and polysaccharide hydrogels showing the droplet profiles as insets and quantification of the measured CA values for different hydrogels.

Precursors can be delivered by injecting directly into the microchannel or target tissue and cross-linked *in situ* to form hydrogels.[40] The precursors must be able to flow through the syringe easily, that is, they have to exhibit a certain amount of yield stress while maintaining shear-thinning properties (decreasing viscosity with increasing shear rate).[4] In 3D bioprinting, the requirements for the printability share similarities with the injectability of precursors.[41−43] The viscosity should be high enough to maintain the shape, and the precursor should have an ability to stack layer-by-layer during the process and before cross-linking.[44] Shear-thinning properties and yield stress are also essential as they result in less shear force during the extrusion.[45]

In our study, the characterization of the precursors started with the analysis of the dynamic viscosity, fiber-forming ability, yield stress, and shear-thinning profiles of each precursor having different MD. Next, the Power law model was applied to the data to confirm the relationship between the shear-thinning coefficients and injectability.[28] Finally, the photo-cross-linked hydrogels were assessed for their physical properties (G'/G'' and hydrophilicity) in different photo-cross-linking conditions.

Quantification of the MD. Tuning of the ratio of the methacrylate anhydride, reaction time, pH, and temperature led to different MDs in the polymer backbone. The higher MD in polypeptides and polysaccharides was achieved by increasing the nucleophilicity of amine (polypeptides) and hydroxy (polysaccharides) groups at basic pH, which in turn promoted the rapid nucleophilic attack of the hydroxy/amine groups onto the anhydride linkage.[24] The flexibility of the tunable functional polymers allowed us to manipulate the properties of precursors and hydrogels, which is an important prerequisite for research studies using hydrogel-based scaffolds.[46]

Yield Stress of Precursors. The presence of yield stress for a particular precursor is highly advantageous for the application by injection. It contributes to the injectability of precursors as it quantifies the initial force required to generate the flow. In addition, the yield stress also helps the injected precursor to experience better retention on the injection site, allowing shape-specific fitting.[4] In other words, the existence of yield stress for a precursor indicates resistance against flow before and after injection.[5] An existing yield stress limit would also suggest that the precursor probably can be printed using 3D bioprinter as it helps the printed structure to resist deformation and maintain the printed shape (Tables 2 and 5). Precursors with good injectability/printability exhibit a sharp drop in viscosity during the flow (increasing shear stress) and thus show a distinct yield stress value.[25]

Fiber Formation and Shear-Thinning Properties of Precursors. In addition to the existence of a distinct yield stress value, another feature contributing to the injectability or printability of a precursor is its ability to readily flow from a nozzle. In our study, the fiber formation test intended to mimic injecting and bioprinting processes; thus, the nozzle size was chosen to match the real injecting/bioprinting situation.[25] In both cases, the flowability is governed by the shear response exhibited by the precursor under an increasing rate of applied shear stress. To successfully inject or 3D bioprint via extrusion, the initial precursor formulation must exhibit shear-thinning behavior, that is, decreasing dynamic viscosity as a function of increasing shear rate and also have the ability to stack layer-by-layer after printing.[4,5,44] In addition to the shear performance of the precursor, a feasible precursor for extrusion-based bioprinting has to be able to form a consisted, cylindrical fiber, rather than droplets when extruded out of a nozzle. This behavior can be prescreened simply by manual dispensing with a syringe and a nozzle without the need for an actual bioprinter. To further quantify the shear-thinning behavior of the precursors, shear-thinning coefficients were calculated from the Power law equation (Table 3). These coefficients were then used to predict whether the precursor could be used for 3D bioprinting. The criteria for choosing a linear region from the viscosity−shear rate curves for the Power trendline fit depended on the shape of the curve. Some of the specimens, such as ColMA and AlgMA, easily slipped out from the geometry during the rheological measurement. As a result, they showed a sharp drop after the increase of the shear rate, and the region for the Power law analysis was chosen from the middle of the linear curve after the drop. It is obvious that precursors with 30% of MD had an n value close to 1, which corresponded to the results of the manual dispensing experiment showing droplet formation. However, GelMA30 had an n value below 0.2, which suggests that it should be highly shear-thinning, but it still could not form a coherent fiber in the manual dispensing test. In this case, the K value needs to be considered as it relates to the flowability and viscosity of precursors. If the K value is too low, the precursor forms a droplet. The flowability of GelMA60 is critically

https://dx.doi.org/10.1021/acs.biomac.0c01322
Biomacromolecules XXXX, XXX, XXX−XXX

Table 5. Requirements for the Photocross-linkable Precursors for Various Fabrication Methods[a]

fabrication method	viscosity (Pa·s)	shear response	yield stress (Pa)	layer stacking ability	references	suitable precursors (5 w/v %)
casting 2D (in a well plate, thin film)	low–high, viscosity depends on the application	not required	not required	not required	52	all investigated materials
casting (by spin coating)	low–high (0.025 to 10^4), viscosity affects the film thickness, but no actual rule reported for suitable viscosity	no/weak shear-thinning, the shear response is considered and observed from the viscosity–shear rate graphs, Newtonian fluidic behavior affects the film deposition during spin coating	not required	not required	35,37,53,54	all investigated materials
casting 3D (bulk hydrogels)	N/A, difficulty in handling and need to centrifuge for viscous precursors	not required	not required	not required	24,39	all investigated materials
injecting (restricted environment)	low–moderate	weak shear-thinning	>1, low yield stress is required for easy injection	N/A	4,55	GelMA60 (RT, 16 °C), ColMA60, HAMA60, AlgMA60
injecting (non-restricted environment)	high viscosity (10^4 to 10^5), viscosity affects the gel loading speed	shear-thinning (n is not defined)	N/A, yield stress should be relatively low for smooth injection	N/A	56–58	GelMA60 (RT, 16 °C), ColMA60, HAMA60, AlgMA60
extrusion-based 3D bioprinting	moderate–high	shear-thinning ($n < 0.2$)	100–10,000 Pa, for bioinks in general, <100 Pa, for photocross-linkable materials	yes, the ability to retain their shape after the extrusion	4,25,52,59	GelMA60, (RT, 16 °C), ColMA60

[a]Restricted environment = *in vivo*, surgical injection, non-restricted environment = injection in, e.g., microfluidic devices (body-on-a-chip application).

https://dx.doi.org/10.1021/acs.biomac.0c01322
Biomacromolecules XXXX, XXX, XXX−XXX

dependent on temperature, and decreasing temperature leads to a higher viscosity, enabling the material to exhibit shear-thinning behaviors. According to the previously published studies, GelMA is a thermosensitive material, which rapidly transitions from liquid to solid as a result of decrease in temperature.[12,47] For many applications, this property allows controlling the extrudability by tuning between the liquid–solid stage and also to fabricate 3D constructs at low temperature.[12]

Rheology of Photocross-linked Hydrogels. The gelation time of the hydrogels was highly dependent on the applied UV intensity. The precursors with 30% MD required longer UV exposure time and higher UV intensity to form stable hydrogels, compared to 60% MD precursors. Many of the 60% MD hydrogels (HAMA, GelMA, and ColMA) had no differences in the storage/loss moduli from 120 s of exposure time onward because they probably had reached saturated cross-linking already at that point. ColMA tended to photopolymerize faster than GelMA because of its amino acid composition and folding geometry. It has been shown by Bell *et al.*, 2015 that even unmodified collagen can be photopolymerized with multiphoton cross-linking.[48] However, AlgMA required higher UV intensity and longer exposure time to form a stable structure. The average mesh size reduced in the presence of high MD and high UV intensity as a result of the higher cross-linking density (Table 4). ColMA30 and ColMA60 had similar mesh sizes because they might have reached the saturation stage of cross-linking already at 120 s. Moreover, the higher cross-linking density can be seen from the increase in the difference between G' and G''. G' values were always higher with the higher MD and UV intensity. In the case of AlgMA60 at 120 s exposure time (50 mW/cm^2), the results showed the highest value of G', but the resulting hydrogel was weak because of low difference in G' and G'' compared to HAMA60, ColMA60, and GelMA60.

In conclusion, the cross-linking density increased with the increasing MD, UV intensity, and exposure time. The variation of G' in AlgMA60 was high because of the high viscosity and stickiness of the precursor, which made the transfer into the mold difficult. The concentration of hydrogels was fixed to 5 w/v %, but the viscosity of precursors and the stiffness of the hydrogels varied as a result of different molecular weight ranges of the starting biopolymers, which in turn resulted in variations in the cross-linking density. In 3D bioprinting applications, photocross-linking conditions (the exposure time and UV intensity) need to be optimized to achieve complicated scaffold structures while maintaining the cell viability.[12] The two different MDs (30 and 60%) and the resulting variable cross-linking densities and stiffness properties of the investigated hydrogels allow the tailoring of the end products, such as scaffolds, according to the particular needs of the cells or tissue. Furthermore, by controlling the exposure time and UV intensity, the stiffness of the constructs can be further tuned to match the stiffness of the specific tissue type.[38]

Hydrophilicity of Photocross-linked Hydrogels. The hydrophilicity of the hydrogels was chosen to be evaluated at the maximum cross-linking conditions used in our study (50 mW/cm^2, 120 s) because hydrogels cross-linked in these conditions were stable in shape. The hydrogels with a low cross-linking degree were difficult to measure as the water instantly spread when it made contact with a moist surface. In ColMA60, the short gelation time combined with a high cross-linking density led to the formation of a tight network, which resulted in oozing of water out of the hydrogel in a phenomenon called syneresis.[49,50]

As expected, the methacrylated polysaccharides (hyaluronan and alginate) had lower CA values than methacrylated polypeptides (gelatin and collagen) because of the higher number of hydrophilic groups in polysaccharides.[51] Furthermore, the morphological properties or surface roughness can affect the CA value of the hydrogels. Hence, glass coverslips were used to flatten the surface of the specimens during the casting process to minimize surface roughness. However, some variation in the surface quality may have appeared when the specimen was detached from the mold.

Evaluation of Fabrication Methods for Precursors. The wide range of materials and MD in our study allows flexibility in choosing a proper precursor for each fabrication method: casting-, injecting-, or extrusion-based 3D bioprinting. As summarized in Tables 4 and 5, we evaluated each precursor to determine their potential to meet the requirements of a particular fabrication method. An obvious drawback of the precursors in our study was the relatively low viscosity as many of the precursors could be fabricated into 3D hydrogels only by using casting into a mold. In addition, high-enough viscosity is an essential requirement for the precursors to achieve shear-thinning behavior and thus, effortless injection. We found that ColMA60 has the optimum properties to be fabricated into the hydrogel with all of the methods reported in Table 5. However, it is expensive to be prepared in high volume, and thus, it is advisable to mix it with other cheaper materials. GelMA60 in low temperature (16 °C) also allows flexibility in choosing an application method because it is less expensive and it maintained high viscosity during the process. Low-cost materials would be beneficial for preparing precursors in high volume such as for 3D bioprinting.

All precursors were suitable for casting, as mentioned earlier. However, they might need a preliminary cross-linking phase (pre-UV treatment or additional calcium chloride for alginate-based materials) to increase their viscosity and improve their shear-thinning profiles for feasible injection and 3D bioprinting. During the fabrication tests, it became clear that another critical factor in the hydrogel preparation is the difficulty in handling. The difficulty depends on the solubility of the biopolymers during the preparation and handling of the precursors because of their stickiness or high viscosity, as summarized in Table 4. Some precursors, such as AlgMA and GelMA, were very sticky to be cast in a mold; hence, centrifugation and shaking in the incubator were needed, which might have created some variation in the results of rheological measurements. These precursors might work better in application with a syringe. In addition, the hydrophilicity of the hydrogels was examined as it can affect cell mixing and cell attachment.

■ CONCLUSIONS

The two selected polypeptides (collagen and gelatin) and two polysaccharides (alginate and hyaluronic acid) were successfully methacrylated to the 30 and 60% MD. Because these methacrylated polymers, together with the PI (precursors), can be used in many fabrication methods utilizing photocross-linking, it is essential to understand their processing-related properties.

As anticipated, the biopolymers and the MD of precursors influenced the viscosity, yield stress, shear-thinning behavior, and fiber-forming capability. We also showed that, as expected,

https://dx.doi.org/10.1021/acs.biomac.0c01322
Biomacromolecules XXXX, XXX, XXX−XXX

also material source and cross-linking conditions affected the properties of the photocross-linked hydrogels. Based on our systematical characterizations, we recommend that precursors with low viscosity, low yield stress, and poor shear-thinning properties should not be used for injecting and 3D bioprinting. Instead, such precursors can be fabricated into 2D and 3D hydrogels by casting with a supporting mold. Furthermore, the assessment of injectability and printability needs a more thorough investigation of the rheological properties of the precursors. For successful 3D bioprinting, a proper fiber formation, layer stacking ability, and shape fidelity are required. In addition, photocross-linking conditions during bioprinting should be optimized in order to minimize the number of radical species generated, which are cytotoxic to cells when present in excess.

To summarize, our data provides grounds for the selection of a suitable fabrication method for the selected precursor. The insight evaluation also helps to choose correct parameters for photocross-linking of precursors into hydrogels with various modifiable properties. In future studies, these tunable precursors will be further explored in 3D bioprinting for the fabrication of complex 3D hydrogel scaffolds.

■ ASSOCIATED CONTENT

Supporting Information

The Supporting Information is available free of charge at https://pubs.acs.org/doi/10.1021/acs.biomac.0c01322.

Additional UV spectra, H NMR spectra, images of the layer stacking test with manual dispensing, and images of the fiber formation test (PDF)

■ AUTHOR INFORMATION

Corresponding Authors

Vijay Singh Parihar − *Biomaterials and Tissue Engineering Group, BioMediTech, Faculty of Medicine and Health Technology, Tampere University, 33720 Tampere, Finland;* orcid.org/0000-0002-6044-2121; Email: vijay.parihar@tuni.fi

Minna Kellomäki − *Biomaterials and Tissue Engineering Group, BioMediTech, Faculty of Medicine and Health Technology, Tampere University, 33720 Tampere, Finland;* orcid.org/0000-0003-4321-1820; Email: minna.kellomaki@tuni.fi

Authors

Hatai Jongprasitkul − *Biomaterials and Tissue Engineering Group, BioMediTech, Faculty of Medicine and Health Technology, Tampere University, 33720 Tampere, Finland;* orcid.org/0000-0003-0646-7712

Sanna Turunen − *Biomaterials and Tissue Engineering Group, BioMediTech, Faculty of Medicine and Health Technology, Tampere University, 33720 Tampere, Finland; Brinter Limited, 20520 Turku, Finland;* orcid.org/0000-0002-6823-8811

Shambhavee Annurakshita − *Photonics Laboratory, Tampere University, 33720 Tampere, Finland;* orcid.org/0000-0002-1780-7199

Complete contact information is available at: https://pubs.acs.org/10.1021/acs.biomac.0c01322

Author Contributions

S.T. and V.S.P. contributed equally. The manuscript was written through the contributions of all authors. Chemical modification and material characterizations have been carried out by H.J. and V.S.P. Data interpretation has been carried out by S.T., V.S.P., and M.K. Spin-coating has been performed by S.A. All authors have given approval to the final version of the manuscript.

Notes

The authors declare no competing financial interest.

■ ACKNOWLEDGMENTS

S.A. would like to thank the Jenny and Antti Wihuri Foundation for financial support. The rest of us are grateful to the Centre of Excellence in Body-on-Chip Research (CoEBoC) by the Academy of Finland for financial support (decision # 312409) and to the University funding for CoEBoC.

■ ABBREVIATIONS

AlgMA, alginate methacrylate;; ColMA, collagen methacrylate; GelMA, gelatin methacrylate; HAMA, hyaluronan methacrylate; MA, methacrylate anhydride; MD, methacrylation degree; ECM, extracellular matrix; RT, room temperature; CA, contact angle; G', storage modulus; G'', loss modulus; PI, photoinitiator

■ REFERENCES

(1) Cernencu, A. I.; Lungu, A.; Stancu, I.-C.; Serafim, A.; Heggset, E.; Syverud, K.; Iovu, H. Bioinspired 3D Printable Pectin-Nanocellulose Ink Formulations. *Carbohydr. Polym.* **2019**, *220*, 12−21.

(2) Mishbak, H. H.; Cooper, G.; Bartolo, P. J. Development and Characterization of a Photocurable Alginate Bioink for Three-Dimensional Bioprinting. *Int. J. Bioprint.* **2019**, *5*, 189.

(3) Pereira, R. F.; Sousa, A.; Barrias, C. C.; Bártolo, P. J.; Granja, P. L. A Single-Component Hydrogel Bioink for Bioprinting of Bioengineered 3D Constructs for Dermal Tissue Engineering. *Mater. Horiz.* **2018**, *5*, 1100−1111.

(4) Townsend, J. M.; Beck, E. C.; Gehrke, S. H.; Berkland, C. J.; Detamore, M. S. Flow Behavior Prior to Crosslinking: The Need for Precursor Rheology for Placement of Hydrogels in Medical Applications and for 3D Bioprinting. *Prog. Polym. Sci.* **2019**, *91*, 126−140.

(5) Rohani Rad, E.; Vahabi, H.; Formela, K.; Saeb, M. R.; Thomas, S. Injectable Poloxamer/Graphene Oxide Hydrogels with Well-Controlled Mechanical and Rheological Properties. *Polym. Adv. Technol.* **2019**, *30*, 2250−2260.

(6) Park, Y. D.; Tirelli, N.; Hubbell, J. A. Photopolymerized Hyaluronic Acid-Based Hydrogels and Interpenetrating Networks. *Biomaterials* **2003**, *24*, 893−900.

(7) Bencherif, S. A.; Srinivasan, A.; Horkay, F.; Hollinger, J. O.; Matyjaszewski, K.; Washburn, N. R. Influence of the Degree of Methacrylation on Hyaluronic Acid Hydrogels Properties. *Biomaterials* **2008**, *29*, 1739−1749.

(8) Darge, H. F.; Andrgie, A. T.; Tsai, H.-C.; Lai, J.-Y. Polysaccharide and Polypeptide Based Injectable Thermo-Sensitive Hydrogels for Local Biomedical Applications. *Int. J. Biol. Macromol.* **2019**, *133*, 545−563.

(9) Nichol, J. W.; Koshy, S. T.; Bae, H.; Hwang, C. M.; Yamanlar, S.; Khademhosseini, A. Cell-Laden Microengineered Gelatin Methacrylate Hydrogels. *Biomaterials* **2010**, *31*, 5536−5544.

(10) Lim, K. S.; Galarraga, J. H.; Cui, X.; Lindberg, G. C. J.; Burdick, J. A.; Woodfield, T. B. F. Fundamentals and Applications of Photo-Cross-Linking in Bioprinting. *Chem. Rev.* **2020**, *120*, 10662−10694.

(11) O'Connell, C. D.; Di Bella, C.; Thompson, F.; Augustine, C.; Beirne, S.; Cornock, R.; Richards, C. J.; Chung, J.; Gambhir, S.; Yue,

Z.; Bourke, J.; Zhang, B.; Taylor, A.; Quigley, A.; Kapsa, R.; Choong, P.; Wallace, G. G. Development of the Biopen: A Handheld Device for Surgical Printing of Adipose Stem Cells at a Chondral Wound Site. *Biofabrication* **2016**, *8*, 015019.
(12) O'Connell, C. D.; Zhang, B.; Onofrillo, C.; Duchi, S.; Blanchard, R.; Quigley, A.; Bourke, J.; Gambhir, S.; Kapsa, R.; Di Bella, C.; Choong, P.; Wallace, G. G. Tailoring the Mechanical Properties of Gelatin Methacryloyl Hydrogels through Manipulation of the Photocrosslinking Conditions. *Soft Matter* **2018**, *14*, 2142−2151.
(13) Li, H.; Liu, S.; Lin, L. Rheological Study on 3D Printability of Alginate Hydrogel and Effect of Graphene Oxide. *Int. J. Bioprint.* **2016**, *2*, 54−66.
(14) Malda, J.; Visser, J.; Melchels, F. P.; Jüngst, T.; Hennink, W. E.; Dhert, W. J. A.; Groll, J.; Hutmacher, D. W. 25th Anniversary Article: Engineering Hydrogels for Biofabrication. *Adv. Mater.* **2013**, *25*, 5011−5028.
(15) Catoira, M. C.; Fusaro, L.; Di Francesco, D.; Ramella, M.; Boccafoschi, F. Overview of Natural Hydrogels for Regenerative Medicine Applications. *J. Mater. Sci.: Mater. Med.* **2019**, *30*, 115.
(16) Chimene, D.; Kaunas, R.; Gaharwar, A. K. Hydrogel Bioink Reinforcement for Additive Manufacturing: A Focused Review of Emerging Strategies. *Adv. Mater.* **2020**, *32*, 1902026−22.
(17) Annabi, N.; Tamayol, A.; Uquillas, J. A.; Akbari, M.; Bertassoni, L. E.; Cha, C.; Camci-Unal, G.; Dokmeci, M. R.; Peppas, N. A.; Khademhosseini, A. 25th Anniversary Article: Rational Design and Applications of Hydrogels in Regenerative Medicine. *Adv. Mater.* **2014**, *26*, 85−124.
(18) Tiwari, S.; Bahadur, P. Modified Hyaluronic Acid Based Materials for Biomedical Applications. *Int. J. Biol. Macromol.* **2019**, *121*, 556−571.
(19) Shelke, N. B.; James, R.; Laurencin, C. T.; Kumbar, S. G. Polysaccharide Biomaterials for Drug Delivery and Regenerative Engineering. *Polym. Adv. Technol.* **2014**, *25*, 448−460.
(20) Raemdonck, K.; Martens, T. F.; Braeckmans, K.; Demeester, J.; De Smedt, S. C. Polysaccharide-Based Nucleic Acid Nanoformulations. *Adv. Drug Delivery Rev.* **2013**, *65*, 1123−1147.
(21) Zhu, T.; Mao, J.; Cheng, Y.; Liu, H.; Lv, L.; Ge, M.; Li, S.; Huang, J.; Chen, Z.; Li, H.; Yang, L.; Lai, Y. Recent Progress of Polysaccharide-Based Hydrogel Interfaces for Wound Healing and Tissue Engineering. *Adv. Mater. Interfaces* **2019**, *6*, 1900761.
(22) Khoury, L. R.; Popa, I. Chemical Unfolding of Protein Domains Induces Shape Change in Programmed Protein Hydrogels. *Nat. Commun.* **2019**, *10*, 1−9.
(23) Ravichandran, R.; Islam, M. M.; Alarcon, E. I.; Samanta, A.; Wang, S.; Lundström, P.; Hilborn, J.; Griffith, M.; Phopase, J. Functionalised Type-I Collagen as a Hydrogel Building Block for Bio-Orthogonal Tissue Engineering Applications. *J. Mater. Chem. B* **2015**, *4*, 318−326.
(24) Koivusalo, L.; Kauppila, M.; Samanta, S.; Parihar, V. S.; Ilmarinen, T.; Miettinen, S.; Oommen, O. P.; Skottman, H. Tissue Adhesive Hyaluronic Acid Hydrogels for Sutureless Stem Cell Delivery and Regeneration of Corneal Epithelium and Stroma. *Biomaterials* **2019**, *225*, 119516.
(25) Paxton, N.; Smolan, W.; Böck, T.; Melchels, F.; Groll, J.; Jungst, T. Proposal to Assess Printability of Bioinks for Extrusion-Based Bioprinting and Evaluation of Rheological Properties Governing Bioprintability. *Biofabrication* **2017**, *9*, 044107.
(26) Araiza-Verduzco, F.; Rodríguez-Velázquez, E.; Cruz, H.; Rivero, I. A.; Acosta-Martínez, D. R.; Pina-Luis, G.; Alatorre-Meda, M. Photocrosslinked Alginate-Methacrylate Hydrogels with Modulable Mechanical Properties: Effect of the Molecular Conformation and Electron Density of the Methacrylate Reactive Group. *Materials* **2020**, *13*, 534.
(27) Hoffman, A. S. Hydrogels for Biomedical Applications. *Adv. Drug Delivery Rev.* **2012**, *64*, 18−23.
(28) Nguyen, K. T.; West, J. L. Photopolymerizable Hydrogels for Tissue Engineering Applications. *Biomaterials* **2002**, *23*, 4307−4314.
(29) Smeds, K. A.; Grinstaff, M. W. Photocrosslinkable Polysaccharides for in Situ Hydrogel Formation. *J. Biomed. Mater. Res.* **2001**, *54*, 115−121.
(30) Jia, S.; Tang, Z.; Guan, Y.; Zhang, Y. Order-Disorder Transition in Doped Microgel Colloidal Crystals and Its Application for Optical Sensing. *ACS Appl. Mater. Interfaces* **2018**, *10*, 14254−14258.
(31) Trujillo, V.; Kim, J.; Hayward, R. C. Creasing Instability of Surface-Attached Hydrogels. *Soft Matter* **2008**, *4*, 564−569.
(32) Yang, X.; Ma, C.; Li, C.; Xie, Y.; Huang, X.; Jin, Y.; Zhu, Z.; Liu, J.; Li, T. Three Dimensional Responsive Structure of Tough Hydrogels. *Electroact. Polym.* **2015**, *9430*, 94301F.
(33) Yang, J. M.; Olanrele, O. S.; Zhang, X.; Hsu, C. C. Fabrication of Hydrogel Materials for Biomedical Applications. *Adv. Exp. Med. Biol.* **2018**, *1077*, 197−224.
(34) George, J. P.; Beeckman, J.; Woestenborghs, W.; Smet, P. F.; Bogaerts, W.; Neyts, K. Preferentially Oriented $BaTiO_3$ thin Films Deposited on Silicon with Thin Intermediate Buffer Layers. *Nanoscale Res. Lett.* **2013**, *8*, 1−7.
(35) Lee, U. G.; Kim, W.-B.; Han, D. H.; Chung, H. S. A Modified Equation for Thickness of the Film Fabricated by Spin Coating. *Symmetry* **2019**, *11*, 1183.
(36) Mitzi, D. B.; Kosbar, L. L.; Murray, C. E.; Copel, M.; Afzali, A. High-Mobility Ultrathin Semiconducting Films Prepared by Spin Coating. *Nature* **2004**, *428*, 299−303.
(37) Tyona, M. D. A Comprehensive Study of Spin Coating as a Thin Film Deposition Technique and Spin Coating Equipment. *Adv. Mater. Res.* **2013**, *2*, 181−193.
(38) Pepelanova, I.; Kruppa, K.; Scheper, T.; Lavrentieva, A. Gelatin-Methacryloyl (GelMA) Hydrogels with Defined Degree of Functionalization as a Versatile Toolkit for 3D Cell Culture and Extrusion Bioprinting. *Bioengineering* **2018**, *5*, 55.
(39) Caffarel-Salvador, E.; Tuan-Mahmood, T.-M.; McElnay, J. C.; McCarthy, H. O.; Mooney, K.; Woolfson, A. D.; Donnelly, R. F. Potential of Hydrogel-Forming and Dissolving Microneedles for Use in Paediatric Populations. *Int. J. Pharm.* **2015**, *489*, 158−169.
(40) Mathew, A. P.; Uthaman, S.; Cho, K.-H.; Cho, C.-S.; Park, I.-K. Injectable Hydrogels for Delivering Biotherapeutic Molecules. *Int. J. Biol. Macromol.* **2018**, *110*, 17−29.
(41) Bertlein, S.; Brown, G.; Lim, K. S.; Jungst, T.; Boeck, T.; Blunk, T.; Tessmar, J.; Hooper, G. J.; Woodfield, T. B. F.; Groll, J. Thiol−Ene Clickable Gelatin: A Platform Bioink for Multiple 3D Biofabrication Technologies. *Adv. Mater.* **2017**, *29*, 1703404.
(42) Gao, T.; Gillispie, G. J.; Copus, J. S.; PR, A. K.; Seol, Y.-J.; Atala, A.; Yoo, J. J.; Lee, S. J. Optimization of Gelatin Alginate Composite Bioink Printability Using Rheological Parameters: A Systematic Approach. *Biofabrication* **2018**, *10*, 034106.
(43) Markstedt, K.; Mantas, A.; Tournier, I.; Martínez Ávila, H.; Hägg, D.; Gatenholm, P. 3D Bioprinting Human Chondrocytes with Nanocellulose-Alginate Bioink for Cartilage Tissue Engineering Applications. *Biomacromolecules* **2015**, *16*, 1489−1496.
(44) Townsend, J. M.; Dennis, S. C.; Whitlow, J.; Feng, Y.; Wang, J.; Andrews, B.; Nudo, R. J.; Detamore, M. S.; Berkland, C. J. Colloidal Gels with Extracellular Matrix Particles and Growth Factors for Bone Regeneration in Critical Size Rat Calvarial Defects. *AAPS J.* **2017**, *19*, 703−711.
(45) Panwar, A.; Tan, L. Current Status of Bioinks for Micro-Extrusion-Based 3D Bioprinting. *Molecules* **2016**, *21*, 685.
(46) Pepelanova, I.; Kruppa, K.; Scheper, T.; Lavrentieva, A. Gelatin-Methacryloyl (GelMA) Hydrogels with Defined Degree of Functionalization as a Versatile Toolkit for 3D Cell Culture and Extrusion Bioprinting. *Bioengineering* **2018**, *5*, 55.
(47) Pahoff, S.; Meinert, C.; Bas, O.; Nguyen, L.; Klein, T. J.; Hutmacher, D. W. Effect of Gelatin Source and Photoinitiator Type on Chondrocyte Redifferentiation in Gelatin Methacryloyl-Based Tissue-Engineered Cartilage Constructs. *J. Mater. Chem. B* **2019**, *7*, 1761−1772.
(48) Bell, A.; Kofron, M.; Nistor, V. Multiphoton Crosslinking for Biocompatible 3D Printing of Type I Collagen. *Biofabrication* **2015**, *7*, 035007.

https://dx.doi.org/10.1021/acs.biomac.0c01322
Biomacromolecules XXXX, XXX, XXX−XXX

(49) Boral, S.; Saxena, A.; Bohidar, H. B. Syneresis in Agar Hydrogels. *Int. J. Biol. Macromol.* **2010**, *46*, 232−236.
(50) Mizrahi, S. *Syneresis in Food Gels and Its Implications for Food Quality*; Woodhead Publishing Limited, 2010.
(51) Basiak, E.; Lenart, A.; Debeaufort, F. Effects of Carbohydrate/Protein Ratio on the Microstructure and the Barrier and Sorption Properties of Wheat Starch−Whey Protein Blend Edible Films. *J. Sci. Food Agric.* **2017**, *97*, 858−867.
(52) Pereira, R. F.; Bártolo, P. J. 3D Photo-Fabrication for Tissue Engineering and Drug Delivery. *Engineering* **2015**, *1*, 090−112.
(53) Zheng, S. Y.; Tian, Y.; Zhang, X. N.; Du, M.; Song, Y.; Wu, Z. L.; Zheng, Q. Spin-Coating-Assisted Fabrication of Ultrathin Physical Hydrogel Films with High Toughness and Fast Response. *Soft Matter* **2018**, *14*, 5888−5897.
(54) Aguilar, R. G.; López, J. O. Low Cost Instrumentation for Spin-Coating Deposition of Thin Films in an Undergraduate Laboratory. *Lat. Amer. J. Phys. Educ.* **2011**, *5*, 368−373.
(55) Mantha, S.; Pillai, S.; Khayambashi, P.; Upadhyay, A.; Zhang, Y.; Tao, O.; Pham, H. M.; Tran, S. D. Smart Hydrogels in Tissue Engineering and Regenerative Medicine. *Materials* **2019**, *12*, 3323.
(56) Sobrino, A.; Phan, D. T. T.; Datta, R.; Wang, X.; Hachey, S. J.; Romero-López, M.; Gratton, E.; Lee, A. P.; George, S. C.; Hughes, C. C. W. 3D Microtumors in Vitro Supported by Perfused Vascular Networks. *Sci. Rep.* **2016**, *6*, 1−11.
(57) Alarçin, E.; Lee, T. Y.; Karuthedom, S.; Mohammadi, M.; Brennan, M. A.; Lee, D. H.; Marrella, A.; Zhang, J.; Syla, D.; Zhang, Y. S.; Khademhosseini, A.; Jang, H. L. Injectable Shear-Thinning Hydrogels for Delivering Osteogenic and Angiogenic Cells and Growth Factors. *Biomater. Sci.* **2018**, *6*, 1604−1615.
(58) Huang, J.; Li, Z.; Hu, Q.; Chen, G.; Ren, Y.; Wu, X.; Ren, J. Bioinspired Anti-Digestive Hydrogels Selected by a Simulated Gut Microfluidic Chip for Closing Gastrointestinal Fistula. *iScience* **2018**, *8*, 40−48.
(59) Mouser, V. H. M.; Melchels, F. P. W.; Visser, J.; Dhert, W. J. A.; Gawlitta, D.; Malda, J. Yield Stress Determines Bioprintability of Hydrogels Based on Gelatin-Methacryloyl and Gellan Gum for Cartilage Bioprinting. *Biofabricaion* **2016**, *8*, 035003.

https://dx.doi.org/10.1021/acs.biomac.0c01322
Biomacromolecules XXXX, XXX, XXX−XXX

PUBLICATION II

Two-Step Crosslinking to Enhance the Printability of Methacrylated Gellan Gum Biomaterial Ink for Extrusion-Based 3D Bioprinting

Jongprasitkul, H.; Turunen, S.; Parihar, V.S.; Kellomäki, M.

Bioprinting 2022, 25, No. e00185
https://doi.org/10.1016/j.bprint.2021.e00185

Bioprinting 25 (2022) e00185

Contents lists available at ScienceDirect

Bioprinting

journal homepage: www.sciencedirect.com/journal/bioprinting

Two-step crosslinking to enhance the printability of methacrylated gellan gum biomaterial ink for extrusion-based 3D bioprinting

Hatai Jongprasitkul [a], Sanna Turunen [a,b], Vijay Singh Parihar [a,*], Minna Kellomäki [a]

[a] Biomedical and Tissue Engineering Group, BioMediTech, Faculty of Medicine and Health Technology, Tampere University, 33720, Tampere, Finland
[b] Brinter Limited, 20520, Turku, Finland

ARTICLE INFO

Keywords:
Gellan gum
Biomaterial ink
3D bioprinting
Hydrogel
Ionic crosslinking
Photocrosslinking
Printability

ABSTRACT

Photocrosslinkable bioinks have gained interest in 3D bioprinting due to their versatility and ease of use. However, a specific functional group, such as methacrylate or photo-click chemistry, is needed in the polymer backbone to enable photocrosslinking. Methacrylated gellan gum (GGMA) precursor has been proven to possess good rheological properties for an injectable hydrogel due to its inherent viscosity. It can also be photocrosslinked *in situ* at the target site. Unfortunately, the GGMA precursors alone are unable to maintain a stable filament shape after extrusion from the nozzle. In this study, a two-step crosslinking technique involving ionic and photocrosslinking was used to make the GGMA biomaterial ink printable. In the presence of an ionic crosslinker (Ca^{2+}), GGMA transformed from a liquid precursor to a weak extrudable hydrogel followed by photocrosslinking turning the weak hydrogel into true hydrogel with good shape fidelity. The printability of various GGMA ink compositions was prescreened thoroughly by characterising their fibre formation and rheological properties. A quantitative approach was introduced to quantify the experimental printability of different GGMA/$CaCl_2$ ink compositions from the printed two-layered grid structures. According to the results, 2% GGMA with 90 mM calcium chloride provided a formulation with the best printability. The optimum ink formulation was then used to print 3D structures. This optimised GGMA ink was printed with consistent fibres and provided high printability during the fabrication. The 3D printed structures still lacked high resolution compared to the control structures. In conclusion, the two-step crosslinking technique provided biomaterial ink with good printability and enabled the printing of genuine 3D constructs. Hence, pre-crosslinked GGMA may be applicable for a wide range of bioprinting applications.

1. Introduction

Extrusion-based bioprinting requires bioinks, which are mostly made of soft hydrogels or water-soluble polymers [1,2]. The development of such bioinks must meet specific requirements for fluid properties such as viscosity, shear-thinning, layer stackability and cell encapsulation [3–5]. The choice of bioink depends on the application in question (e.g., soft/hard tissues, biosensors) [6]. So far, hydrogel precursors have been the most used material choice of bioinks for extrusion-based 3D bioprinters due to their biocompatibility, high hydrophilicity, cell-friendly characteristics (promotion of cell growth and cell attachment), and tunability of mechanical properties. However, in order to create suitable hydrogels for extrusion-based bioprinting, the printability and cell survivability must be optimised throughout the printing process [7–10].

As the specialised materials suited for bioprinting have become an important research field, it has come relevant to define the terminology bit further. Groll et al. have clearly defined the terms bioink and biomaterial ink [11,12]. According to their definition, cells are a mandatory component of a bioink. Hence, aqueous compositions of polymers or hydrogel precursors that may include biologically active molecules but without living cells are not considered bioinks but instead biomaterial inks [12]. In our study, we use the term biomaterial ink (in short, "ink") for the material formulations as we have not yet formulated the materials with living cells.

The properties of Gellan gum (GG) can be modified to suit 3D bioprinting applications [13]. These properties, including molecular weight, polymer concentration and the type of crosslinker, affect the characteristics of GG hydrogels [14]. For biofabrication purposes, the GG chain is commonly functionalised with methacrylate groups (MA) to transform it photocrosslinkable and enable mechanical tunability of the

* Corresponding author.
E-mail address: vijay.parihar@tuni.fi (V.S. Parihar).

https://doi.org/10.1016/j.bprint.2021.e00185
Received 17 September 2021; Received in revised form 16 November 2021; Accepted 28 November 2021
Available online 7 December 2021

hydrogel [15–17]. Methacrylated GG (GGMA) precursor has shown good rheological properties to be used as an injectable hydrogel, so assumably it also suits bioprinting [18].

Unfortunately, the GGMA precursors alone lack the stability to maintain the 3D structure, although the prescreening results based on the rheological data, Power-law modelling, and filament formation imply that the material is extrudable. In fact, it has become clear that prescreening of printability does not provide sufficient data to predict the quality of printing outcome, although it is an important first step in the process of developing and characterising new bioinks for extrusion-based 3D bioprinting [5,15].

According to previously published research studies, gellan gum/GGMA is usually mixed with materials having good shear-thinning properties, such as chitosan, gelatin or synthetic polymers, to achieve good shape fidelity during the printing process [14,16,17]. The blending of bioink with other materials makes the preparation more complex, is time-consuming, and can yield bath-to-batch variations of each polymer. Moreover, a bioink without blending or stand-alone bioink could bridge the gap between academia and industry, as it offers versatility in both research and commercialisation.

To overcome these challenges, we present here a two-step crosslinking approach, which turns unprintable GGMA into fibre-forming, stackable biomaterial ink capable of forming 3D hydrogel constructs via extrusion-based 3D bioprinting.

In our study, we applied a pre-crosslinking approach (physical crosslinking with Ca^{2+}) via coordination bonding of carboxylate groups to calcium ions, providing sufficient stability to maintain the shape before photocrosslinking [19]. The previously published studies have shown that GGMA precursor has an ability to transform from solution to weak hydrogel under low temperature, pH and ionic conditions [13,20,21]. However, the physically crosslinked GG hydrogels alone cannot maintain their stability *in vivo* after implantation due to the exchange of divalent cations with monovalent ones present at higher concentrations in the physiological environment [20,22]. Thus, we hypothesised that the introduction of two-step crosslinking would improve the printability and printing resolution of the low polymer content GGMA compared to photocrosslinking alone. The two-step crosslinking protocol with ions and UV light was applied to maintain the shape fidelity and printing resolution during the printing at room temperature.

We highlighted the relationship between the two-step crosslinking technique and the printing outcome through stepwise printability evaluations. Therefore, we investigated the parameters that influence printability, including polymer concentration, degree of calcium ionic crosslinking, and UV irradiation time. Different GGMA and calcium chloride ink mixtures were evaluated through three steps: 1) pre-screening printability and rheological profiles, 2) printing parameters, and 3) post-printing analysis. The ink formulations were evaluated for their fibre formability, and the semi-quantitative measurement of 3D printed structures was used to obtain the highest printing resolution. Then, the optimised biomaterial ink was selected to print 3D structures to assess the printing accuracy and swelling behaviour after printing. The study provided a systematical approach to succeed 3D constructs using two-step crosslinking in GGMA inks. We also proposed simple quantitative tests to obtain a high aspect ratio from different ink compositions.

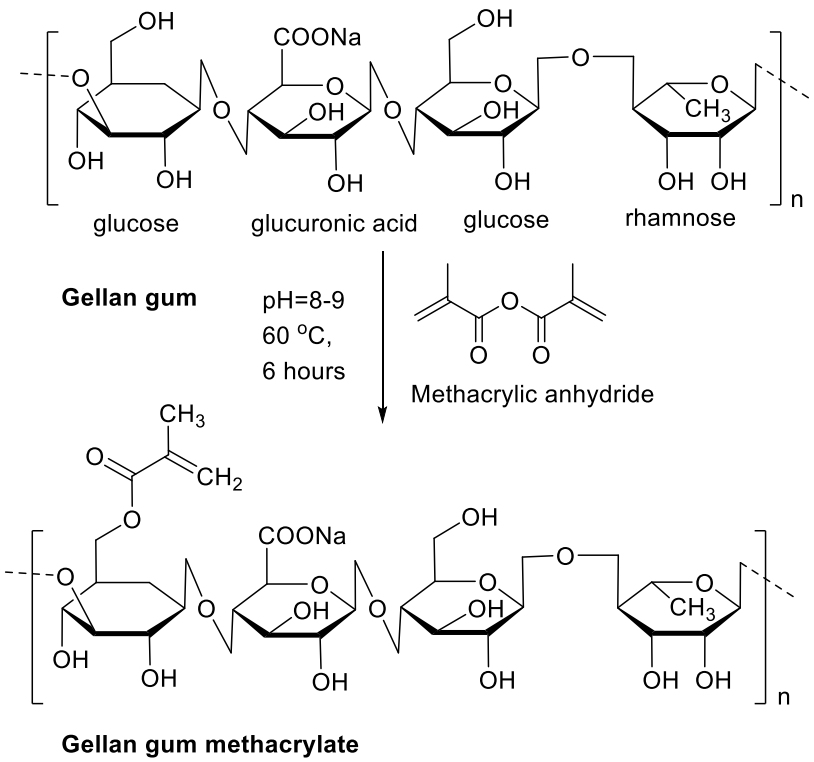

Fig. 1. Schematic illustration of the synthesis of GGMA.

2. Materials and methods

2.1. Synthesis and characterisation of modification degree of GGMA biomaterial inks

In this study, low acyl gellan gum (GG) was modified with a 15% degree of methacrylation (MA) (Fig. 1). GGMA with 15% MA was synthesised as follows. Low acyl gellan gum (Gelzan, purchased from Merck KGaA, USA) was purified to remove all divalent cations using the method reported elsewhere [23]. The purified GG was modified with functional methacrylate groups to enable photocrosslinking. Briefly, 1 g of GG was dissolved in 100 mL of DI water at 90 °C for 30 min, then cooled to 50 °C. Next, 8 mL of methacrylic anhydride (Merck KGaA, USA) was slowly added dropwise in the reaction mixture while stirring to maintain homogeneity for 3 h. Simultaneously, the pH was periodically adjusted to 8.5 with 5 M NaOH, and the reaction was continued for 6 h. GGMA was then transferred to dialysis membranes (11–14 kDa molecular weight-cutoff (MWCO) membrane (Spectra/Por, Repligen Corp., USA)) and dialysed against DI water for 5 days to remove any unreacted methacrylate anhydride. Water was changed 2–3 times a day until the solution became clear. The amount of unreacted methacrylic acid was monitored from dialysis water for 120 h using UV spectra (UV-3600 Plus, Shimadzu Corp., Japan) at a wavelength 350−500 nm to confirm the complete removal of excess methacrylic acid from the product. The resulting GGMA was lyophilised and stored in a −40 °C dried refrigerator. The methacrylation degree of GG was quantified via ^{1}H-NMR. The NMR spectra were recorded with the JEOL-500 MHz instrument (SCZ500R, JEOL Resonance, Japan) in D_2O solvent. The spectra were acquired at RT.

2.2. Formulation of GGMA biomaterial inks and pre-crosslinking techniques

The GGMA inks were dissolved in DPBS solution with a presence of a photoinitiator (0.5% w/v, Irgacure 2959 purchased from Merck KGaA, USA) in an incubator at 37 °C. Three different GGMA concentrations were formulated: 1, 2 and 3% w/v and two pre-crosslinking methods were tested: low temperature (4 °C) and ionic crosslinking. Ionically pre-crosslinked biomaterial ink was prepared by using 0, 22.5, 45 or 90 mM $CaCl_2$ (final concentration). The pH of all GGMA inks with different formulations was adjusted to 7.5 to gain proper viscosity. The tested formulations were: $GGMA_{\_4°C}$ = GGMA at 4 °C, $GGMA_{\_22.5mM}$ = GGMA with 22.5 mM $CaCl_2$, $GGMA_{\_45mM}$ = GGMA with 45 mM $CaCl_2$ and $GGMA_{\_90mM}$ = GGMA with 90 mM $CaCl_2$. After that, the ink formulations were evaluated according to Fig. 2.

2.3. Prescreening of printability of GGMA biomaterial inks

The prescreening protocol has been previously reported [5]. A simple method to determine the printability of a biomaterial ink in extrusion-based bioprinting is to observe the filament formation and layer stacking ability. All the inks were loaded into a 10 mL cartridge and capped with a nozzle of 200 μm in diameter. The cartridge was clamped in a vertical position to minimise the variation of temperature. The biomaterial ink was extruded by an automatic dispenser, varying

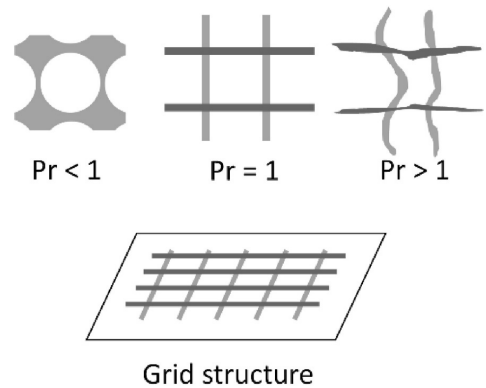

Fig. 3. Pore geometry evaluation and calculation of the printability (Pr) value. Ideally, Pr =1, indicating perfectly square-shaped pores.

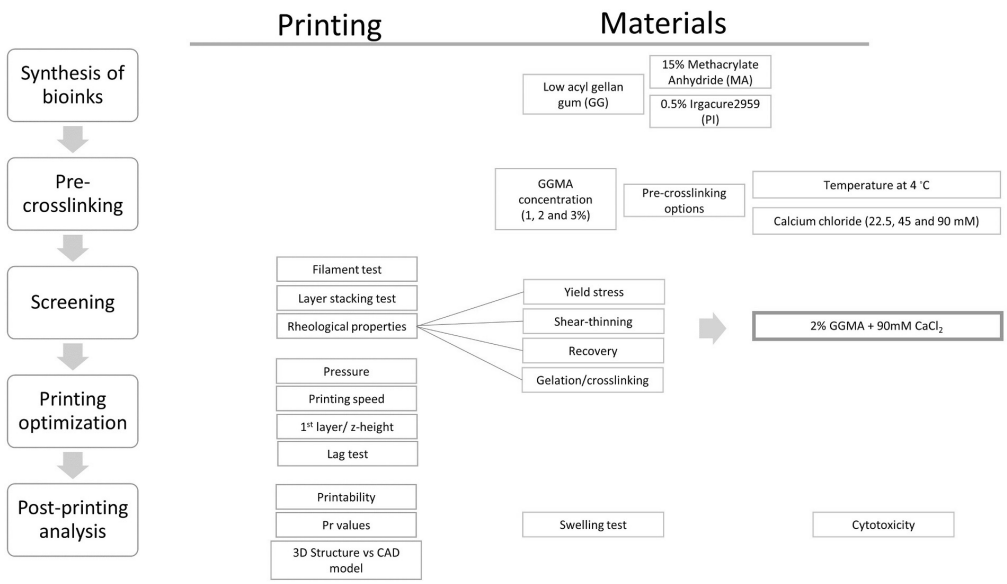

Fig. 2. Evaluation of GGMA biomaterial ink and development process.

the dispensing pressure between 0.1 and 2 bars and simultaneously observing the flow. The initial pressure was adjusted until the fibre started to flow, then slowly increased until the fibre was produced smoothly. The filament formation of different ink compositions was observed at RT and captured by a high-resolution mirrorless camera.

2.4. Rheological measurements of GGMA biomaterial inks

All rheological experiments were performed on a rotational rheometer (Discovery HR-2, TA Instruments Inc., USA) in parallel plate geometry (12 mm plate, 2.5 mm gap size). The temperature-dependent behaviour of GGMA was performed in flow mode (temperature sweep, 4−37 °C) with a constant shear rate (0.01 s^{-1}) at the rate of 2 °C/min (300 s soaking time). The results were plotted as a viscosity vs temperature graph.

For viscosity, yield stress, shear-thinning and recovery behaviour, the measurements were also performed in flow mode. The yield stress was determined using the shear rate-shear stress curve. The yield point was defined as the intersection point of the Y-axis at 0 shear rate in the shear stress-shear rate diagrams, indicating the point at which the material first started to flow. Shear-thinning was performed in flow mode with a shear rate ranging from 0.01−800 s^{-1}. Recovery behaviour measurements were performed to characterise the material's recovery behaviour by applying a low shear rate of 0.01 s^{-1} for 200 s, followed by a high shear rate of 500 s^{-1} for 100 s and finally, a low shear rate of 0.01 s^{-1} for 200 s.

Gelation/crosslinking time evaluation was performed via *in situ* polymerisation using a rotational rheometer and external UV lamp (BlueWave 50 UV curing spot lamp, DYMAX Corp., USA) at 365 nm in wavelength and 25 mW/cm^2 in UV intensity. Viscoelasticity (storage and loss moduli, G' and G'') was measured at RT as a function of time (500 s, UV lamp was activated at 100 s) while strain and frequency were kept constant at 1% and 1 Hz, respectively.

2.5. Shear-thinning coefficients of GGMA biomaterial inks

The Power-law regression model was applied to confirm the shear-thinning properties of the inks from the linear region of the viscosity-shear rate plots, calculated from Equation (1). The linear part of the curve from non-Newtonian region was chosen, where the viscosity drops with increasing shear rate.

$$\mu = K\dot{\gamma}^{n-1} \tag{1}$$

The flow index *n* relates to the shear-thinning abilities of the precursor, with n = 1 indicating Newtonian behaviour, n = 0.6 indicating weakly shear-thinning material, and n $\leq$ 0.2 meaning high shear-thinning properties and therefore good extrudability [3,24].

2.6. Quantitative evaluation of printability of GGMA biomaterial inks

Biomaterial inks were prepared as previously described, then loaded into a 10 mL cartridge (Optimum® syringe barrels, Nordson EFD, USA) and transferred in an incubator (37 °C) for 30 min to remove any air bubbles. Next, the cartridge was installed into a multi-material 3D bioprinter (BRINTER® 3D BIOPRINTER, Brinter Ltd., Finland). A 200 μm plastic UV shielded tapered nozzle (SmoothFlow™, Nordson EFD, USA) was attached to the cartridge and inserted into an air-pressure controlled Pneuma Tool print head (Fig. 4). To optimise the parameters, the pressure was set according to the previous prescreening test. Printing speed and print head temperature were constant at 8 mm/s and RT.

Biomaterial inks having ideal rheological properties, shear-thinning, and recovery behaviour produce coherent filaments, which are able to stack without merging [25,26]. Even though some of our GGMA ink candidates exhibited adequate results in both rheological and quantitative printability assessments, they could not be printed into 3D constructs. They either suffered from structure collapse, or upper layers started to merge with the lower layer. The next step for the practical printing assessment was to print grid patterns and apply a quantitative method to evaluate the shape of the printed pores using Equation (2):

$$Pr = \frac{\pi}{4}\frac{1}{C} = \frac{L^2}{16A}, \tag{2}$$

in which C is the circularity of the enclosed pore, L means perimeter and A the pore area. We defined the biomaterial inks' printability (Pr) based on the squareness of the pores inside the grid structure. Pr value 1 indicates a perfect square shape. A CAD model for the square grids (20 x 20 x 0.4 mm^3) was drawn with AutoDesk Fusion 360 software and used as a standard for this assessment. Appropriately conditioned inks can produce smooth filaments with a constant width and stack into a 3D structure, yielding square pores in the fabricated construct with a Pr value of 1 (Fig. 3 and Fig. S4). On the other hand, poorly conditioned inks demonstrate the liquid-like or irregularly shaped filament, giving Pr value less than 1 or more than 1, respectively. The higher Pr value is a result of excessive pre-crosslinking. The lower Pr value is an indication of an inadequate degree of pre-crosslinking. To determine the Pr value of each ink with various printing parameter combinations, optical images of printed constructs were analysed in ImageJ to measure the circularity of the pores (n=5).

To obtain a perfect 3D construct, we determined pre-flow and post-flow delays via lag time calculation before and after the ink deposition. We found out that the flow of the inks showed delay after applying pressure and when changing a printing layer. This caused the structure to deform and collapse after fibre deposition in the subsequent layers (Fig. S3).

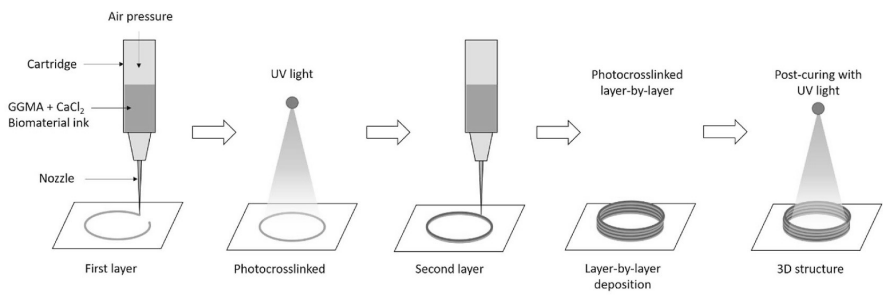

Fig. 4. Process flow of the extrusion-based 3D bioprinting process.

2.7. Printing accuracy and structural integrity of 3D printed GGMA hydrogels

After obtaining the best printable biomaterial ink formulation and optimal printing parameters, we assessed the structural integrity. We chose Nivea Creme (Nivea Creme, Beiersdorf Global AG, Germany) as a control printing material. It gave high geometric accuracy with minimal deviation compared to the CAD model [3,27]. The ink was printed into cylinders (10 mm in outer diameter) with different heights (1, 2.5 and 5 mm). Each structure was cured in a layer-by-layer fashion using the bioprinter's integrated UV/Vis LED module at a wavelength of 365 nm with 25 mW/cm^2 intensity for 10 s for each layer and 60 s for the post-curing process. The overview of the printing process is illustrated in Fig. 4. The dimensions of the cylinders were compared to the printed control structure to determine the printing accuracy. The structural integrity of each 3D printed structure was calculated as the ratio between dimensions of GGMA and control structure (1 = perfect structure, <1 = smaller in dimension, >1 = bigger dimensions than the control) [28].

For further in-depth structural analysis, the average mesh size and crosslinking density were determined from rheological measurement results [5,29]. The average mesh size (ξ, nm) calculation was applied using the storage moduli (G') of resulting hydrogels (the best formulation ink, 2% GGMA$_{90mM}$) at 0, 60, 120 and 180 s UV exposure time. Equation (3) estimates the average mesh size (ξ) of hydrogels at different exposure times:

$$(\xi) = \left(\frac{G' N}{RT}\right)^{-1/3}, \tag{3}$$

where G′ is the storage modulus of the hydrogel, N is the Avogadro constant (6.023 × 1023 mol^{-1}), R is the molar gas constant (8.314 JK^{-1}mol^{-1}), and T is the temperature (298 K).

Moreover, crosslinking density (n_e, mol/m^3) of the hydrogels were calculated using the storage modulus from the linear region of the frequency sweep test (a frequency range of 0.1–100 Hz). The data provided the total number of elastically active junction points in the network per unit of volume, using Equation (4).

$$n_e = \frac{G_e}{RT}, \tag{4}$$

where G_e is the average value of storage modulus from the linear region of oscillatory frequency sweep measurement.

2.8. Swelling of 3D printed GGMA hydrogels

The swelling ratio of the printed hydrogels was determined in DI water and cell culture media (Dulbecco's Modified Eagle's medium, DMEM). The GGMA was printed into cylinders with a height of 1 mm. Each experiment condition was tested with GGMA at a concentration of 2% GGMA$_{90mM}$. All samples were cured using 365 nm UV light at an intensity of 25 mW/cm^2 in a layer-by-layer fashion with 10 s exposure time followed by 60 s post-curing. The obtained hydrogels at zero time point were defined with a weight of W_0. The hydrogels were then immersed in the solution (DI water or DMEM) until equilibrium was reached and weighed (W_s). The swelling ratio was calculated at time points of 1, 2, 3, 4, 5, 24, 36 and 48 h using Equation (5).

$$Swelling\ Ratio = \frac{W_s - W_0}{W_0} \times 100\%. \tag{5}$$

3. Results

3.1. Synthesis and characterisation of modification of GGMA biomaterial inks

GGMA was functionalised by methacrylation of purified GG polymer. The purity of dialysed GGMA was confirmed by UV absorption spectra (Fig. S1). The methacrylation degree of GGMA was characterised and verified by using ^{1}H-NMR. The degree of methacrylation was calculated by comparing the integrated protons' peaks from methyl group on rhamnose ring of gellan gum (d =1.26 ppm) with a methyl group on the methacrylate moiety (d= 1.90 ppm) and vinylic protons on carbon-carbon double bond (d= 5.72 and 6.13 ppm) (Fig. S2).

3.2. Formulations and prescreening printability of GGMA biomaterial inks

GG and GGMA are capable of physical gelation via temperature change and ionic crosslinking. GGMA was prepared at different concentrations (1, 2 and 3% w/v). Initial testing screened the fibre-forming ability (in the air) of the pre-crosslinked GGMA. It was observed that GGMA solution alone at RT immediately formed a droplet after being extruded. Due to temperature-dependent viscosity, GGMA at 4 °C was more viscous and was able to form weak hydrogels. However, it could form a fibre only for a short time and was not able to maintain its shape after extruding from a nozzle. (The rheological data presented in the next section confirmed this phenomenon). According to Fig. 8, the ionic pre-crosslinking of GGMA was carried out by adding Ca^{2+} ions and varying the concentration of GGMA (1, 2 and 3% w/v) and $CaCl_2$ solution (22.5, 45 and 90 mM). A mild ionic crosslinking of GGMA enabled the formation of a weak hydrogel, which was soft and extrudable. According to the results, all concentrations of GGMA with 45 or 90 mM of $CaCl_2$ (1% GGMA$_{45mM}$, 1% GGMA$_{90mM}$, 2% GGMA$_{45mM}$, 2% GGMA$_{90mM}$, 3% GGMA$_{45mM}$ and 3% GGMA$_{90mM}$) were able to form coherent fibres that were assumed to be good candidates for 3D printing.

3.3. Rheological properties of GGMA inks and their pre-crosslinking methods

The evaluation of the rheological behaviour of GGMA was divided into three parts: yield stress, shear-thinning, and recovery behaviour. The shear-thinning profiles of each GGMA formulation were assessed to confirm the reliability of the prescreening method and to predict the extrudability. The Power-law model was applied to calculate the shear-

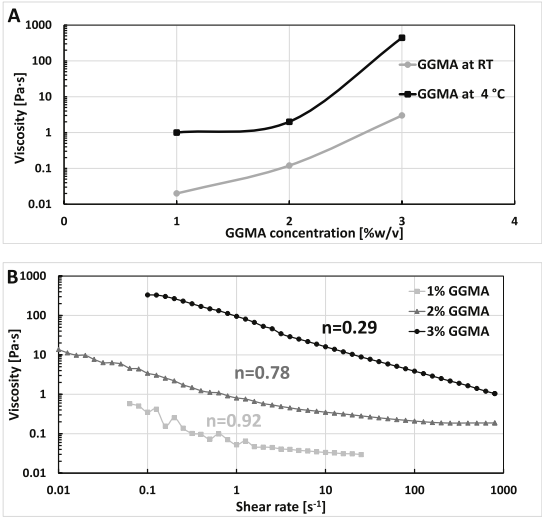

Fig. 5. A) The effect of temperature on GGMA at RT and 4 °C for various concentrations (1, 2 and 3%), B) Shear-thinning properties of 1, 2 and 3% GGMA concentrations at 4 °C.

thinning coefficients (*n* values). According to Fig. 5A and B, the viscosity of GGMA changed as a function of temperature. The results showed that 3% $GGMA_{4\ °C}$ without ionic crosslinking exhibited shear-thinning behaviour with decreasing viscosity as a function of increasing shear rate ($n = 0.29$). On the other hand, the prescreening method showed contradictory results. 3% $GGMA_{4\ °C}$ formed a temporary fibre in the air and lost its properties a few seconds after being extruded from a nozzle. 1 and 2% $GGMA_{4\ °C}$ exhibited Newtonian fluid behaviour.

Ionic pre-crosslinking resulted in the improvement of the shear-thinning behaviour, as shown in Fig. 6. 1% $GGMA_{22.5mM}$ and 1% $GGMA_{45mM}$ had a lot of variance due to the lack of viscosity and hence *n* values could not be obtained. 2% $GGMA_{22.5mM}$ was weakly shear-thinning ($n = 0.55\pm0.01$). Most of the 2 and 3% GGMA gels with 45 or 90 mM $CaCl_2$ (2% $GGMA_{45mM}$, 2% $GGMA_{90mM}$, 3% $GGMA_{45mM}$ and 3% $GGMA_{90mM}$) exhibited Non-Newtonian behaviour as the viscosity decreased as a function of increasing shear rate. The *n* values from the Power-law equation for 2% $GGMA_{45mM}$, 2% $GGMA_{90mM}$, 3% $GGMA_{45mM}$ and 3% $GGMA_{90mM}$ gels were 0.35 ± 0.03, 0.10 ± 0.03, 0.26 ± 0.2 and 0.22 ± 0.30, accordingly. In addition, 1% $GGMA_{90mM}$ and 3% $GGMA_{22.5mM}$ had some shear-thinning properties (*n* values were lower than 0.3).

Yield stress values of GGMA at different polymer and $CaCl_2$ concentrations were evaluated. According to Fig. 6, all concentrations of $GGMA_{22.5mM}$ have a low yield point, are low in viscosity and do not exhibit yield stress. In addition, 1% $GGMA_{45mM}$ cannot gain enough yield stress to show yielding behaviour. 2% and 3% GGMA with 45 or 90 mM $CaCl_2$ (2% $GGMA_{45mM}$, 2% $GGMA_{90mM}$, 3% $GGMA_{45mM}$ and 3% $GGMA_{90mM}$) showed a clear yield point. After the shear rate was increased, they exhibited Non-Newtonian behaviour and started to flow.

Recovery testing was performed to predict the recoverability of materials after being extruded from the print head. Ideally, GGMA should recover fast back to the initial viscosity level once printed on the substrate. According to Fig. 6, 1% $GGMA_{22.5mM}$ and 1% $GGMA_{45mM}$ were unable to be measured due to low viscosity, and the inks were completely splashed out from the geometry at a higher shear rate. In addition, 3% $GGMA_{90mM}$ was disintegrated and slipped out during the measurement because the ink appeared to be a hard and fragile hydrogel. Fig. 6 shows the recovery results for 1% $GGMA_{90mM}$, 2% $GGMA_{22.5mM}$, 2% $GGMA_{45mM}$, 2% $GGMA_{90mM}$, 3% $GGMA_{22.5mM}$ and 3% $GGMA_{45mM}$. Only 1% $GGMA_{90mM}$ and 2% $GGMA_{90mM}$ gels were able to rapidly recover their viscosity back to 90% of the original value after removing the shear. On the other hand, 2% $GGMA_{22.5mM}$, 2% $GGMA_{45mM}$, 3% $GGMA_{22.5mM}$, and 3% $GGMA_{45mM}$ did not recover their original viscosity quickly but required a longer recovery time (100 s for 2% GGMA) to reach back to their initial viscosity. The material properties of 3% GGMA changed permanently as a result of the high shear rate.

3.4. Gelation time of GGMA inks via in situ photo-rheology

As shown in Fig. 7, *in situ* photo-rheology was used to measure the gelation kinetics of GGMA at different concentrations after exposure to UV light. All GGMA concentrations rapidly gelated and crosslinked within 10 s and reached the maximum crosslinking state at 60 s. The concentration of GGMA had a significant effect on the final storage modulus, but the gelation time did not differ dramatically between various tested polymer concentrations.

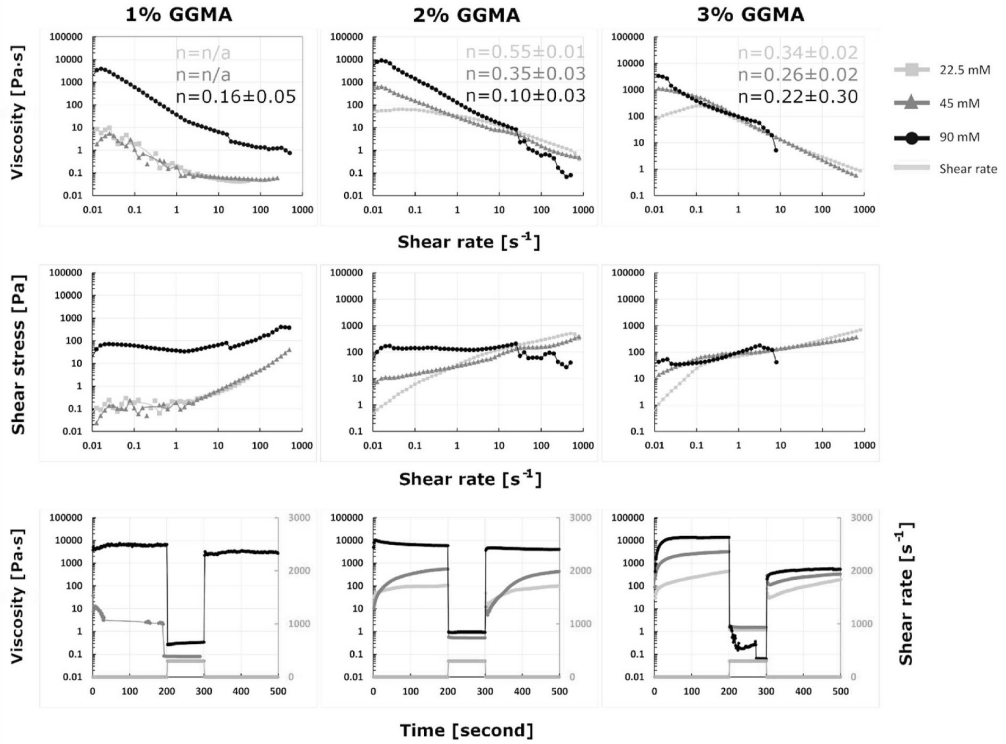

Fig. 6. Rheological properties: shear-thinning, yield stress and recovery for various GGMA and $CaCl_2$ concentrations at RT.

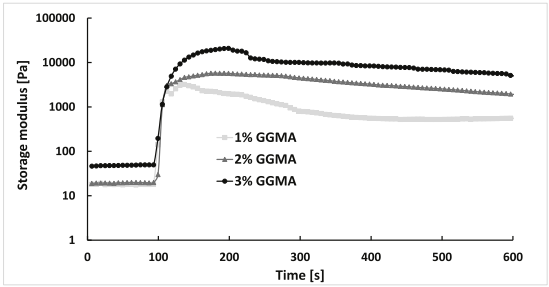

Fig. 7. In situ photorheology of 1%, 2% and 3% GGMA at RT.

3.5. Quantitative evaluation of printability of GGMA inks and ionic pre-crosslinking

Pr values were calculated for each combination of GGMA and $CaCl_2$ concentrations. Fig. 8 illustrates Pr values of GGMA with concentrations of 1, 2 and 3% w/v pre-crosslinked with $CaCl_2$ concentration of 0, 22.5, 45 or 90 mM. Ink is referred to as printable when the Pr value is 0.9–1.1 (Fig. 9). It was clear that GGMA without pre-crosslinking was unprintable at RT/4 °C even though 3% GGMA had the highest viscosity. Fig. 8 shows the relationship between various concentrations of GGMA mixed with various concentrations of $CaCl_2$. Pr value of $GGMA_{\_22.5mM}$ could not be quantified at all due to insufficient ionic crosslinking. The Pr value of 1% $GGMA_{\_45mM}$ could not be defined due to poor gelation. For 1% $GGMA_{\_90mM}$, Pr value was 0.78±0.4.

On the other hand, 3% $GGMA_{\_90mM}$ appeared as overgelated ink due to excessive ionic crosslinking. It required high pressure to be extruded and formed a tough hydrogel inside the nozzle, resulting in variable-sized printed fibre and irregularly shaped pores (Pr = 1.1± 0.3). Printability of 2% $GGMA_{\_90mM}$ and 3% $GGMA_{\_45mM}$ fell into the proper region of printability, being 0.97 and 1.1, respectively. However, 2% GGMA produced smooth and coherent grid structures as compared to the crooked and uneven shape of 3% $GGMA_{\_45mM}$ grids. 2% $GGMA_{\_45mM}$ with the value of 0.82±0.04 was also printable but was not viscous enough to maintain the grid shape.

3.6. Printing accuracy and structural integrity

The CAD models of cylinders had a wall height of 1, 2.5 or 5 mm and consisted of 6, 16 or 33 layers. The printed GGMA structures were compared to the printed control structure to calculate the %error and

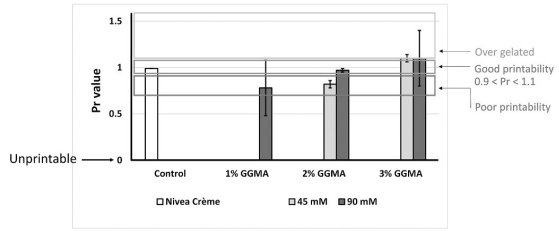

Fig. 9. The calculated Pr values for Nivea Creme (control) and various GGMA formulations with different amounts of $CaCl_2$ pre-crosslinking.

structural integrity (Fig. 10). Table 1 shows all measured dimensions of GGMA 3D structures: cylinder height, diameter (inner and outer) and wall thickness.

The average mesh sizes (ξ) and crosslinking densities (n_e) were calculated using Equations (3) and (4). The calculated parameters can be found in the supporting information (Table S1). Crosslinked hydrogels (2% $GGMA_{\_90mM}$) with the 180 s of UV exposure time had a smaller mesh size than crosslinked hydrogels with 60 s or no exposure. On the other hand, the longest UV exposure time (180 s) yielded the highest value of crosslinking density.

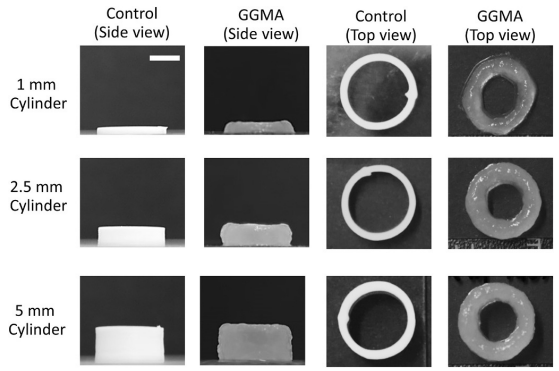

Fig. 10. Side-views and top-views of printed cylinders for the evaluation of printing accuracy and structural integrity, The scale bar = 5 mm.

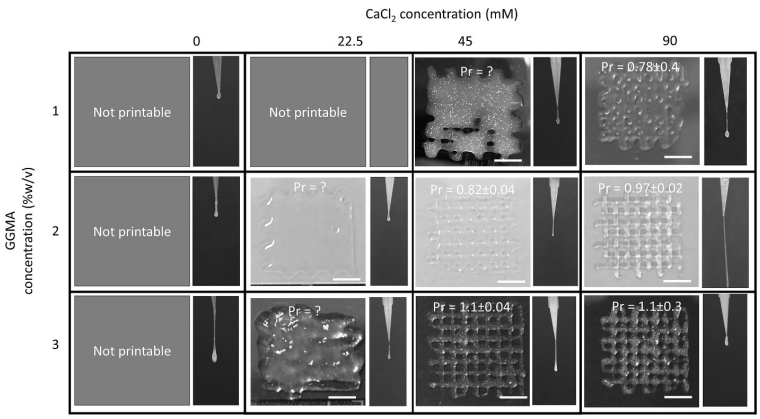

Fig. 8. The fibre formation results and printed grid structures of GGMA/$CaCl_2$ inks in terms of printability at RT. The scale bar is 5 mm.

Table 1
Dimensions of the printed cylinders, including the percentage error, compared to the control cylinder and structural integrity ratio.

1 mm cylinder [6 layers]	Control dimensions [mm]	GGMA dimensions [mm]	Error [%]	Structural integrity ratio
height	1.3±0.1	1.7±0.2	30.7±5.1	1.31±0.05
outer diameter	11.0±0.2	11.2±0.2	1.8±0.2	1.02±0.01
inner diameter	8.80±0.2	6.5±0.3	26.2±2.7	0.73±0.04
wall thickness	1.2±0.1	3.0±0.1	150.7±10.8	2.50±1.30
2.5 mm cylinder [16 layers]	**Control dimensions [mm]**	**GGMA dimensions [mm]**	**Error [%]**	**Structural integrity ratio**
height	3.2±0.1	3.7±0.3	15.6±3.7	1.15±0.06
outer diameter	11.0±0.1	11.7±0.2	6.3±1.5	1.06±0.01
inner diameter	8.8±0.2	6.2±0.1	28.5±2.8	0.70±0.04
wall thickness	1.2±0.2	3.1±0.1	158.7±12.5	2.58±0.28
5 mm cylinder [33 layers]	**Control dimensions [mm]**	**GGMA dimensions [mm]**	**Error [%]**	**Structural integrity ratio**
height	5.8±0.1	7.2±0.2	24.21±1.2	1.24±0.02
outer diameter	11.2±0.2	11.2±0.1	10.7±5.8	1.04±0.02
inner diameter	8.4±0.2	5.6±0.2	33.3±5.3	0.66±0.01
wall thickness	1.4±0.2	3.2±0.1	128.5±7.2	2.28±0.22

3.7. Swelling of the 3D printed structures

The printed structures were immersed in DI water and DMEM for 48 h and periodically weighted at different time points (Figs. S5 and S6). Samples (in DI water and DMEM) without UV post-curing were completely disintegrated after 30 min in an incubator at 37 °C. As shown in Fig. 11, samples immersed in water quickly absorbed water into the structures after only 30 min, resulting in enormous swelling up to almost 200% at the 5-h time point. The swelling saturated after 10 h immersion in water, then slowly decreased after 24 h (% swelling reduced to ~100%) and became steady until 48 h. When immersed in DMEM, the samples gradually shrank and reached the equilibrium stage after 5 h. The swelling ratio of the samples in DMEM stayed constant until the end of the swelling study.

4. Discussion

In this study, we have developed a two-step crosslinking technique using ionic pre-crosslinking together with photocrosslinking to enhance the printability of GGMA biomaterial ink. Hence, we ended up using ionic $CaCl_2$ crosslinking of GGMA precursors by tuning the polymer and Ca^{2+} concentrations. While the pre-crosslinking technique using $CaCl_2$ is a well-known and widely used approach for alginate and nanocellulose inks, it has not been previously used for GGMA biomaterial inks [30,31]. Also, the mixture of gellan gum and calcium ions has been reported to increase the elastic modulus of the resulting bulk hydrogels [20,32]. However, the combination has not been studied from the 3D printability perspective. The incorporation of Ca^{2+} into GGMA improves the viscosity of the inks, even with low GGMA concentrations, and enables them to sustain the 3D shape before photocrosslinking. However, the tuning of the Ca^{2+} concentration needs to be meticulous, as incorrect Ca^{2+} amount can lead to poor printability (either too liquid or too viscous ink) [3].

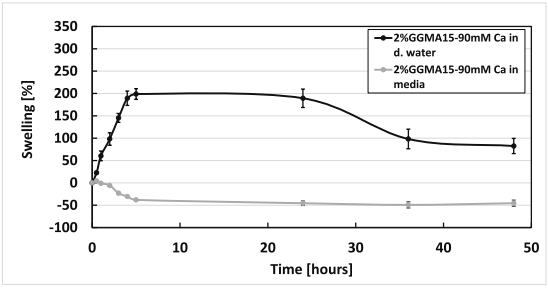

Fig. 11. Swelling behaviour of the printed GGMA structures. The samples were immersed in two different media: deionised water and DMEM.

To optimise the printing outcome, we evaluated the effect of different ratios of GGMA and $CaCl_2$ on printing results. After applying ionic pre-crosslinking, weak hydrogels were obtained. They were soft and extrudable and maintained their shape after being deposited from the nozzle in the printing process. Photocrosslinking was applied layer-by-layer to turn the weak hydrogels into true hydrogels with stable 3D shapes. We combined several assessment methods (Fig. 2) into a step-by-step process to measure the true printability of the inks [25]: pre-screening of extrudability (fibre formation), rheological measurements (shear-thinning, yield stress and recovery behaviour), and quantification of printability (Pr value) from the printed grids [33].

Shear-thinning properties especially have been used in several research studies to show the printability of novel biomaterial inks [34, 35]; however, those characteristics alone cannot guarantee that the inks can be successfully printed. According to our prescreening printability data, GGMA should have been printable at room temperature (RT) if the polymer concentration was high enough. However, the experimental printing tests showed otherwise. Without pre-crosslinking, GGMA inks at RT could not be printed into 3D structures as they did not form fibres nor had appropriate rheological behaviour. On the contrary, GGMA precursors at low temperature (4 °C) showed good shear-thinning properties (*n* value was lower than 0.3) but behaved like liquid after being deposited on the substrate. The explanation for this result could be that the GGMA precursor was cooled in the syringe, but the temperature suddenly rose after the printed filament was exposed to the room temperature on the printing substrate. Hence, the viscosity of the GGMA ink had to be improved by applying ionic pre-crosslinking.

We found that Ca^{2+} played an essential role in determining the viscosity and shear-thinning coefficients of GGMA inks. The viscosity changed as a function of the $CaCl_2$ concentration. These pre-crosslinked inks also had a high shape fidelity after extrusion. However, GGMA (1–3% w/v) pre-crosslinked with a low concentration of $CaCl_2$ (22.5 mM) had poor printability and could not form a consistent fibre. Their rheological profiles also supported our findings of the poor printability as the samples could not recover back to their initial viscosity after the high shear rate, suggesting an insufficient ionic pre-crosslinking. According to the results, it is apparent that low polymer concentration requires more Ca^{2+} pre-crosslinking to gain enough viscosity for 3D printing, while inks with higher polymer concentration can be printed with lower Ca^{2+} concentration. In general, pre-crosslinked GGMA inks with Ca^{2+} displayed rapid viscosity recovery after removing the high shear rate. The recovery test results also showed that a higher Ca^{2+} amount in GGMA ink improved recovery behaviour in all polymer concentrations, except in 3% $GGMA_{90mM}$. 3% GGMA_90 mM appeared as solid hydrogel and was not extrudable. In addition, according to Cao et al. [35] and Coutinho et al. [20], even a 90 mM concentration of $CaCl_2$ as a crosslinker barely affects the ink's biocompatibility and shows no significant effect on the viability of encapsulated cells (both fibroblasts and neural cells) [31].

Photorosslinking kinetics of the GGMA inks were monitored using *in situ* photorheology. As observed from Fig. 7, the storage moduli of all GGMA concentrations immediately increased after exposure to the UV

light. The storage moduli increased dramatically as a function of the curing time and reached a plateau after 60 s. The possible reason for the plateaued curve is that the precursors became fully crosslinked, as explained in the literature [36]. The exposure times for the layer-by-layer curing during printing and post-curing phase were chosen to match the conditions of the *in situ* photorheology, i.e. 25 mW/cm^2 intensity for 10 s for each layer and 60 s for the post-curing process.

Quantitative printability evaluation was defined via Pr value, which other researchers have used as a guideline for the selection of bioprinting parameters [25,26,37,38]. According to Ouyang et al. [25], the Pr value should be in the range of 0.9–1.1. In our study, the printability improved when the concentration increased for either GGMA or $CaCl_2$. In the inks with low Pr values (less than 0.8), the pores inside the grid structures were fused and were evaluated as having poor printability. On the other hand, in the inks with high Pr values (more than 1.1), the square shape of the pores deviated from the CAD model and were also assigned as having poor printability.

In addition to the Pr value evaluation, the dimensions of the printed 3D structures were measured to estimate the printing error (i.e., the deviation from the control structure dimensions) and structural integrity. Nivea Creme was chosen as a control for the evaluation because it exhibits good fibre formation. The formed fibres are highly consistent and maintain their shape without merging/breaking during the printing. The grid constructs attach well to the glass slide and keep the shape of a crosshatch [3]. Also, the printed Nivea Creme structures have only a slight deviation from the CAD model and thus represent a perfect example of material behaviour during the printing process. The structural analysis of printed 3D structures and comparison to control samples was adopted from Gao et al. [28]. According to the structural integrity analysis, all GGMA structures ended up being a bit bigger than the control structures in all dimensions because the rheological recovery degree of GGMA was only 70–90%, and the structural integrity ratio was more than 1.0. The extruded fibres on the glass substrate were swollen and had pronounced dimensions in every layer. The wall thickness had the highest deviation, and the deviation increased as a function of the number of the printed layers. The wall thickness of the GGMA cylinders was considerably more prominent than in the control cylinders as the GGMA fibres spread, resulting in a high deviation in the inner diameter. Another reason for the deviation could be the slanted cylinder walls, resulting in measurement errors in the wall heights. The average mesh size and crosslinking density will not directly explain the pore size of hydrogels but will provide more structural insight since pore size is related to mesh size [29]. In addition, the average mesh size values reflect the crosslinking density (smaller mesh sizes lead to higher crosslinking density). These values are crucial in evaluating the suitability of these photocrosslinked hydrogels for biomedical applications. The average mesh size of 2% GGMA_90 mM was around 10–15 nm, which is comparable to other natural hydrogels having a mesh size of 5–100 nm [39]. The size range of 5–100 nm allows the exchange of small molecules, such as nutrients and growth factors, while the flow of non-covalently entrapped larger molecules may be hindered. Anyhow, most proteins and peptides in human cells can easily diffuse through our GGMA gels since their diameter is less than 7 nm [40].

The swelling/shrinking behaviour is normally studied to confirm the mechanical stability of hydrogels in aqueous media [33]. The printed GGMA structures shrank immediately in the DMEM solution, suggesting they were influenced by the cations in the solution. On the contrary, the samples in water swell and quickly uptook the water, losing their integrity over time because DI water has no ions. These results are supported by the previous studies of alginate and gellan gum hydrogels. The shrinking phenomenon has also been observed by Coutinho et al. [20] when the hydrogels were immersed in media containing Ca^{2+}. According to the swelling test of bulk hydrogels done by Xu et al. [32] and Coutinho et al. [20], solid GGMA hydrogels swell at a slower rate compared to our printed GGMA structures. This difference results from the fact that the surface area of hydrogels strongly influences the swelling kinetics. Our cylinder-shaped printed structures have a higher surface area than the solid bulk hydrogels and thus swell faster.

5. Conclusions

In this study, we successfully developed a two-step crosslinking technique to achieve 3D printed structures from GGMA biomaterial inks with extrusion-based bioprinting. With a sufficient amount of calcium chloride precrosslinker, GGMA transformed from a liquid precursor to a weak printable hydrogel, which could be further photocrosslinked into a true hydrogel with good shape fidelity. The printing parameters were optimised through stepwise characterisation of printability and rheological properties. According to the prescreening results, viscosity data and shear-thinning coefficients alone cannot guarantee the success of 3D printing. They do not predict the actual printing outcome, which is governed by gravitational forces and the surface properties of the printing substrate. However, the rheological data was valuable to predict the extrudability of the inks out from a nozzle. Our ink optimisation process showed that the polymer and calcium chloride concentration affected the printability of GGMA inks. We found that out of the studied combinations, 2% $GGMA_{\_90mM}$ and 3% $GGMA_{\_45mM}$ were best in printing. 2% $GGMA_{\_90mM}$ was selected as the best combination, and 3D printed cylinders were achieved with the height of 1, 2.5 and 5 mm. However, the printed outcome still lacked high resolution compared to the control samples and the CAD model. The study highlights that the two-step crosslinking approach is an effective way to convert unprintable GGMA ink into stackable material capable of forming 3D constructs. Our qualitative and quantitative analyses can be applied to other bioinks/biomaterial inks in the field of biofabrication, as well.

CRediT authorship contribution statement

Hatai Jongprasitkul: Conceptualization, Methodology, Investigation, Formal analysis, Writing – original draft, Visualization, Validation. **Sanna Turunen:** Conceptualization, Methodology, Investigation, Formal analysis, Validation, Writing – original draft, Supervision. **Vijay Singh Parihar:** Conceptualization, Methodology, Resources, Formal analysis, Validation, Writing – review & editing, Data curation, Supervision. **Minna Kellomäki:** Conceptualization, Methodology, Funding acquisition, Project administration, Writing – review & editing, Supervision.

Declaration of competing interest

The authors declare that they have no known competing financial interests or personal relationships that could have appeared to influence the work reported in this paper.

Acknowledgement

The authors are grateful to The Centre of Excellence in Body-on-Chip Research (CoEBoC) by the Academy of Finland for financial support (decision #312409, #326587 and #336663) and to the Tampere University funding for CoEBoC. We would like to thank Ms Niina Alén for the development of UV-based method for measuring the purity of the dialysed product.

Appendix A. Supplementary data

Supplementary data to this article can be found online at https://doi.org/10.1016/j.bprint.2021.e00185.

References

[1] I.T. Ozbolat, M. Hospodiuk, Current advances and future perspectives in extrusion-based bioprinting, Biomaterials 76 (2016) 321–343, https://doi.org/10.1016/j.biomaterials.2015.10.076.

[2] M. Amr, M. Counts, J. Kernan, A. Mallah, J. Mendenhall, B. Van Wie, N. Abu-lail, B. A. Gozen, Bioprinting 3D printed , mechanically tunable , composite sodium alginate , gelatin and Gum Arabic (SA-GEL-GA) scaffolds, Bioprinting 22 (2021), e00133, https://doi.org/10.1016/j.bprint.2021.e00133.

[3] N. Paxton, W. Smolan, T. Böck, F. Melchels, J. Groll, T. Jungst, Proposal to assess printability of bioinks for extrusion-based bioprinting and evaluation of rheological properties governing bioprintability, Biofabrication 9 (2017), 44107, https://doi.org/10.1088/1758-5090/aa8dd8.

[4] C.J. Ferris, K.J. Gilmore, S. Beirne, D. McCallum, G.G. Wallace, M. Het Panhuis, Bio-ink for inkjet printing of living cells, Tech. Proc. 2013 NSTI Nanotechnol. Conf. Expo, NSTI-Nanotech 2013 2 (2013) 261–264.

[5] H. Jongprasitkul, S. Turunen, V.S. Parihar, S. Annurakshita, M. Kellomaki, Photocross-linkable methacrylated polypeptides and polysaccharides for casting, injecting, and 3D fabrication, Biomacromolecules 22 (2021) 481–493, https://doi.org/10.1021/acs.biomac.0c01322.

[6] M.K. Włodarczyk-Biegun, A. del Campo, 3D bioprinting of structural proteins, Biomaterials 134 (2017) 180–201, https://doi.org/10.1016/j.biomaterials.2017.04.019.

[7] S.A. Bencherif, A. Srinivasan, F. Horkay, J.O. Hollinger, K. Matyjaszewski, N. R. Washburn, Influence of the degree of methacrylation on hyaluronic acid hydrogels properties, Biomaterials 29 (2008) 1739–1749, https://doi.org/10.1016/j.biomaterials.2007.11.047.

[8] A. Isaacson, S. Swioklo, C.J. Connon, 3D bioprinting of a corneal stroma equivalent, Exp. Eye Res. 173 (2018) 188–193, https://doi.org/10.1016/j.exer.2018.05.010.

[9] H. Li, S. Liu, L. Li, Rheological study on 3D printability of alginate hydrogel and effect of graphene oxide, Int. J. Bioprinting. 2 (2016) 54–66, https://doi.org/10.18063/IJB.2016.02.007.

[10] L.E. Bertassoni, M. Cecconi, V. Manoharan, M. Nikkhah, J. Hjortnaes, A.L. Cristino, G. Barabaschi, D. Demarchi, M.R. Dokmeci, Y. Yang, A. Khademhosseini, Hydrogel bioprinted microchannel networks for vascularization of tissue engineering constructs, Lab Chip 14 (2014) 2202–2211, https://doi.org/10.1039/c4lc00030g.

[11] M.E. Cooke, D.H. Rosenzweig, The rheology of direct and suspended extrusion bioprinting, APL Bioeng 5 (2021), 011502, https://doi.org/10.1063/5.0031475.

[12] J. Groll, J.A. Burdick, D.W. Cho, B. Derby, M. Gelinsky, S.C. Heilshorn, T. Jüngst, J. Malda, V.A. Mironov, K. Nakayama, A. Ovsianikov, W. Sun, S. Takeuchi, J. J. Yoo, T.B.F. Woodfield, A definition of bioinks and their distinction from biomaterial inks, Biofabrication 11 (2019), 013001, https://doi.org/10.1088/1758-5090/aaec52.

[13] T.M. Robinson, S. Talebian, J. Foroughi, Z. Yue, C.D. Fay, G.G. Wallace, Fabrication of aligned biomimetic gellan gum-chitosan microstructures through 3D printed microfluidic channels and multiple in situ cross-linking mechanisms, ACS Biomater. Sci. Eng. 6 (2020) 3638–3648, https://doi.org/10.1021/acsbiomaterials.0c00260.

[14] C.J. Ferris, K.J. Gilmore, G.G. Wallace, M. In Het Panhuis, Modified gellan gum hydrogels for tissue engineering applications, Soft Matter 9 (2013) 3705–3711, https://doi.org/10.1039/c3sm27389j.

[15] H.H. Mishbak, G. Cooper, P.J. Bartolo, Development and characterization of a photocurable alginate bioink for three-dimensional bioprinting, Int. J. Bioprinting. 5 (2019) 12–26, https://doi.org/10.18063/IJB.V5I2.189.

[16] V.H.M. Mouser, F.P.W. Melchels, J. Visser, W.J.A. Dhert, Yield stress determines bioprintability of hydrogels based on gelatin-methacryloyl and gellan gum for cartilage bioprinting, Biofabrication 8 (2016) 1–24, https://doi.org/10.1088/1758-5090/8/3/035003.

[17] D. Wu, Y. Yu, J. Tan, L. Huang, B. Luo, L. Lu, C. Zhou, 3D bioprinting of gellan gum and poly (ethylene glycol) diacrylate based hydrogels to produce human-scale constructs with high-fidelity, Mater. Des. 160 (2018) 486–495, https://doi.org/10.1016/j.matdes.2018.09.040.

[18] S. Pacelli, P. Paolicelli, I. Dreesen, S. Kobayashi, A. Vitalone, M.A. Casadei, Injectable and photocross-linkable gels based on gellan gum methacrylate: a new tool for biomedical application, Int. J. Biol. Macromol. 72 (2015) 1335–1342, https://doi.org/10.1016/j.ijbiomac.2014.10.046.

[19] J. Hazur, R. Detsch, E. Karakaya, J. Kaschta, J. Teßmar, D. Schneidereit, O. Friedrich, D.W. Schubert, A.R. Boccaccini, Improving alginate printability for biofabrication: establishment of a universal and homogeneous pre-crosslinking technique, Biofabrication 12 (2020), 045004, https://doi.org/10.1088/1758-5090/ab98e5.

[20] D.F. Coutinho, S.V. Sant, H. Shin, J.T. Oliveira, M.E. Gomes, N.M. Neves, A. Khademhosseini, R.L. Reis, Modified Gellan Gum hydrogels with tunable physical and mechanical properties, Biomaterials 31 (2010) 7494–7502, https://doi.org/10.1016/j.biomaterials.2010.06.035.

[21] S.R. Van Tomme, G. Storm, W.E. Hennink, In situ gelling hydrogels for pharmaceutical and biomedical applications, Int. J. Pharm. 355 (2008) 1–18, https://doi.org/10.1016/j.ijpharm.2008.01.057.

[22] J. Silva-Correia, B. Zavan, V. Vindigni, T.H. Silva, J.M. Oliveira, G. Abatangelo, R. L. Reis, Biocompatibility evaluation of ionic- and photo-crosslinked methacrylated gellan gum hydrogels: in vitro and in vivo study, Adv. Healthc. Mater. 2 (2013) 568–575, https://doi.org/10.1002/adhm.201200256.

[23] D.M. Kirchmajer, B. Steinhoff, H. Warren, R. Clark, M. In Het Panhuis, Enhanced gelation properties of purified gellan gum, Carbohydr. Res. 388 (2014) 125–129, https://doi.org/10.1016/j.carres.2014.02.018.

[24] E. Reina-Romo, S. Mandal, P. Amorim, V. Bloemen, E. Ferraris, L. Geris, Towards the experimentally-informed in silico nozzle design optimization for extrusion-based bioprinting of shear-thinning hydrogels, Front. Bioeng. Biotechnol. 9 (2021) 1–14, https://doi.org/10.3389/fbioe.2021.701778.

[25] L. Ouyang, R. Yao, Y. Zhao, W. Sun, Effect of bioink properties on printability and cell viability for 3D bioplotting of embryonic stem cells, Biofabrication 8 (2016) 1–12, https://doi.org/10.1088/1758-5090/8/3/035020.

[26] G. Gillispie, P. Prim, J. Copus, J. Fisher, A.G. Mikos, J.J. Yoo, A. Atala, S.J. Lee, Assessment methodologies for extrusion-based bioink printability, Biofabrication 12 (2020), 022003, https://doi.org/10.1088/1758-5090/ab6f0d.

[27] L. Horvath, Y. Umehara, C. Jud, F. Blank, A. Petri-Fink, B. Rothen-Rutishauser, Engineering an in vitro air-blood barrier by 3D bioprinting, Sci. Rep. 5 (2015) 7974, https://doi.org/10.1038/srep07974.

[28] T. Gao, G.J. Gillispie, J.S. Copus, A.K. Pr, Y.-J. Seol, A. Atala, J.J. Yoo, S.J. Lee, Optimization of gelatin alginate composite bioink printability using rheological parameters: a systematic approach, Biofabrication 10 (2018), 34106, https://doi.org/10.1088/1758-5090/aacdc7.

[29] J. Karvinen, T.O. Ihalainen, M.T. Calejo, I. Jönkkäri, M. Kellomäki, Characterization of the microstructure of hydrazone crosslinked polysaccharide-based hydrogels through rheological and diffusion studies, Mater. Sci. Eng. C 94 (2019) 1056–1066, https://doi.org/10.1016/j.msec.2018.10.048.

[30] A.A. Aldana, F. Valente, R. Dilley, B. Doyle, Development of 3D bioprinted GelMA-alginate hydrogels with tunable mechanical properties, Bioprinting 21 (2021), e00105, https://doi.org/10.1016/j.bprint.2020.e00105.

[31] T. Gonzalez-Fernandez, A.J. Tenorio, K.T. Campbell, E.A. Silva, J.K. Leach, Alginate-based bioinks for 3D bioprinting and fabrication of anatomically accurate bone grafts, Tissue Eng. (2021) 1–14, https://doi.org/10.1089/ten.tea.2020.0305.

[32] Z. Xu, Z. Li, S. Jiang, K.M. Bratlie, Chemically modified gellan gum hydrogels with tunable properties for use as tissue engineering scaffolds, ACS Omega 3 (2018) 6998–7007, https://doi.org/10.1021/acsomega.8b00683.

[33] A. Ribeiro, M.M. Blokzijl, R. Levato, C.W. Visser, M. Castilho, W.E. Hennink, T. Vermonden, J. Malda, Assessing bioink shape fidelity to aid material development in 3D bioprinting, Biofabrication 10 (2018), 014102, https://doi.org/10.1088/1758-5090/aa90e2.

[34] E.A. Kiyotake, A.W. Douglas, E.E. Thomas, S.L. Nimmo, M.S. Detamore, Development and quantitative characterization of the precursor rheology of hyaluronic acid hydrogels for bioprinting, Acta Biomater. 95 (2019) 176–187, https://doi.org/10.1016/j.actbio.2019.01.041.

[35] N. Cao, X.B. Chen, D.J. Schreyer, Influence of calcium ions on cell survival and proliferation in the context of an alginate hydrogel, ISRN Chem. Eng. (2012), 516461, https://doi.org/10.5402/2012/516461.

[36] K.S. Lim, J.H. Galarraga, X. Cui, G.C.J. Lindberg, J.A. Burdick, T.B.F. Woodfield, Fundamentals and applications of photo-cross-linking in bioprinting, Chem. Rev. 120 (2020) 10662–10694, https://doi.org/10.1021/acs.chemrev.9b00812.

[37] P. Zhuang, W.L. Ng, J. An, C.K. Chua, L.P. Tan, Layer-by-layer ultraviolet assisted extrusion-based (UAE) bioprinting of hydrogel constructs with high aspect ratio for soft tissue engineering applications, PLoS One 14 (2019) 1–21, https://doi.org/10.1371/journal.pone.0216776.

[38] A. Schwab, R. Levato, M. D'Este, S. Piluso, D. Eglin, J. Malda, Printability and shape fidelity of bioinks in 3D bioprinting, Chem. Rev. 120 (2020) 11028–11055, https://doi.org/10.1021/acs.chemrev.0c00084.

[39] J. Li, D.J. Mooney, Designing hydrogels for controlled drug delivery, Nat. Rev. Mater. 1 (2016) 1–18, https://doi.org/10.1038/natrevmats.2016.71.

[40] E.R. Aurand, K.J. Lampe, K.B. Bjugstad, Defining and designing polymers and hydrogels for neural tissue engineering, Neurosci. Res. 72 (2012) 199–213, https://doi.org/10.1016/j.neures.2011.12.005.

PUBLICATION III

Sequential Cross-linking of Gallic Acid-Functionalized GelMA-Based Bioinks with Enhanced Printability for Extrusion-Based 3D Bioprinting

Jongprasitkul, H.; Turunen, S.; Parihar, V.S.; Kellomäki, M.

Biomacromolecules 2023, 24(1), 502-514.
https://doi.org/10.1021/acs.biomac.2c01418

BioMACROMOLECULES

pubs.acs.org/Biomac

Article

Sequential Cross-linking of Gallic Acid-Functionalized GelMA-Based Bioinks with Enhanced Printability for Extrusion-Based 3D Bioprinting

Hatai Jongprasitkul, Sanna Turunen, Vijay Singh Parihar,* and Minna Kellomäki

Cite This: *Biomacromolecules* 2023, 24, 502−514

Read Online

ACCESS | Metrics & More | Article Recommendations | Supporting Information

ABSTRACT: The printability of a photocross-linkable methacrylated gelatin (GelMA) bioink with an extrusion-based 3D bioprinter is highly affected by the polymer concentration and printing temperature. In this work, we developed a gallic acid (GA)-functionalized GelMA ink to improve the printability at room and physiological temperatures and to enable tissue adhesion and antioxidant properties. We introduced a sequential cross-linking approach using catechol−Fe^{3+} chelation, followed by photocross-linking. The results show that the ink formulation with 0.5% (w/v) Fe^{3+} in GelMA (30% modification) with 10% GA (GelMA30GA-5Fe) provided the optimum printability, shape fidelity, and structural integrity. The dual network inside the printed constructs significantly enhanced the viscoelastic properties. Printed cylinders were evaluated for their printing accuracy. The printed structures of GelMA30GA-5Fe provided high stability in physiological conditions over a month. In addition, the optimized ink also offered good tissue adhesion and antioxidant property. This catechol-based sequential cross-linking method could be adopted for the fabrication of other single-polymer bioinks.

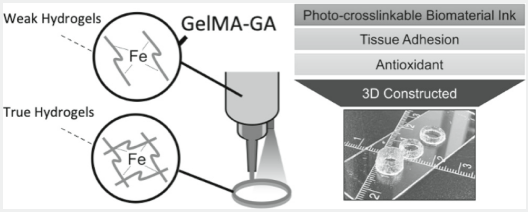

INTRODUCTION

3D bioprinting technologies are creating versatility in tissue engineering applications, such as using 3D tissue constructs as scaffolds, wound repairing, disease modeling, and organ-on-chip applications. Methacrylated gelatin (GelMA) has gained wide attention for mimicking the extracellular matrix,[1−4] as GelMA can form hydrogels under UV light in the presence of a photoinitiator. Recently, GelMA has been one of the most used choices for bioinks to build 3D constructs using additive manufacturing. GelMA-based bioinks harness excellent biological properties and tunability that are preferential for 3D cell culture, including the skin, muscle, and cartilage.[5] However, GelMA is difficult to form into complex 3D structures at room temperature (RT) or at low concentrations.[6] The printability of GelMA is highly dependent on the polymer concentration and printing temperature.[7] Therefore, more attention should be given to improving the printability and shape fidelity of GelMA bioinks because they allow the building of tissue-like constructs at high resolution.[6,8] However, enhancing GelMA's properties by increasing the concentration (>10%) leads to high cross-linking density and stiffness of the cured ink that adversely affects cell viability.[9] Furthermore, printing at low temperatures for an extended time can also induce more cold injuries to cells and can cause irreversible cell damage.[10] In addition, the cartridge, nozzle, and print-bed temperatures are not easily kept steady, which can lead to discontinuous extrusion. The most common way to improve GelMA's printability is to incorporate other polymers, such as hyaluronic acid, alginate, gellan gum, chitosan, or synthetic polymers, to reinforce the hydrogel network.[9,11] On the other hand, combining the bioink with other materials is not always ideal. It can cause unnecessary complexity and increase bioink's preparation time, as reported in several publications studying single-component bioinks.[12] In recent years, several stand-alone bioinks, formed with different chemical modifications and cross-linking techniques, have been explored to maximize the printability in extrusion-based 3D bioprinting.[13] Dopamine-functionalized biopolymers and catechol-based biomaterials have been extensively explored as they mimic mussel adhesive protein that provides adhesion on wet tissue surfaces.[14−16] It is noteworthy to mention that the hydrogel-based scaffolds with tissue adhesive properties help in the integration with surrounding tissue surfaces.

Gallic acid (GA) is a polyhydroxy aromatic compound with three phenol units, which are well known as catechol moieties. GA is also recognized for its tissue adhesive properties and antioxidant activity.[17] However, according to our own findings,

Received: November 28, 2022
Revised: December 12, 2022
Published: December 22, 2022

https://doi.org/10.1021/acs.biomac.2c01418
Biomacromolecules 2023, 24, 502−514

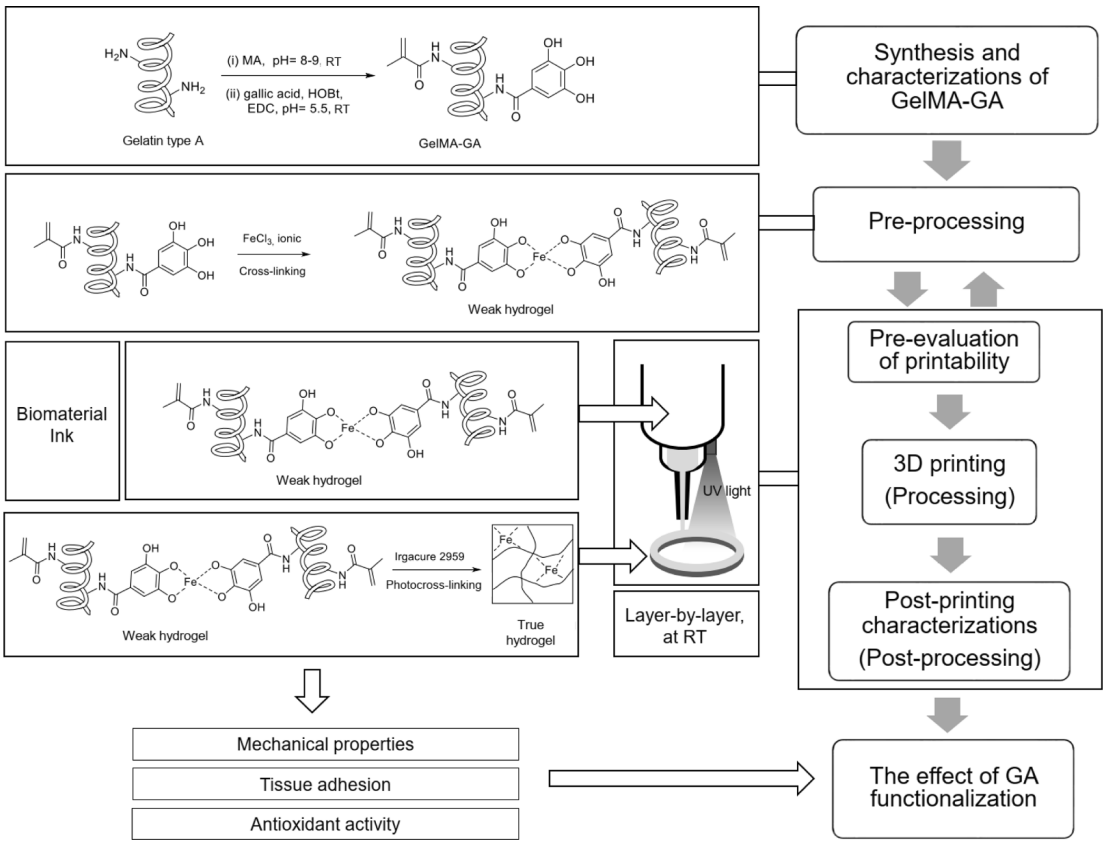

Figure 1. This schematic contains the set of biomaterial ink characterizations. (1) Synthesis and characterization of GelMAGA biomaterial inks, (2) preprocessing: optimization of different ink formulations, influenced by catechol−Fe^{3+} chelation, (3) pre-evaluation of printability in terms of Pr value and stackability, (4) processing: 3D printing and photocross-linking, (5) post-printing characterizations: 3D printing accuracy and structural integrity, and (6) the effect of GA functionalization: tissue adhesive, antioxidant, and mechanical properties. Weak hydrogels = viscous enough to be extrudable. True hydrogels = mechanically stable enough to maintain the structural integrity after printing.[24]

GA alone could not improve the rheological behavior of the GelMA ink as the printability of GelMA and GA-functionalized GelMA (GelMAGA) appears similar. Catechol-functionalized polymers with metal ions have been proven to have rapid network formation, pH-tunable cross-linking, and self-healing activity.[15,18] The concentration of metal ions and pH can be used to precisely control the polymer network and their rheological properties.[16] However, only a few studies have reported the application of GA−metal ion coordination chemistry to obtain printable biomaterial inks.[17,19−21]

In this work, we functionalized gelatin with methacrylate (MA) and GA to create printable biomaterial inks by modulating the viscosity of the precursor using catechol/iron complexation. We hypothesized that the addition of a pre-cross-linker into a low-concentration GelMAGA could improve the printability and initial shape fidelity at RT/physiological temperature. Therefore, we propose a sequential cross-linking strategy by introducing two types of cross-linking techniques: catechol−Fe^{3+} chelation, followed by photocross-linking. The interactions between a gallate-tethered cationic polymer and metal ions resulted in shear-thinning behavior.[18,21] The optimization was done by pre-cross-linking GelMAGA (5% w/v) with iron(III) chloride ($FeCl_3$) with varying concentrations of $FeCl_3$ (0.25, 0.5, and 1% w/v) to create a weak extrudable hydrogel. The pre-cross-linking strategies have been widely used in alginate and gellan gum-based bioinks.[22,23] Moreover, GA (10% degree of modification)-functionalized GelMA can enhance tissue adhesion and offer antioxidant properties. Our study contains a set of biomaterial ink characterizations, as shown in Figure 1: (1) synthesis of biomaterial inks, (2) pre-processing, (3) pre-evaluation, (4) processing (3D printing), (5) post-printing characterizations, and (6) the effect of additional functionalization (tissue adhesive, antioxidant, and mechanical properties). In the pre-processing phase, the rheology of the ink formulations (GelMAGA and $FeCl_3$) was measured, and a fiber formation test was performed to optimize the ink composition before printing. A printable set of inks were obtained with appropriate viscosity and rheological profiles. The pre-evaluation method was applied to further assess the printability of pre-cross-linked hydrogels with respect to the geometry of the printed constructs. In the processing step, layer-by-layer UV photo-cross-linking was used after printing to ensure the shape fidelity of the 3D constructs. In post-printing characterizations, the

https://doi.org/10.1021/acs.biomac.2c01418
Biomacromolecules 2023, 24, 502−514

Table 1. Biomaterial Ink Compositions with Various Modification Degrees of Methacrylate and GA and Fiber Quality[a]

formula	degree of methacrylation [%]	degree of GA modification [%]	$FeCl_3$[% w/v]	fiber quality
GelMA30 (RT)	30	0	0	droplet
GelMA60 (RT)	60	0	0	droplet
GelMA30GA (RT)	30	10	0	droplet
GelMA60GA (RT)	60	10	0	droplet
GelMA30GA-2.5Fe (RT)	30	10	0.25	discontinuous fiber
GelMA60GA-2.5Fe (RT)	60	10	0.25	discontinuous fiber
GelMA30GA-5Fe (RT)	30	10	0.5	continuous fiber
GelMA30GA-5Fe (37 °C)	30	10	0.5	continuous fiber
GelMA60GA-5Fe (RT)	60	10	0.5	discontinuous fiber

[a]GelMA = gelatin methacrylate; GelMAGA = gelatin methacrylate functionalized with GA; GelMAGA-Fe = Fe^{3+} pre-cross-linked gelatin methacrylate functionalized with GA.

accuracy of printed constructs was measured. Long-term stability of the printed structures was observed in the incubated environment (swelling and dissolution test). The effect of grafting the GA onto GelMA was evaluated by oscillatory measurement (mechanical properties), tack test (tissue adhesion), and antioxidant activity.

■ MATERIALS AND METHODS

Materials. Gelatin type A (300 bloom strength, porcine skin), methacrylic anhydride, GA (3,4,5-trihydroxybenzoic acid), 1-ethyl-3-(3-dimethylaminopropyl)-carbodiimide hydrochloride (EDC), 1-hydroxybenzotriazole hydrate (HOBt), glycine, trinitrobenzene sulfonic acid (TNBS), $FeCl_3$, and Irgacure 2959 (I2959) were purchased from Merck KGaA, Darmstadt, Germany. A dialysis membrane with a molecular weight cutoff (MWCO) of 14 kDa was purchased from Spectra/Por, Repligen Corp., USA. DI water (deionized water, Miele Aqua Purificator G 7795, Siemens) and u.p. water (ultra-pure, Sartorius Arium Mini, 0.055 μS/cm) were used. Dulbecco's phosphate-buffered saline (DPBS) was prepared in the laboratory. All solvents were of analytical quality.

Synthesis of Biomaterial Inks (GelMA and GelMAGA). GelMAGA was synthesized using a two-step reaction. GelMA batches with 30 and 60% degrees of methacrylation were synthesized as previously described[3,7] *via* nucleophilic reaction of residual amine on gelatin molecules and methacrylic anhydride. Briefly, 10% w/v of gelatin type A was dissolved in DPBS under the basic conditions (pH 9) at 60 °C. Next, methacrylic anhydride was added dropwise, and the degree of functionalization was controlled by varying the ratio of gelatin and methacrylic anhydride in each modification. The pH was maintained at 9 after each addition of methacrylic anhydride. The reaction was carried out at 50 °C for 3 h. After completion, the reaction mixture was dialyzed with a 14 kDa MWCO membrane at 40 °C against DI water for 72 h (water was changed twice daily). GelMA was then lyophilized and stored at 4 °C. The degree of methacrylation was confirmed using UV-spectral measurement (Shimadzu UV-3600 plus UV−vis−NIR spectrophotometer).[3,25] After that, GelMA30 and GelMA60 were functionalized with GA using the protocol reported previously.[26] GelMAGA was synthesized *via* a carbodiimide coupling reaction using EDC. HOBt was added (1 equiv) with respect to GelMA. The degree of GA functionalization was controlled using EDC (0.2 equiv). The reaction was let to proceed for 4 h (pH 5). The unreacted GA and EDC were removed by dialysis (MWCO = 3500 Da, regenerated cellulose membrane) in 1 M NaCl (pH 5.3) at 4 °C for 3 days, followed by dialysis against DI water for 24 h. At last, the solution was freeze-dried. The degree of GA was characterized by UV spectra. The calculation of the number of free amine groups in gelatin type A, GelMA, and GelMAGA was done using the calibration curve of the glycine standard[27] (Figure S1).

Preparation of Biomaterial Ink Formulations. GelMA and GelMAGA inks were dissolved at 5% w/v in a photoinitiator solution at 40 °C (Irgacure 2959, 0.5% w/v in DPBS) and stirred for 2 h until they were completely homogeneous. The pH was tuned to 7.5 to gain proper viscosity. The studied biomaterial ink formulations were GelMA, GelMAGA, and GelMAGA with a pre-cross-linker ($FeCl_3$). Gelatin methacrylate with 30 and 60% degrees of modifications was named GelMA30 and GelMA60, respectively. GelMA30 and GelMA60 functionalized with GA were termed GelMA30GA and GelMA60GA, respectively. GelMA30GA and GelMA60GA with $FeCl_3$ were GelMA30GA-xFe and GelMA60GA-xFe, respectively, where x indicated the concentration of $FeCl_3$ (2.5 is 0.25% and 5 is 0.5% w/v). All the formulations are listed in Table 1.

Prescreening and Flow Behavior of Biomaterial Inks. Biomaterial inks were evaluated using the pre-processing method: formulation of inks, fiber formation, and rheological measurements to prescreen the printability without loading the ink into the 3D bioprinter. We followed the simple prescreening protocols published previously:[22] filament formation and stackability test. The biomaterial inks with different formulations (Table 1) were loaded into a 10 mL cartridge and capped with a tapered UV-shielded nozzle (200 μm in diameter, Nordson EFD, Germany). The ink filament was formed in the air at RT (24 °C) and at 37 °C by an automatic dispenser, and a video was recorded simultaneously with a camera. The ink compositions were chosen based on filament characteristics. The filament was deposited on the glass surface to investigate the stackability.

The flow behavior of different ink formulations was evaluated by a rotational rheometer (Discovery HR-2, TA Instruments Inc., USA) with a plate−plate geometry (12 mm in diameter, a gap size of 2.5 mm). The measurements were recorded at RT. The rheological tests performed were temperature ramp (viscosity−temperature), *in situ* photo-polymerization (gelation time), shear-thinning (viscosity−shear rate), yield stress, and recovery behavior. The temperature-dependent behavior was measured with a temperature sweep varying from 40 to 4 °C at the rate of 2 °C/min. The gelation times of the inks were determined *via in situ* photo-polymerization using a rheometer with an external UV source (BlueWave 50 UV curing spot lamp, DYMAX Corp., USA). The UV intensity was measured using a power meter console (PM100USB, Thorlabs Inc., USA) coupled with an S310C thermal sensor. The estimation of UV light intensity as a function of the distance from the light source is described in Figure S2. Viscoelasticity was measured using oscillatory mode at RT as a function of time (500 s, a UV lamp at a wavelength of 365 nm and 25 mW/cm^2 in UV intensity, UV light was activated at 100 s), while strain and frequency were kept constant at 1% and 1 Hz, respectively. The shear-thinning properties of the inks were also determined in flow mode, with the shear rate varying from 0.01 to 800 s^{-1}. The shear-thinning coefficients and yield stress values were determined from the linear region of the graph using eqs 1 and 2, respectively. Shear-thinning coefficients were calculated using the power law, eq 1.

$$\mu = K\gamma^{n-1} \tag{1}$$

The flow behavior index n describes the shear-thinning ability of the ink. If $n = 1$, the ink follows Newtonian behavior. If $n > 0.6$, the material is weakly shear-thinning and if $n \leq 0.2$, the ink has good shear-thinning properties and excellent printability.

https://doi.org/10.1021/acs.biomac.2c01418
Biomacromolecules 2023, 24, 502−514

Yield stress values were determined from the yield stress−shear rate plot, where the shear stress begins to increase from the intersection at the *Y*-axis, using the Herschel−Bulkley model (eq 2).

$$\tau = \tau_0 + K\gamma^n \tag{2}$$

where τ is the shear stress measured on the inks and τ_0 is the yield stress. The yield point determines the flow initiation of the inks at the level of the applied shear stress.

The recovery behavior test (thixotropy) is to characterize the bioink's ability to recover its viscosity after a high shear rate has been applied. The measurements were performed at a low shear rate (0.01 s^{-1} for 200 s) to simulate at-rest conditions before extrusion, followed by a high shear rate (500 s^{-1} for 100 s) to mimic shear forces in the nozzle tip during extrusion, and finally a low shear rate (0.01 s^{-1} for 200 s) to simulate bioink recovery after extrusion.

Pre-Evaluation of Printability. After obtaining the best printable biomaterial ink formulation and optimal printing parameters, we assessed the structural integrity. The shape and stackability of the printed filament are the first parameters that can ensure a successful printing process and yield high printing resolution. Thus, the true printability was quantified by semi-quantitative measurement from the shape of the printed structures. Prescreened biomaterial ink formulations were loaded into a 10 mL cartridge (Optimum syringe barrels, Nordson EFD, USA) and transferred in an incubator (37 °C) for 30 min to remove any air bubbles. Next, the cartridge was installed into a multi-material 3D bioprinting platform (Brinter One, Brinter Ltd., Finland) by capping it with a 200 μm plastic UV-shielded tapered nozzle (SmoothFlow, Nordson EFD, USA). A pneumatically operated Pneuma Tool printhead was used for printing. The printing pressure was set according to the prescreening test results. Printing speed and printhead temperature were kept constant at 8 mm/s and RT, respectively. 3D constructs were printed using the layer-by-layer deposition approach, followed by photocross-linking to stabilize the structure (an integrated UV/vis LED module was used at a wavelength of 365 nm with 25 mW/cm^2 intensity for 10 s for each layer and 60 s for the post-curing process).

As previously described,[22] the printability assessment of different biomaterial ink compositions was done by printing two-layered grid patterns. The shape of the printed pores is evaluated using eq 3.

$$\mathrm{Pr} = \frac{\pi}{4}\cdot\frac{1}{C} = \frac{L^2}{16A} \tag{3}$$

in which C is the circularity of the enclosed pore, L is the perimeter, and A is the pore area. The printability (Pr) of the biomaterial ink compositions was determined by the squareness of the pores inside the grid structure. The Pr value of 1 indicates a perfect square shape. A computer-aided design (CAD) model for the square grids (20 × 20 × 0.4 mm^3) was drawn with Autodesk Fusion 360 software and used as a standard for this assessment.

3D Printing. 3D printed cylinders were used to evaluate the ability of the inks to support the weight of each layer while maintaining the printing resolution. We chose poloxamer (40% w/v, Kolliphor P 407, BASF Corp., USA) as a control printing material. It gave high geometric accuracy with minimal deviation compared to the CAD model. The prescreened ink was printed into cylinders (10 mm in outer diameter) with different heights (1.5, 2.5, and 5 mm). Each structure was cured in a layer-by-layer fashion using the bioprinter's integrated UV/vis LED module at a wavelength of 365 nm with 25 mW/cm^2 intensity for 10 s for each layer and 60 s for the post-curing process. The dimensions of the cylinders were measured from photos with ImageJ and compared with the printed control structure to determine the printing accuracy. The filaments of the prescreened inks and the control material were observed with a contact angle camera (Theta Lite, CMOS 1/2″ USB 3.0 digital camera with fixed zoom, a resolution of 1280 × 1024 pixels, Biolin Scientific, Sweden) to measure the width of the filaments (OneAttension v2.1).

Tissue Adhesion Test. To observe the impact of GA on the adhesive properties of the ink, a tack test was performed for GelMA and GelMAGA using a rotational rheometer at RT. Chicken skins and porcine muscles (freshly purchased from the market) were harvested and glued to the 12 mm geometry, and the inks were placed on the bottom of the plate.[14,28] After that, the geometry with animal tissue attached was moved in contact with the inks with a constant compressive force (0.1 N) for 120 s to establish a uniform molecular contact between the tissue and the ink. Subsequently, the inks were *in situ* photopolymerized with a UV lamp for 120 s. Thereafter, the geometry was pulled up at a constant velocity of 20 μm/s to record the change in axial force as a function of time. A graph was then plotted to observe the influence of GA in GelMA on adhesive properties. The harvested tissue was kept moist during the measurement.

Antioxidant Activity. A 2,2-diphenylpicrylhydrazyl (DPPH) radical scavenging assay was used as a preliminary assessment of the changes in the antioxidant properties upon modification of GelMA with GA. The free radical scavenging activity of GelMAGA was evaluated using the DPPH method.[17,29] GelMAGA was dissolved in DI water at 2 mg/1 mL concentration, followed by 1 mL of DPPH solution (1 mg/12 mL in methanol). After incubation at 25 °C for 30 min, the absorbance of the resulting solution was measured at 517 nm using a UV−vis spectrophotometer. The DPPH scavenging activity (%) is calculated from eq 4.

$$\text{DPPH scavenging activity (\%)} = \frac{A_1}{A_2} \times 100 \tag{4}$$

where A_1 is the absorbance of blank DPPH solution that was used under the same reaction conditions in the absence of synthesized polymers and A_2 is the absorbance of DPPH solution in the presence of polymer samples.

Viscoelastic Properties. To determine the effect of GA functionalization on mechanical properties, the oscillatory measurements were carried out in the linear viscoelastic region using an amplitude sweep (0.1−100% strain range and at a constant frequency of 1 Hz) and a frequency sweep (a frequency range of 0.1−100 Hz and at a constant strain of 1%). The biomaterial inks were cast in the molds (2.5 mm height, diameter of 12 mm) and were exposed to 365 nm UV light (25 mW/cm^2) for 120 s. Each sample was placed between the 12 mm geometry and the platform with a gap size of 2.5 mm. Storage modulus (G') and loss modulus (G'') were obtained from the slopes. After that, tan δ was calculated from G' and G'' to determine the viscoelastic properties and plotted as a tan δ−strain curve.

For further in-depth structural analysis, the average mesh size and cross-linking density were determined from oscillatory measurement results.[30] The average mesh size (ξ, nm) calculation was applied using the storage moduli (G') of resulting hydrogels (the best formulation ink) at 120 s UV exposure time. Equation 5 estimates the average mesh size (ξ) of hydrogels at different exposure times

$$(\xi) = \left(\frac{G'N}{RT}\right)^{-1/3} \tag{5}$$

where G' is the storage modulus of the hydrogel, N is the Avogadro constant (6.023 × 10^{23} mol^{-1}), R is the molar gas constant (8.314 J K^{-1} mol^{-1}), and T is the temperature (298 K).

Moreover, cross-linking density (n_e, mol/m^3) of the hydrogels was calculated using the storage modulus from the linear region of the frequency sweep test. The data provided the total number of elastically active junction points in the network per unit of volume using eq 6.[30]

$$n_e = \frac{G_e}{RT} \tag{6}$$

where G_e is the average value of storage modulus from the linear region of oscillatory frequency sweep measurement.

Stability Study. The chosen biomaterial ink was printed into 3D grid structures (10 × 10 × 5 mm^3). Subsequently, an extra photocross-linking method was applied to the printed structures to gain an additional stability during the incubation.[11] Briefly, the printed structures were immersed in DPBS containing 0.05% of

https://doi.org/10.1021/acs.biomac.2c01418
Biomacromolecules 2023, 24, 502−514

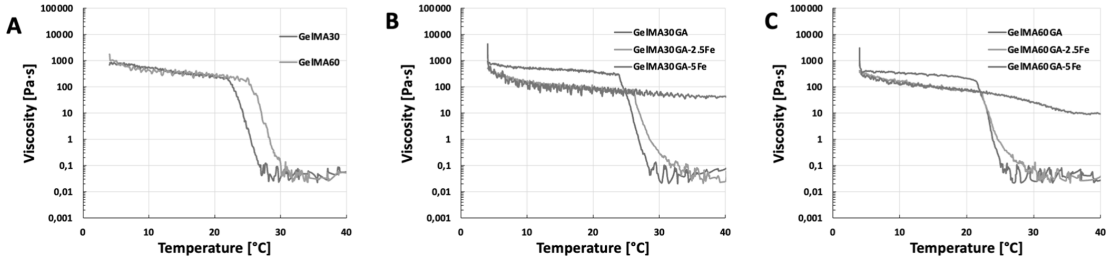

Figure 2. Rheological measurement of viscosity as a function of temperature. All samples were measured over the temperature range from 4 to 40 °C. (A) GelMA with 30 and 60% degrees of methacrylation, (B) GelMA30GA group with/without Fe^{3+}, and (C) GelMA60GA group with/without Fe^{3+}.

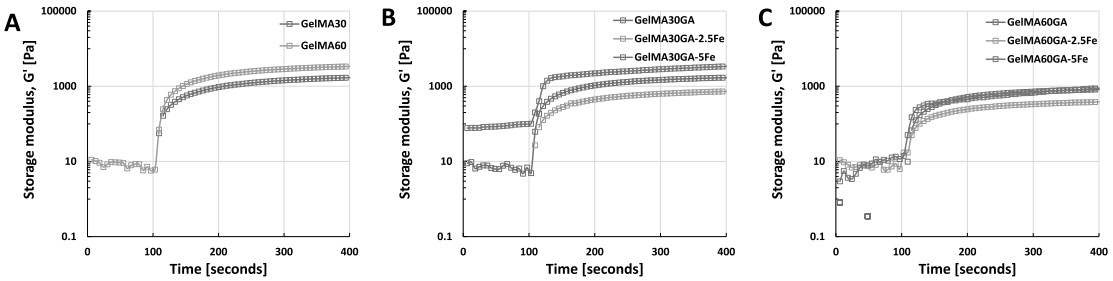

Figure 3. *In situ* photo-polymerization test to observe the gelation time of each ink formulation (time sweep of oscillatory measurement, 25 mW/cm^2 for 300 s, at RT). (A) Pure GelMA30 and GelMA60, (B) GelMA30GA group with/without Fe^{3+}, and (C) GelMA60GA group with/without Fe^{3+}.

Irgacure 2959 and exposed to UV light (10 mW/cm^2) for 5 min. Post-stabilization, the printed samples were immersed in the solution (DI water, DPBS, or DMEM) at 37 °C. The structures were weighed at time points 0, 1, 2, 3, 5, 7, 15, and 30 d. At the zero time point, the samples were defined with a weight of W_0. At every time point, the samples were removed from the solution and the excess solution from the surface was removed to obtain the W_s. The swelling ratio was calculated as W_s/W_0.

Statistical Analysis. The results of oscillatory measurements were presented as mean ± standard deviation (SD). The analysis was performed using Student's *t*-test to determine the differences between groups, and the significance was defined at $p < 0.05$.

■ RESULTS

Characterizations of Synthesized Biomaterial Inks. The biomaterial inks were synthesized with various modification degrees, as listed in Table 1. The degree of methacrylation of GelMA30 and GelMA60 was obtained as ∼31 ± 5% (∼0.09 mmol/g) and ∼64 ± 5% (∼0.18 mmol/g) (batch-to-batch variations), confirmed by the TNBSA assay (Figure S3). The degree of GA modification on GelMA was quantified using UV/vis absorption measurements (GA ∼10% or ∼0.03 mmol/g) (Figure S3). The degree of methacrylation and GA modification were calculated based on the measurements of free amines in modified gelatin with respect to unmodified gelatin, as shown in Table S1. The pH dependency of GA further confirmed the conjugation.[26] GelMAGA solution turned brown at the basic condition (∼pH 8), indicating that GA functionalization was successful in the GelMA backbone (Figure S4).

Prescreening of Bioink Formulations. The concentrations of biomaterial inks were set to 5% w/v in DPBS (0.5% w/v I2959). To obtain the high printability and stability at RT, pre-cross-linker $FeCl_3$ was applied to GelMAGA using various concentrations. The biomaterial inks and the fiber quality were assessed as a function of methacrylation in GelMAGA and $FeCl_3$ concentration, as shown in Table 1. The fiber quality was assessed from the fiber formation ability of the inks after being extruded from the nozzle. From Table 1, GelMA30, GelMA60, GelMA30GA, and GelMA60GA (5% w/v) at RT were extruded as droplets. GelMA30GA-2.5Fe and GelMA60-2.5GA could not form stable enough fiber during the extrusion at RT, as they hardly formed a continuous fiber. At RT and at 37 °C, GelMA30GA-5Fe produced approximately 5 cm long coherent filaments. However, GelMA60-5Fe produced irregular and discontinuous fiber. We also tuned the concentration of Fe^{3+} into 1% w/v in both GelMA30GA and GelMA60GA, but the inks were too gelated and clogged the nozzle.

Flow Behavior of Biomaterial Inks. To further deepen the study of the ink properties, the flow behavior of the inks was measured in terms of viscosity as a function of temperature. Figure 2A−C presents the temperature dependence of viscosity between 4 and 40 °C. The viscosity of GelMA (Figure 2A) and GelMAGA (Figure 2B,C, blue and orange curves) without (or with 2.5Fe) additional cross-linker ($FeCl_3$) decreased significantly after 25 °C, whereas GelMA30GA-5Fe and GelMA60GA-5Fe (Figure 2B,C, green curve) had steady viscosity levels, which only slowly fell after reaching 30 °C.

In situ photo-polymerization (Figure 3A−C) shows the gelation time of all ink formulations (storage modulus as a function of time). All inks showed an increase in storage modulus right after being exposed to UV light and reached the maximum cross-linking degree after 60 s. The gelation time and storage moduli of GA-functionalized GelMA did not differ from the pure GelMA. However, $FeCl_3$ in GelMAGA required

https://doi.org/10.1021/acs.biomac.2c01418
Biomacromolecules 2023, 24, 502−514

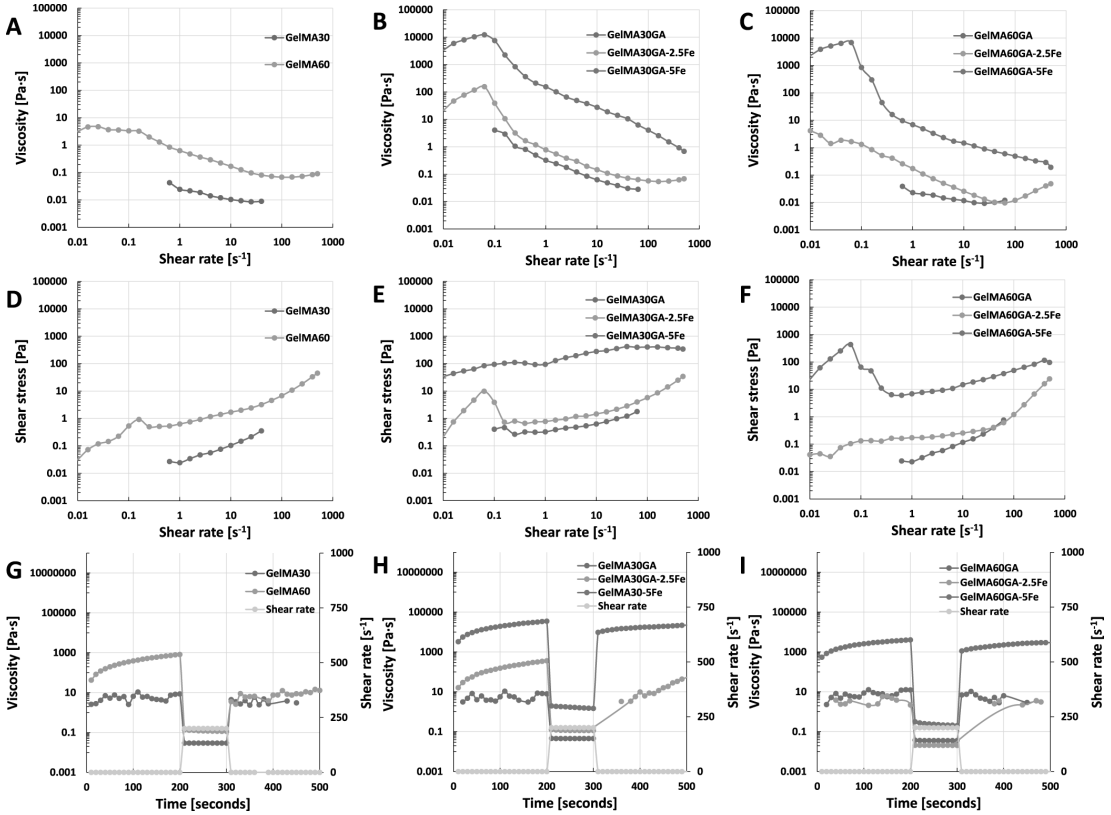

Figure 4. Rheological measurements in the flow mode: shear-thinning (A−C), yield stress (D−F), and recovery behavior (G−I) at RT. (A,D,G) Pure GelMA30 and GelMA60, (B,E,H) GelMA30GA group with/without Fe^{3+}, and (C,F,I) GelMA60GA group with/without Fe^{3+}.

more than 60 s before the storage modulus reached the plateau.

Figure 4A−I presents the flow curve, shear-thinning, and recovery behavior of different ink formulations at 37 °C. All the ink formulations provided $n < 1$, which proves shear-thinning behavior. In detail, it was observed that GelMA30 and GelMA60 at RT have a weak shear-thinning ability because of low viscosity and low yield stress (Figure 4A,D,G). Shear-thinning coefficients of $n > 0.6$ also confirmed the results, and the prescreened results also showed droplet formation as the material was extruded out from the nozzle.

However, GA functionalization alone could not improve the shear-thinning behavior of the inks and showed almost similar results to GelMA (Figure 4, blue curves). The addition of 0.25 or 0.5% w/v of $FeCl_3$ in GelMA30GA and GelMA60GA significantly improved viscosity, shear-thinning, yield stress, and recovery behavior. GelMA30GA-5Fe and GelMA60GA-5Fe had more obvious shear-thinning ability than GelMA30-GA-2.5Fe and GelMA60GA-2.5Fe, as shown in Table 2. In addition, in Figure 4H,I and Table 2, GelMA30GA-5Fe and GelMA60GA-5Fe rapidly recovered back their viscosity (∼73 and 72% recovery) after removing the high shear rate. In comparison, 0.25% w/v $FeCl_3$ inks could not recover their viscosity and permanently lost their properties (Figure 4B,C,E,F,H,I, orange curves). According to the curves (Figure 4C,F, green curves), the viscosity of GelMA60GA-5Fe had a sharp drop with an increasing shear rate (0.1 s^{-1}), which correlates with the irregular shape of the extruded filaments.

Table 2. Flow Behavior of Each Ink Formulation: Viscosity, Shear-Thinning Coefficients, Yield Stress, and Recovery Rate during the Extrusion

compositions	n	viscosity [Pa·s]	K	τ_0 [Pa]	recovery rate [%]
GelMA30	0.82	1.22	0.01	0.04	
GelMA60	0.41	4.62	0.73	0.07	
GelMA30GA	0.28	4.05	0.43	0.08	
GelMA60GA	0.92	0.05	0.01	0.02	
GelMA30GA-2.5Fe	0.42	76	0.80	0.74	
GelMA60GA-2.5Fe	0.26	4.16	0.16	0.04	
GelMA30GA-5Fe	0.03	7940	276	83	∼73
GelMA60GA-5Fe	0.23	6371	21	21	∼72

Pre-Evaluation of Printability. As shown in Figure 5, the prescreened inks, GelMA30GA-5Fe and GelMA60GA-5Fe, were printed into grid structures at RT. In addition, GelMA30GA-5Fe was also printed at 37 °C. GelMA60GA-5Fe was extruded as small fragments formed from the cross-linked hydrogel, resulting in random-sized filaments when fabricating multiple stacked layers. GelMA30GA-5Fe was fabricated with high resolution when printed into two or six layers. At the elevated temperature, the geometry of the grids

https://doi.org/10.1021/acs.biomac.2c01418
Biomacromolecules 2023, 24, 502−514

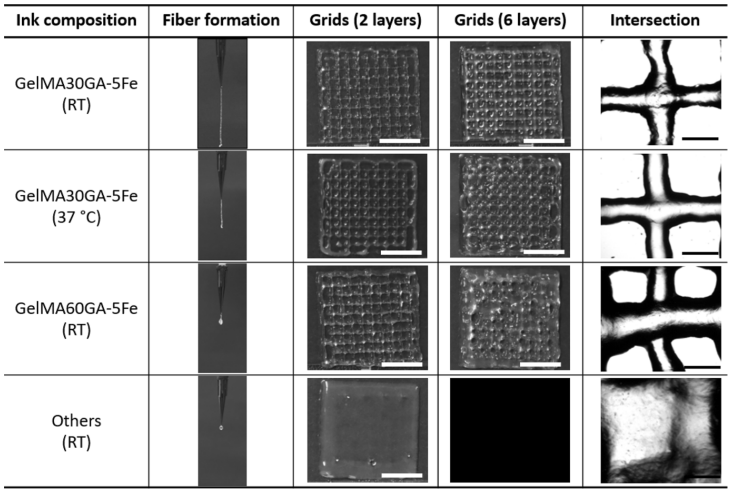

Figure 5. Prescreening of biomaterial inks: fiber formation, two-layered and six-layered printed grids, and close-up of filament intersections. Scale bar = 10 mm (white), 1 mm (black).

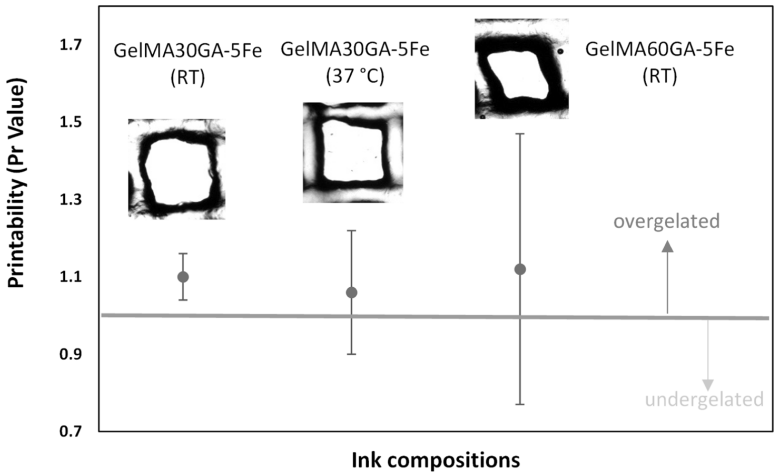

Figure 6. Calculated Pr values for the determination of the actual printability of GelMA30GA-5Fe at RT, GelMA30GA-5Fe at 37 °C, and GelMA60GA-5Fe at RT. The green line indicates the perfect printability value of 1. The Pr values are represented as mean ± standard deviation (n = 20).

and filaments was not constant; instead, multilayered constructs started to collapse. The images of filament intersections showed that all pre-screened inks were able to stack without merging. The printability (Pr value) was calculated from the pore geometry inside the grids. Figure 6 shows that the average Pr values of all inks were close to each other (Pr = 1.1), had irregular shapes, and fell into the over-gelation area of the graph. However, the standard deviation values increased when the methacrylate modification was higher, supported by the filament formation data and the printing results. Also, the temperature-responsive behavior of GelMA resulted in irregularly shaped multilayered constructs (Figure 5, GelMA30GA-5Fe at 37 °C).

3D Printed Structures. The CAD models of cylinders had a wall height of 1.5, 2.5, or 5 mm and consisted of 9, 16, or 33 layers. The dimensions of GelMA30-5Fe printed structures, including outer diameters and heights (Figure 7A,B), were measured and compared to printed Poloxamer to calculate the printing accuracy. All outer diameters of cylinders were consistent across all the structures (10.1−10.3 mm compared to 10 mm of the CAD model), except for the 5 mm GelMA30GA-5Fe cylinder, which has a measured height of 11 mm. In Figure 7C, the CA camera images show that the filament width of Poloxamer was close to the nozzle orifice, which was 0.2 mm. The filament width of GelMA30GA-5Fe swelled after being extruded (0.45 mm), resulting in higher cylinders. The shape fidelity of the 3D construct was confirmed by further characterization of filament shapes. The printed cylinders from three ink types, Poloxamer (RT), GelMA30GA-5Fe (RT), and GelMA60 (16 °C), were observed to confirm

https://doi.org/10.1021/acs.biomac.2c01418
Biomacromolecules 2023, 24, 502−514

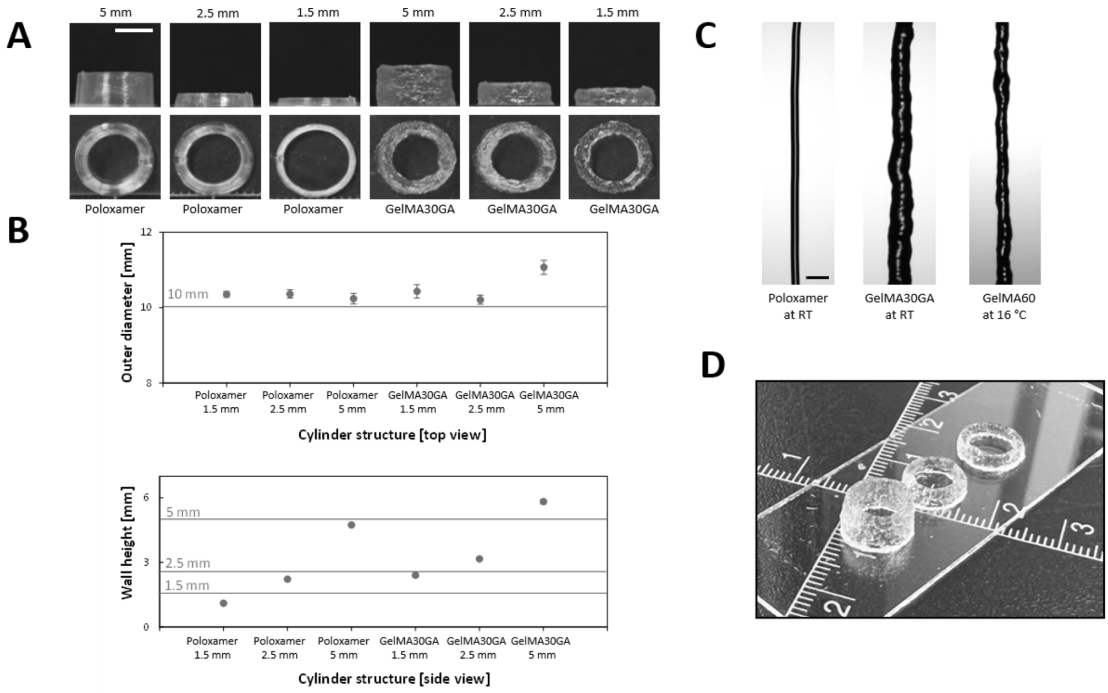

Figure 7. 3D printed structures of GelMA30GA-5Fe ink and control material (poloxamer). (A) Top and side views of printed structures with 1.5, 2.5, and 5 mm wall heights (theoretical heights from CAD models). Scale bar = 5 mm (white). (B) Measured outer diameters and wall heights of cylinders compared to the heights from the CAD model (red lines). (C) Extruded filaments to observe filament widths of poloxamer at RT, GelMA30GA-5Fe at RT, and 5% w/v GelMA60 at 16 °C. Scale bar = 0.5 mm (black). (D) Examples of printed cylinders of GelMA30GA-5Fe. The ruler scale is in centimeter.

the printed structure resolution. The comparison of the top and side views of the structures showed that GelMA30GA-5Fe was able to maintain good shape fidelity and enabled the printing of multilayered 3D constructs (Figure 7A). Figure 7D illustrates the overview of all printed cylinders.

Viscoelastic Properties. The oscillatory measurement data demonstrated that the addition of GA in GelMA30 led to a significant increase in the storage modulus values, but no such increase was observed for GelMA60 versus GelMA60GA (Figure 8A). The inks with $FeCl_3$ yielded a significantly higher storage modulus compared to the samples without GA and $FeCl_3$. Figure 8B shows that dual cross-linking using photocross-linking with $FeCl_3$ resulted in higher elasticity than photocross-linking GelMA and GelMAGA without $FeCl_3$. At low strain (1%), all samples displayed higher storage modulus and with increasing strain (100%), the storage modulus was reduced, while the loss modulus increased. The results were supported by the tan δ value, which is the ratio between G' and G'' in Table 3. The tan δ value gave values significantly lower than 1. The tan δ value of GelMA30GA-5Fe and GelMA60GA-5Fe slowly increased after 10% strain compared to GelMA and GelMAGA (<5% strain), indicating that the gels were highly elastic. The average mesh sizes (ξ) and cross-linking densities (n_e) were calculated using eqs 4 and 5 and are shown in Table 3. GA-functionalized GelMA hydrogels had higher cross-linking density, which led to stiffer hydrogels and smaller average mesh size. On the other hand, GelMA60 and GelMA60GA did not show a significant improvement in G', resulting in an insignificant difference in the cross-linking densities and average mesh sizes ($p > 0.05$). In comparison to all other ink formulations, GelMAGA with $FeCl_3$ had a significantly smaller average mesh size due to the higher values of G' and cross-linking densities ($p < 0.05$).

Stability Test: Swelling Behavior and Dissolution Test. The results of the stability test of the printed constructs, including swelling behavior in water and dissolution test in DPBS and DMEM, are presented in Figure 9. GelMAGA showed rapid initial swelling in water during the first 3 days (swelling ratio 1.51 ± 0.03), followed by slow degradation after the following days, but ultimately it remained stable for 1 month (swelling ratio 1.24 ± 0.22). In addition, the samples in DMEM absorbed a small amount of buffer and remained stable with swelling ratios of 1.05 ± 0.05 and 0.93 ± 0.03, respectively. However, the hydrogel in DPBS dissolved over a period of 7 days (swelling ratio 0.95 ± 0.05) and remained stable until the end of the observation.

Tissue Adhesive Properties. A tack test was performed to investigate the tissue adhesive properties of different inks using the chicken skin and porcine muscle. Both GelMA and GelMAGA showed tissue adhesive properties (Figure S5). However, GA-modified GelMA required greater pull-up force from the *in situ* photocross-linked hydrogels (higher negative force) than GelMA.

Antioxidant Properties. The DPPH reagent underwent a visual change in color from deep purple to deep orange in GelMA30GA and GelMA60GA because of the antioxidant

https://doi.org/10.1021/acs.biomac.2c01418
Biomacromolecules 2023, 24, 502−514

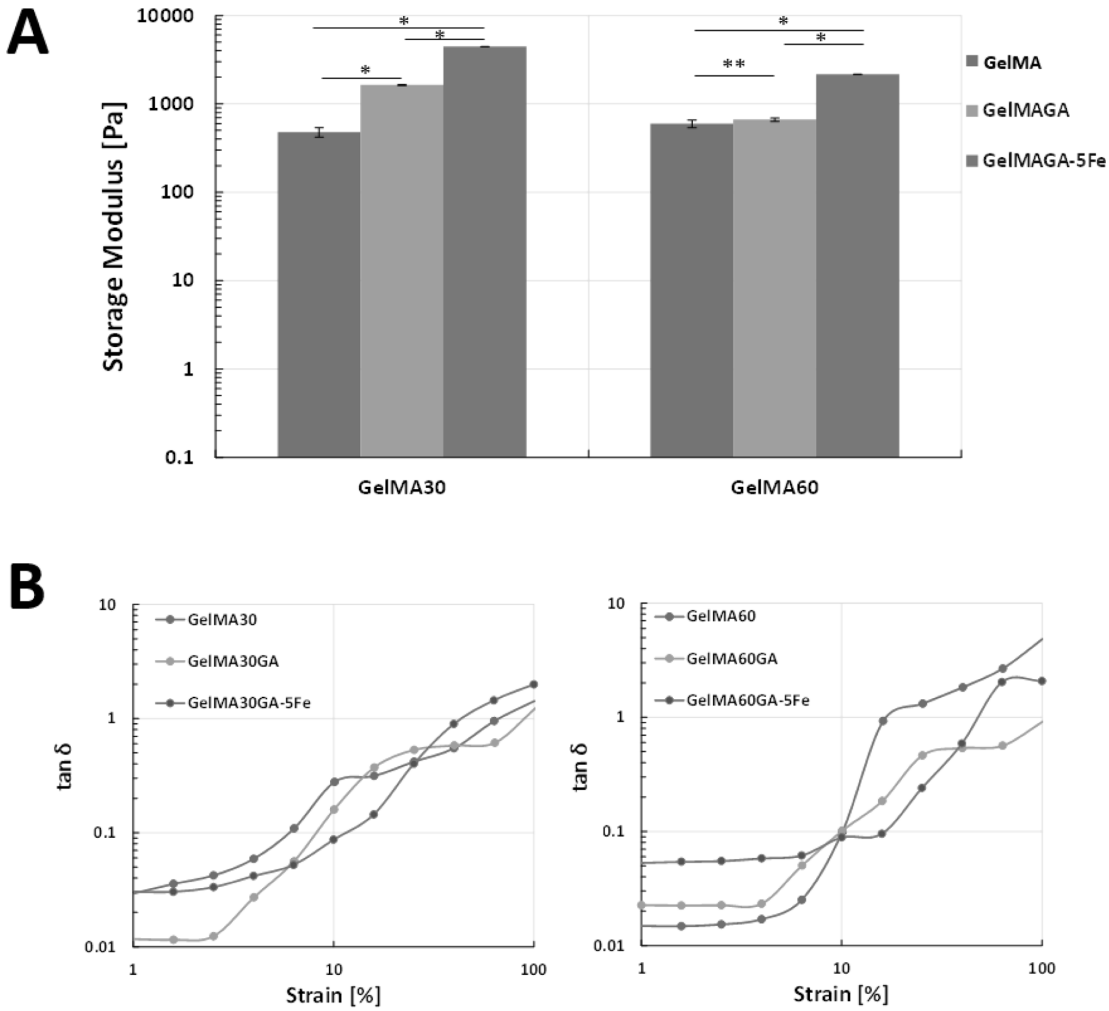

Figure 8. Oscillatory measurements of all hydrogel samples: GelMA30, GelMA60, GelMA30GA, GelMA60GA, GelMA30GA-5Fe, and GelMA60GA-5Fe, measured *via* frequency and amplitude sweeps at RT. The error bars indicate the standard deviation of storage modulus for each ink, presented as mean ± SD (n = 10, *p < 0.05, **insignificant). (A) Storage moduli of hydrogels in frequency sweep, (B) tan δ value, calculated from the ratio between G' and G'' from amplitude sweep to observe the elasticity of hydrogels.

Table 3. Storage and Loss Moduli, Calculated Average Mesh Sizes (ξ), and Cross-linking Densities (n_c) for the Investigated Ink Compositions

	G' [Pa]	G'' [Pa]	ξ [nm]	n_c[mol/m^3]
GelMA30	478 ± 7	14 ± 2	20.52	0.19
GelMA60	594 ± 5	8 ± 1	19.06	0.24
GelMA30GA	1631 ± 26	34 ± 5	13.62	0.66
GelMA60GA	662 ± 30	15 ± 1	18.38	0.27
GelMA30GA-5Fe	4454 ± 38	135 ± 9	9.75	1.87
GelMA60GA-5Fe	2166 ± 43	115 ± 1	12.38	0.87

properties imparted by GA. The UV−vis spectroscopy measurement of 2 mg/mL GelMA30GA and GelMA60GA in the presence of DPPH displayed 26 and 37% reduction (Figure S6) in absorption, indicating potential antioxidant properties.

DISCUSSION

The printability of biomaterial inks/bioinks is highly dependent on viscosity and flow behavior. The common approaches to improve the printability of GelMA are to increase the polymer concentration, lower the printing temperature, or mix it with other polymers.[8] GelMA has been printed on its own with a concentration higher than 10% w/v at RT.[6,10,31] However, high concentrations of polymers can result in reduced nutrient and oxygen transport for cells.[32] Printing 5% w/v GelMA at low printing temperature (16−17 °C) could generate more cell injuries, and the temperature might not be homogeneously distributed throughout the cartridge, nozzle, and printing bed.[10,33]

To overcome the temperature-related issues, we synthesized GelMAGA from GelMA having two degrees of methacrylation

https://doi.org/10.1021/acs.biomac.2c01418
Biomacromolecules 2023, 24, 502−514

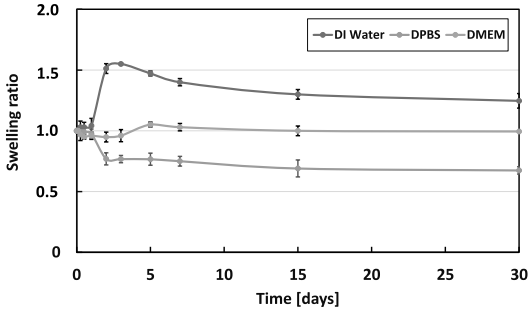

Figure 9. Stability test of 3D printed GelMA30GA-5Fe structures in DI water, DPBS, and DMEM for 30 days. The mean (n = 3) and standard deviation are shown.

(30 and 60%), followed by 10% GA conjugation to GelMA.[15,33] Furthermore, the rheological properties were enhanced by pre-cross-linking with $FeCl_3$*via* catechol−Fe^{3+} chelation, allowing lower polymer concentrations to be printable at RT or physiological temperature. Adding Fe^{3+} to GelMAGA inks can enhance the viscosity, providing primary cross-linking of the ink. After printing each layer, the ink was stabilized by photocross-linking (i.e., secondary cross-linking method). This sequential cross-linking approach significantly improves the printability of low-concentration GelMA-based bioinks (5% w/v).

All synthesized biomaterial inks were screened according to our pre-processing method. The prescreened results also showed that 0.5% $FeCl_3$ in GelMAGA provided a favorable viscosity for the biomaterial inks, which were able to form a filament at RT due to noncovalent interactions of catechol−Fe^{3+} chelation. The coordination bonding between the trivalent ferric ions and hydroxyl groups of the GA leads to the formation of a loose hydrogel network and, hence, increases the viscosity of the inks.[34] However, extruded GelMA60GA-5Fe filament was slightly overgelated, and it could not support its own weight in the air, resulting in a discontinuous filament. The concentration of 0.25% w/v $FeCl_3$ in GelMAGA was not high enough to maintain the shape of the ink and led to droplet formation in the prescreening tests. Furthermore, the prescreening test showed that GelMA30GA-5Fe had good filament formation and stackability.

In general, printable biomaterial inks/bioinks are shear-thinning, having a viscosity that decreases with an increase in shear rate.[35−39] The inks should exhibit yield stress, that is, have appropriate shear stress that must be overcome to make the ink flow. However, too high shear stress can cause the ink to burst and cause cell damage when printing with cells. Also, the initial viscosity value should be recovered at least up to 80% of the original level within seconds after printing.[36,40] The temperature sweep of the flow mode showed that the viscosity of GelMAGA with Fe^{3+} was not much affected by the temperature change from RT to 37 °C. It indicates that primary cross-linking of Fe^{3+} can stabilize the ink at an elevated temperature. Instead, the viscosity of the inks slowly decreased after 4 °C compared to GelMA or GelMAGA. In general, increasing the gelatin modification degree decreases the physical interactions between the macromolecules, resulting in lower precursor viscosities and lower sol−gel transition temperatures.[41] The results show that GelMA60GA ink displayed less thermostability compared to GelMA30GA. Similar behavior has been described previously: high modification of GelMA disturbs the triple helix structure due to reduced ionic and dipole−dipole interaction between gelatin molecules, resulting in a looser physical network that leads to the lower thermostability of the hydrogel network.[41]

The values of shear-thinning coefficients and yield stress were used to explain printability. GelMA30GA-5Fe and GelMA60GA-5Fe had high zero shear viscosity and did not flow immediately after the beginning of the measurement. Thus, both inks possessed yield stress, confirmed by the plotting of the Herschel−Bulkley model. All GelMAGA inks with and without Fe^{3+} were shear-thinning, supported by the Power-law model results, giving $n < 1$. However, our previously published study indicates that the n value should be lower than 0.2 to ensure high printability.[22] In addition, low zero shear viscosity can result in poor fiber formation because of a lack of shape fidelity after being extruded from the nozzle.[42]Figure 4C shows that the viscosity of GelMA60GA-5Fe dropped sharply when the geometry started to move. This may be related to overgelation of the Fe^{3+} network. The recovery behavior tests demonstrated that GelMA30GA-5Fe and GelMA60GA-5Fe could recover 70% of their initial viscosity after removing the high shear. This results from the reversible interaction between GA and Fe^{3+} ions.[43] We interpreted that the multiple long-range ionic interactions due to quadruple hydrogen bonds between Fe^{3+} and the phenolic groups resulted in favorable shear-thinning and recovery behavior of the inks.[44]

Based on the prescreening and rheological measurements, GelMA30GA-5Fe and GelMA60GA-5Fe were chosen to be evaluated for their printability (Pr) using a 3D bioprinter. Bioinks with excellent printability will exhibit constant shape and square pores in the printed grid structures. The calculated Pr values were similar, but the standard deviations varied, indicating the random pore geometries in GelMA60-5Fe grids. On the contrary, GelMA30-5Fe showed almost similar Pr values at RT and 37 °C. When printed into six-layered grids, GelMA30GA-5Fe at 37 °C and GelMA60GA-5Fe at RT resulted in irregular grid structures, which collapsed during printing.

GelMA30GA-5Fe was chosen to be printed into cylinders as well and further studied for its mechanical properties and stability. Previous studies have shown that UV light might not penetrate through the 3D structures, but photocross-linking in a layer-by-layer manner during the printing can increase the homogeneity of the printed structures.[45] The measured cylinder diameters were quite similar to the control, but the wall heights differed from the CAD model, which probably resulted from the die swelling of the filament after being extruded from the nozzle. The inaccuracy of the printed 3D constructs was also supported by the filament shape characterization showing die swelling of GelMA30GA-5Fe (RT). By comparing the top and side views of the cylinders, it is obvious that GelMA30GA-5Fe was still able to maintain good shape fidelity and enabled multilayered printing.

According to the oscillatory measurement, the storage moduli of GelMA30G-5Fe and GelMA60GA-5Fe were significantly higher than that for the ink without GA and Fe^{3+}. In addition, GA and Fe^{3+} improved the elasticity of the resulting GelMA hydrogels, as shown in Figure 8B, because of the double network formed between GA and Fe^{3+}. The interconnectivity and integrity due to photocross-linking and catechol−Fe^{3+} chelation provided a more stable network than in a single network GelMA (single photocross-linking).[21,26,46]

https://doi.org/10.1021/acs.biomac.2c01418
Biomacromolecules 2023, 24, 502−514

Dual cross-linking in the GelMAGA-Fe hydrogels yielded a smaller mesh size and higher cross-linking density as compared to the single network in the GelMA hydrogel. However, the denser polymer network can limit the transport of oxygen and nutrients to the cells.[30,47]

Swelling and dissolution tests were performed to evaluate the stability of GelMAGA printed structures in water, DPBS, and DMEM under a physiological environment.[47,48] The structures were stable for over a month in the aqueous solution at 37 °C, with a slight change during the first 2 days. In the previously reported studies, the weight of GelMA hydrogels increased by almost 60% in PBS after just 24 h.[6,10,48] In comparison, our GelMA30GA-5Fe swelled less than 10% and the printed structures were able to maintain internal and external architecture until the end of the observation period. As assumed, the cross-linking density and average mesh size influenced the swelling capacity of the hydrogel.[30] The higher cross-linking density resulted from the dual network formation leading to a reduction in water absorption.[49] In addition, we observed that GelMAGA-Fe displays considerable tissue adhesive and antioxidant properties, as shown in Figures S4 and S5. Adhesive biomaterial inks can be useful as a printable glue, and they expand the bioink application possibilities, enabling, for example, printing directly to the defect site for wound dressing purposes.[20,26]

■ CONCLUSIONS

We developed a GA-functionalized GelMA-based biomaterial ink utilizing a two-step sequential cross-linking approach: metal−ligand complexation followed by photocross-linking. The pre-cross-linked GA-modified GelMA with Fe^{3+} (GelMA30GA-5Fe) showed higher viscosity and better rheological profile than GelMA ink alone, resulting in superb printability. It was also printable into 3D constructs with good shape fidelity compared to the ink without a pre-cross-linker. The dual network achieved by catechol−Fe^{3+} chelation and photocross-linking also improved the elastic modulus in the hydrogels, compared to GelMA and GelMAGA. The printed structures of GelMA30GA-5Fe ink showed good stability and a low swelling ratio in the physiological environment over a month. In addition, GA provided tissue adhesion and antioxidant properties. The catechol-based adhesive printable inks can offer the tissue-engineered scaffolds better attachment on the surface of target organs or tissues without using additional glue. Moreover, the GA-modified GelMA ink opens up new possibilities for wound dressing materials that can be utilized for *in situ* bioprinting at the defect site.

■ ASSOCIATED CONTENT

Supporting Information

The Supporting Information is available free of charge at https://pubs.acs.org/doi/10.1021/acs.biomac.2c01418.

> Calibration curve for residual amine concentration using glycine standard; measured UV light intensity versus distance from the light source; additional UV spectra of Gelatin type A, GelMA, and GelMAGA; calculation of the degree of methacrylation and gallic acid modification; further confirmation of GelMAGA conjugation; tack test of GelMA30, GelMA60, GelMA30GA, and GelMA60GA; and DPPH radical scavenging assay of GelMA30GA and GelMA60GA (PDF)

■ AUTHOR INFORMATION

Corresponding Author

Vijay Singh Parihar − *Biomaterials and Tissue Engineering Group, BioMediTech, Faculty of Medicine and Health Technology, Tampere University, Tampere 33720, Finland;* orcid.org/0000-0002-6044-2121; Email: vijay.parihar@tuni.fi

Authors

Hatai Jongprasitkul − *Biomaterials and Tissue Engineering Group, BioMediTech, Faculty of Medicine and Health Technology, Tampere University, Tampere 33720, Finland;* orcid.org/0000-0003-0646-7712

Sanna Turunen − *Biomaterials and Tissue Engineering Group, BioMediTech, Faculty of Medicine and Health Technology, Tampere University, Tampere 33720, Finland; Brinter Ltd, Turku 20520, Finland;* orcid.org/0000-0002-6823-8811

Minna Kellomäki − *Biomaterials and Tissue Engineering Group, BioMediTech, Faculty of Medicine and Health Technology, Tampere University, Tampere 33720, Finland;* orcid.org/0000-0003-4321-1820

Complete contact information is available at: https://pubs.acs.org/10.1021/acs.biomac.2c01418

Author Contributions

The manuscript was written through the contributions of all authors. Chemical modification and material characterizations have been carried out by H.J., V.S.P., and S.T. Data interpretation has been carried out by H.J., S.T., V.S.P., and M.K. All authors have given approval to the final version of the manuscript.

Notes

The authors declare no competing financial interest.

■ ACKNOWLEDGMENTS

The authors are grateful to The Centre of Excellence in Body-on-Chip Research (CoEBoC) by the Academy of Finland for financial support (decisions #312409, #326587, and #336663) and to the Tampere University funding for CoEBoC.

■ ABBREVIATIONS

GelMA, methacrylated gelatin; MA, methacrylate; GA, gallic acid; UV, ultraviolet; RT, room temperature; G', storage modulus; G'', loss modulus; PI, photoinitiator; CAD, computer-aided design; DI, deionized

■ REFERENCES

(1) Matai, I.; Kaur, G.; Seyedsalehi, A.; McClinton, A.; Laurencin, C. T. Progress in 3D Bioprinting Technology for Tissue/Organ Regenerative Engineering. *Biomaterials* **2020**, *226*, 119536.

(2) Ng, W. L.; Chua, C. K.; Shen, Y. F. Print Me An Organ! Why We Are Not There Yet. *Prog. Polym. Sci.* **2019**, *97*, 101145.

(3) O'Connell, C. D.; Zhang, B.; Onofrillo, C.; Duchi, S.; Blanchard, R.; Quigley, A.; Bourke, J.; Gambhir, S.; Kapsa, R.; Di Bella, C.; Choong, P.; Wallace, G. G. Tailoring the Mechanical Properties of Gelatin Methacryloyl Hydrogels through Manipulation of the Photocrosslinking Conditions. *Soft Matter* **2018**, *14*, 2142−2151.

(4) Ouyang, L.; Highley, C. B.; Rodell, C. B.; Sun, W.; Burdick, J. A. 3D Printing of Shear-Thinning Hyaluronic Acid Hydrogels with Secondary Cross-Linking. *ACS Biomater. Sci. Eng.* **2016**, *2*, 1743−1751.

(5) Shie, M. Y.; Lee, J. J.; Ho, C. C.; Yen, S. Y.; Ng, H. Y.; Chen, Y. W. Effects of Gelatin Methacrylate Bio-Ink Concentration on

Mechano-Physical Properties and Human Dermal Fibroblast Behavior. *Polymers* **2020**, *12*, 1930.
(6) Yin, J.; Yan, M.; Wang, Y.; Fu, J.; Suo, H. 3D Bioprinting of Low-Concentration Cell-Laden Gelatin Methacrylate (GelMA) Bioinks with a Two-Step Cross-Linking Strategy. *ACS Appl. Mater. Interfaces* **2018**, *10*, 6849−6857.
(7) Jongprasitkul, H.; Turunen, S.; Parihar, V. S.; Annurakshita, S.; Kellomäki, M. Photocross-Linkable Methacrylated Polypeptides and Polysaccharides for Casting, Injecting, and 3D Fabrication. *Biomacromolecules* **2021**, *22*, 481−493.
(8) Ouyang, L.; Highley, C. B.; Sun, W.; Burdick, J. A. A Generalizable Strategy for the 3D Bioprinting of Hydrogels from Nonviscous Photo-Crosslinkable Inks. *Adv. Mater.* **2017**, *29*, 1604983.
(9) Zhuang, P.; Ng, W. L.; An, J.; Chua, C. K.; Tan, L. P. Layer-by-Layer Ultraviolet Assisted Extrusion-Based (UAE) Bioprinting of Hydrogel Constructs with High Aspect Ratio for Soft Tissue Engineering Applications. *PLoS One* **2019**, *14*, No. e0216776.
(10) Gu, Y.; Zhang, L.; Du, X.; Fan, Z.; Wang, L.; Sun, W.; Cheng, Y.; Zhu, Y.; Chen, C. Reversible Physical Crosslinking Strategy with Optimal Temperature for 3D Bioprinting of Human Chondrocyte-Laden Gelatin Methacryloyl Bioink. *J. Biomater. Appl.* **2018**, *33*, 609−618.
(11) Ouyang, L.; Armstrong, J. P. K.; Lin, Y.; Wojciechowski, J. P.; Lee-Reeves, C.; Hachim, D.; Zhou, K.; Burdick, J. A.; Stevens, M. M. Expanding and Optimizing 3D Bioprinting Capabilities Using Complementary Network Bioinks. *Sci. Adv.* **2020**, *6*, 1−14.
(12) Tarassoli, S. P.; Jessop, Z. M.; Jovic, T.; Hawkins, K.; Whitaker, I. S. Candidate Bioinks for Extrusion 3D Bioprinting—A Systematic Review of the Literature. *Front. Bioeng. Biotechnol.* **2021**, *9*, 1−15.
(13) Hölzl, K.; Lin, S.; Tytgat, L.; Van Vlierberghe, S.; Gu, L.; Ovsianikov, A. Bioink Properties before, during and after 3D Bioprinting. *Biofabrication* **2016**, *8*, 032002.
(14) Salzlechner, C.; Haghighi, T.; Huebscher, I.; Walther, A. R.; Schell, S.; Gardner, A.; Undt, G.; da Silva, R. M. P.; Dreiss, C. A.; Fan, K.; Gentleman, E. Adhesive Hydrogels for Maxillofacial Tissue Regeneration Using Minimally Invasive Procedures. *Adv. Healthc. Mater.* **2020**, *9*, 1901134.
(15) Krogsgaard, S. M. M.; Behrens, M.; Pedersen, M. A.; Birkedal, J. S.; Birkedal, H. Self-Healing Mussel-Inspired Multi-PH-Responsive Hydrogels. *Biomacromolecules* **2013**, *14*, 297−301.
(16) Holten-Andersen, N.; Harrington, M. J.; Birkedal, H.; Lee, B. P.; Messersmith, P. B.; Lee, K. Y. C.; Waite, J. H. PH-Induced Metal-Ligand Cross-Links Inspired by Mussel Yield Self-Healing Polymer Networks with near-Covalent Elastic Moduli. *Proc. Natl. Acad. Sci. U.S.A.* **2011**, *108*, 2651−2655.
(17) Samanta, S.; Rangasami, V. K.; Sarlus, H.; Samal, J. R. K.; Evans, A. D.; Parihar, V. S.; Varghese, O. P.; Harris, R. A.; Oommen, O. P. Interpenetrating Gallol Functionalized Tissue Adhesive Hyaluronic Acid Hydrogel Polarizes Macrophages to an Immunosuppressive Phenotype. *Acta Biomater.* **2022**, *142*, 36−48.
(18) Krogsgaard, M.; Andersen, A.; Birkedal, H. Gels and Threads: Mussel-Inspired One-Pot Route to Advanced Responsive Materials. *Chem. Comm.* **2014**, *50*, 13278−13281.
(19) Samanta, S.; Rangasami, V. K.; Murugan, N. A.; Parihar, V. S.; Varghese, O. P.; Oommen, O. P. An Unexpected Role of an Extra Phenolic Hydroxyl on the Chemical Reactivity and Bioactivity of Catechol or Gallol Modified Hyaluronic Acid Hydrogels. *Polym. Chem.* **2021**, *12*, 2987−2991.
(20) Włodarczyk-Biegun, M. K.; Paez, J. I.; Villiou, M.; Feng, J.; del Campo, A. Printability Study of Metal Ion Crosslinked PEG-Catechol Based Inks. *Biofabrication* **2020**, *12*, 035009.
(21) Wang, L.; Zhang, X.; Yang, K.; Fu, Y. V.; Xu, T.; Li, S.; Zhang, D.; Wang, L. N.; Lee, C. S. A Novel Double-Crosslinking-Double-Network Design for Injectable Hydrogels with Enhanced Tissue Adhesion and Antibacterial Capability for Wound Treatment. *Adv. Funct. Mater.* **2020**, *30*, 1904156.
(22) Jongprasitkul, H.; Turunen, S.; Parihar, V. S.; Kellomäki, M. Two-Step Crosslinking to Enhance the Printability of Methacrylated Gellan Gum Biomaterial Ink for Extrusion-Based 3D Bioprinting. *Bioprinting* **2022**, *25*, No. e00185.
(23) Wang, M. D.; Zhai, P.; Schreyer, D. J.; Zheng, R. S.; Sun, X. D.; Cui, F. Z.; Chen, X. B. Novel Crosslinked Alginate/Hyaluronic Acid Hydrogels for Nerve Tissue Engineering. *Front. Mater. Sci.* **2013**, *7*, 269−284.
(24) Morris, E. R.; Nishinari, K.; Rinaudo, M. Gelation of Gellan - A Review. *Food Hydrocoll* **2012**, *28*, 373−411.
(25) Pepelanova, I.; Kruppa, K.; Scheper, T.; Lavrentieva, A. Gelatin-Methacryloyl (GelMA) Hydrogels with Defined Degree of Functionalization as a Versatile Toolkit for 3D Cell Culture and Extrusion Bioprinting. *Bioengineering* **2018**, *5*, 55.
(26) Shin, M.; Lee, H. Gallol-Rich Hyaluronic Acid Hydrogels: Shear-Thinning, Protein Accumulation against Concentration Gradients, and Degradation-Resistant Properties. *Chem. Mater.* **2017**, *29*, 8211−8220.
(27) Sisso, A. M.; Boit, M. O.; DeForest, C. A. Self-Healing Injectable Gelatin Hydrogels for Localized Therapeutic Cell Delivery. *J. Biomed. Mater. Res. A* **2020**, *108*, 1112−1121.
(28) Koivusalo, L.; Kauppila, M.; Samanta, S.; Parihar, V. S.; Ilmarinen, T.; Miettinen, S.; Oommen, O. P.; Skottman, H. Tissue Adhesive Hyaluronic Acid Hydrogels for Sutureless Stem Cell Delivery and Regeneration of Corneal Epithelium and Stroma. *Biomaterials* **2019**, *225*, 119516.
(29) Lai, J. Y.; Luo, L. J. Antioxidant Gallic Acid-Functionalized Biodegradable in Situ Gelling Copolymers for Cytoprotective Antiglaucoma Drug Delivery Systems. *Biomacromolecules* **2015**, *16*, 2950−2963.
(30) Karvinen, J.; Ihalainen, T. O.; Calejo, M. T.; Jönkkäri, I.; Kellomäki, M. Characterization of the Microstructure of Hydrazone Crosslinked Polysaccharide-Based Hydrogels through Rheological and Diffusion Studies. *Mater. Sci. Eng. C* **2019**, *94*, 1056−1066.
(31) Billiet, T.; Gevaert, E.; De Schryver, T.; Cornelissen, M.; Dubruel, P. The 3D Printing of Gelatin Methacrylamide Cell-Laden Tissue-Engineered Constructs with High Cell Viability. *Biomaterials* **2014**, *35*, 49−62.
(32) Nichol, J. W.; Koshy, S. T.; Bae, H.; Hwang, C. M.; Yamanlar, S.; Khademhosseini, A. Cell-Laden Microengineered Gelatin Methacrylate Hydrogels. *Biomaterials* **2010**, *31*, 5536−5544.
(33) Luo, C.; Xie, R.; Zhang, J.; Liu, Y.; Li, Z.; Zhang, Y.; Zhang, X.; Yuan, T.; Chen, Y.; Fan, W. Lower-Temperature Three-Dimensional Printing of Tissue Cartilage Engineered with Gelatin Methacrylamide. *Tissue Eng. Part C Methods* **2020**, *26*, 306−316.
(34) Fazary, A. E.; Taha, M.; Ju, Y. H. Iron Complexation Studies of Gallic Acid. *J. Chem. Eng. Data* **2009**, *54*, 35−42.
(35) Ding, H.; Chang, R. C. Printability Study of Bioprinted Tubular Structures Using Liquid Hydrogel Precursors in a Support Bath. *Appl. Sci.* **2018**, *8*, 403.
(36) Paxton, N.; Smolan, W.; Böck, T.; Melchels, F.; Groll, J.; Jungst, T. Proposal to Assess Printability of Bioinks for Extrusion-Based Bioprinting and Evaluation of Rheological Properties Governing Bioprintability. *Biofabrication* **2017**, *9*, 044107.
(37) Gillispie, G.; Prim, P.; Copus, J.; Fisher, J.; Mikos, A. G.; Yoo, J. J.; Atala, A.; Lee, S. J. Assessment Methodologies for Extrusion-Based Bioink Printability. *Biofabrication* **2020**, *12*, 022003.
(38) Gao, T.; Gillispie, G. J.; Copus, J. S.; PR, A. K.; Seol, Y.-J.; Atala, A.; Yoo, J. J.; Lee, S. J. Optimization of Gelatin Alginate Composite Bioink Printability Using Rheological Parameters: A Systematic Approach. *Biofabrication* **2018**, *10*, 034106.
(39) Townsend, J. M.; Beck, E. C.; Gehrke, S. H.; Berkland, C. J.; Detamore, M. S. Flow Behavior Prior to Crosslinking: The Need for Precursor Rheology for Placement of Hydrogels in Medical Applications and for 3D Bioprinting. *Prog. Polym. Sci.* **2019**, *91*, 126−140.
(40) Jiang, Y.; Zhou, J.; Feng, C.; Shi, H.; Zhao, G.; Bian, Y. Rheological Behavior, 3D Printability and the Formation of Scaffolds with Cellulose Nanocrystals/Gelatin Hydrogels. *J. Mater. Sci.* **2020**, *55*, 15709−15725.

(41) Rebers, L.; Granse, T.; Tovar, G. E. M.; Southan, A.; Borchers, K. Physical Interactions Strengthen Chemical Gelatin Methacryloyl Gels. *Gels* **2019**, *5*, 4.
(42) Schwab, A.; Levato, R.; D'Este, M.; Piluso, S.; Eglin, D.; Malda, J. Printability and Shape Fidelity of Bioinks in 3D Bioprinting. *Chem. Rev.* **2020**, *120*, 11028−11055.
(43) Oh, D. X.; Kim, S.; Lee, D.; Hwang, D. S. Tunicate-Mimetic Nanofibrous Hydrogel Adhesive with Improved Wet Adhesion. *Acta Biomater.* **2015**, *20*, 104−112.
(44) Lee, S. C.; Gillispie, G.; Prim, P.; Lee, S. J. Physical and Chemical Factors Influencing the Printability of Hydrogel-Based Extrusion Bioinks. *Chem. Rev.* **2020**, *120*, 10834−10886.
(45) Levato, R.; Visser, J.; Planell, J. A.; Engel, E.; Malda, J.; Mateos-Timoneda, M. A. Biofabrication of Tissue Constructs by 3D Bioprinting of Cell-Laden Microcarriers. *Biofabrication* **2014**, *6*, 035020.
(46) Bhagat, V.; Becker, M. L. Degradable Adhesives for Surgery and Tissue Engineering. *Biomacromolecules* **2017**, *18*, 3009−3039.
(47) Santos, E.; Hernández, R. M.; Pedraz, J. L.; Orive, G. Novel Advances in the Design of Three-Dimensional Bio-Scaffolds to Control Cell Fate: Translation from 2D to 3D. *Trends Biotechnol.* **2012**, *30*, 331−341.
(48) Ibañez, R. I. R.; do Amaral, R. J. F. C.; Reis, R. L.; Marques, A. P.; Murphy, C. M.; O'Brien, F. J. 3D-Printed Gelatin Methacrylate Scaffolds With Controlled Architecture and Stiffness Modulate the Fibroblast Phenotype Towards Dermal Regeneration. *Polymers* **2021**, *13*, 2510.
(49) Hoti, G.; Caldera, F.; Cecone, C.; Rubin Pedrazzo, A. R.; Anceschi, A.; Appleton, S. L.; Khazaei Monfared, Y. K.; Trotta, F. Effect of the Cross-Linking Density on the Swelling and Rheological Behavior of Ester-Bridged β-Cyclodextrin Nanosponges. *Materials* **2021**, *14*, 478.

https://doi.org/10.1021/acs.biomac.2c01418
Biomacromolecules 2023, 24, 502−514

PUBLICATION IV

pH-Responsive Gallol Functionalized Hyaluronic Acid-based Tissue Adhesive Hydrogels for Injecting and 3D Bioprinting

Jongprasitkul, H.; Parihar, V.S.; Turunen, S.; Kellomäki, M.

ACS Applied Materials & Interfaces 2023, 15(28), 33972-33984.
https://doi.org/10.1021/acsami.3c02961

ACS APPLIED MATERIALS & INTERFACES

www.acsami.org

Research Article

pH-Responsive Gallol-Functionalized Hyaluronic Acid-Based Tissue Adhesive Hydrogels for Injection and Three-Dimensional Bioprinting

Hatai Jongprasitkul, Vijay Singh Parihar,* Sanna Turunen, and Minna Kellomäki

Cite This: *ACS Appl. Mater. Interfaces* 2023, 15, 33972−33984

Read Online

ACCESS | Metrics & More | Article Recommendations | Supporting Information

ABSTRACT: The major challenges of hyaluronic acid-based bioinks in extrusion-based three-dimensional bioprinting are poor printability and low printing accuracy. To tackle the challenges, we developed a bioink in which two components are blended: gallic acid-functionalized hyaluronic acid (HAGA) and hyaluronic acid methacrylate (HAMA). In the precursor phase, the blend's HAGA component enables pH-dependent viscosity modulation that results in improved injectability and printability at physiological temperature. Postprinting, the blend's HAMA component is photocrosslinked to create a true hydrogel with a complementary network of both HAGA and HAMA. The ready structures of the HAGA-HAMA hydrogel showed sufficient printing quality and accuracy compared to plain HAMA. The blend also displayed enhanced viscoelastic properties and stable swelling behavior. In addition to the pH tunability, the HAGA component also imparted tissue adhesion and antioxidant activity. This bioink has the potential to be printed directly on an infected wound site due to its adhesiveness to tissue and dimensional stability in situ.

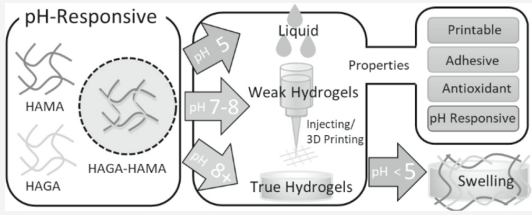

KEYWORDS: *hyaluronic acid, gallic acid, pH-responsive, bioprinting, bioink blend, photocrosslinking*

■ INTRODUCTION

Hyaluronic acid-based (HA) hydrogels have been considered an attractive choice for bioinks. The various reactive functional groups allow HA hydrogels to be chemically modified by the conjugation of biorthogonal moieties or bioactive molecules.[1,2] Modification with methacrylate (MA) groups is the most common way to obtain highly versatile bioinks and a hydrogel network can be formed via photopolymerization reaction.[3−5] Recently, hyaluronic acid methacrylate (HAMA), with a high degree of MA-modification, has been used for light-based three-dimensional (3D) bioprinting, such as stereolithographic and digital light processing.[6] However, the printing of HAMA using an extrusion-based 3D bioprinter remains challenging due to its low mechanical properties, poor printability, and poor printing accuracy.[7] HAMA's printability can be improved by blending it with high shear-thinning or stimuli-responsive precursors/hydrogels to create a complementary network, which can compensate for the HAMA's insufficient properties.[8−13] Over the past decades, the development of tissue adhesive hydrogels has been reported with various techniques, including mussel-inspired chemistry and supramolecular interactions.[14] However, the integration between high printability, stimuli-responsiveness, and tissue adhesion in one biomaterial ink is still challenging.

To improve the printability of bioinks, blending bioinks with high-molecular-weight polymers could be an alternative option. However, the physical blending of two different molecular weight polymers may create an immiscible mixture as blending requires compatibility of polymer properties.[15] Furthermore, the biological functions might be disrupted because a higher pressure is required during the printing process.[16,17] Precrosslinking techniques are an effective way to convert unprintable inks into printable ones capable of forming 3D constructs. Precrosslinking techniques create a weak hydrogel network, giving enough stability to sustain shape fidelity during the printing.[18] Several precrosslinking approaches have been studied to improve the printability of bioinks for extrusion-based 3D bioprinting.[19] The most common ways are to utilize ionic crosslinking (e.g., for alginate, gellan gum),[20−22] enzymatic crosslinking (collagen),[23] pH (chitosan),[24] or temperature changes (gelatin).[25−27]

Stimuli-responsive hydrogels have also been investigated as candidates for bioinks and can be induced by exposing the ink to various environmental changes, including pH, temperature, light, and ions.[28] These properties provide versatility to bioinks, as they harness the on-demand tunability of bioinks

Received: March 1, 2023
Accepted: June 26, 2023
Published: July 6, 2023

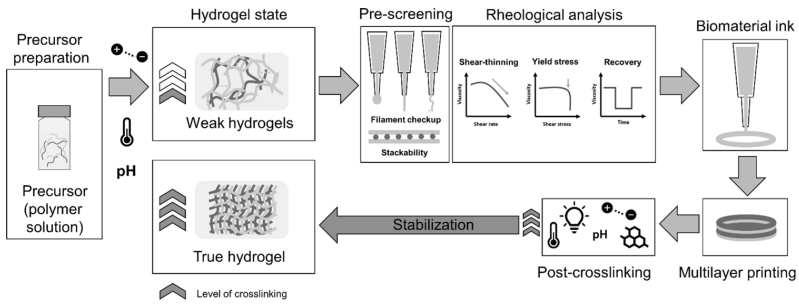

Figure 1. Flow chart demonstrates the process of biomaterial ink evaluation through the definitions of precursor, weak hydrogel, true hydrogel, and biomaterial ink. (precursor → weak hydrogel → biomaterial ink → true hydrogel). Precursor, polymer solution or pre-hydrogel solution without crosslinking. Weak hydrogel, weakly crosslinked hydrogel (extrudable). Biomaterial ink, printable precursor (weak hydrogel) or precursor candidate for 3D bioprinting that has been screened for printability through various evaluation steps: precursor preparation, precrosslinking, prescreening for printability (filament formation and stackability), rheological analysis (degree of shear-thinning, yield stress, and recovery behavior), 3D printing (multilayer printing), and postcrosslinking (stabilization). True hydrogel, crosslinked hydrogels with mechanically stable to maintain the structural integrity after printing.[36]

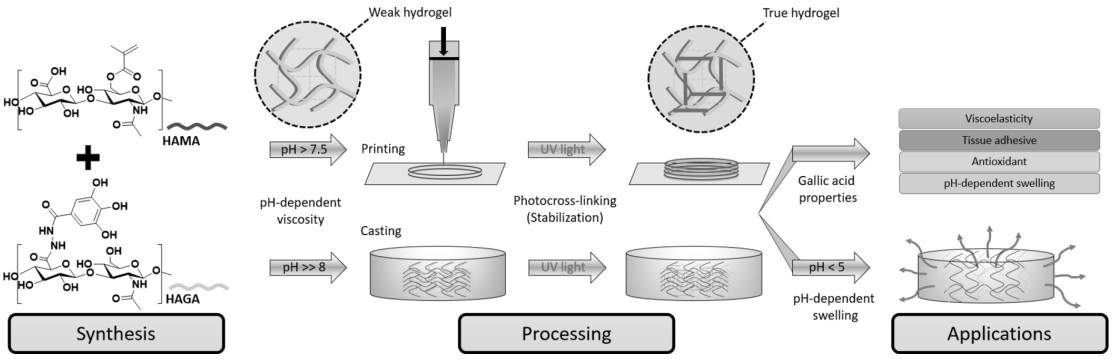

Figure 2. Schematics of HAGA and HAMA blend, combining the viscosity modulation of pH-dependent precursors for casting and extrusion-based 3D bioprinting. 3D printing of the complementary network hydrogel is done in two steps: first, the viscosity of the precursor is enhanced via pH change to obtain proper printability, described as "ink", and next, photocrosslinking is used after printing. The GA-based hydrogels demonstrate viscoelasticity, tissue adhesion, and antioxidant and pH-dependent swelling behavior.

and can be used for various applications.[29] The pH-responsive hydrogels have gained wide interest because of their excellent adaptation in physiological conditions for in situ bioprinting applications.[30] Moreover, pH-stimuli can better control bioink's stability in the defect site due to the different pH during healing stages.[31,32] Only a few reports have explored the pH-responsive properties of bioinks to obtain printable hydrogels; for example, the pH-induced chitosan hydrogel was printed into a concentrated NaOH bath, forming the intramolecular−intermolecular hydrogen bonds.[24]

Moreover, an injectable hydrogel with self-healing and tissue adhesive properties is an interesting class of hydrogels. Self-healing injectable hydrogels can temporarily fluidize under shear stress and recover their original structure and mechanical properties after the release of the applied stress. This ability makes them easily injectable at the wound site. Additionally, as self-healing injectable hydrogels possess tissue adhesive properties, they can adhere effectively to the wound site and facilitate sutureless implantation of hydrogel constructs.[33] Shin and Lee have reported the combination of gallol-tethered hyaluronic acid and oligo-epigallocatechin (OEGCG) gels with pH-dependent behavior for injectable hydrogels at basic conditions.[1]

In this work, as a novel component for bioink, we developed gallic acid-functionalized hyaluronic acid (HAGA) to establish pH-responsiveness that can control the printability of precursors as well as both the mechanical and swelling behavior of hydrogels. GA is a polyphenol compound with three phenol units known as catechol moieties and is also recognized for its tissue adhesive properties and antioxidant activity.[34] We hypothesized that the precursor blend of HAGA-HAMA could achieve high printability and injectability at pH 7.5−8. The pH change serves as a precrosslinking method for the precursor during printing followed by UV postcrosslinking to stabilize the printed constructs. The precursor formulations could be printed without any additional viscosity enhancers. The HAGA component enhances pH responsiveness at basic pH, which results in an increase of tissue adhesion via phenolic group oxidation. This phenomenon mimics mussel adhesion due to the higher interaction of reductive cysteine-rich proteins.[35]

This article reports the synthesis of HAGA with 10 and 20% GA modification and HAMA with 15% methacrylation and

https://doi.org/10.1021/acsami.3c02961
ACS Appl. Mater. Interfaces 2023, 15, 33972−33984

their blending to a 1:1 volume ratio. The evaluation of biomaterial ink printability was addressed in this article through an evaluation process illustrated in Figure 1, which is based on our previous studies.[7,21,36] The rheological characterization of the HAGA-HAMA precursor at different pH was performed. Furthermore, the effect of GA functionalization on the viscoelastic properties of hydrogels was investigated. Additionally, HAGA conjugation provided tissue-adhesive properties and antioxidant activity to the HAGA-HAMA hydrogel. The schematics in Figure 2 describe the entire process of synthesis, processing, and postprocessing of the HAGA-HAMA precursor. We also highlight that the pH-responsive precursors offer a flexible way to control the ink's viscosity for printing. Furthermore, the viscoelastic properties and tissue adhesiveness of the photocrosslinked hydrogels can be easily modified by changing the pH and degree of GA modification.

■ MATERIALS AND METHODS

Hyaluronic acid (M_w 100 kDa) was purchased from LifeCore Biomedical (Chaska, USA). Methacrylic anhydride, gallic acid (3,4,5-trihydroxy benzoic acid), hydrazine hydrate, 1-ethyl-3-(3-dimethyl aminopropyl)-carbodiimide hydrochloride (EDC), 1−hydroxy benzotriazole hydrate (HOBt), dimethyl sulfoxide (DMSO), and Irgacure 2959 (I2959) were purchased from Merck KGaA, Darmstadt, Germany. Dialysis membranes used for purification were purchased from Spectra Por-6 (MWCO 3500). DI water (deionized water, Miele Aqua Purificator G 7795, Siemens) was used. Dulbecco's phosphate-buffered saline (DPBS) was prepared in the lab. All solvents were of analytical quality. Nuclear magnetic resonance (NMR) analysis was carried out on an NMR spectrometer (Varian Mercury 300 MHz, Agilent Technologies, Inc., USA).

Synthesis of Hyaluronic Acid Methacrylate. Methacrylated hyaluronic acid (HAMA) with ∼15% MA was prepared by adjusting the ratio of methacrylic anhydride in the reaction, as has been described previously in ref 7. In brief, 400 mg of sodium hyaluronate was dissolved in 100 mL of deionized water at pH 9. Next, methacrylic anhydride was added dropwise, providing the amount equal to the defined modification (500 μL). The reaction was carried out for 7 h at 4 °C while maintaining pH ∼ 8. After that, the reaction mixture was dialyzed with a 3.5 kDa MWCO membrane against deionized water for 72 h (2 × 2 L, 12 h) at RT. Thereafter, the solution was lyophilized, and the product was obtained. The MA in HAMA was quantified by 1H NMR. The measurement was performed at RT. The synthesis procedure of HAMA is displayed in Figure S-1.

Synthesis of Gallic Acid-Functionalized Hyaluronic Acid. 400 mg of HA (1 mmol of HA, in equivalent) was dissolved in 75 mL of DI water followed by the addition of 1 mmol N-hydroxy benzotriazole (HOBt, 153 mg, 1 equiv). The gallic acid hydrazide (Figure S-2) (GA-Hyd, 184 mg, 1 equiv) was separately dissolved in 25 mL of DMSO and added to the stirred reaction mixture solution dropwise and allowed additional stirring for 30 min. The pH of the reaction solution was adjusted to 4.75 using 1 M HCl and 1 M NaOH. For the 10 and 20% GA modification, 0.15 mmol (29 mg, 0.15 equiv) and 0.30 mmol (57.5 mg, 0.30 equiv) of EDC were added, respectively. The mixture was stirred overnight. The reaction mixture was then loaded into a dialysis bag (Spectra Por-6, MWCO 3500 g/mol) and dialyzed against dilute HCl (pH = 3.5) containing 100 mM NaCl (6 × 2 L, 48 h) and then dialyzed against deionized water (4 × 2 L, 24 h). The solution was lyophilized to obtain a white solid fluffy material. The conjugation of gallic acid and the degree of modification of gallic acid in the hyaluronic acid was further ascertained by the presence of distinctive aromatic peaks at 6.98 and 6.93 ppm of GA in the 1H NMR spectrum. The HAGA synthesis is displayed in Figure S-3.

Preparation of pH-Responsive Precursors. All precursors were prepared at a concentration of 5% w/v in DPBS. The PI, Irgacure 2959, was added into the HAMA precursor at a concentration of 0.5% w/v. The precursors of HAGA and HAMA were mixed into a ratio of 1:1 with two formulations: HAGA10-HAMA15 and HAGA20-HAMA15. The pH of all precursor formulations was slowly adjusted using 0.5 M NaOH and varied into acidic (pH = 4 and 5), neutral (pH = 7), and basic (pH = 8 and 9) pH.

pH-Dependent Rheological Behavior of Precursors. The rheological characterizations were carried out on a rheometer (Discovery HR-2, TA Instruments Inc., USA) using a plate-to-plate geometry with a diameter of 12 mm. Different formulations of precursor with different pH were measured using flow mode. The measurements were made at 37 °C. The rheological tests of precursors were in situ photopolymerization (gelation time), flow measurements, and recovery behavior. The flow measurement (shear-thinning and yield stress) was carried out at a shear rate of 1−200 s^{-1} to determine the viscosity and flow behavior. For recovery behavior, the measurement was performed by using three intervals of a low shear rate (0.01 s^{-1} for 200 s), followed by a high shear rate (500 s^{-1} for 100 s) and finally, a low shear rate (0.01 s^{-1} for 200 s) to screen the viscosity recovery of precursors after extrusion. The gelation time of the precursors was quantified via in situ photopolymerization using a rheometer with an external UV lamp (BlueWave 50 UV curing spot lamp, DYMAX Corp., USA). Shear-thinning coefficients and yield stress were calculated using the Power-Law Equation and the Herschel−Bulkley model, as previously described[7,21] and explained in the Supporting Information (eqs S-1, S-2). The viscosity of the precursors at high pH was obtained from the Cox-Merz rule (eq S-3) and transformed from the oscillatory measurement (frequency sweep, 0.1−500 rad/s, constant strain 1%).

Prescreening of Injectability and Printability. The injectability of the hydrogels was confirmed using a commercial needle with a diameter of 22G (BD MicrolanceTM 3, Becton Dickinson S.A.). For printability, we followed simple prescreening protocols published previously:[7,21] filament formation and stackability tests. The different precursor formulations were loaded into a 1 mL syringe and capped with 410 μm steel nozzle types. The nozzles were purchased from Nordson EFD, Germany. The precursor filament was formed in air at RT (24 °C) and at 37 °C to observe filament quality and extrudability and then deposited on the glass surface to investigate the stackability. The images of filaments were captured using a camera (Theta Lite, CMOS 1/2" USB 3.0 digital camera with fixed zoom, resolution of 1280 × 1024 pixels, Biolin Scientific, Sweden). Based on our previous studies (Figure 1), we defined the prescreening test for biomaterial ink printability and divided filaments into three categories: droplet, smooth, and irregular filament. A droplet filament indicates that the extruded precursor is too liquid and is not recommended for 3D bioprinting. A smooth filament, on the other hand, indicates that the extruded precursor exhibits smooth, uniform, and consistent filament, which is considered a good candidate for 3D bioprinting. An irregular filament indicates an over-gelation condition of the precursor, exhibiting the nonuniformed and fractured filament after being extruded from the nozzle.

Evaluation of Printability. Filament quality checkup and 3D printing ability were assessed to determine the printability of precursor formulations. The most optimal precursor formulation was described as "ink" and printed using an extrusion-based 3D bioprinter (Brinter One, Brinter Ltd., Finland). A 410 μm steel nozzle was used in all printing tests. The ink filament checkup was done by printing lines with different pressure and printing speed values. Extrusion pressure ranged between 2000 and 3000 mbar, and the printing speed was set to 4, 6, or 8 mm/s. The filament widths were captured and measured using Image processing software (Fiji-ImageJ). The filament widths were compared to the nozzle size to determine the printability. After that, the best printing parameters were chosen to continue with multilayer printing (two and four-layered grid structure). The shapes of the pores in the printed grids were evaluated to obtain the pore geometry and *Pr* value (Figure S-11, eq S-4), as previously described.[21] The four-layered grid structures were printed to assess the inks' ability to support the weight of each layer while maintaining the printing resolution without collapse. The

https://doi.org/10.1021/acsami.3c02961
ACS Appl. Mater. Interfaces 2023, 15, 33972−33984

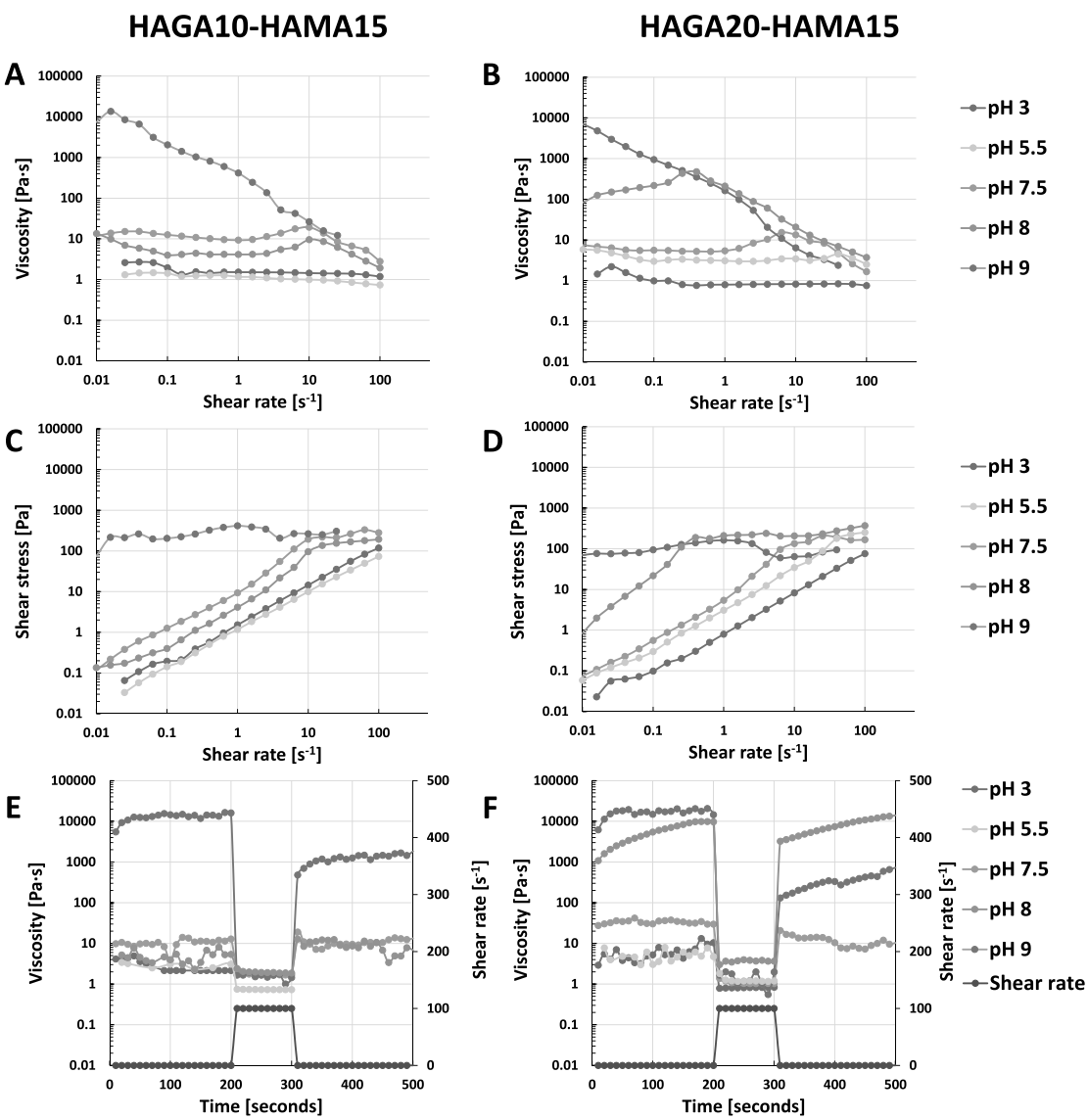

Figure 3. Rheological measurements of precursor mixtures of HAGA10-HAMA15 and HAGA20-HAMA15 at different pH (3, 5.5, 7.5, 8 and 9): shear-thinning (A, B), yield stress (C, D), and recovery behavior (E, F) at 37 °C.

multilayered structures were postcured using the bioprinter's integrated UV/vis LED module at a wavelength of 365 nm with 25 mW/cm^2 intensity for 120 s.

Hydrogel Preparation. The pH of precursor formulations was adjusted into acidic (pH 5), neutral (pH 7), and basic (pH 8). After that, the precursors were cast into the molds (2.5 mm height, diameter of 12 mm) and were left for 30 min to settle down. Next, the precursors were exposed to 365 nm UV light (25 mW/cm^2) for 120 s (BlueWave 50 UV curing spot lamp, DYMAX Corp., USA).

Mechanical Properties of Hydrogels. To evaluate the viscoelastic behavior of the hydrogels with and without photo-crosslinking, oscillatory measurement was employed using a rheometer with a plate-to-plate geometry (12 mm of diameter). The amplitude sweep was carried out to determine the linear viscoelastic region of the materials (0.1−100% strain). Subsequently, frequency sweep measurements were carried out from 0.1 to 100 Hz at a fixed strain of 1% and at a gap distance of 2.5 mm at 25 °C. The storage and loss moduli (G', G'') correlating to the elastic and viscous attributes of the hydrogel samples were measured and calculated into loss tangent (tan δ). Stress relaxation was also measured with a rheometer (12 mm plate-to-plate geometry) to evaluate the effect of gallic acid in hydrogels compared to plain HAMA hydrogel. The hydrogel samples were tested with 20% strain at a constant rate for 500 s, giving the stress response over time. Crosslinking density (n_e, mol/m^3) and average mesh size (ξ, nm) were estimated by calculating the difference between G' and G'' (eqs S-5, S-6). To screen the strain recovery or self-healing behavior of the hydrogels, G' and G'' were measured under the repeating seven cycles of low (1%) and ultrahigh

https://doi.org/10.1021/acsami.3c02961
ACS Appl. Mater. Interfaces 2023, 15, 33972−33984

oscillation strain (800%) conditions at 25 °C and oscillation frequency remained constant at 1 Hz, using 12 mm diameter stainless steel parallel plate geometry. The holding period of each cycle was set at 60 s. The self-healing properties of GA-based hydrogels were evaluated via a cutting-healing method. The hydrogels were first cut into two separate pieces, after which the cut edges were faced together at 37 °C for 30 min.

pH-Dependent Swelling of Hydrogels. All hydrogel samples with and without postcrosslinking were immersed in 0.1 M phosphate-buffered saline (PBS) solution with different pH (5, 7, and 9) to examine their stability (K_2HPO_4 and KH_2PO_4 were varied from 5.841 and 94.16 mM to 93.48 and 6.523 mM to obtain the desired pH). The hydrogels were maintained at 37 °C ± 0.5 °C in a shaking incubator at 90 rpm until various time points (0, 1, 2, 3, 5, 7, and 15 days). At the zero time point, the samples were defined with a weight of W_0. At every time point, the samples were removed from the solution, and the residual solution from the surface was removed to obtain the W_s. The swelling ratio was calculated as W_s/W_0.

Degradation Study. Enzymatic degradation of the material was performed using hyaluronidase at a concentration of 50 U/mL in DPBS at pH 7.4. Three parallel hydrogel samples of 250 μL HAMA15, HAGA10-HAMA15, and HAGA20-HAMA15 were prepared in the molds. Similarly to the swelling test, hydrogel samples were submerged in 1 mL hyaluronidase DPBS solution until various time points (0, 1, 2, 3, 5, and 7 days). At the zero-time point, the samples were defined as having an initial weight of W_0. At every time point, the samples were removed from the hyaluronidase buffer, the residual buffer from the surface was removed to obtain the W_m, and the enzyme buffer was replaced after each measurement. The degradation weight percentage was calculated as $W_m/W_0 \times 100$.

Adhesive Properties. A tack test was performed for HAMA and HAGA-HAMA using a rotational rheometer at RT to observe the adhesive properties. The protocol has been reported in a previous study.[2] In brief, chicken skins and porcine muscles (freshly purchased from the market) were carefully cut into circular sheets having a 12 mm diameter and attached to the upper and bottom plates. Next, the precursors were injected between two tissue layers. The upper plate with the attached animal tissue was then pressed with a uniform compressive force (0.1 N) for 120 s to settle the tissue and the precursor. Subsequently, hydrogels were formed by in situ photocrosslinking with a UV lamp for 120 s. Thereafter, the upper plate was pulled up in axial motion at a constant velocity of 20 μm/s. The change in axial force was recorded at the point of detachment. A graph was then plotted to observe the influence of gallic acid on the adhesive properties of the precursor compared to HAMA without gallic acid. Each test contained five parallel samples. The tissue used for the adhesive study was moist throughout the measurement.

Antioxidant Properties. Free radical scavenging activity of HAGA-HAMA was evaluated using the DPPH (2,2,1-diphenyl-1-picrylhydrazyl) method.[36] HAGA was dissolved in DI water at 30 μg/1 mL concentration, followed by 1 mL of DPPH solution (1 mg/12 mL in methanol). After incubation at 25 °C for 30 min, the absorbance was measured at 517 nm using a UV−vis spectrophotometer. The DPPH scavenging activity (%) was calculated from eq 1.

$$\text{DPPH scavenging activity (\%)} = \frac{A_1}{A_2} \times 100 \quad (1)$$

where A_1 is the absorbance of DPPH solution in the presence of samples, and A_2 is the absorbance of blank DPPH solution that was used under the same reaction conditions in the absence of synthesized polymers.

Statistical Analysis. The results of the oscillatory measurements were presented as mean ± standard deviation (SD). The analysis was performed using Student's *t*-test to determine the differences between groups, and the significance was defined at $p < 0.05$.

■ RESULTS

Development of pH-Responsive Precursors. The HAGA precursors were synthesized with calculated modification degrees of 10 and 20% and were obtained as ∼12 and ∼21%, as confirmed by H1-NMR (Figure S-8A,B and Figure S-9A,B). The degree of methacrylation of the HAMA15 precursor was approximately 16%, quantified by H1-NMR (Figure S-10A,B). According to the appearance, the precursors were liquid under acidic conditions (pH 3−5), gained more viscosity at pH 7.5−8, and became true hydrogels under basic conditions (pH 8.5−9). The preliminary testing was performed to screen the precursors' injectability and printability after extruding from the nozzle. In Figure S-12, at pH 3−7.5, the precursor displayed a droplet-like filament, whereas the filaments of the precursor at pH 7.5−8 were coherent. The precursor at pH > 8 was unable to form a coherent filament; instead, it was irregular and too solid. In addition, 5% w/v of HAMA precursor displayed a liquid-like filament and was not a good candidate for 3D bioprinting (Figure S-15A).

Flow Behavior of pH-Responsive Precursors. Figure 3 illustrates the flow curve of shear-thinning and recovery behavior of precursors at different pH. The values of shear-thinning coefficients and yield stress were used to explain the injectability and printability. In detail, all precursors at low pH (3−5) exhibited low viscosity and behaved liquid-like. This was confirmed by the shear-thinning coefficients of $n > 0.9$ (Table S-1), describing the precursor as a Newtonian fluid. The precursors started to gelate when the pH reached 7.5, resulting in higher viscosity as the pH increased.

At acidic and neutral pH, all precursor formulations were liquid and partially slipped out of the plate-to-plate geometry after applying the shear. According to the viscosity curve of HAGA10-HAMA15 at pH 7.5−8 (Figure 3A), Newtonian behavior was observed at a low shear rate, revealing the extended plateau region, finally demonstrating non-Newtonian behavior at 10 s^{-1} shear rate. The values of shear-thinning coefficients are listed in Table S-1. On the other hand, as shown in Figure 3B, HAGA20-HAMA15 at pH 5−7.5 was weakly shear-thinning as the viscosity started to drop at a high shear rate (above 10 s^{-1}). HAGA20-HAMA15 at pH 8 showed improvement in shear-thinning behavior at a shear rate above 1 s^{-1}, giving $n < 0.2$ (Table S-1). In addition, HAGA10-HAMA15 and HAGA20-HAMA15 at pH 8 did not have high yield stress, implying that high printing pressure is not required to extrude the material (Figure 3C,D). The recovery behavior graphs are represented in Figure 3E,F. HAGA20-HAMA15 at pH 8 rapidly recovered to its original viscosity (∼80%) after removing the high shear rate. In contrast, at pH 9, HAGA10-HAMA15 and HAGA20-HAMA15 lost half of their viscosity after removing the shear.

At pH 9, both HAGA10-HAMA15 and HAGA20-HAMA15 became true hydrogels. The Power-Law model was applied, and shear-thinning coefficients of $n < 0.2$ were obtained. In contrast, they required high shear stress to reduce the viscosity and could not recover their original viscosities (∼40−50% recovery). Based on the rheological results, HAGA20-HAMA15 at pH 8 provided high viscosity, proper yield stress, shear-thinning properties, and recovery behavior. Hence, it was selected as the biomaterial ink candidate for injecting and 3D printing tests. In addition, in situ photopolymerization (Figure S-13) shows the gelation time of all precursor formulations at different pH after being exposed to UV light (storage modulus as a function of time).

Evaluation of Printability. After the printability of precursors was prescreened using filament analysis (filament

https://doi.org/10.1021/acsami.3c02961
ACS Appl. Mater. Interfaces 2023, 15, 33972−33984

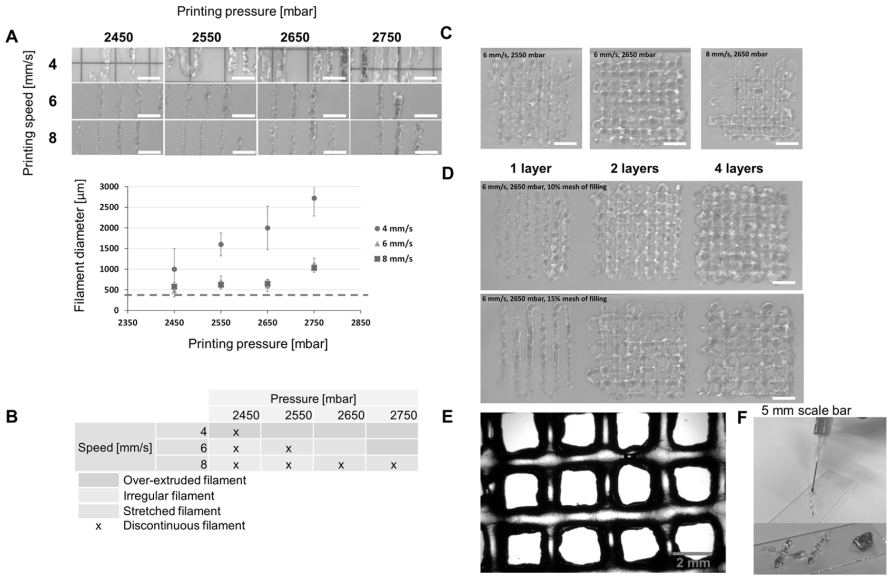

Figure 4. Printability of biomaterial inks (HAGA20-HAMA15 at pH 7.5−8, 37 °C) and 3D printing tests. (A) Filament of printed biomaterial inks with various pressure and printing speed values. The graph illustrates how filament diameter is affected by pressure and printing speed. The red line is used as a guideline to compare the filament diameter with the actual nozzle size. The error bars indicate the standard deviation of filament diameter for each ink, presented as mean (n = 10) ± SD. (B) Printability window: an over-extruded filament (red color), irregular filament (yellow color), stretched filament (green color), or discontinuous filament (x symbol). (C) Images of two-layer printed grids to screen the optimal printing parameters. (D) Images of multilayer printing of one, two, and four layers using the optimal printing parameters and different filling percentages to determine the achievable printing resolution. (E) Example of a microscopic image of an optimal printed grid structure for *Pr* value calculation and stackability of 2 filament layers (6 mm/s, 2650 mbar). (F) Example of the prescreening results of injectability and stackability of biomaterial inks.

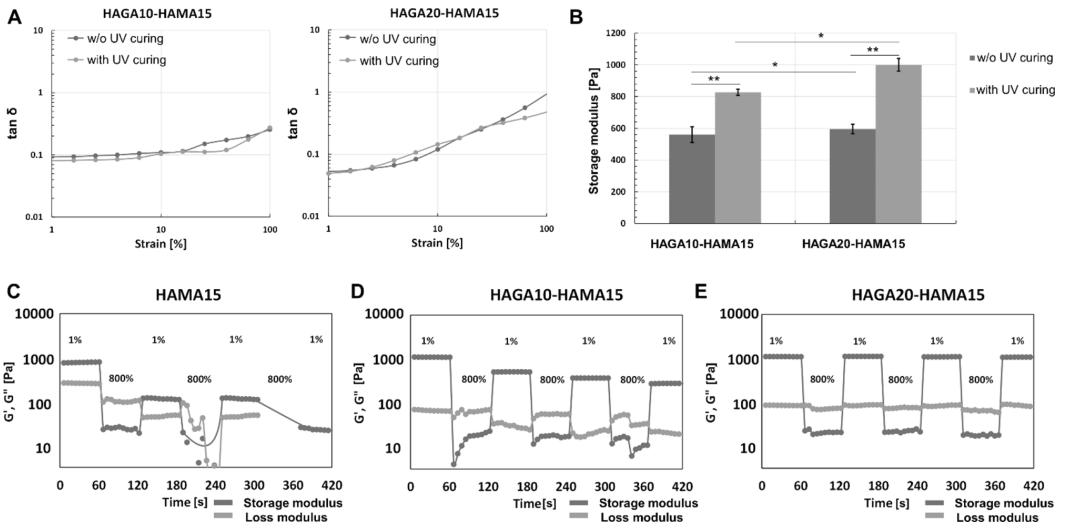

Figure 5. Oscillatory measurements of all hydrogel samples, tested using frequency and amplitude sweeps. (A) tan δ value, calculated from the ratio between G' and G'' from the amplitude sweep to observe the viscoelasticity of hydrogels (with and without UV). (B) Storage moduli of hydrogels (with and without UV) obtained from the linear region of amplitude and frequency curves. The error bars indicate the standard deviation of storage modulus for each ink, presented as mean ± SD (n = 10, *p < 0.05, **insignificant). (C−E) Comparison of strain recovery behavior of hydrogels with the complementary network (HAGA10-HAMA15 and HAGA20-HAMA15) and without the complementary network (HAMA15). The strain recovery behavior was measured through seven cycles of strain (1% strain → 800% strain → 1% strain).

https://doi.org/10.1021/acsami.3c02961
ACS Appl. Mater. Interfaces 2023, 15, 33972−33984

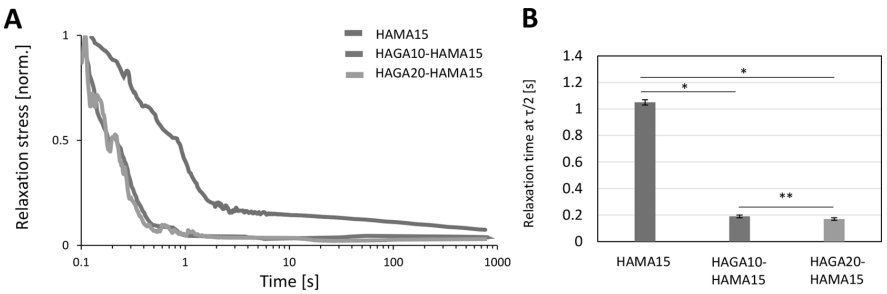

Figure 6. Stress relaxation tests on HAGA-HAMA and HAMA hydrogels. (A) Hydrogel samples were tested with 5% strain, which was then held at a constant rate for 1000 s. (B) Quantification of stress relaxation in the time scale at which the stress is relaxed to half of its initial value. The error bars indicate the standard deviation of storage modulus for each ink, presented as mean ± SD (n = 10, *p < 0.05, **insignificant).

formation and stackability) and rheology (shear-thinning, yield stress, and recovery behavior), the integrity of multilayered constructs and the effect of printing parameters were evaluated using *Pr* value calculation and filament width measurement. Figure 4A shows the printed filaments at different printing conditions. Low printing speed (4 mm/s) fed excessive ink on the printing bed, resulting in over-deposited filaments. However, the ink started to extrude at the pressure of 2450 mbar and could not form a smooth filament. The printing speeds of 6 and 8 mm/s resulted in continuous thin filaments having thickness close to the nozzle diameter. Figure 4A also shows the measured filament thicknesses compared to the nozzle size. However, some discontinuous filaments were observed at the pressure values of 2450 and 2550 mbar. The thickness of filaments can be used to predict the accuracy of the printing process.[37] The thickness of continuous filaments was around 577 ± 8 μm. The printing pressure of 2650 mbar and a speed of 6 mm/s resulted in a continuous filament and were chosen for multilayered grid (2 × 2 cm^2) printing. The filament characteristics and printing parameters were collected in the table and marked as the printability window to narrow the printing parameters (Figure 4B). The red color indicates over-extruded filaments caused by too high printing pressure and speed. The irregularly shaped filaments caused by unfeasible printing speed with proper pressure were marked with yellow. The green color shows the part of the printability window where the printing pressure and speed meet the minimum requirements, giving well-defined filaments. The x symbol demonstrates the filament breakage during the printing, yielding poor printing results. Figure 4C visualizes how irregular grid structures were formed if inappropriate printing parameters were chosen. Figure 4D shows the successful 3D printed grids (2 and 4 layers) using optimized printing parameters with different degrees of filling for the CAD model (to change the size of the internal pore size in the grid). The printability of HAGA20-HAMA15 was evaluated by varying the printing parameters, such as printing pressure (2450−2750 mbar) and speed (4−8 mm/s). Ideally, the proper printing parameters provide stability and shape fidelity for the printed structure, which allows the 3D stacking of filaments in a layer-by-layer fashion. Figure 4F shows the result of injectability and stackability of HAGA20-HAMA15 using a commercially available needle at RT and 37 °C. The material was stackable on the glass slide. Subsequently, the *Pr* values were calculated from the grid constructs from the optimal printing parameters (Figure S-16 and Table S-2).

Viscoelastic Properties of Hydrogels. The storage moduli of hydrogels were evaluated using oscillatory measurement (amplitude and frequency sweeps) with and without photocrosslinking (Figure 5). As mentioned in the Materials and Methods section, HAGA-HAMA formulations were adjusted to basic pH to be gelated into true hydrogels. The rheological analyses represented that with and without UV curing, gels remained stable during the rheological testing. Both formulations consistently yielded higher storage moduli after photocrosslinking (560 ± 11, 827 ± 26, 595 ± 12, and 1060 ± 25 Pa for HAGA10-HAMA15 without UV-curing, UV-cured HAGA10-HAMA15, HAGA20-HAMA15 without UV-curing, and UV-cured HAGA20-HAMA15, respectively). Moreover, Figure 5A demonstrates that UV-cured and hydrogels without UV-curing resulted in viscoelasticity and high stability (tan δ values lower than 1), but there were no significant differences between the two formulations (Figure 5B). The average mesh sizes (ξ) and crosslinking densities (n_e) were calculated using eqs S-5 and S-6 and are listed in Table S-3. Stress relaxation on HAMA and HAGA-HAMA gels was evaluated to observe the effect of GA functionalization in the hydrogel networks. As shown in Figure 5C−E, the dynamic strain recovery properties of the complementary network hydrogels were assessed using the continuous seven-step strain (1% strain → 800% strain → 1% strain). At high strain (800%), the hydrogels reached the critical strain, which was converted into a viscous state (G'' dominates G'). At low strain (1%), the hydrogels exhibited an elastic state (G' dominates G''). During the cyclic test, the rapid transition between elastic and viscous states between low and high strain indicates the strain recovery behavior of the hydrogels. The HAGA-HAMA hydrogels showed high elastic recoverability of the polymeric networks (especially HAGA20-HAMA15), suggesting the dynamic nature of the complementary network between gallol moieties and photocrosslinking. In contrast, HAMA15 groups lost their original properties after the first high strain. Figure 6A confirms that HAGA-HAMA hydrogels have enhanced stress relaxation behavior. When comparing the relaxation behavior of HAMA15, HAGA10-HAMA15, and HAGA20-HAMA15, we observed that the HAGA-HAMA groups displayed a faster relaxation time (at 0.5 relaxation stress), which was approximately 0.2 ± 0.01, 0.18 ± 0.01, and 1.05 ± 0.02 s for HAGA20-HAMA15, HAGA10-HAMA15, and HAMA15 respectively, as shown in Figure 6B. However, the relaxation amplitude and relaxation time between HAGA10-

https://doi.org/10.1021/acsami.3c02961
ACS Appl. Mater. Interfaces 2023, 15, 33972−33984

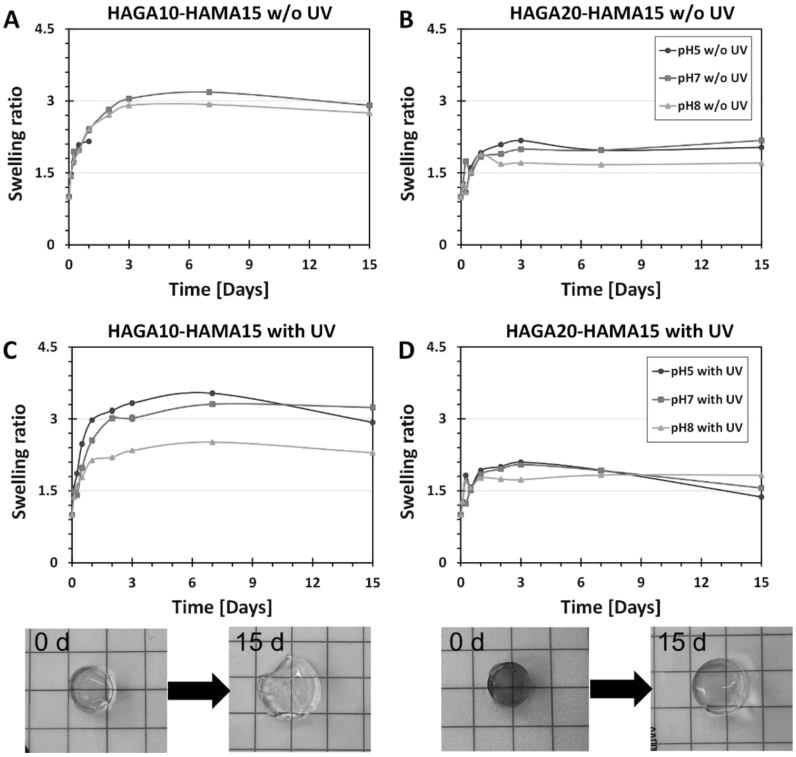

Figure 7. Time-dependent swelling behavior of HAGA10-HAMA15 and HAGA20-HAMA gels (n = 10, the error bars indicate the SD) as a response to different pH (5−8). The swelling ratio of hydrogels (A) HAGA10-HAMA15 and (B) HAGA20-HAMA15. The hydrogels before and after swelling are shown here as examples, 1 cm^2 grid scale.

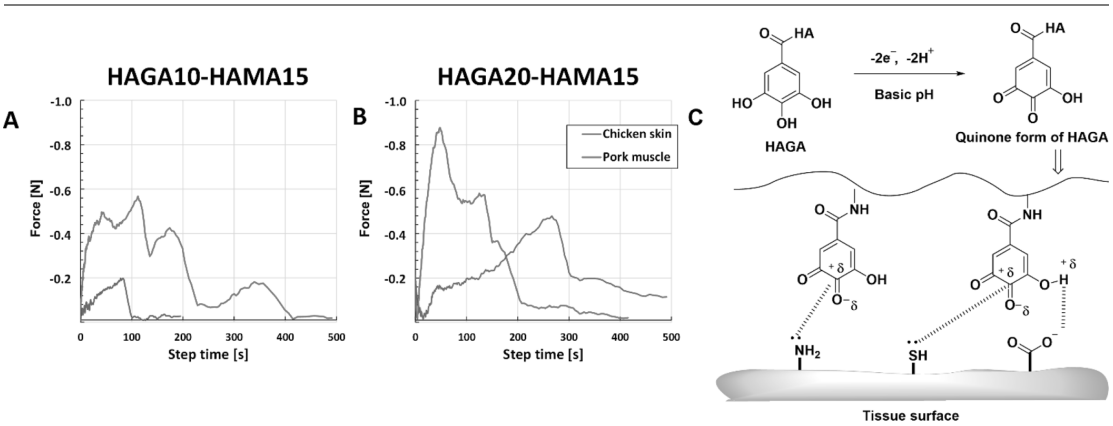

Figure 8. Measurement of tissue adhesion force of hydrogels (n = 4) (A) HAGA10-HAMA15 and (B) HAGA20-HAMA15 by the tack adhesion test. The precursors were in situ photocrosslinked and adhered to the surface of animal tissues. (C) Adhesion chemistry between hydrogels and the tissue surface due to nucleophilic group interactions and quinone.

HAMA15 and HAGA20-HAMA15 were not significantly different.

pH-Dependent Swelling of Hydrogels. The swelling studies were performed to investigate the stability of the HAGA-HAMA gels (with and without UV curing) under physiological conditions (pH 7.4) and at acidic conditions (pH 5.0), in which the GA modification starts to degrade, and at basic conditions (pH 8.0) (Figure 7). HAGA10-HAMA15 hydrogels without photocrosslinking (Figure 7A) disintegrated after the first time point of observation in the acidic conditions, but HAGA20-HAMA15 hydrogels without photocrosslinking (Figure 7B) were stable until the end of the observation. In

https://doi.org/10.1021/acsami.3c02961
ACS Appl. Mater. Interfaces 2023, 15, 33972−33984

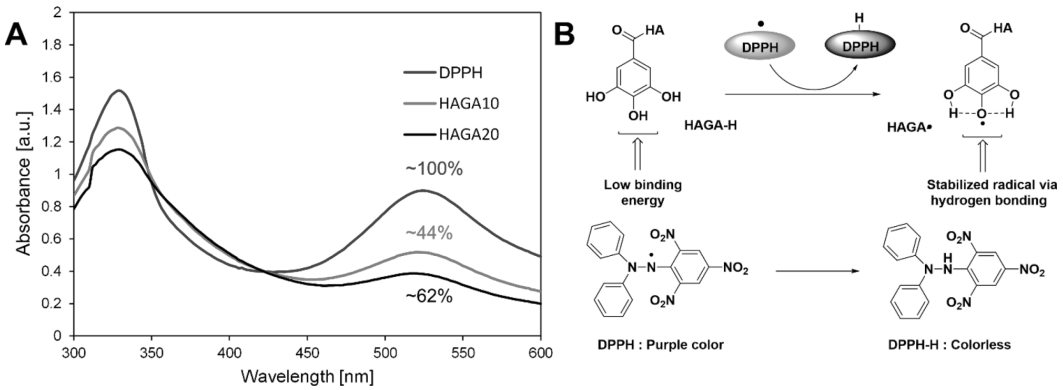

Figure 9. Antioxidant properties of HAGA10 and HAGA20. (A) UV−vis spectrum of HAGA10 and HAGA20 exhibited a reduction of absorbance at 530 nm, compared to DPPH alone. (B) DPPH radical scavenging mechanism that is responsible for the antioxidant activity of HAGA.

contrast, both UV-cured HAGA10-HAMA15 (Figure 7C) and HAGA20-HAMA15 (Figure 7D) hydrogels showed rapid initial swelling followed by degradation in acidic buffer, but the HAGA20-HAMA15 gels displayed a significantly lower swelling ratio (∼4.1 ± 0.03 and ∼2.2 ± 0.02 swelling ratio, respectively). Under physiological conditions and at basic pH, HAGA20-HAMA15 gels (with and without UV) were stable, but HAGA10-HAMA15 gels at pH 7 swelled more than HAGA20-HAMA15 gels.

Adhesive Properties. A tack test was performed to investigate the tissue adhesive properties of different inks using chicken skin and porcine muscle. Both HAGA10-HAMA15 (Figure 8A) and HAGA10-HAMA15 (Figure 8B) showed tissue adhesive properties. However, a higher modification degree of GA (HAGA20) required higher force to pull the tissue from the in situ photocrosslinked hydrogels (negative force) compared to gels with a lower modification degree of GA (HAGA10). Figure 8C shows the mechanism of wet adhesion on tissue surfaces.

Antioxidant Properties. A DPPH radical scavenging assay was used as a preliminary assessment of the changes in the antioxidant properties upon modification of HA with GA. The DPPH reagent underwent a visual change in color from deep purple to deep orange in HAGA10 and HAGA20 due to the antioxidant properties imparted by GA. The antioxidant properties of GA were confirmed again by comparing it with pure DPPH, which did not change its color, and was considered as 100% absorption. The UV−vis spectroscopy measurement of 30 μg/mL HAGA10 and HAGA20 in the presence of DPPH displayed ∼44 and ∼62% reduction in absorption (Figure 9A), indicating potential antioxidant properties. Figure 9B illustrates the mechanism of radical quenching by gallol moieties.

■ DISCUSSION

Among all kinds of stimuli-responsive hydrogels, pH-responsive hydrogels have been extensively explored due to their potential for various applications, such as injectable and self-healing hydrogels as well as drug delivery systems.[31] In addition, the pH-responsiveness in precursors enables control over the precursor viscosity and mechanical, swelling, and degradation properties of hydrogels. The pH-responsive precursors can be bioprinted at neural-basic pH (7.3−9.8) on damaged skin[31] and be triggered to degrade at low pH (4−6) on healed skin.[32] In bioprinted wound dressing applications, the pH-responsive non-Newtonian precursors enable the in situ bioprinting of the precursor in the wound and allow the shape-specific fitting and stability of the printed construct.[38]

In this study, we synthesized pH-responsive hyaluronic acid-(HA)-based precursors grafted with the gallic acid (GA) moiety (the degrees of GA functionalization were ∼10 and 20% with respect to the disaccharide repeat units). GA was conjugated to polysaccharides via carbohydrazide linkages utilizing the carboxylic group on the polymer backbone and hydrazide group from amine-functionalized GA using carbodiimide coupling chemistry.[1,39] The carboxylate residues of GA were modified to a hydrazide derivative as they are known to undergo proficient EDC coupling at acidic pH (4.7−4.8). The successful conjugation of GA was confirmed as the solution turned light brown at basic pH (∼8), indicating that GA functionalization was successful in the HA backbone, as also demonstrated in our previous study of GelMAGA.[36] We hypothesized that the precursor blend (HAGA-HAMA) would provide the pH-responsive properties necessary to improve both printability and injectability. We decided to test higher (20%) and lower (10%) gallic acid modifications to understand the effect of the gallic moiety on pH responsiveness. To simplify the study, the ratio between HAMA and HAGA was fixed to 1:1, and the HAMA hydrogel was used as a control.

A series of rheological characterizations were performed to study the pH-dependent precursor properties. Shear-thinning behavior in non-Newtonian precursors has been used in several research studies to show the printability of precursors.[20,40] The Power-Law model was applied to the flow curve to calculate the shear-thinning coefficients (n and K values). These coefficients were used to prescreen whether the precursor is injectable or printable. In general, the linear region from the viscosity−shear rate curve has been used for the Power-Law trendline fit.[7,18,36] HAGA-HAMA precursors undergo a rapid sol−gel transition between pH 7.5 and 8, which results in increased viscosity at higher pH levels due to denser crosslinked network formation via oxidized gallol moieties. However, the precursor at basic pH became the true hydrogel and slipped from the parallel plate at high-velocity centrifugal movement during the measurement. Therefore, the Cox−Merz rule was applied to convert the frequency sweep to a viscosity-

https://doi.org/10.1021/acsami.3c02961
ACS Appl. Mater. Interfaces 2023, 15, 33972−33984

shear rate graph (eq S-3 and Figure S-14). The Cox−Merz rule is a correlational relationship that can predict the shear rate-dependent viscosity based on the oscillatory data.[41] We applied the rule when the measurement of precursors became impossible at a shear rate above 5 s^{-1} due to the rotational movement of the geometry. Precursors at acidic pH had an n value close to 1, which led to droplet formation. On the other hand, precursors at neutral and basic pH had an n value below 0.2, making them highly shear-thinning. To further evaluate the printability, the recovery behavior of the precursors was evaluated. Upon removal of the high shear rate, HAGA20-HAMA15 at pH 8 recovered its initial viscosity, suggesting the thixotropic behavior.

In general, the precursors for injecting and 3D bioprinting must exhibit shear-thinning behavior, displaying a decreasing dynamic viscosity as a function of increasing shear rate and also have the recovery behavior as well as the ability to stack layer-by-layer during printing.[18,38] According to the results, precursor formulations at neutral pH could not provide enough stackability, as the filaments merged after being deposited on the substrate. We have recently shown that the rheological data alone cannot guarantee a 100% success rate for printing.[7,21] To confirm the printability, the printability window was formulated to provide the influence of printing pressure and printing speed on the filament diameter and quality, giving the proper printability data. When the pressure was increased, filaments swelled, leading to poor accuracy. Increasing the printing speed resulted in thinner filaments but could also cause discontinuous filaments if the speed did not match the pressure. To investigate the feasibility of 3D printing HAGA20-HAMA15 at pH 7.5−8, 3D cylinders were printed to observe the stackability of multilayered structures (Figure S-17). We found that the cylinders with lower heights of 1 and 2.5 mm could stack successfully. However, the structural integrity of 5 mm cylinders was poor due to the ink's inability to support its weight, which resulted in structural collapse after the fifth layer was printed.

The pH-induced crosslinking, together with photocrosslinking, provided a complementary network in the HAGA-HAMA hydrogel. To verify the gallol-mediated complementary network formation in the HAGA-HAMA hydrogels, we performed oscillatory and stress relaxation measurements. We observed the complementary network of HAGA-HAMA before and after photocrosslinking, and we found that HAGA-HAMA displayed more stress relaxation than HAMA alone. According to Chaudhuri et al., living tissues behave viscoelastic and have stress relaxation.[42] The addition of photocrosslinking led to increased storage modulus, higher crosslinking density and more elastic gels (tan δ), indicating more stable matrix formation. In general, GA functionalized hydrogels possess strain recovery and self-healing behavior.[1,2,34] Therefore, a series of rheological recovery tests were conducted with G' and G'' under the seven cycles of low and high strain to determine the superiority of complementary networks in hydrogels. After the first cycle, HAMA hydrogels lost their initial G' value because HAMA hydrogels were covalently formed by a single network, resulting in brittleness in the hydrogel structure.[43] The strain recovery of hydrogels may increase due to the addition of secondary crosslinking, such as interpenetrating and complementary network.[1,13,44,45] According to the results, the G' of the HAGA10-HAMA15 and HAGA20-HAMA15 hydrogels under high dynamic strain decreased due to the deformation of the hydrogel network. After the low strain, they quickly returned to the original G' value as the hydrogel construct recovered, especially in hydrogels with higher GA modification. In addition, the self-healing properties of the HAGA20-HAMA15 hydrogels were evaluated using a cutting-healing test. After 30 min of incubation at 37 °C, the separated hydrogel discs were merged with each other (Figure S-18). However, HAGA-HAMA hydrogels at high basic pH levels produced a brownish color, which might reduce the transparency of the precursor, affecting the UV light penetration and hindering photocrosslinking. Hence, the results of in-situ photorheology (Figure S-13) showed a slight improvement in storage modulus upon UV exposure. Moreover, GA has been proven to be an antioxidant, leading to radical inhibition, ultimately reducing the degree of photocrosslinking.

The pH-dependent swelling was investigated to further confirm the concept of the complementary network and controlled swelling properties of HAGA-HAMA hydrogels. The acidic media pH led to higher water uptake and increased the swelling of hydrogels. At basic and neutral media pH, the GA hydrogels exhibited stable swelling over the period of observation. The HAGA20-HAMA15 hydrogels illustrated a slower swelling rate than the HAGA10-HAMA15 hydrogels, especially after day 1. The complementary network limited the hydrogel swelling and reduced the average mesh size (ξ), resulting in reduced water uptake into the hydrogels. According to the previously published studies,[46,47] crosslinking density (n_e) and average mesh size (ξ) influence hydrogel's swelling capacity. The higher crosslinking density results in additional network formation; subsequently, the network structure of hydrogel is formed, which reduces the water absorption. To further confirm the gallol-mediated complementary network formation in the HAGA-HAMA hydrogels, an enzymatic degradation study was performed in the presence of hyaluronidase in DPBS at pH 7.4, as shown in Figure S-19. Both groups of HAGA-HAMA hydrogels exhibited slower degradation than the plain HAMA hydrogel, especially after day 1. The HAMA hydrogels degraded quickly after 4 days, and the remaining mass was lost at the end of the observation. The interpenetrating crosslinking between photocrosslinking and gallol-mediated network in the HAGA-HAMA hydrogels limited their enzymatic degradation by bulk erosion, resulting in a slower degradation that proceeded through surface erosion.

In general, HA has been shown to enhance wound healing and modulate inflammation.[34] GA possesses a large variety of bioactive characteristics, including anti-carcinogenic, anti-mutagenic, and anti-inflammatory properties.[34] Recently, we have shown that a GA-functionalized GelMA displayed antioxidant and tissue adhesive properties.[36] We aimed to incorporate the advantages of two moieties into our precursor by grafting GA on the HA backbone. The tissue adhesive behavior of the HAGA-HAMA was determined by a tack test. HAGA20-HAMA15 displayed a high negative force with chicken skin and pork muscles compared to HAGA10-HAMA15. Our developed HAGA-HAMA blends showed a significantly stronger adhesion compared to previous reports on tissue adhesive hydrogels with similar functionalization.[2] The surface of biological tissues has a variety of amino acids that has several nucleophilic groups available for interaction with electrophilic groups.[48] Although the exact mechanism for tissue adhesion is unclear, we anticipate that catechol groups on the gallic acid oxidized to a quinone provide adhesion to biological tissues by forming covalent bonds with the residual

https://doi.org/10.1021/acsami.3c02961
ACS Appl. Mater. Interfaces 2023, 15, 33972−33984

nucleophilic moieties (amines, thiol, and hydroxyl groups) on the tissue surfaces.[49] This tissue adhesion in a moist environment paves the path for developing the class of biomaterials that can be used as bio-glue in contact with the body fluids. The biomaterial inks without tissue adhesion may detach from the substrate or the formerly printed layers during the printing process, which results in poor resolution and structural deformation.

Antioxidant properties of HAGA-HAMA were confirmed by the DPPH radical quenching assay, which was used as a preliminary test to estimate the antioxidant properties upon the incorporation of gallic acid. The catechol group is known to scavenge free radicals and show antioxidant properties. In addition, GA derivatives have also been found in many phytomedicines with various biological and pharmaceutical activities, including free radical scavenging effect, induction of cancer cell apoptosis, and protection of cells from UV- or irradiation-induced damage.[49] As shown in Figure 9B, the GA derivatives demonstrate antioxidant properties due to the formation of radical intermediate on the para-hydroxyl group stabilized by strong intramolecular hydrogen bonding.[50]

■ CONCLUSIONS

The HAGA precursor with pH-responsive properties can be blended with other nonviscous precursors to improve the processability (printability, type of crosslinking and gelation time), printing accuracy, and tissue attachment. The complementary network of HAGA-HAMA hydrogels formed via pH change and photocrosslinking enhanced the viscoelasticity properties and the stability of hydrogels. HAGA-HAMA hydrogels exhibited controlled swelling properties, were capable of swelling under acidic conditions and became stable at neutral and basic pH. Moreover, the presence of GA moiety in the hydrogel network offered antioxidant and tissue-adhesive properties. Overall, we provided the fundamental connection of chemistry, rheology, and 3D fabrication, which can help to standardize the 3D bioprinting protocol from bioink development to post-processing. Moreover, our pH-responsive precursor is capable of opening a new venue for 4D bioprinting with several applications in tissue engineering and drug delivery.

■ ASSOCIATED CONTENT

Supporting Information

The Supporting Information is available free of charge at https://pubs.acs.org/doi/10.1021/acsami.3c02961.

Synthesis of hyaluronic acid methacrylate (HAMA), synthesis of a hydrazide derivative of gallic acid (GA-Hyd), synthesis of gallic acid conjugated hyaluronic acid (HAGA), ^{1}H-NMR spectra of methyl ester, 13C-NMR spectra of gallic acid methyl ester, ^{1}H-NMR spectra of GA-Hyd, 13C-NMR spectra of GA-Hyd, ^{1}H-NMR of HAGA10, ^{1}H-NMR of HAGA10 (expanded), ^{1}H-NMR of HAGA20, ^{1}H-NMR of HAGA20 (expanded), ^{1}H-NMR of HAMA15, ^{1}H-NMR of HAMA15 (expanded), pore geometry evaluation and calculation of the printability (*Pr*) value, filament quality of plain HAMA15, HAGA10-HAMA15 and HAGA20-HAMA15 at pH 3−5, 7.5−8 and >8, gelation time of HAGA10-HAMA15 and HAGA20-HAMA15, Power-Law model equation, Cox-Merz rule explanation, HAGA10-HAMA15 and HAGA20-HAMA15 after applying Power-Law and Cox-Merz rule, values of shear-thinning coefficients, HAMA15 and HAGA20-HAMA15 (neutral pH) printing test, *Pr* value calculation (equation), the example of biomaterial ink printability assessment from the macrostructure (HAGA20-HAMA15 at pH 7.5−8, *Pr* values of printed grid structures, 3D printed cylinder structures of HAGA20-HAMA15 at pH 7.5−8, crosslinking density and mesh size calculation equation, the calculated mesh size and crosslinking density values, self-healing behavior, and degradation study (PDF)

■ AUTHOR INFORMATION

Corresponding Author

Vijay Singh Parihar − *Biomaterials and Tissue Engineering Group, BioMediTech, Faculty of Medicine and Health Technology, Tampere University, 33720 Tampere, Finland;* orcid.org/0000-0002-6044-2121; Email: vijay.parihar@tuni.fi

Authors

Hatai Jongprasitkul − *Biomaterials and Tissue Engineering Group, BioMediTech, Faculty of Medicine and Health Technology, Tampere University, 33720 Tampere, Finland;* orcid.org/0000-0003-0646-7712

Sanna Turunen − *Biomaterials and Tissue Engineering Group, BioMediTech, Faculty of Medicine and Health Technology, Tampere University, 33720 Tampere, Finland; Brinter Ltd, 20520 Turku, Finland;* orcid.org/0000-0002-6823-8811

Minna Kellomäki − *Biomaterials and Tissue Engineering Group, BioMediTech, Faculty of Medicine and Health Technology, Tampere University, 33720 Tampere, Finland;* orcid.org/0000-0003-4321-1820

Complete contact information is available at: https://pubs.acs.org/10.1021/acsami.3c02961

Author Contributions

The manuscript was written through the contributions of all authors. Chemical modification and material characterizations have been carried out by H.J. and V.S.P. Data interpretation has been carried out by H.J., V.S.P, and M.K. All authors have given approval for the final version of the manuscript.

Notes

The authors declare no competing financial interest.

■ ACKNOWLEDGMENTS

The authors are grateful to The Centre of Excellence in Body-on-Chip Research (CoEBoC) by the Academy of Finland for financial support (decision #312409, #326587 and #336663) and to the Tampere University funding for the CoEBoC consortium.

■ ABBREVIATIONS

HA, hyaluronic acid
GA, gallic acid
HAGA, gallic acid-functionalized hyaluronic acid
HAMA, hyaluronic acid methacrylate
PI, photoinitiator

■ REFERENCES

(1) Shin, M.; Lee, H. Gallol-Rich Hyaluronic Acid Hydrogels: Shear-Thinning, Protein Accumulation against Concentration Gradients,

and Degradation-Resistant Properties. *Chem. Mater.* **2017**, *29*, 8211−8220.
(2) Samanta, S.; Rangasami, V. K.; Sarlus, H.; Samal, J. R. K.; Evans, A. D.; Parihar, V. S.; Varghese, O. P.; Harris, R. A.; Oommen, O. P. Interpenetrating Gallol Functionalized Tissue Adhesive Hyaluronic Acid Hydrogel Polarizes Macrophages to an Immunosuppressive Phenotype. *Acta Biomater.* **2022**, *142*, 36−48.
(3) Bagheri, A.; Jin, J. Photopolymerization in 3D Printing. *ACS Appl. Polym. Mater.* **2019**, *1*, 593−611.
(4) Zheng, Z.; Eglin, D.; Alini, M.; Richards, G. R.; Qin, L.; Lai, Y. Visible Light-Induced 3D Bioprinting Technologies and Corresponding Bioink Materials for Tissue Engineering: A Review. *Engineering* **2021**, *7*, 966−978.
(5) Lim, K. S.; Galarraga, J. H.; Cui, X.; Lindberg, G. C. J.; Burdick, J. A.; Woodfield, T. B. F. Fundamentals and Applications of Photo-Cross-Linking in Bioprinting. *Chem. Rev.* **2020**, *120*, 10662−10694.
(6) Hossain Rakin, R.; Kumar, H.; Rajeev, A.; Natale, G.; Menard, F.; Li, I. T. S.; Kim, K. Tunable Metacrylated Hyaluronic Acid-Based Hybrid Bioinks for Stereolithography 3D Bioprinting. *Biofabrication* **2021**, *13*, No. 044109.
(7) Jongprasitkul, H.; Turunen, S.; Parihar, V. S.; Annurakshita, S.; Kellomaki, M. Photocross-Linkable Methacrylated Polypeptides and Polysaccharides for Casting, Injecting, and 3D Fabrication. *Biomacromolecules* **2021**, *22*, 481−493.
(8) Giuseppe, M. d.; Law, N.; Webb, B.; Macrae, R. A.; Liew, L. J.; Sercombe, T. B.; Dilley, R. J.; Doyle, B. J. Mechanical Behaviour of Alginate-Gelatin Hydrogels for 3D Bioprinting. *J. Mech. Behav. Biomed. Mater.* **2018**, *79*, 150−157.
(9) Vorwald, C. E.; Gonzalez-Fernandez, T.; Joshee, S.; Sikorski, P.; Leach, J. K. Tunable Fibrin-Alginate Interpenetrating Network Hydrogels to Support Cell Spreading and Network Formation. *Acta Biomater.* **2020**, *108*, 142−152.
(10) Cao, N.; Chen, X. B.; Schreyer, D. J. Influence of Calcium Ions on Cell Survival and Proliferation in the Context of an Alginate Hydrogel. *ISRN Chem. Eng.* **2012**, *2012*, No. 516461.
(11) Duchi, S.; Onofrillo, C.; O'Connell, C. D.; Blanchard, R.; Augustine, C.; Quigley, A. F.; Kapsa, R. M. I.; Pivonka, P.; Wallace, G.; di Bella, C.; Choong, P. F. M. Handheld Co-Axial Bioprinting: Application to in Situ Surgical Cartilage Repair. *Sci. Rep.* **2017**, *7*, 5837.
(12) O'Connell, C. D.; Zhang, B.; Onofrillo, C.; Duchi, S.; Blanchard, R.; Quigley, A.; Bourke, J.; Gambhir, S.; Kapsa, R.; Di Bella, C.; Choong, P.; Wallace, G. G. Tailoring the Mechanical Properties of Gelatin Methacryloyl Hydrogels through Manipulation of the Photocrosslinking Conditions. *Soft Matter* **2018**, *14*, 2142−2151.
(13) Ouyang, L.; Armstrong, J. P. K.; Lin, Y.; Wojciechowski, J. P.; Lee-Reeves, C.; Hachim, D.; Zhou, K.; Burdick, J. A.; Stevens, M. M. Expanding and Optimizing 3D Bioprinting Capabilities Using Complementary Network Bioinks. *Sci. Adv.* **2020**, *6*, No. eabc5529.
(14) Zhao, Y.; Song, S.; Ren, X.; Zhang, J.; Lin, Q.; Zhao, Y. Supramolecular Adhesive Hydrogels for Tissue Engineering Applications. *Chem. Rev.* **2022**, *122*, 5604−5640.
(15) Gao, Q.; Kim, B. S.; Gao, G. Advanced Strategies for 3D Bioprinting of Tissue and Organs Analogs Using Alginate Hydrogel Bioinks. *Mar. Drugs* **2021**, *19*, 708.
(16) Panwar, A.; Tan, L. P. Current Status of Bioinks for Micro-Extrusion-Based 3D Bioprinting. *Molecules* **2016**, *21*, 685.
(17) Deo, K. A.; Singh, K. A.; Peak, C. W.; Alge, D. L.; Gaharwar, A. K. Bioprinting 101: Design, Fabrication, and Evaluation of Cell-Laden 3D Bioprinted Scaffolds. *Tissue Eng. Part A* **2020**, *26*, 318−338.
(18) Paxton, N.; Smolan, W.; Böck, T.; Melchels, F.; Groll, J.; Jungst, T. Proposal to Assess Printability of Bioinks for Extrusion-Based Bioprinting and Evaluation of Rheological Properties Governing Bioprintability. *Biofabrication* **2017**, *9*, No. 044107.
(19) GhavamiNejad, A.; Ashammakhi, N.; Wu, X. Y.; Khademhosseini, A. Crosslinking Strategies for 3D Bioprinting of Polymeric Hydrogels. *Small* **2020**, *16*, No. 2002931.
(20) Gao, T.; Gillispie, G. J.; Copus, J. S.; PR, A. K.; Seol, Y.-J.; Atala, A.; Yoo, J. J.; Lee, S. J. Optimization of Gelatin Alginate Composite Bioink Printability Using Rheological Parameters: A Systematic Approach. *Biofabrication* **2018**, *10*, No. 034106.
(21) Jongprasitkul, H.; Turunen, S.; Parihar, V. S.; Kellomäki, M. Two-Step Crosslinking to Enhance the Printability of Methacrylated Gellan Gum Biomaterial Ink for Extrusion-Based 3D Bioprinting. *Bioprinting* **2022**, *25*, No. e00185.
(22) Xu, Z.; Li, Z.; Jiang, S.; Bratlie, K. M. Chemically Modified Gellan Gum Hydrogels with Tunable Properties for Use as Tissue Engineering Scaffolds. *ACS Omega* **2018**, *3*, 6998−7007.
(23) Kim, W.; Kim, G. Intestinal Villi Model with Blood Capillaries Fabricated Using Collagen-Based Bioink and Dual-Cell-Printing Process. *ACS Appl. Mater. Interfaces* **2018**, *10*, 41185−41196.
(24) Maiz-Fernández, S.; Pérez-álvarez, L.; Silván, U.; Vilas-Vilela, J. L.; Lanceros-Méndez, S. PH-Induced 3D Printable Chitosan Hydrogels for Soft Actuation. *Polymers (Basel)* **2022**, *14*, 650.
(25) Luo, C.; Xie, R.; Zhang, J.; Liu, Y.; Li, Z.; Zhang, Y.; Zhang, X.; Yuan, T.; Chen, Y.; Fan, W. Lower-Temperature Three-Dimensional Printing of Tissue Cartilage Engineered with Gelatin Methacrylamide. *Tissue Eng. Part C Methods* **2020**, *26*, 306−316.
(26) Gu, Y.; Zhang, L.; Du, X.; Fan, Z.; Wang, L.; Sun, W.; Cheng, Y.; Zhu, Y.; Chen, C. Reversible Physical Crosslinking Strategy with Optimal Temperature for 3D Bioprinting of Human Chondrocyte-Laden Gelatin Methacryloyl Bioink. *J. Biomater. Appl.* **2018**, *33*, 609−618.
(27) Janmaleki, M.; Liu, J.; Kamkar, M.; Azarmanesh, M.; Sundararaj, U.; Nezhad, A. S. Role of Temperature on Bio-Printability of Gelatin Methacryloyl Bioink in Two-Step Cross-Linking Strategy for Tissue Engineering Applications. *Biomed. Mater.* **2021**, *16*, No. 015021.
(28) Serna, J. A.; Rueda-gensini, L.; Céspedes-valenzuela, D. N.; Cifuentes, J.; Cruz, J. C.; Muñoz-camargo, C. Recent Advances on Stimuli-responsive Hydrogels Based on Tissue-derived Ecms and Their Components: Towards Improving Functionality for Tissue Engineering and Controlled Drug Delivery. *Polymers (Basel)* **2021**, *13*, 3263.
(29) Teixeira, M. C.; Lameirinhas, N. S.; Carvalho, J. P. F.; Silvestre, A. J. D.; Vilela, C.; Freire, C. S. R. A Guide to Polysaccharide-Based Hydrogel Bioinks for 3D Bioprinting Applications. *Int. J. Mol. Sci.* **2022**, *23*, 6564.
(30) Li, W.; Wang, M.; Wang, S.; Wang, X.; Avila, A.; Kuang, X.; Mu, X.; Garciamendez, C. E.; Jiang, Z.; Manríquez, J.; Tang, G.; Guo, J.; Mille, L. S.; Robledo, J. A.; Wang, D.; Cheng, F.; Li, H.; Flores, R. S.; Zhao, Z.; Delavaux, C.; Wang, Z.; López, A.; Yi, S.; Zhou, C.; Gómez, A.; Schuurmans, C.; Yang, G. Y.; Wang, Y.; Zhang, X.; Zhang, X.; Zhang, Y. S. An Adhesive Bioink toward Biofabrication under Wet Conditions. *Small* **2023**, No. e2205078.
(31) Haidari, H.; Kopecki, Z.; Sutton, A. T.; Garg, S.; Cowin, A. J.; Vasilev, K. Ph-Responsive "Smart" Hydrogel for Controlled Delivery of Silver Nanoparticles to Infected Wounds. *Antibiotics* **2021**, *10*, 49.
(32) Jiang, H.; Ochoa, M.; Waimin, J. F.; Rahimi, R.; Ziaie, B. A PH-Regulated Drug Delivery Dermal Patch for Targeting Infected Regions in Chronic Wounds. *Lab Chip* **2019**, *19*, 2265−2274.
(33) Bertsch, P.; Diba, M.; Mooney, D. J.; Leeuwenburgh, S. C. G. Self-Healing Injectable Hydrogels for Tissue Regeneration. *Chem. Rev.* 2023 *123*, 834−873. DOI: 10.1021/acs.chemrev.2c00179.
(34) Samanta, S.; Rangasami, V. K.; Murugan, N. A.; Parihar, V. S.; Varghese, O. P.; Oommen, O. P. An Unexpected Role of an Extra Phenolic Hydroxyl on the Chemical Reactivity and Bioactivity of Catechol or Gallol Modified Hyaluronic Acid Hydrogels. *Polym. Chem.* **2021**, *12*, 2987−2991.
(35) Han, L.; Yan, L.; Wang, K.; Fang, L.; Zhang, H.; Tang, Y.; Ding, Y.; Weng, L. T.; Xu, J.; Weng, J.; Liu, Y.; Ren, F.; Lu, X. Tough, Self-Healable and Tissue-Adhesive Hydrogel with Tunable Multifunctionality. *NPG Asia Mater.* **2017**, *9*, e372−e372.
(36) Jongprasitkul, H.; Turunen, S.; Parihar, V. S.; Kellomäki, M. Sequential Cross-Linking of Gallic Acid-Functionalized GelMA-Based

Bioinks with Enhanced Printability for Extrusion-Based 3D Bioprinting. *Biomacromolecules* **2023**, *24*, 502−514.
(37) Włodarczyk-Biegun, M. K.; Paez, J. I.; Villiou, M.; Feng, J.; Del Campo, A. Printability Study of Metal Ion Crosslinked PEG-Catechol Based Inks. *Biofabrication* **2020**, *12*, No. 035009.
(38) Townsend, J. M.; Beck, E. C.; Gehrke, S. H.; Berkland, C. J.; Detamore, M. S. Flow Behavior Prior to Crosslinking: The Need for Precursor Rheology for Placement of Hydrogels in Medical Applications and for 3D Bioprinting. *Prog. Polym. Sci.* **2019**, *91*, 126−140.
(39) Queiroz, M. F.; Sabry, D. A.; Sassaki, G. L.; Rocha, H. A. O.; Costa, L. S. Gallic Acid-Dextran Conjugate: Green Synthesis of a Novel Antioxidant Molecule. *Antioxidants* **2019**, *8*, 478.
(40) Pepelanova, I.; Kruppa, K.; Scheper, T.; Lavrentieva, A. Gelatin-Methacryloyl (GelMA) Hydrogels with Defined Degree of Functionalization as a Versatile Toolkit for 3D Cell Culture and Extrusion Bioprinting. *Bioengineering* **2018**, *5*, 55.
(41) Boni, R.; Ali, A.; Giteru, S. G.; Shavandi, A.; Clarkson, A. N. Silk Fibroin Nanoscaffolds for Neural Tissue Engineering. *J. Mater. Sci. Mater. Med.* **2020**, *31*, 81.
(42) Chaudhuri, O.; Gu, L.; Klumpers, D.; Darnell, M.; Bencherif, S. A.; Weaver, J. C.; Huebsch, N.; Lee, H. P.; Lippens, E.; Duda, G. N.; Mooney, D. J. Hydrogels with Tunable Stress Relaxation Regulate Stem Cell Fate and Activity. *Nat. Mater.* **2016**, *15*, 326−334.
(43) Dhand, A. P.; Davidson, M. D.; Galarraga, J. H.; Qazi, T. H.; Mauck, R. L.; Burdick, J. A.; Locke, R. C. Simultaneous One-Pot Interpenetrating Network Formation to Expand 3D Processing Capabilities. *Adv. Mater.* **2022**, *34*, No. 2202261.
(44) Park, Y. D.; Tirelli, N.; Hubbell, J. A. Photopolymerized Hyaluronic Acid-Based Hydrogels and Interpenetrating Networks. *Biomaterials* **2003**, *24*, 893−900.
(45) Kang, B.; Vales, T. P.; Cho, B. K.; Kim, J. K.; Kim, H. J. Development of Gallic Acid-Modified Hydrogels Using Interpenetrating Chitosan Network and Evaluation of Their Antioxidant Activity. *Molecules* **2017**, *22*, 1976.
(46) Karvinen, J.; Ihalainen, T. O.; Calejo, M. T.; Jönkkäri, I.; Kellomäki, M. Characterization of the Microstructure of Hydrazone Crosslinked Polysaccharide-Based Hydrogels through Rheological and Diffusion Studies. *Mater. Sci. Eng. C* **2019**, *94*, 1056−1066.
(47) Dave, P. N.; Gor, A. Natural Polysaccharide-Based Hydrogels and Nanomaterials: Recent Trends and Their Applications. In *Handbook of Nanomaterials for Industrial Applications*; Elsevier, 2018; *1*, 36−66.
(48) Bovone, G.; Dudaryeva, O. Y.; Marco-Dufort, B.; Tibbitt, M. W. Engineering Hydrogel Adhesion for Biomedical Applications via Chemical Design of the Junction. *ACS Biomater. Sci. Eng.* **2021**, *7*, 4048−4076.
(49) Zhou, D.; Li, S.; Pei, M.; Yang, H.; Gu, S.; Tao, Y.; Ye, D.; Zhou, Y.; Xu, W.; Xiao, P. Dopamine-Modified Hyaluronic Acid Hydrogel Adhesives with Fast-Forming and High Tissue Adhesion. *ACS Appl. Mater. Interfaces* **2020**, *12*, 18225−18234.
(50) Leopoldini, M.; Prieto Pitarch, I.; Russo, N.; Toscano, M. S. Conformation, and Electronic Properties of Apigenin, Luteolin, and Taxifolin Antioxidants. A First Principle Theoretical Study. *J. Phys. Chem. A* **2004**, *108*, 92−96.

https://doi.org/10.1021/acsami.3c02961
ACS Appl. Mater. Interfaces 2023, 15, 33972−33984